Formulation and Aerosol Delivery of Nano-Sized Biomaterials

By

Eugene Raj Arulmuthu

A Doctoral Thesis

Submitted in partial fulfilment of the requirements for the award of Doctor of Philosophy of Loughborough University

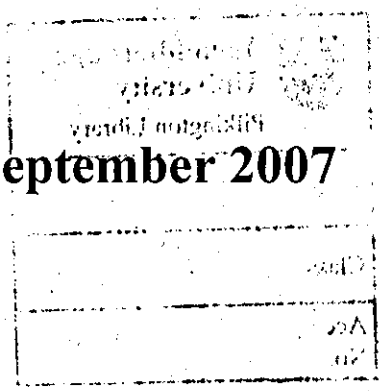

September 2007

Dedication

To my Parents,

to Joseline and

to Ashish & Ashwin.

Abstract

The aim of this research has been to study and develop the engineering principles associated with the impact of formulation and device parameters on the safe delivery of nano-sized biomaterials such as plasmid DNA. In the present investigation, Omron U22 and U03 mesh nebulisers operating at frequencies of ~175 kHz and ~65 kHz respectively were used. Since the U22 device is a recently introduced mesh nebuliser for respiratory drug delivery, detailed characterisation, experimentation, modelling and analysis was carried out for this device.

Plasmids of size 5.7, 8.7, 13 and 20 kb were purified from *Escherichia coli* cells and used for nebulisation experiments. Experiments on the nebulisation of plasmid DNA using the U22 device in a bio-safety cabinet showed no damage to the sc structure of the 5.7 kb plasmid, but almost complete damage to the 20 kb plasmid in the condensed aerosols collected using a fabricated aerosol collection apparatus. The damage to the sc structure of plasmid DNA was analysed using gel electrophoresis, PicoGreen assay and atomic force microscope (AFM). Engineering analysis was performed using computational fluid dynamics (CFD) modeling to determine the shear and elongational strain rates in the mesh nozzle of nebuliser. The estimated maximum hydrodynamic force on plasmid DNA based on the Ryskin equation was calculated in picoNewton (pN) from the actual molecular size of the sc structure and predicted strain rates. Optimisation of the formulation and device parameters were carried out using Design of Experiments (DOE) to predict damage to the sc structure. Formulation of the 20 kb plasmid with polyethyleneimine (PEI) resulted in safe aerosol delivery using the mesh nebuliser. *In vitro* transfection studies in suspension-adapted Chinese Hamster Ovary (CHO-S) cells resulted in successful integration of Green Fluorescent Protein (GFP) from the 5.7 kb plasmid after nebulisation.

The commercially available U22 mesh nebuliser promises to be a useful pulmonary device for the successful delivery of plasmid DNA for non-viral gene therapy. Realisation of this promise however will require both innovations in the design of experiments, formulation and methods of studying plasmid DNA damage as demonstrated in this thesis.

Table of Contents

		Page
Abstract		i
Abbreviations		xi
List of Tables		xviii
List of Figures		xx
Acknowledgments		xxviii
Chapter 1. Introduction		1
1	Context of the Research	1
1.1	Delivery of non-viral gene therapeutic	2
1.2	Statement of the problem	3
1.3	Structure of the PhD thesis	3
Chapter 2. Review of Literature		6
2.1	Introduction to the chapter	6
2.2	Gene therapy	6
2.2.1	Vectors for gene therapy	7
2.2.2	Non-viral gene therapeutics	9
2.2.3	Plasmid DNA-based non-viral gene therapeutic	10
2.2.3.1	Therapeutic gene	10
2.2.3.2	Gene expression plasmids	10
2.2.3.2.1	Production and processing of plasmid DNA	11
2.2.3.2.2	Quality of plasmid DNA for gene therapy	12
2.2.4	Gene therapy clinical trials	13
2.3	Formulation for non-viral gene delivery	15
2.4	Non-viral gene delivery	17

2.4.1	Route for plasmid DNA delivery into cells	18
2.4.1.1	Endocytosis	19
2.4.1.2	Dissociation of plasmid DNA from non-viral carrier	20
2.4.1.3	Plasmid DNA uptake in nucleus	20
2.5	Delivery systems for administration	21
2.5.1	Parenteral delivery	21
2.5.1.1	Subcutaneous injection	22
2.5.1.2	Intravenous injection	22
2.5.1.3	Intramuscular injection	23
2.5.2	Oral delivery	24
2.5.3	Nasal delivery	24
2.5.4	Transdermal delivery	25
2.5.5	Ocular delivery	26
2.5.6	Pulmonary delivery	27
2.6	Devices used for pulmonary delivery	29
2.6.1	Pressurised metered dose inhalers	30
2.6.2	Dry powder inhalers	30
2.6.3	Nebulisers	31
2.6.3.1	Jet nebuliser	31
2.6.3.2	Ultrasonic nebuliser	31
2.6.3.2.1	Conventional type	32
2.6.3.2.1	Mesh type	32
2.6.4	Alternative aerosolisation methods	33
2.6.4.1	Electro-mechanical device	34
2.6.4.1	Electro-hydrodynamic device	35
2.6.5	Targeted delivery by magnetofection	36
2.7	Theory of aerosol generation from an ultrasonic nebuliser	36
2.7.1	Capillary theory	37
2.7.2	Cavitation theory	37
2.8	Aerosol gene delivery	37

2.9 Roadmap to non-viral gene therapy 38
2.10 Conclusions 40

Chapter 3. Materials and Methodology..... 41

3.1 Materials/ Equipment 41
3.1.1 Chemicals 41
3.1.2 Delivery device 41
3.1.3 Plasmid DNA 41
3.1.4 Equipment used for the experiments 43
3.2 Methodology 44
3.2.1 Operation of a U22 mesh nebuliser 44
3.2.2 Operation of a U03 mesh nebuliser 45
3.2.3 Characterisation of the mesh nebuliser 46
3.2.4 Aerosol collection apparatus 46
3.2.5 High-speed imaging of aerosolisation 47
3.2.6 Purification of plasmid DNA from cells 48
3.2.7 Analysis of plasmid DNA 49
3.2.7.1 DNA concentration and purity measurements 50
3.2.7.2 Agarose gel electrophoresis 50
3.2.7.2.1 Preparation of buffers and agarose gel 51
3.2.7.2.2 Loading of DNA samples in the agarose gel 51
3.2.7.2.3 Quantification of agarose gel 52
3.2.7.3 PicoGreen assay 53
3.2.7.4 Atomic force microscopy 53
3.2.8 Formulation of plasmid DNA 54
3.2.8.1 Formulation using liposomes 54
3.2.8.2 Formulation using DEAE-dextran 55
3.2.8.3 Formulation using PEI 55
3.2.9 Transfection studies 55

3.2.9.1 Chinese hamster ovary cells 56
3.2.9.2 Maintenance of CHO-S cells 56
3.2.9.3 Preparation of PEI-pDNA complexes using 5.7 kb plasmid 56
3.2.9.4 PEI-pDNA transfection of CHO-S cells 57
3.2.9.5 Determination of viable cell density and percentage viability 57
3.2.9.6 Flow cytometric analysis 58
3.3 Summary 58

Chapter 4. Purification and nebulisation of plasmid DNA..... 59

4.1 Introduction 59
4.2 Purification of plasmid DNA 60
4.2.1 5.7 kb and 20 kb plasmids 60
4.2.2 8.7 kb and 13 kb plasmids 61
4.3 Characterisation of a U22 mesh nebuliser 62
4.3.1 Dimensions of the nebuliser mesh 62
4.3.2 Aerosol particle size distribution 65
4.3.3 Nebulisation rate 65
4.4 Characterisation of a U03 mesh nebuliser 66
4.5 Aerosol delivery of plasmid DNA 67
4.6 Nebulisation of plasmid DNA in a U22 mesh nebuliser 69
4.6.1 Assessment of pDNA damage 69
4.6.1.1 Agarose gel electrophoresis for pDNA damage 69
4.6.1.1.1 5.7 kb plasmid 70
4.6.1.1.2 8.7 kb plasmid 74
4.6.1.1.3 20 kb plasmid 75
4.6.1.2 Atomic force microscopy for plasmid DNA imaging 77
4.6.1.2.1 5.7 kb plasmid 77
4.6.1.2.2 20 kb plasmid 79
4.6.1.3 PicoGreen assay for analysis of DNA damage 80

4.6.1.3.1 5.7 kb plasmid 81
4.6.1.3.2 20 kb plasmid 86
4.6.2 Summary of pDNA nebulisation in a U22 mesh nebuliser 87
4.7 Nebulisation of plasmid DNA in a U03 mesh nebuliser 88
4.8 Discussion 90
4.9 Conclusion 94

Chapter 5. Nebulisation of plasmid DNA: DOE..... 96

5.1 Introduction to Design of Experiments (DOE) 96
5.2 Nebulisation of 20 kb plasmid – Response surface method 97
5.2.1 Choice of variables and levels 97
5.2.2 Experimental design 98
5.2.3 Statistical analysis of Box-Behnken design 99
5.2.4 Model diagnostic plots 102
5.2.5 Model predictions: Response surface contour and 3D plots 102
5.2.5.1 Effect of nozzle size 104
5.2.5.1.1 Nozzle size 3 um 104
5.2.5.1.2 Nozzle size 4 um 104
5.2.5.1.3 Nozzle size 5 um 104
5.2.5.2 Effect of DNA concentration 108
5.2.5.2.1 DNA concentration 10 µg/mL 108
5.2.5.2.2 DNA concentration 20 µg/mL 108
5.2.5.2.3 DNA concentration 30 µg/mL 112
5.2.5.3 Effect of NaCl concentration 112
5.2.5.3.1 NaCl concentration 0 mM 112
5.2.5.3.2 NaCl concentration 150 mM 112
5.2.5.3.3 NaCl concentration 300 mM 113
5.2.5.4 Response from model predictions 117
5.2 Aerosol characterisation from the U22 mesh nebuliser 117

5.4 Discussion 119
5.4 Conclusions 120

Chapter 6. Engineering analysis on nebulisation of pDNA..... 122

6.1 Introduction 122
6.2 Droplet formation from capillary waves 122
6.3 High-speed imaging of aerosolisation 125
6.3.1 Introduction 125
6.3.2 Aerosolisation using the U22 mesh nebuliser 125
6.3.2.1 Aerosolisation from 5 µl droplet without mesh 126
6.3.2.2 Aerosolisation of 0.5 µl liquid film without and with mesh 127
6.3.2.3 Nebulisation of plasmid DNA without and with mesh 128
6.3.2.4 Analysis of high-speed imaging 129
6.3.3 Discussion 131
6.4 Background to engineering analysis 132
6.4.1 Mechanism of degradation of supercoiled plasmid DNA 133
6.4.2 Time scales involved in process 135
6.4.2.1 DNA relaxation time scales 136
6.4.2.2 Process time scale 138
6.4.2.3 Inertial time scale 138
6.4.2.4 Particle relaxation time scale 139
6.4.2.5 Capillary time scale 139
6.4.2.6 Viscous time scale 140
6.4.2.7 Summary of time scales 140
6.5 Mechanics of fluid flow through nebuliser 141
6.5.1 CFD methodology 141
6.5.1.1 Model geometry and boundary conditions 141
6.5.1.2 CFD simulation for fluid flow through nozzle 143
6.5.1.3 Grid dependency studies 145

6.5.1.4 Estimated hydrodynamic force on pDNA from strain rates 148
6.5.2 Discussion 153
6.6 Prediction of plasmid DNA size for safe delivery 159
6.6.1 Degradation of plasmid DNA in a U22 mesh nebuliser 159
6.6.2 Degradation of plasmid DNA in a U03 mesh nebuliser 159
6.6.3 Discussion 161
6.7 Conclusions 159

Chapter 7. Device parameters influencing pDNA damage 163

7.1 Introduction 163
7.2 Influence of size on damage: DOE using factorial design 163
7.2.1 Choice of variables and levels 163
7.2.2 Experimental design 164
7.2.3 Analysis of factorial design 165
7.2.4 Model adequacy plots 166
7.2.5 Model predictions: Main effects and interaction plots 168
7.2.6 Model predictions: Contour and surface plots 170
7.2.7 Discussion 170
7.2.8 Summary 172
7.3 Influence of frequency on damage: DOE using factorial design 172
7.3.1 Choice of variables and levels 172
7.3.2 Experimental design 173
7.3.3 Analysis of factorial design 174
7.3.4 Model adequacy plots 175
7.3.5 Model predictions: Main effects and interaction plots 177
7.3.6 Model predictions: Contour and surface plots 179
7.3.7 Predicted damage at intermediate frequencies 179
7.3.8 Discussion 181
7.3.9 Summary 182

7.4 Conclusions 182

Chapter 8. Formulation of 20 kb pDNA for nebulisation..... 183

8.1 Introduction 183
8.2 Formulation of 20 kb plasmid 185
8.2.1 Nebulisation of unformulated 20 kb plasmid 186
8.2.1.1 Analysis of pDNA damage 186
8.2.2 Nebulisation of pDNA with liposomes 188
8.2.3 Nebulisation of pDNA formulations with DEAE-dextran 188
8.2.3.1 Analysis of pDNA damage 189
8.2.3.2 Atomic force microscopy 192
8.2.3.2.1 Visualisation of pDNA/DD formulations 192
8.2.3.2.2 Size of pDNA/DD formulations 196
8.2.4 Nebulisation of pDNA formulations with PEI 196
8.2.4.1 Analysis of pDNA damage 197
8.2.3.2 Atomic force microscopy 198
8.3 Discussion 200
8.4 Conclusions 200

Chapter 9. Transfection of CHO-S cells using plasmid DNA ... 201

9.1 Introduction 201
9.2 Choice of formulation substrate and concentration 202
9.3 Transfection of CHO-S cells 202
9.3.1 PEI complexed 5.7 kb plasmid 203
9.3.1.1 Cell density measurements 204
9.3.1.2 Fluorescence measurements 204
9.3.2 Nebulised 5.7 kb plasmid complexed with PEI 206
9.3.2.1 Plasmid in TE buffer 206

9.3.2.1.1 Cell density measurements 207
9.3.2.1.2 Flow cytometry analysis 208
9.3.2.2 Plasmid in HBS buffer 210
9.3.2.2.1 Flow cytometry analysis 210
9.3.2.2.2 Microscopy 212
9.4 Discussion 212
9.5 Conclusions 215

Chapter 10. Conclusions 217

10.1 Introduction 217
10.2 Conclusions 218
10.3 Key parameters for delivery of supercoiled plasmid 220
10.4 Scope for future work 220
10.4.1 Studies on multiphase modelling and device parameters 221
10.4.2 Nebulisation for cystic fibrosis gene therapy 222

References 224

Publications..... 248

Appendix..... 249

Abbreviations

AGE	Agarose gel electrophoresis
AFM	Atomic force microscopy
AN	After nebulisation
ANOVA	Analysis of variance
ATA	Aurintricarboxylic acid
BN	Before nebulisation
CHO-S	Chinese hamster ovary suspension-adapted
CF	Cystic fibrosis
CFD	Computational fluid dynamics
CFTR	Cystic fibrosis transmembrane conductance regulator
CGE	Capillary gel electrophoresis
cGMP	Current good manufacturing practice
CNS	Central nervous system
COPD	Chronic obstructive pulmonary disease
DC-Chol	3β[(N-(n',N'-dimethylaminoethane)-carbamoyl]cholesterol
DEAE	Diethylaminoethyl
df	Degrees of freedom
DNA	Deoxyribonucleic acid
DOE	Design of experiments

DOPE	Dioleoylphosphatidylethanolamine
DOSPA	2,3-dioleyloxy-*N*-[2-(sperminecarboxamido) ethyl]-*N*,*N*-dimethyl-1-propanaminium trifluoroacetate
DOTAP	1,2-diacyl-3-trimethylammonium propane
DOTMA	N[1-(2,3-dioleyloxy)propyl]-N,N,N-trimethylammonium chloride)
DPI	Dry powder inhalers
DRV	Dehydration-rehydration vesicles
dsDNA	double-stranded DNA
pDMAEMA	Poly(2-dimethylamino) ethyl methacrylate
pDNA	plasmid DNA
PNA	peptide nucleic acid
EGFP	Enhanced green fluorescent protein
EMEA	European medicines evaluation agency
EtBr	Ethidium bromide
FPF	Fine particle fraction
GALT	Gut-associated lymphoid tissues
GI tract	Gastro-intestinal tract
GSD	Geometric standard deviation
HBS	HEPES-buffered saline
HEPES	Hydroxyethylpiperazine-N'-2-ethanesulfonic acid
HIV	Human immunodeficiency virus
HVJ	Hemagglutinating virus of Japan

i.m.	Intramuscular
i.d.	Intradermal
kb	kilo basepair (1 basepair = 623 gm.mole^{-1})
LB	Luria broth
Lf	linear form
MMAD	Mass median aerodynamic diameter
NALT	Nasal-associated lymphoid tissues
NC	Nebuliser chamber
NLS	Nuclear localisation signal
NPC	Nuclear pore complex
N/P	PEI Nitrogen to DNA phosphate ratio
oc	open circular
PBS	Phosphate-buffered saline
PCR	Polymerase chain reaction
PEG	Polyethylene glycol
PEI	Polyethylenimine
PG	PicoGreen
PLL	Poly-L-Lysine
pMDI	Pressurised metered dose inhalers
pN	PicoNewton
PRESS	Predicted residual sum of squares

RFU	Relative fluorescence units
RNAi	Ribonucleic acid interference
RNAa	Ribonucleic acid activation
rpm	revolutions per minute
RSM	Response surface method
sc	supercoiled
SEM	Scanning electron microscope
SFM	Serum free medium
siRNA	Short interfering RNA
SMSS	Sequential model sum of squares
ssDNA	Single-stranded DNA
TBE	Tris-Borate EDTA
TE	Tris-EDTA
TESP	TappingMode^{TM} etched silicon probes
ULB	Ultra low binding
USP	United States pharmacopoeia
ZI	Zygo interferometer

Symbols

A_{260}/A_{280}	Measure of DNA purity; DNA ratio by absorbance at 260 to 280 nm
b	Optical path length

k	Dimensionless constant based on Ryskin equation
k_{ratio}	DNA binding constant ratio (= k_{BN}/k_{AN}, = k_{BD}/k_{AD})
L_{sc}	Length of the supercoiled DNA molecule
L_{AFM}	AFM length of the supercoiled DNA molecule
X_{nozzle}	Nozzle size (μm)
$X_{plasmid}$	Plasmid size (kb)
C_{DNA}	DNA concentration ($\mu g.mL^{-1}$)
C_{NaCl}	NaCl concentration (mM)
$C_{polymer}$	Polymer (sc pDNA) concentration ($gm.cm^{-3}$) in Ryskin equation
C_o/C (C)	Ratio of intact sc before nebulisation (C_o) to that after nebulisation
D	Droplet diameter (m)
$Damage_{sc}$	Percentage damage to the sc structure
$\frac{\partial u}{\partial z}$	Elongational strain rate on molecule aligned with local streamlines
$0.5\frac{\partial u}{\partial r}$	Elongational strain rate on molecule oriented at 45° to the streamlines
λ	Capillary wavelength (m)
γ	Surface tension ($N.m^{-1}$)
ρ_L	Density of liquid ($kg.m^{-3}$)
η_s	Solvent viscosity ($kg.m^{-1}.s^{-1}$)
f	Frequency of vibrator horn (Hz = $cycles.s^{-1}$)

υ	Kinematic viscosity ( )
ω	Angular frequency ($rad.s^{-1}$)
a	Amplitude of vibrator horn (m)
a_{th}	Threshold amplitude (m)
V	Velocity of transducer or vibrator horn ($m.s^{-1}$)
V_{rms}	RMS velocity of transducer or vibrator horn ($m.s^{-1}$)
$\dot{\gamma}$	Strain rate (s^{-1})
β	Pressure amplitude ($N.m^{-2}$)
c	Velocity of sound (m/s)
h	Film thickness (m)
U	Velocity scale ($U = f.a$)
$[\eta]$	Intrinsic viscosity
M	Molecular weight of DNA ($gm.mole^{-1}$)
R	Gas constant
T	Temperature (K)
K_θ	Hydrodynamic coefficient ($dl.g^{-1}.(g.mol^{-1})^{-1/2}$)
R_{rms}	Root mean square separation of the ends of the molecule
Φ	Universal hydrodynamic constant ($dl.cm^{-3}.mol^{-1}$)
τ_r	Relaxation time (s)
$\tau_{r_{Zimm}}$	Chain relaxation time according to Zimm model (s)

τ_f	Process timescale (s)
τ_u	Inertial timescale (s)
τ_{St}	Particle relaxation timescale based on Stokes number (s)
τ_σ	Capillary timescale (s)
τ_μ	Viscous timescale (s)
g	Acceleration due to gravity ($m.s^{-2}$)

Dimensionless numbers

We	Weber number ($We = \frac{\rho_L U^2 h}{\sigma}$)
Re	Reynolds number ($\mathrm{Re} = \frac{\rho_L U h}{\eta}$)
Fr	Froude number ($Fr = \frac{U^2}{ga}$)
De	Deborah number ($De = \tau\dot{\gamma}$)

List of Tables

Table 2.1: Viral and non-viral vectors for gene therapy	8
Table 2.2: Quality assurance tests of plasmid DNA preparation for gene therapy	12
Table 2.3: Main gene therapy vectors in the clinical phase of the gene therapy trials	15
Table 2.4: Targeting aerosols to the lung via inhalation [Hanes et al., 2003]	28
Table 2.5: Technical specifications for next-generation mesh nebulisers	34
Table 3.1: Equipment/software used for experiments	43
Table 4.1: Plasmid DNA purity for 5.7 kb and 20 kb plasmids by A_{260}/A_{280} ratio (n=6)	61
Table 4.2: Plasmid DNA purity for 8.7 kb and 13 kb plasmids by A_{260}/A_{280} ratio	61
Table 4.3: Dimensions of mesh of the U22 nebuliser mesh	64
Table 4.4: Damage to sc pDNA in some reported aerosolisation devices	68
Table 4.5: Summary of PicoGreen results on damage to 5.7 kb plasmid	85
Table 4.6: Absorbance measurements of nebulisation samples of 20 kb plasmid	87
Table 4.7: Summary of plasmid DNA nebulisation in a U22 mesh nebuliser	88
Table 5.1: Variables and levels chosen for experimental design	98
Table 5.2: Box-Behnken experimental design and experimental response	99
Table 5.3: Statistical analysis of Box-Behnken design based on SMSS	100
Table 5.4: Lack of Fit Tests for Box-Behnken design	100
Table 5.5: Model summary statistics for Box-Behnken design	100
Table 5.6: Analysis of Variance (ANOVA)	101

Table 5.7: Characterisation of distilled water aerosols from the U22 nebuliser with 3 μm and 4 μm nozzle sizes.	117
Table 6.1: Theoretical predictions of the effect of frequency and physical properties on droplet size and strain rate in a mesh nebuliser.	125
Table 6.2: Computed time scales associated with aerosolisation of 5.7 and 20 kb plasmids.	140
Table 6.3: Grid dependency studies with triangular and quadrilateral meshes.	146
Table 6.4: Summary of forces reported for stretching/damaging DNA.	151
Table 7.1: Variables and levels chosen for factorial design of experiments.	164
Table 7.2: A 2^2 factorial experimental design for plasmid and nozzle sizes as variables.	164
Table 7.3: Estimated effects and coefficients for % damage in coded units.	165
Table 7.4: Analysis of variance (ANOVA)	166
Table 7.5: Variables and levels chosen for factorial design of experiments	173
Table 7.6: A 2^2 factorial experimental design for plasmid size and frequency as variables	173
Table 7.7: Estimated effects and coefficients for % damage in coded units	174
Table 7.8: Analysis of variance (ANOVA)	175
Table 8.1: Nebulisation of unformulated 20 kb plasmid (n=2)	186
Table 8.2: Analysis of DNA damage to pDNA formulations of DEAE-dextran (n=2)	190
Table 8.3: Size of DD/plasmid DNA nanoparticles determined by AFM	196
Table 9.1: Average cell density and transfection efficiency (n=3) for 5.7 kb plasmid	210
Table 10.1: Summary of the key parameters for delivery of supercoiled plasmid	221

List of Figures

Figure 2.1: Gene therapy clinical trials: (a) vectors used, (b) diseases addressed (Data taken from website http://www.wiley.co.uk/genetherapy/clinical/ as of July 2007).	**14**
Figure 2.2: Comparison of the main vectors used in gene therapy clinical trials (Data taken from website http://www.wiley.co.uk/genetherapy/clinical/ dated as of July 2007).	**15**
Figure 2.3: A schematic showing the trafficking of a cationic lipid/plasmid DNA complex during the transfection process in targeted cells.	**19**
Figure 2.4: Human respiratory system showing anatomy of the lower airways comprising trachea, bronchi and alveoli.	**28**
Figure 2.5: Roadmap to non-viral gene therapy.	**39**
Figure 3.1: A U22 (MicroAIR® NE-U22) mesh nebuliser.	**42**
Figure 3.2: A U03 (U1 NE-U03) mesh nebuliser.	**42**
Figure 3.3: Principle of operation of the U22 mesh nebuliser [Kishida et al., 2003] showing the medication container and the mesh of the device; the vibrator horn is powered by a DC volt supply of 3V; plasmid DNA sample from the 'nebuliser chamber' is taken to check integrity of supercoiled (sc) structure.	**44**
Figure 3.4: U03 mesh nebuliser: a) sketch of the device, b) schematic of medication container showing nozzle mesh and nebuliser chamber; liquid is drawn through the annular section and forced through the mesh resulting in generation of aerosols.	**45**
Figure 3.5: Aerosol collection apparatus from a U22 mesh nebuliser, same apparatus was used for the U03 mesh nebuliser.	**47**
Figure 3.6: (a) Vibrator horn (diameter at the top of the horn is 3.5 mm) of the U22 mesh nebuliser, (b) schematic of a high speed imaging set-up.	**48**
Figure 4.1: Figure 4.1: DNA homogeneity of purified supercoiled 5.7 kb and 20 kb plasmids determined by densitometric scan of an agarose gel; *sc 5.7 kb – 96.57%, sc 20 kb – 96.61%* (an ethidium bromide correction factor of 1.36 was applied to the sc structure)	**60**
Figure 4.2: Figure 4.2: DNA homogeneity of purified supercoiled 8.7 kb and 13 kb plasmids determined by densitometric scan of agarose gel; *sc*	**62**

8.7 kb – 96.34%, sc 13 kb – 96.9% (an ethidium bromide correction factor of 1.36 was applied to the sc structure).	
Figure 4.3: Scanning electron micrograph of the mesh of a U22 nebuliser showing (a) arrangement of nozzles on the mesh, (b) single nozzle and (c) distance between nozzles.	63
Figure 4.4: Cross-section of a nebuliser mesh of the U22 mesh nebuliser; A and B represent total mesh thickness.	64
Figure 4.5: Average particle size distribution of aerosols during nebulisation from U22 mesh nebuliser (n=3).	65
Figure 4.6: Nebulisation rate in the U22 mesh nebuliser (a) distilled water – 0.44 mL/min, (b) saline solution – 0.45 mL/min (n=4).	66
Figure 4.7: Agarose gel electrophoresis of nebulisation of 5.7 kb plasmid: a) TE buffer; lanes 2 and 3: BN and AN samples in TE buffer; lanes 3, 4 and 5: BN, NC and AN samples in TE buffer showing open-circular (oc), linear form (Lf) and supercoiled (sc) forms of the plasmid; b) TE buffer with 160 mM NaCl; lanes 1, 2 and 3: BN, NC and AN samples in TE buffer with 160mM NaCl showing oc, Lf and sc forms of the plasmid.	71
Figure 4.7 c) & d): Agarose gel electrophoresis of nebulisation of 5.7 kb plasmid: c) and d) densitometer scans showing peaks of open-circular (oc), linear form (lf) and supercoiled (sc) of Figure 4.7 a) and b) respectively resulting in less than 5% damage to the sc form in both cases.	72
Figure 4.8: Agarose gel electrophoresis of nebulisation of 5.7 kb plasmid: a) PBS buffer: BN and AN samples; b) HEPES buffer: BN and AN samples; c) TE with 150mM NaCl: BN and AN samples; open-circular (oc) form of the 5.7 kb plasmid is damaged in the AN samples; DM – DNA marker.	73
Figure 4.9: Densitometric scans of agarose gel from nebulisation of 8.7 kb plasmid formulated in: a) TE buffer, b) TE buffer with 150 mM NaCl; % damage to sc structure in a) 45% and b) 6.5%; BN – before nebulisation, AN – after nebulisation.	74
Figure 4.10: Agarose gel electrophoresis study of nebulisation of 20 kb plasmid: lanes 2, 3 and 4: BN, NC and AN samples in TE buffer; lanes 5, 6 and 7: BN, NC and AN samples in TE buffer with 160mM NaCl showing supercoiled (sc) form of the plasmid.	76
Figure 4.11: Distribution of sheared DNA fragments after nebulisation of the 20 kb plasmid generated from the densitometric scans of an agarose gel (n=2); 'x' is the DNA molecular size in kb determined from DNA marker as a reference.	77

Figure 4.12: Structural analysis of sc structure of 5.7 kb plasmid DNA by AFM imaging in air: a) before nebulisation, scan size of 0.75 x 0.75 μm, scale bar – 250 nm; b) after nebulisation showing sc structure and sheared fragments of 5.7 kb, scan size of 2.5 x 2.5 μm, scale bar – 500 nm.	78
Figure 4.13: Structural analysis of sc structure of 20 kb plasmid DNA by AFM imaging in air: a) before nebulisation; b) after nebulisation showing sheared fragments of 5.7 kb, scan size of 2.5 x 2.5 μm, scale bar – 500 nm for both images.	79
Figure 4.14: Structural analysis of sc structure of condensed 20 kb plasmid DNA; scan size of 7.5 x 7.5 μm, scale bar – 2500 nm.	80
Figure 4.15: A standard DNA fluorescence graph using PicoGreen assay for 5.7 kb plasmid at a) high concentration (0-800 ng/mL), b) low concentration (0-3 ng/mL) range (n=3).	82
Figure 4.16: PicoGreen assay for 5.7 kb plasmid exposed to alkaline denaturation at pH 12; k_{BD} = 0.0154, k_{AD} = 0.0108, k_{ratio} = 1.43 (n=3).	82
Figure 4.17: PicoGreen assay for 5.7 kb plasmid exposed to chemical degradation at 60°C for 24 hours; k_{BD} = 0.0032, k_{AD} = 0.0017, k_{ratio} = 1.88 (n=3).	83
Figure 4.18: PicoGreen assay for 5.7 kb plasmid exposed to chemical degradation at 60°C for 48 hours; k_{BD} = 0.008, k_{AD} = 0.0127, k_{ratio} = 0.63 (n=2).	84
Figure 4.19: PicoGreen assay for 5.7 kb plasmid exposed to nebulisation; k_{BN} = 0.0036, k_{AN} = 0.004, k_{ratio} = 0.9 (n=3).	84
Figure 4.20: A standard graph using PG assay for a 20 kb plasmid (n=3).	86
Figure 4.21: PicoGreen assay of nebulisation samples of 20 kb plasmid exposed to alkaline denaturation (n=3).	87
Figure 4.22: Densitometric scans of agarose gel electrophoresis of nebulisation of plasmids in U1 nebuliser: a) 5.7 kb, b) 8.7 kb, c) 20 kb (20 μg/mL), d) 20 kb (30 μg/mL); % damage to sc structure after nebulisation in a) 24.3%, b) 55.9%, c) 92.5%, d) 90.7%.	89
Figure 5.1: Diagnostic plot: a) Normal probability; b) Actual versus Predicted response.	103
Figure 5.2: Response surface contour and 3D plots of the effect of 3 μm nozzle on damage to the sc structure of 20 kb plasmid	105

Figure 5.3: Response surface contour and 3D plots of the effect of 4 μm nozzle size on the damage to the sc structure of 20 kb plasmid	106
Figure 5.4: Response surface contour and 3D plots of the effect of 5 μm nozzle size on damage to the sc structure of 20 kb plasmid	107
Figure 5.5: Response surface contour and 3D plots of the effect of 10 μg/mL DNA concentration on damage to the sc structure of 20 kb plasmid.	109
Figure 5.6: Response surface contour and 3D plots of the effect of 20 μg/mL DNA concentration on damage to the sc structure of 20 kb plasmid.	110
Figure 5.7: Response surface contour and 3D plots of the effect of 30 μg/mL DNA concentration on the damage to the sc structure of 20 kb plasmid.	111
Figure 5.8: Response surface contour and 3D plots of the effect of 0 mM NaCl concentration on damage to the sc structure of 20 kb plasmid.	114
Figure 5.9: Response surface contour and 3D plots of the effect of 150 mM NaCl concentration on the damage to the sc structure of 20 kb plasmid.	115
Figure 5.10: Response surface contour and 3D plots of the effect of 300 mM NaCl concentration on the damage to the sc structure of 20 kb plasmid.	116
Figure 5.11: Minimum predicted damage to sc structure of 20 kb plasmid for DNA and NaCl concentrations at nozzle sizes of: a) 3 μm, b) 4 μm, c) 5 μm.	118
Figure 6.1: Imaging of aerosols from 5μl droplet on vibrator without mesh.	127
Figure 6.2: High speed imaging of PBS solution aerosols generated by the mesh nebuliser (a) without mesh and (b) with mesh in place.	128
Figure 6.3: Nebulisation of 20 kb plasmid with and without mesh. Lanes 1,5 – before nebulisation (BN), lanes 2,6 – nebuliser chamber (NC), lanes 3,7 – after nebulisation (AN), DM - λHindIII DNA marker.	129
Figure 6.4: Agarose gel electrophoresis of nebulisation of 5.7 kb plasmid in TE buffer (lanes 2,3) and TE buffer with 150 mM NaCl (lanes 4,5); Chemical degradation of nebulisation samples (lanes 6 to 9); DM – DNA marker, BN – before nebulisation, AN – after nebulisation.	134

Figure 6.5: Densitometric scans of agarose gel (shown in Figure 6.4) of chemical degradation of nebulisation samples (lanes 6 to 9).	135
Figure 6.6: a) Section of a nozzle of the mesh used in the U22 mesh nebuliser; diameter of the nozzle – 3μm; frequency of the vibrator horn – 175 kHz. b) Dimensions and boundary conditions for the axi-symmetric domain of a nozzle of the nebuliser mesh; boundary conditions - velocity inlet at the vibrator horn, pressure outlet at the nozzle exit; wall at the nozzle wall; slip adjacent to the nozzle wall; symmetry axis at the axis of the nozzle.	142
Figure 6.7: Contours of velocity stream lines for steady state simulation of the flow of fluid through the nozzle of the mesh nebuliser.	144
Figure 6.8: CFD simulations of strain rates (in s^{-1}) used to determine the maximum hydrodynamic force near the nozzle of the mesh nebuliser (a) elongational strain rate and (b) shear strain rate; Inset shows the strain rates in the nozzle exit.	145
Figure 6.9: Grid dependency studies for triangular and quadrilateral meshes (a) average strain rate at nozzle, (b) Average velocity at nozzle and average pressure drop between inlet and nozzle for triangular and quadrilateral meshes.	147
Figure 6.10: Percentage of plasmid DNA exposed to computed hydrodynamic shear force upon passage through nozzle exit of mesh nebuliser (a) 5.7 kb plasmid, (b) 20 kb plasmid, (c) formulated 20 kb plasmid; Arrows indicate the forces defining the DNA stretching and deformation region as given in Table 6.4.	152
Figure 6.11: Distribution of DNA fragments of 20 kb plasmid based on molecular size after nebulisation as observed in agarose gel electrophoresis.	157
Figure 6.12: A schematic for generation of DNA fragments from degradation of 20 kb plasmid; a total of eight scissions are required to generate fragments of size 2.5 kb with the star symbol representing a scission.	158
Figure 6.13: Limiting size for safe aerosol delivery of supercoiled plasmid DNA in the U22 mesh nebuliser (% damage data taken from Table 4.7).	160
Figure 6.14: Limiting size for safe aerosol delivery of supercoiled plasmid DNA in the U03 mesh nebuliser (% damage data taken from Figure 4.22).	160
Figure 7.1: Normal plot of standardised effects for plasmid and nozzle sizes	167

Figure 7.2: Pareto chart of standardised effects for plasmid and nozzle sizes	168
Figure 7.3: Main effects plot of plasmid and nozzle sizes for % damage to sc structure.	169
Figure 7.4: Interactions plot of plasmid and nozzle sizes for % damage to sc structure.	169
Figure 7.5: Model predictions from factorial design of plasmid and nozzle sizes: a) contour and b) surface plots of damage to sc structure of the plasmid.	171
Figure 7.6: Normal plot of standardised effects for plasmid size and device frequency	176
Figure 7.7: Pareto chart of standardised effects for plasmid size and device frequency	176
Figure 7.8: Main effects plot of plasmid size and device frequency for % damage to sc structure	178
Figure 7.9: Interactions plot of plasmid size and device frequency for % damage to sc structure.	178
Figure 7.10: Model predictions from factorial design of plasmid size and device frequency: a) contour and b) surface plots of damage to sc structure of the plasmid.	180
Figure 7.11: Prediction of damage to the sc structure of 5.7 kb and 20 kb plasmid at intermediate frequencies at a nozzle size of 3 μm.	181
Figure 8.1: Densitometric scans of agarose gel from nebulisation of 20 kb pDNA at DNA concentrations of: a) 15, b) 7.5, c) 5 μg/mL.	187
Figure 8.2: Agarose gel electrophoresis of nebulisation samples of (i) naked 20 kb plasmid, (ii) 20 kb plasmid complexed with DOTAP/DOPE and (iii) 20 kb plasmid complexed with DOTAP/Cholesterol; damage to the sc structure of naked plasmid observed, DM – DNA marker, BN – before nebulisation, NC – Nebuliser chamber and AN – after nebulisation.	189
Figure 8.3: Densitometric scans of agarose gel from nebulisation of 20 kb pDNA complexed with DEAE-dextran at N/P ratios of: a) 0.1, b) 0.2 and c) 0.4.	191
Figure 8.4: AFM image of sc structure and DD/sc pDNA complex (N/P ratio 0.1) before nebulisation. Inset shows DD/sc pDNA complex with protruding strands of pDNA after nebulisation (scale bar for inset – 250	192

nm, height – 5 nm).	
Figure 8.5: AFM images of DD/plasmid DNA complex (N/P ratio 0.2) before nebulisation (height – 5 nm), (c) & (d) after nebulisation (height – 10 nm); scale bar – 250 nm for all the images.	194
Figure 8.6: AFM images of unwinding of DNA strand from DD/sc pDNA complex at N/P ratio of 0.2 before nebulisation (height – 5 nm); scale bar – 250 nm.	194
Figure 8.7: AFM images of DD/plasmid DNA complex at N/P ratio of 0.4 before nebulisation (a) nanoparticles (scale bar – 600 nm, height – 5 nm), (b) aggregates (scale bar – 250 nm, height – 10 nm).	195
Figure 8.8: AFM images of DD/plasmid DNA complex at N/P ratio of 0.4 after nebulisation (scale bar – 250 nm, height – 20 nm).	195
Figure 8.9: Formulation studies of 20kb plasmid DNA: PicoGreen assay showing relative fluorescence unit (RFU) of plasmid formulated in TE buffer and PEI/20 kb plasmid DNA before (BN) and after nebulisation (AN) (n=3).	198
Figure 8.10: Formulation studies of 20kb plasmid DNA: Structural analysis by AFM imaging in air of PEI/20 kb plasmid formulated in PBS after washing the samples with de-ionised water; a) before nebulisation; scan size of 4.35 x 4.35 μm, scale bar – 500 nm; b) after nebulisation, scan size of 0.8 x 0.8 μm, scale bar – 200 nm; height 5 nm for both images.	199
Figure 9.1: Viable cell density of Chinese hamster ovary cells transfected with before and after nebulisation samples of PEI formulated 5.7 kb plasmid. Control refers to untransfected CHO-S cells (n=2).	204
Figure 9.2: Cell specific relative fluorescence units for untransfected and transfected CHO-S cells based on fluorescence measurements using a microplate reader at excitation wavelength of 483nm and emission wavelength of 530nm for GFP quantification after 24 and 48 hours of incubation (n=3).	205
Figure 9.3: Cell density of CHO-S cells transfected with unebulised and nebulised samples of 5.7 kb plasmid complexed with PEI after an incubation time of 48 hours. Control refers to untransfected CHO-S cells (n=3).	207
Figure 9.4: Effect of nebulisation and DNA concentration on transient transfection: GFP intensity measured using a Flow cytometer for a) untransfected CHO-S cells, b) unnebulised and c) nebulised pDNA at 20 μg/mL DNA concentration, d) nebulised pDNA at 30 μg/mL DNA concentration in TE complexed with PEI, after incubation time of 48 hours; % values indicate the transfection efficiency in terms of the	209

percent of eGFP positive cells in a transfected cell population.	
Figure 9.5: Effect of nebulisation and formulation on transient transfection: GFP intensity measured using a Flow cytometer for a) untransfected CHO-S cells, b) unnebulised and c) nebulised pDNA at 20 μg/mL concentration, in HBS complexed with PEI, after incubation time of 48 hours; % values indicate the percentage of eGFP positive cells in a transfected cell population (n=3).	211
Figure 9.6: Microscopic image of a) untransfected and b) transfected CHO-S cells.	213
Figure A.1: Agarose gel electrophoresis of nebulisation of 5.7 kb plasmid in buffers showing the supercoiled (sc) and open-circular (oc) forms of the plasmid: lanes 1 and 2: BN and AN samples in PBS buffer; lanes 3 and 4: BN and AN samples in HEPES buffer; lanes 5 and 6: BN and AN samples in TE buffer with 150 mM NaCl; lanes 7 – DNA marker.	249
Figure A.2: Agarose gel electrophoresis of nebulisation of 5.7 kb plasmid in buffers showing the supercoiled (sc) and open-circular (oc) forms of the plasmid: a) PBS buffer; lanes 1 and 2: BN and AN samples in PBS buffer; lanes 3 and 4: BN and AN samples in TE buffer; lanes 5 and 6: BN and AN samples in TE buffer with 150 mM NaCl; lanes 7 and 8: BN and AN samples in TE buffer with 300 mM NaCl.	250
Figure A.3: Agarose gel electrophoresis of nebulisation of 5.7 kb plasmid in TE buffer showing the supercoiled (sc) and open-circular (oc) forms of the plasmid: lanes 1 – DNA Marker; lanes 2 and 3: BN and AN samples with 20 μg/mL DNA concentration; lanes 4 and 5: BN and AN samples with 10 μg/mL DNA concentration; lanes 6 and 7: BN and AN samples with 5 μg/mL μg/mL DNA concentration.	251
Figure A.4: Agarose gel electrophoresis of nebulisation of 8.7 kb plasmid in TE buffer showing the supercoiled (sc) and open-circular (oc) forms of the plasmid: lanes 1 – BN; 2 – NC; 3 – AN samples; 4 – Lamba HindIII DNA marker.	252
Figure A.5: Agarose gel electrophoresis of nebulisation of 8.7 kb plasmid in TE buffer showing the supercoiled (sc) and open-circular (oc) forms of the plasmid: lanes 1 – BN; 2 – NC; 3 – AN samples; 4 – Lamba HindIII DNA marker.	253
Figure A.6: Agarose gel electrophoresis of nebulisation of 8.7 kb plasmid in buffers showing the supercoiled (sc) and open-circular (oc) forms of the plasmid: TE Buffer – control; TE Buffer with 150mM NaCl, lanes 2 and 3 –BN and AN; TE Buffer, lanes 4 and 5 –BN and AN.	254

Acknowledgements

I would not have completed my PhD research without the help of many people who deserve my heartfelt acknowledgement.

Firstly, I sincerely thank my research supervisors at Loughborough University, Professor David J Williams FREng and Mr. Henk K Versteeg, and at the Advanced Centre for Biochemical Engineering, University College London, Professor Mike Hoare FREng. Professor Williams deserves special appreciation for initiating this collaborative research with UCL and for providing me with the support that has enabled me to carry out the research at both institutions. I appreciate his confidence in my abilities and his help in guiding me to overcome both my research and other problems. Professor Williams has been an excellent mentor and tutor, and I look forward to continuing this relationship in the future. I also have really appreciated the guidance of Mr. Henk Versteeg and thank him in particular for his meticulous approach to reviewing my work; his constructive suggestions have helped me improve my research contribution immensely. I appreciate the significant support of Professor Mike Hoare particularly for allowing me to perform the research experiments at UCL and thank him for many valuable comments.

Secondly, I sincerely thank staff and colleagues in Loughborough University and University College London, particularly Professors John Ward and Nigel Titchener-Hooker, Dr. Andrew Tait, Dr. Helen Baldascini, Dr. Eli Keshavarz-Moore, Dr. Clive Osborne, Professor Graham Hargrave, Mr. Andrew Sandaver, Dr. Yong Khoo, Dr. Leon Lobo, Mr. Brian Mace, Mr. David Travis and Mr. Jagpal Singh all of who have assisted me in my research. A special thanks goes to my friend and research colleague, Dr.Immanuel Sebastine for all his help. I also thank all my colleagues in the Healthcare Engineering Group for their support particularly Dr.Paul Hourd, Dr.Amit Chandra and Dr.Yang Liu.

Lastly, I thank my family. I especially thank my wife for her support and encouragement throughout my research. Thanks to my two sons for being so patient with me for the past three years. I heartily appreciate the prayers and best wishes of my Dad. Above all, I thank God for providing me His grace and wisdom to complete this research. I also thank Central Food Technological Research Institute, India, especially Dr. N.G.Karanth and Dr. M.C.Misra for their support.

CHAPTER 1. INTRODUCTION

1 Context of the Research

The identification of the genes in the human genome project has opened up opportunities for the treatment of genetic and acquired human diseases. The advent of recombinant DNA technology has seen the production of recombinant proteins from therapeutic genes using cell culture technology. The targeted delivery of therapeutic genes to diseased cells promises a better approach than such proteins. The disadvantages of direct administration of proteins include bioavailability, systemic toxicity, *in vivo* stability, high hepatic and renal clearance rates, and the high cost of manufacturing [Han et al., 2000]. The vectors reported in gene therapy clinical trials are predominantly viral, with a steady increase in the use of non-viral vectors. The disadvantages of viral vectors including insert-size limitation, safety (immunogenicity) and manufacture, have led to an increased focus on the use of non-viral vectors for gene therapy. The main hurdle for the successful application of gene therapy is the safe delivery of the vector to the targeted cells to obtain efficient gene expression.

Presently, plasmid DNA is the most common vector for non-viral gene therapy, although non-viral genetic techniques such as RNAi (RNA interference) and RNAa (RNA activation) have been recently discovered. The challenge for delivery of plasmid DNA for non-viral gene therapy is the retention of the fragile supercoiled (sc) structure of the plasmid during formulation and delivery to the targeted site. In order to ensure regulatory compliance and maximum bioavailability to the cells, the sc structure of plasmid DNA needs to be preserved intact during delivery. Pulmonary delivery of plasmid DNA is a promising emerging non-invasive delivery route using respiratory devices such as nebulisers and dry powder inhalers. Nebulisers have the advantages of less challenging formulation requirements, large dosage handling capability, ease of operation and continuous aerosol delivery.

This thesis reports the results of a close collaboration between Loughborough University and University College London. Research has focussed on the use of a mesh nebuliser for safe delivery of the sc structure of different sized plasmids, determination of the sc structure of plasmids using AFM, CFD modelling to predict the hydrodynamic force on the sc structure, alternative formulations and bio-efficacy studies on transfection of aerosolised plasmid DNA in a mammalian cell line such as Chinese Hamster Ovary cells. This introductory chapter presents the basic aspects of gene delivery, a brief statement of the problem and the structure of the thesis.

1.1 Delivery of non-viral gene therapeutic

Vectors for gene transfer may be classified based on the mode of delivery as '*in vivo*' and '*ex-vivo*'. *In vivo* delivery is the transfer of genetic material either locally (eg. intra-muscular, intra-tumoral injection, inhalation, local permeation) or systemically (intravenous injection) to the intact body. *Ex vivo* delivery occurs when the transfer of genetic material is performed on cells or tissues that are first explanted, cultured in the laboratory, and then re-implanted into the patient. In this thesis, an ultrasonic mesh nebuliser has been used for engineering studies on the aerosol delivery of plasmid DNA for *in vivo* gene delivery.

Pulmonary delivery of therapeutics is a non-invasive approach for the treatment of respiratory diseases. With the recent approval in the pulmonary delivery of insulin, this delivery route also offers promise for the treatment of systemic diseases. A number of challenges to the pulmonary delivery of plasmid DNA via conventional jet nebulisation include damage to the sc structure due to the shearing effects associated with nebulisation, the requirement to produce aerosol droplet sizes appropriate for optimal delivery to the peripheral lung and to maximise the dose of DNA delivered to lung surfaces. Non-viral polyplexes are emerging as suitable candidates for use in pulmonary inhalation gene therapy. PEI-based formulations appear to be good candidates for aerosol delivery of genes for the treatment of a variety of genetic pulmonary disorders, including lung tumors. This thesis focusses on the study of both formulation for delivery and delivery of plasmid vectors via nebulisers and the engineering required to enable this delivery.

1.2 Statement of the problem

Aerosolisation of plasmid DNA is a challenge using pulmonary devices due to the requirement to protect the fragile supercoiled structure against damage. The main objective of this investigation was to study and develop the engineering principles associated with the impact of formulation and device parameters on the safe delivery of plasmid DNA. The motivation for the work resulted from the need for development of a supercoiled plasmid DNA-based formulation for safe aerosol delivery using a commercial drug delivery device with potential applications for the treatment of respiratory and systemic diseases. The main advantage of using a clinically proven nebuliser device is that it can be readily tested in pre-clinical trials for the safe and efficient delivery of plasmid DNA and does not require regulatory approval as a device.

1.3 Structure of the PhD thesis

The structure of the PhD thesis is summarised here to provide a concise description of the chapters for the reader. Chapter 2 provides a detailed review of work on the basic aspects of gene therapy with an emphasis on aerosol non-viral gene delivery of plasmid DNA and current status of gene therapy clinical trials. A review of the delivery systems reported in the literature shows the significance of pulmonary drug delivery. A description of the drug delivery devices used for the respiratory tract with emphasis on nebuliser devices and the scope for targeted pDNA delivery using magnetofection are summarised. The theories postulated for aerosol generation from an ultrasonic nebuliser are discussed. The chapter ends with a roadmap to non-viral gene therapy starting with the formulation of plasmid DNA and ending with gene therapy clinical trials.

Chapter 3 presents the materials and methodology adopted for the experiments. The principle of operation of the mesh nebulisers, MicroAir® (NE-U22) and U1 (NE-U03), designated as U22 and U03 mesh nebulisers respectively are discussed. The methods used for the purification, formulation, nebulisation and analysis of plasmid DNA are discussed. The protocol adopted for high-speed imaging of aerosol generation and

transfection of suspension adapted Chinese hamster ovary (CHO-S) cells with the formulated plasmid is described in detail.

Chapter 4 discusses the purification and nebulisation of plasmid DNA. In this chapter, super-coiled plasmids of size 5.7, 8.7, 13 and 20 kb are purified from *E. coli* cells and the purity of sc structure assessed as per the specifications recommended for gene therapy. The characterisation of the mesh nebulisers in terms of nozzle dimensions and nebulisation rate is determined. The integrity of the sc structure upon nebulisation of the plasmid formulations in the U22 and U03 mesh nebulisers is determined using agarose gel electrophoresis, and the PicoGreen assay. Analysis of the gel electrophoresis and the PicoGreen assay results suggested that the sc structure of the 5.7 kb plasmid was intact while that of the 20 kb plasmid was damaged after nebulisation. Atomic force microscopy (AFM) enabled visual examination of the sc structure of the 5.7 and 20 kb plasmids before and after nebulisation.

Chapter 5 discusses an initial experimental and statistical modelling study to identify the effect of formulation and device parameters on damage to the sc structure upon nebulisation of a 20 kb plasmid using a response surface method (RSM) based on design of experiments (DOE). The RSM study enabled development of a response equation to predict the damage to the sc structure of the 20 kb plasmid upon nebulisation. Analysis of the model suggested the minimum predicted damage to the sc structure at different nozzle sizes and ionic concentrations.

In chapter 6, engineering analysis of the nebulisation of plasmid DNA is reported. High-speed imaging of aerosol generation from the mesh nebuliser is examined to determine the residence time and pressure amplitudes in the nozzle of the nebuliser and consider the possible effect of cavitation on damage to the sc structure. The mechanism of supercoiled plasmid degradation and the time scales involved in the aerosolisation process are discussed. Estimation of the maximum hydrodynamic force on the sc structure from the mechanics of fluid flow through the nozzle of the mesh nebuliser using computational fluid dynamics and AFM imaging is reported. The extent of plasmid DNA degradation after nebulisation for different sized plasmids enables a linear extrapolation of the plasmid size for safe delivery of the sc structure.

Chapter 7 discusses the parameters influencing plasmid DNA damage in the mesh nebuliser. DOE studies to determine the influence of plasmid size and damage with respect to key device parameters such as nozzle size and frequency are discussed. Damage to the 20 kb plasmid was observed to be higher with the 3 μm nozzle than with the 5 μm nozzle. Nebulisation using the U03 mesh nebuliser operated at 65 kHz resulted in more damage to plasmids of size <13 kb than using the U22 mesh nebuliser at 175 kHz. The interaction between the parameters and damage to sc structure of the plasmid is reported.

Chapter 8 discusses the formulation of the 20 kb plasmid to protect the sc structure during nebulisation in the mesh nebuliser. Formulation with an adjuvant and cationic gene delivery agent such as DEAE-dextran resulted in retention of 15% of the sc structure on nebulisation. Formulation of the 20 kb plasmid with PEI resulted in protection of the sc structure as confirmed by PicoGreen assay. AFM imaging of the formulated plasmid nanoparticles enabled visualisation of the extent of complexation of sc pDNA with the cationic substrate.

In chapter 9, transfection studies on suspension-adapted Chinese Hamster Ovary (CHO-S) cells using formulated 5.7 kb plasmid bearing the Green fluorescent protein (GFP) gene before and after nebulisation are reported. Formulation of the 5.7 kb plasmid was attempted prior to transfection in order to transfect the cells efficiently in suspension culture medium. Lower GFP expression was observed with PEI formulated 5.7 kb plasmid after nebulisation than with before nebulisation, possibly due to compaction of the nanoparticle during the nebulisation process. However, the nebulised 5.7 kb plasmid when formulated with PEI prior to transfection resulted in comparable transfection efficiency to the unnebulised plasmid. The plasmid DNA delivery efficiency in the transfected cells using the condensed aerosols determined using a flow cytometer is reported to validate the earlier results that the sc structure of the 5.7 kb plasmid is not damaged upon aerosolisation.

Chapter 10 discusses the conclusions of the research and the key parameters for aerosol delivery of supercoiled plasmid DNA in a mesh nebuliser. This chapter summarises the contribution of the research in the aerosol delivery of plasmid DNA for non-viral gene therapy. The opportunities for future research and the next steps for further work in this area are highlighted.

CHAPTER 2. REVIEW OF LITERATURE

2.1 Introduction to the chapter

This chapter provides a review of gene therapy and focuses on plasmid DNA as a non-viral gene therapeutic. A brief overview of the therapeutic genes used in gene therapy, the production and processing of plasmid DNA, and the quality of plasmid DNA are discussed. The present status of plasmid DNA in gene therapy clinical trials is analysed based on the data available in the clinical trials website (www.wiley.co.uk/genetherapy/clinical). From this information, it is clear that there is scope for increasing use of plasmid DNA in future gene therapy clinical trials. The formulation of plasmid DNA for non-viral gene delivery, the sequence of processes leading to non-viral gene delivery into the cells and the barriers for gene delivery through the pulmonary route are discussed. The different routes for delivery of plasmid DNA are reported with typical therapeutic targets for each route. The devices used for pulmonary delivery such as pMDIs, DPIs and nebulisers are reviewed. The importance of mesh nebulisation technology in pulmonary delivery of macromolecules is highlighted. New aerosolisation devices in development such as those based on electro-mechanical and electro-hydrodynamic approaches and physical methods of targeted gene delivery such as magnetofection are also discussed. The use of a commercial pulmonary delivery device based on mesh technology to deliver the supercoiled structure of plasmid DNA is the central theme of this thesis.

2.2 Gene therapy

The advent of genetic engineering resulting in an unprecedented elucidation of genetic data from genomic sequencing and gene chip analysis, and developments in bioprocess engineering has helped identify and mass produce therapeutic genes, leading to the development of new gene-engineered therapies. Application of human gene therapy has been the hope for new therapeutic approaches [Rubanyi, 2001].

Somatic gene therapy is gene transfer targeted at only the genetic material of tissues that do not contribute to hereditary transmission, for instance muscles, lung, brain, bones, kidney and heart. In contrast, 'germ line' gene therapy refers to gene transfer to germ cells for the modification of the genome for transmission to subsequent generations. The term 'gene therapy' in this thesis refers to 'somatic gene therapy' unless indicated otherwise. The objective of somatic gene therapy is to deliver functional groups of nucleic acids to target cells. The subsequent alteration in the production of a specific protein or changes in protein expression results in a therapeutic benefit.

Over 4000 human diseases are essentially disorders of genes caused by inborn alterations in a single gene. While common therapeutic drugs often treat symptoms, gene therapy focuses on gene transfer for treating or eliminating the cause of a disease [Mountain, 2000]. Gene-based medical interventions will be of critical importance in creating vaccines and antiviral therapies for HIV, hepatitis, herpes and other viral illnesses, as well as for developing new strategies for the prevention and treatment of emerging diseases [Hellermann and Mohapatra, 2003; Liu and Ulmer, 2005]. The field of gene therapy has constantly evolved since its inception, moving from *ex vivo* to direct *in vivo* gene-based medicine [Rolland, 2005]. Although newer delivery techniques are being developed, choosing the right approach for administration of gene medicine to the targeted cells still remains an issue and poses a significant constraint on the success of gene therapy.

2.2.1 Vectors for gene therapy

Gene therapy essentially involves treatment of a disease by delivering therapeutic genes packaged in viral or non-viral vectors to target cells in order to replace malfunctioning or missing genes. The main viral vectors used for gene transfer are retrovirus, adenovirus and adeno-associated virus. Viral vectors have been more efficient in transfection (introduction of therapeutic DNA into cells) than non-viral vectors. Most gene therapy experiments and clinical trials use viral vectors for gene delivery. The first application of gene therapy occurred with the transfer of naked DNA leading to the expression of the transgene [Wolff et al., 1991]. Synthetic non-

viral vectors can be formed by condensing the plasmid DNA containing the therapeutic nucleic acid with cationic lipids or polymers to form lipoplexes or polyplexes respectively, and with both to form lipopolyplexes [Montier et al., 2004]. The disadvantages of viral vectors concerning insert-size limitation, safety (immunogenicity) and manufacture have led to an increased focus on the use of non-viral vectors for gene therapy [El-Aneed, 2004; Rots et al., 2003]. A comparison of the factors considered when choosing between viral and non-viral vectors is shown in Table 2.1. Non-viral vectors have a more positive impact over viral vectors for the success and application of gene therapy.

Table 2.1: Viral and non-viral vectors for gene therapy

Factors	**Vector for gene therapy**		**Reasons for positive impact**
	Viral	**Non-viral**	
Culture of cell lines (*in vitro*)	+++	+++	Simple, robust, and high efficiency of gene transfer
Culture of primary cells (*in vitro*)	+++	+	High gene transfer efficiency due to integration of viruses into host genome.
Overall transfection efficiency	+++	+	Viral vectors achieve higher gene transfer rates *in vivo* and *in vitro* than non-viral.
Transgene capacity	+	+++	Non-viral ability to transfect larger DNA sequences (> 100 kb).
General safety	+	+++	Non-viral systems generally non-infectious.
Cost	+	+++	Non-viral transfection reagents are inexpensive compared to viral.
Time	+	+++	More time required to develop a viral vector compared to non-viral.
Gene delivery - *In vivo* and *Ex vivo*	+	+	Unclear – Major obstacle facing the development of gene therapy

The disadvantage of viral vectors over non-viral for treatment of respiratory diseases such as cystic fibrosis is that repeated administration of the viral vectors is not possible due to recognition by the immune system. Therefore non-viral vectors being non-immunogenic upon repeated administration have distinct advantage over viral vectors.

2.2.2 Non-viral gene therapeutics

Non-viral gene therapeutics have the potential to provide nucleic acid-based drugs that could be more effective than traditional pharmaceuticals. They overcome the limitations associated with the direct administration of therapeutic proteins, which include low bioavailability, systemic toxicity, *in vivo* instability, high hepatic and renal clearance rates, and the high cost of manufacturing [Han et al., 2000].

The simplest non-viral gene therapeutic system uses 'naked' plasmid DNA, which when injected directly into certain tissues, particularly muscles, produces significant levels of gene expression, though lower than those achieved with viral vectors. Since plasmid DNA is susceptible to rapid degradation upon entry into the cell in the extra-cellular milieu, protection from that degradation could be expected to lead to higher levels of gene expression. Plasmid DNA, being anionic in nature, readily forms a complex with cationic substrates such as cationic lipids and cationic polymers.

Another non-viral approach employs a peptide nucleic acid (PNA) clamp to directly and irreversibly modify plasmid DNA, without affecting either its conformation or its ability to be efficiently transcribed. This strategy helps to "functionalise" the gene by direct coupling of ligands (fluorophores, peptides, proteins, sugars or oligonucleotides) to plasmid DNA. The usefulness of this technique is that it provides versatile tools for specific targeting and efficient delivery, thereby overcoming the obstacles of synthetic non-viral gene delivery systems [Zelphati et al., 2003].

A novel non-viral approach, RNA interference (RNAi) is gaining recognition as a powerful tool in gene therapy for post-transcriptional gene silencing [Agami, 2002; Genc et al., 2004]. With RNAi, small sequence specific, double-stranded, short interfering RNA (siRNA) molecules bind to a complementary portion of mRNA and either prevent it from being translated or trigger its destruction. The specific gene-targeting technology of RNAi to shut down the expression of a disease-causing gene has added to the benefits of gene therapy [Orive et al., 2003].

2.2.3 Plasmid DNA-based non-viral gene therapeutic

The use of plasmid DNA as a non-viral vector for gene therapy has shown promise in the development of new therapeutics [Wolff, 2005]. Plasmids are extra-chromosomal DNA capable of being transmitted from cell to cell. They are super-coiled, circular covalently closed (ccc) strands of DNA ranging from 5 kb to 400 kb that replicate independently of the host DNA. The essential components of a non-viral plasmid DNA based gene therapeutic approach include (i) a therapeutic gene encoding a specific protein; (ii) a gene expression plasmid controlling the function of the therapeutic gene within the target cell; and (iii) a gene delivery system controlling the delivery of gene expression plasmid to specific locations within the body.

2.2.3.1 Therapeutic gene

Over 1300 different gene types have been transferred in gene therapy clinical trials worldwide. The diseases addressed by gene therapy clinical trials are reported in section 2.2.4. An example indicates the approach based on gene therapy for the cure of cystic fibrosis (CF) [Moraes and Downey, 2004; Klink et al., 2004]. CF is a common genetic disease occurring due to a recessive genetic mutation that causes deficiencies in the transport of salt across the membranes of secretory cells. This abnormal metabolic transport causes the accumulation of thick, sticky mucus in the respiratory and digestive tracts, leading to recurrent lung infections, pulmonary damage and difficulties in food intake. Clinical trials in CF patients have been conducted using cationic liposomes carrying the genes for the Cystic Fibrosis Transmembrane-conductance Regulator (CFTR) [Rochat and Morris, 2002; Brown, 2002].

2.2.3.2 Gene expression plasmids

Essentially, gene expression occurs in two steps: (i) transcription – a process of converting information encoded in DNA into a molecule of RNA, the messenger RNA (mRNA) and (ii) translation – a process of converting information encoded in the nucleotides of mRNA into a defined sequence of amino acids in a protein. A gene

expression plasmid is a plasmid DNA which is capable of expression of the therapeutic gene into the desired protein.

2.2.3.2.1 Production and processing of plasmid DNA

Preparation of plasmid DNA is a simpler manufacturing process than the viral packaging and purification method [Spack and Sorgi, 2001]. Although non-viral vectors are less effective than viral forms, the relative ease of plasmid DNA production poses no constraint to the quantity of plasmid DNA that could be used for gene therapy [Wahlung et al., 2004]. Recent advances in the large-scale manufacturing process for production of pDNA as a DNA vaccine for an influenza pandemic have been reviewed to explore the potential of non-viral over viral gene therapy [Hoare et al., 2005]. The production of pharmaceutical grade ccc plasmid DNA [Prather et al., 2003] essentially involves the steps of: (i) cloning the therapeutic gene into a plasmid vector, (ii) transforming the plasmid into *Escherichia coli*, (iii) cultivating *E. coli* cells in bioreactors for mass plasmid production and (iv) cell lysis and purification of plasmid DNA. Extensive purification procedures are required to ensure that the gene product contains a high percentage of plasmids in super-coiled form. Interest in producing large quantities of super-coiled plasmid DNA has recently increased as a result of the rapid evolution of gene therapy and DNA vaccines [Ferreira et al., 2000].

Plasmid DNA is a very fragile molecule and is highly susceptible to shear during the manufacturing process. Medium to high shear processes such as mixing, turbulent flow during transport, filtration, lyophilization, and spray-drying are commonly encountered in the operations of a plasmid manufacturing process. Since any breakage in the DNA strand affects the quality and performance of the gene product, especially if the damage is in the promoter or gene-coding region, it is necessary to address the potential of shear related damage that may occur during processing of the DNA [Lengsfeld and Anchordoquy, 2002]. A method for protection of plasmid DNA from high shear induced damage uses simple divalent cations and the lyophilizable alcohol, *tert*-butanol, to self-assemble DNA into condensed, shear-resistant forms [Knight and Adami, 2003]. As a result of their economic importance, the development of plasmid DNA production and purification strategies for gene-therapy vectors have been

performed in pharmaceutical companies within a confidential environment. Consequently, detailed information on large-scale plasmid purification is not available to the scientific community.

2.2.3.2.2 Quality of plasmid DNA for gene therapy

The manufacturing of plasmids compliant to current Good Manufacturing Practice (cGMP) as required by the Food and Drug Administration (FDA) and the European Medicines Evaluation Agency (EMEA) is crucial to obtain a product that is consistent in purity, potency, identity, efficacy and safety [Prazeres and Ferreira, 2004]. Possible contaminants in a plasmid DNA preparation include genomic DNA, RNA, protein, lipids and microflora. The level of contaminants in plasmid DNA preparations can be checked by quality assurance tests (Table 2.2) to meet the specifications required for administration as a gene therapeutic [Schleef and Schmidt, 2004]. Supercoiled multimeric plasmids are of interest for pharmaceutical purpose because they contain multimeric copies of therapeutic gene and can therefore be more efficient vectors [Voβ et al., 2003].

Table 2.2: Quality assurance tests of plasmid DNA preparation for gene therapy

S.No.	Test	Analytical Method
1	DNA concentration	UV-absorption (260 nm)
2	General purity	UV-scan (220–320 nm)
3	Homogeneity (ccc content)	CGE (capillary gel electrophoresis)
4	Purity (visible)	Visual inspection
5	Purity (genomic DNA)	Agarose gel (visual); Southern blot; quantitative PCR (polymerase chain reaction)
6	Purity (RNA)	Agarose gel (visual); fluorescence assay; quantitative PCR
7	Purity (protein)	BCA (Bicinchoninic acid) test
8	Purity (LPS)	LAL (Lymulus amebocyte lysate) test
9	Purity (microorganisms)	Bioburden test; sterility test
10	Identity (vector structure)	Restriction fragment length conforms to reference in AGE (1–3 enzymes)
11	Identity (sequence)	Sequencing (double strand)

2.2.4 Gene therapy clinical trials

The Journal of Gene Medicine clinical trials website (http://www.wiley.co.uk/genetherapy/clinical/) provides updated information on the world-wide clinical trials in gene therapy. The vectors used and the diseases addressed in the gene therapy clinical trials are shown in Figure 2.1. Viral vectors have been the most frequently employed vectors in the clinical trials, with adenovirus and retrovirus being the most widely used. Plasmid (naked) DNA and other non-viral vectors have been used in about one-quarter of the trials. Comparison of the plasmid DNA clinical trial information over the past few years has shown a steady increase in the number of clinical trials [Forde, 2005]. Among the therapeutic targets addressed in gene therapy clinical trials (Figure 2.1b), unmet medical needs such as cancer, cardiovascular, monogenic and infectious diseases have received major attention. Plasmid DNA and viral vector-based cancer vaccines have many inherent features that make them promising cancer vaccine candidates [Anderson and Schneider, in press].

Analysis of the status of gene therapy clinical trials for the four dominant vectors (Figure 2.2) shows that the percentage of open clinical trials with naked/plasmid DNA is higher than that for the adenoviral and retroviral vectors. From Table 2.3, plasmid DNA leads in the percentage of open trials for the clinical phases of testing and also has the least number of closed clinical trials suggesting that results in the early clinical phase are encouraging. Although gene therapy clinical trials have been carried out for more than a decade, the small number of clinical trials in phase III (Table 2.3) suggests that the commonly used gene delivery approach of intervention by injection could be one of the bottlenecks in gene therapy. The route to plasmid DNA delivery into cells is discussed in section 2.4.1. Currently, there are no clinical trials using pDNA for intervention by the pulmonary route [http://clinicaltrials.gov/].

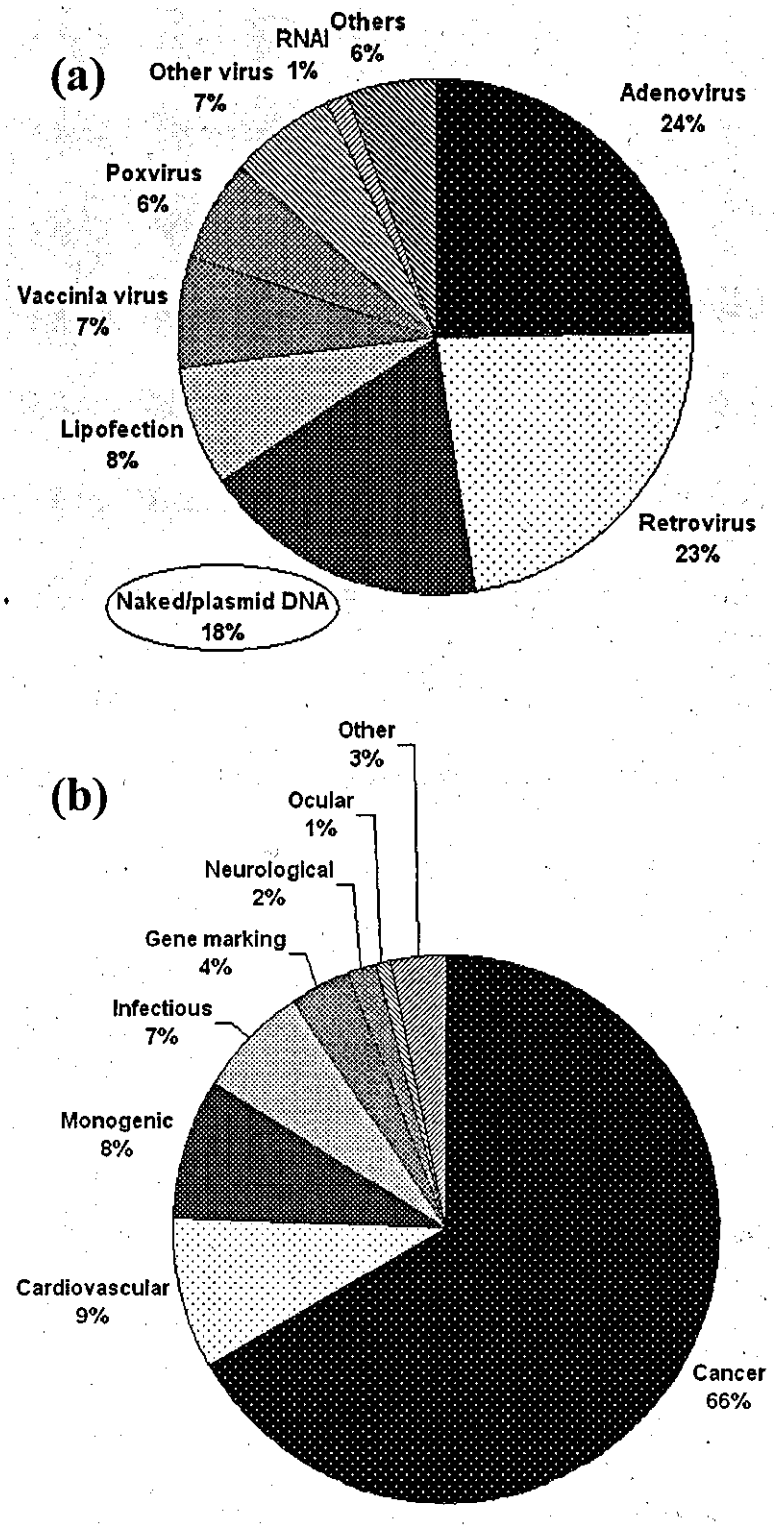

Figure 2.1: Gene therapy clinical trials: (a) vectors used, (b) diseases addressed (Data taken from website http://www.wiley.co.uk/genetherapy/clinical/ as of July 2007).

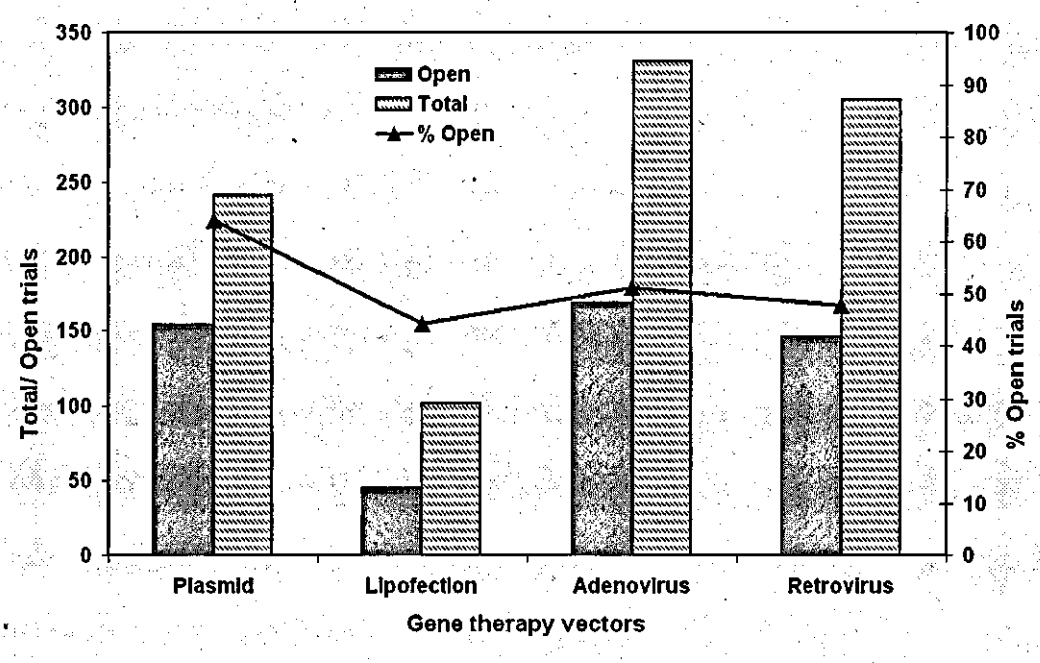

Figure 2.2: Comparison of the main vectors used in gene therapy clinical trials (Data taken from: http://www.wiley.co.uk/genetherapy/clinical/ dated as of July 2007).

Table 2.3: Main gene therapy vectors in the clinical phase of the gene therapy trials

Clinical phase stage	Number of open (in %) trials of the total trials for each vector *			
	Plasmid DNA	Lipofection	Adenovirus	Retrovirus
Phase I	38.6	28.4	32.0	31.5
Phase I/II	12.1	7.8	8.2	12.8
Phase II	11.2	6.9	8.5	3.6
Phase II/III	0.8	0	0.9	0
Phase III	1.2	1.0	1.5	0
Closed	36.1	55.9	48.9	52.1

* - Source: http://www.wiley.co.uk/genetherapy/clinical/ dated as of July 2007.

2.3 Formulation for non-viral gene delivery

The development of non-viral gene transfer methods requires proper formulations that are both effective *in vivo* and non-toxic. The development of non-viral gene vectors for therapeutic delivery must take into account the stability of the vector when exposed to physiological conditions. Aqueous formulations of non-viral vectors at the high

concentrations necessary for clinical trials are very unstable when compared to frozen formulations [Anchordoquy et al., 2004b].

Cationic liposomes (lipoplexes) and cationic polymers (polyplexes) are the most frequently used non-viral gene transfer systems. Lipoplexes have been used as nonviral vectors in human clinical trials of gene therapy worldwide [Martin et al., 2005; Ewert et al., 2005]. Electrostatic interactions between the positive charges of the cationic lipid headgroups and the phosphate DNA backbones are the main driving force for the lipoplex formation [Elouahabi and Ruysscharet, 2005]. Complexes between cationic lipids and plasmid DNA are typically prepared by mixing preformed cationic liposomes and DNA in an aqueous solution [Hirko et al., 2003]. A scalable and extrusion-free method for efficient liposomal encapsulation of plasmid DNA for gene therapy has been reported [Jeffs et al., 2005]. Developing nonviral, pharmaceutical formulations of genes for human therapy is important in functional tumor targeting of gene therapeutics. Ligand-directed lipoplex targeting enables dual expression of ligands such as folate, transferrin or anti-transferrin-receptor antibody, and lipoplexes. Such targeting methods have been used for gene delivery and expression in human breast, prostate, head and neck cancers [Schmidt-Wolf and Schmidt-Wolf, 2003].

The common cationic polymers used for complexing plasmid DNA include poly(ethylenimine) (PEI), poly(L-lysine) (PLL), Chitosan, Dendrimers and Poly(2-dimethylamino) ethyl methacrylate or pDMAEMA. The cationic lipids include *N*[1-(2,3-dioleyloxy)propyl]-*N,N,N*-trimethylammonium chloride) (DOTMA), 3β[(N-(n',N'-dimethylaminoethane)-carbamoyl]cholesterol (DC-Chol), 2,3-dioleyloxy-*N*-[2-(sperminecarboxamido) ethyl]-*N,N*-dimethyl-1-propanaminium trifluoroacetate (DOSPA) and a neutral phospholipid, such as dioleoylphosphatidylethanolamine (DOPE) [Mahato, 2005]. The DNA/cationic polyplexes are generally made in low salt solutions, because the complexes form micron-sized aggregates in either physiological saline or in blood. Polyethylenimine (PEI) is the most efficient nonviral gene vector for transfer of plasmid DNA. Gene transfer efficiency and cytotoxicity with PEI/pDNA complexes depend on the molecular weight of PEI [Demeneix and Behr, 2005]. Smaller PEIs of size < 25-kDa, although less efficient are non-cytotoxic. Increase in gene transfer efficiency with minimal cytotoxicity can be achieved by

cross-linking of small PEIs with potentially biodegradable linkages [Thomas et al., 2005].

Among the biodegradable polymers, cyclodextrin and chitosan provide a suitable substrate for formulation. Cyclodextrins are useful templates for further modification to produce molecular constructs capable of enhanced gene delivery. Polycationic cyclodextrin utility in promoting DNA cellular-uptake is dependent on proteoglycan-mediated binding to cells [Cryan et al., 2004]. PEGylation is a common and effective means of conferring salt stability to polyplexes. The most striking difference between cationic lipids and cationic polymers is the ability of the latter to more efficiently condense plasmid DNA [Agarwal et al., 2005].

Chitosan is a non-toxic biodegradable polysaccharide composed of two subunits, D-glucosamine and N-acetyl-D-glucosamine, linked together by a β(1,4) glycosidic bond. Cationic–charged chitosan interacts with the negatively charged phosphate groups of DNA [Richardson et al., 1999]. Because chitosan is a mucoadhesive polymer, chitosan/DNA complexes are attractive candidates for transfecting gastrointestinal epithelia and/or immune cells in gut-associated lymphoid tissue after being carried across the mucosal boundaries. In one report cells transfected with lactosylated chitosan had a gene expression higher than PEI-mediated transfection [Erbacher et al., 1998].

2.4 Non-viral gene delivery

Recent developments in the formulation of plasmid DNA for production of non-viral gene therapeutics should pave the way for the preparation of gene therapies to treat a wide range of inherited and acquired human diseases. However, the design of an optimal gene delivery system for effective non-viral gene therapy is limiting progress. Gene delivery systems should serve to protect the plasmid DNA from premature degradation in the extra-cellular milieu, mediate non-specific or cell-specific delivery to target cells and facilitate intracellular trafficking [Mahato et al., 1999]. The main hurdle to the success of plasmid DNA based gene therapy is the lack of efficient, specific and safe DNA delivery systems that can permeate the physiological (extracellular) and biological (intracellular) barriers to gene transfer

and expression [Luo, 2004; Davis, 2002; Pilewski, 2002]. The physiological barriers to gene delivery are mainly influenced by the methods of protection of DNA and the delivery route chosen for administration of the gene therapeutic. The biological barriers arise from intracellular events in the gene transfer route which include cell membrane entry, endosomal release, nuclear localization and gene expression [Pouton, 1999]. The immunological barriers to non-viral DNA delivery result from the activation of the innate immune system by the plasmid DNA [Hofland et al., 2004]. A schematic of physical processes involved in gene transfer of cationic plasmid formulation into targeted cells is shown in Figure 2.3.

Polyethylenimine (PEI) is *the* compound with the highest charge density and a high intrinsic endosomolytic activity because of a strong buffer capacity at virtually any pH. PEI is only partially protonated at physiological pH. The positively-charged PEI/pDNA complex enters through the cell membrane by endocytosis resulting in the formation of endosomes. Upon acidification within endosomes or endolysosomes, PEI is thought to act as a proton sponge, with the protonation presumably triggering passive chloride ion influx. Proton and chloride ion accumulation is followed by the influx of water, causing osmotic swelling with subsequent endosome rupture, thus allowing the escape of polyplexes into the cytosol [Kirchies et al., 2001]. Endosomal release resulting in high transfection efficiency is reported for PEIs with molecular weights above approximately 10 kDa. Although the exact mechanism of entry of polyplexes into the nucleus is not understood [Densmore, 2003], it has been reported that formulation aids in high transfection efficiency.

2.4.1 Route for plasmid DNA delivery into cells

Upon administration, non-viral vectors have to encounter extra-cellular barriers before they reach the targeted cells for gene transfer. To reach target cells, non-viral vectors must pass through capillaries, avoid recognition by mononuclear phagocytes, emerge from the blood vessels to the interstitial sites, and bind to the surface of the target cells [Nishikawa et al., 2005]. Cationic vectors may attract serum proteins and blood cells when entering into blood circulation; this attraction results in dynamic changes in their physicochemical properties.

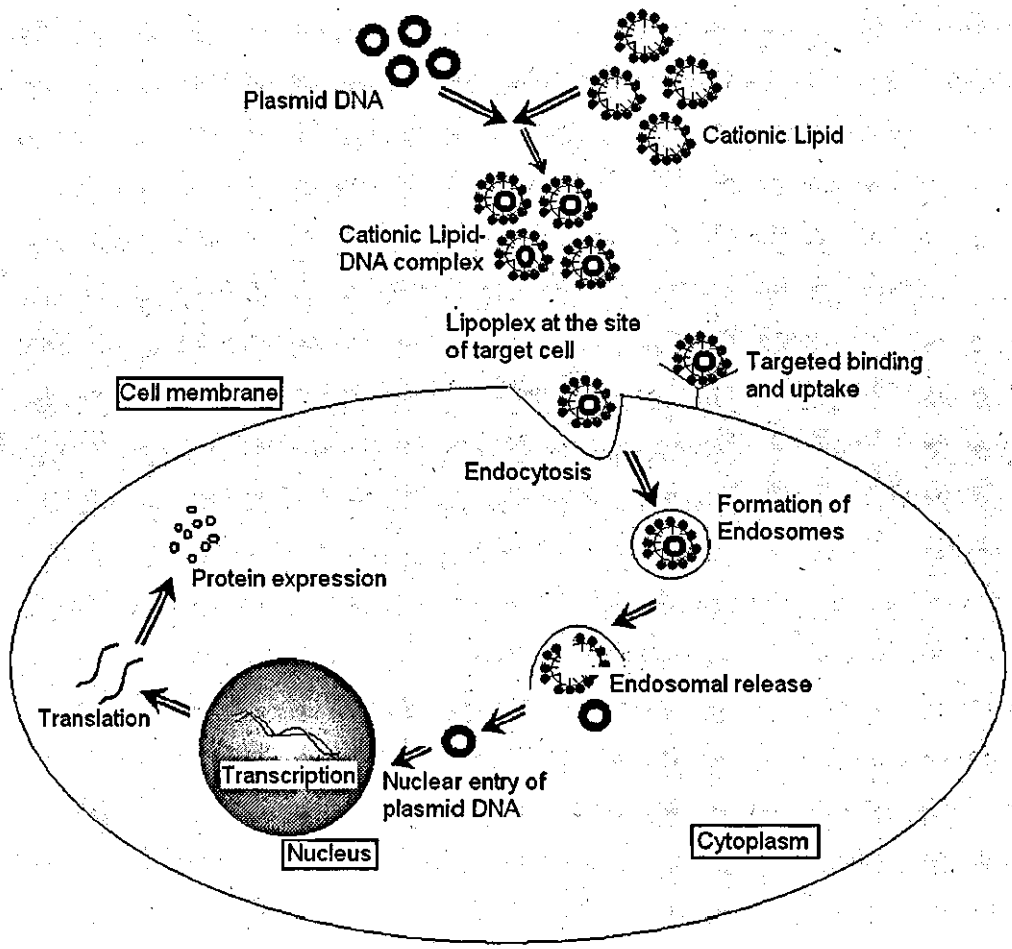

Figure 2.3: A schematic showing the trafficking of a cationic lipid/plasmid DNA complex during the transfection process in targeted cells.

Biological barriers compromise the delivery of plasmid DNA in the targeted cell to gene expression resulting in lower therapeutic efficacy. The sequence of events leading to gene delivery upon entry into the cell include: (i) endocytosis, (ii) dissociation of plasmid DNA from its non-viral carrier, and (iii) pDNA uptake in nucleus for transgene expression [Poulton and Seymour, 2001].

2.4.1.1 Endocytosis

After delivery to the targeted cell, viral/ non-viral vectors enter through endocytosis, an internalisation process for the degradation of foreign/ extracellular material. For

efficient gene transfer, the cytosolic release of plasmid DNA is a prerequisite for nuclear translocation. Since entrapment and degradation of plasmid DNA in endo-lysosomes constitutes a major barrier to gene transfer, proper formulation is essential to encapsulate and protect the plasmid DNA. Formulation of lipoplex with a neutral lipid, DOPE has been shown to increase the efficiency of gene transfer. DOPE promotes the fusion of lipid/DNA particles with endosomal membranes, facilitating membrane disruption and increasing the amount of plasmid molecules released into the cytoplasm. Formulated non-viral vectors based on PEI and HVJ (Hemagglutinating Virus of Japan)-liposome has been characterized to escape endosomal degradation [Kaneda et al., 2002].

2.4.1.2 Dissociation of plasmid DNA from non-viral carrier

Following internalization of the DNA-polycation complex by endocytosis, a large fraction is targeted to the lysosomal compartment by default. Once the plasmid DNA is released in the cytoplasm and before entering the nucleus, it can be quickly degraded by Ca-sensitive cytosolic nucleases. Only a small fraction of internalized plasmid DNA penetrates the cytoplasm. Hence the plasmid DNA should be imported into the nucleus quickly to be transcribed and avoid nuclease attack. It is estimated that at least 10^5 plasmids per cell are required in the extracellular compartment to ensure that a few DNA molecules are taken up into the nucleus of non-mitotic cells [Lechardeur et al., 2005].

2.4.1.3 Plasmid DNA uptake in nucleus

For cellular plasmid-based expression, nuclear import is a rate-limiting step, and intracellular trafficking of pDNA, either naked or complexed to synthetic vectors, is largely uncharacterized. After entry of plasmid DNA into the nucleus, a therapeutic gene has to be transcribed to generate an mRNA, with or without integration into the host's genome. This process would be expected to be common between viral and non-viral vectors. Gene regulation is very much dependent on the transcription and proper

transcription control of a transgene is an important issue in gene therapy [Kamiya et al., 2001].

During non-viral gene transfer, entry of exogenous DNA into the nucleus occurs only in cells that are actively dividing, i.e., when the nuclear envelope breaks down. This is consistent with the observation that well-differentiated, non-dividing airway epithelial cells show very low transfection efficiency. Hence delivery of therapeutic plasmid DNA to a non-proliferating cell nucleus is an inefficient process. Nuclear import of signal-mediated pDNA using nuclear localisation signal (NLS) has been attempted [Tachibana et al., 2001; Munkonge et al., 2003]. One of the main obstacles to the development of gene therapy for the airways is the inability of current viral and non-viral gene transfer vectors to direct sustained expression of a therapeutic transgene. This may be due to several causes including loss of the vector (especially if present in an episomal form), transcriptional silencing of the transgene promoter, loss of the transfected cell through cell turnover, or the generation of an immune response to the transgene product or the transfected cell itself [Ferrari et al., 2002]. The nuclear import of exogenous genes using plasmid DNA/importin-[beta] conjugates has been observed to enhance the nuclear localization of exogenous DNA in a non-viral gene delivery system [Nagaski et al., 2005].

2.5 Delivery systems for administration

The following section examines gene delivery via the following routes for administration of plasmid DNA for gene therapy, namely: (i) parenteral, (ii) oral, (iii) nasal, (iv) transdermal, (v) ocular and (vi) pulmonary delivery.

2.5.1 Parenteral delivery

The three major types of parenteral routes for delivery are (i) subcutaneous, (ii) intravenous and (iii) intramuscular injection. Biodegradable polymeric microspheres based on polylactic acid-co-glycolide and chitosan have been used for parenteral

delivery of drugs containing peptides such as luteinising releasing hormone and growth hormone [Davis, 2006].

2.5.1.1 Subcutaneous injection

Direct DNA injection into skin tissues results in low transfection efficiency compared to viral vector systems due to its rapid degradation by endogenous nuclease activity within tissues. Hence, the coadministration of plasmid DNA and a competitive nuclease inhibitor, aurintricarboxylic acid (ATA) by direct intradermal injection is more effective than the administration of naked DNA [Glasspool-Malone et al., 2000]. Compared to naked DNA immunisation, entrapment of plasmid-based DNA vaccines into liposomes by the dehydration-rehydration vesicle (DRV) method has been shown to enhance both humoral and cell-mediated immune responses to encoded antigens administered by a variety of routes. Effectively entrapping plasmid DNA in DRV vesicles within a range of lipid and non-ionic based vesicle formulations may be a useful system for subcutaneous delivery of DNA vaccines [Perrie et al., 2004]. Some DNA vaccines administered parenterally induced strong systemic humoral and cell mediated immune responses, while mucosal immune responses have generally not been observed [Shroff et al., 1999].

2.5.1.2 Intravenous injection

Hydrodynamics-based gene delivery essentially involves a large-volume, high-speed intravenous injection of naked plasmid DNA (pDNA), which yields a significantly high level of transgene expression *in vivo* [Kobayashi et al., 2005; Fabre, 2005]. Application of hydrodynamics-based procedures to therapeutic vectors for cytokine delivery and small interfering RNA (siRNA) or siRNA-expressing naked vectors *in vivo* have been reported [Tuschl and Borkhardt, 2002]. The delivery of interferon (IFN) genes, which play a crucial role in tumor suppression and rejection, holds considerable promise for *in vivo* cytokine gene therapy. The therapeutic effect of intravenous interferon gene delivery with naked plasmid DNA in murine metastasis models was observed to be better than subcutaneous delivery [Kobayashi et al., 2002].

The potential of dendritic poly(l-lysine) of the 6th generation (KG6) as a nonviral gene carrier *in vivo* of plasmid DNA after intravenous administration in tumor-bearing mice was found to be better than with DOTAP/Chol liposomes and PEI. KG6 carrier developed high transfection ability without significant cytotoxicity *in vitro* [Kawano et al., 2004]. Intravenous RNAi-based gene therapy encapsulates plasmid DNA inside receptor-specific pegylated immunoliposomes (PILs). This RNAi approach achieved a 90% knockdown of brain tumour-specific gene expression with a single intravenous injection in adult rats or mice with intracranial brain cancer [Pardridge, 2004].

2.5.1.3 Intramuscular injection

Intramuscular gene delivery has been carried out using formulations of plasmid DNA with labile sphingosine-based liposomes and phosphatidylcholine. Upon intramuscular injection, the lipoplex DNA was resistant to serum enzymatic digestion and induced an increased inhibition of gene expression as compared with naked DNA. The cationic lipoplexes used for in vivo gene transfer form a weakly compacted structure and are potentially labile in vivo [Baraldo et al., 2002]. The delivery of plasmid DNA coding for intracellular or secreted beta-cell antigen, glutamic acid decarboxylase (GAD) resulted in less effective disease suppression with intramuscular (i.m.) delivery compared to an intradermal (i.d.) or oral route of administration [Li and Escher, 2003]. Although DNA vaccines are highly effective in inducing both cell-mediated and humoral immunity, the uptake of plasmid DNA *in vivo* has only been observed in the cells of the bone marrow and lymph node B cells after intramuscular immunization [Coelho-Castelo et al., 2003]. Further, the administration of plasmid vectors engineered for gene delivery into mammalian muscle did not induce the production of anti-double stranded (ds) DNA and anti-nuclear autoantibodies in normal mice [MacColl et al., 2001]. Peripheral intramuscular immunization in rats using plasmid DNA complexed with PEI was studied to document gene transfer in neurons of the central nervous system (CNS). The results showed that the non-viral neuronal gene delivery method bypasses the blood–brain barrier and suggests a possible therapeutic strategy for noninvasive CNS gene transfer [Wang et al., 2001].

2.5.2 Oral delivery

Oral delivery assumes importance due to the availability of a large mucosal surface housing the immune inductive gut-associated lymphoid tissues (GALT) in the gastro-intestinal (GI) tract. The two main areas of application for oral gene delivery are corrective gene therapy (both local and systemic) and genetic mucosal immunization via the Peyer's Patches, the immune sampling portals that occur in discrete patches in the small intestine [Page and Cudmore, 2001]. Delivery of foreign genes to the digestive tract mucosa by oral administration of non-replicating gene transfer vectors should be a useful method for vaccination and gene therapy. However, an inevitable disadvantage of oral delivery of polyplexes is the disintegration of the complex in the GI tract due to mechanical, chemical and enzymatic barriers. A PLGA microparticle carrier containing PEI polyplexes for the deposition of intact polyplexes in intestinal lymphoid tissue yielded transgene expression [Howard et al., 2004]. A DNA vaccine for treating gastrointestinal diseases comprising plasmid DNA was orally delivered to the intestines using N-acetylated chitosan as a carrier [Kai and Ochiya, 2004]. The delivery of plasmid DNA to the mucosa of the small intestine was confirmed by the results of immunohistochemical analyses using an expression plasmid encoding Human Immunodeficiency Virus env (HIV env) gp120. After oral administration of virus-like particles (VLPs) loaded with HIV env cDNA, significant levels of specific IgG and IgA to HIV env in fecal extracts and sera was obtained [Takamura et al., 2004].

2.5.3 Nasal delivery

In man, the target site for a nasally administered vaccine formulation is believed to be the nasal-associated lymphoid tissue (NALT) situated mainly in the pharynx as a ring of lymphoid tissue, Waldeyer's ring. Waldeyer's ring comprises the nasopharyngeal tonsil, attached to the roof of the pharynx, the paired tubal tonsils, by the Eustachian openings, the paired palatine tonsils at the oropharynx and the lingual tonsil [Sminia and Kraal, 1999]. From a pharmaceutical standpoint, different formulation strategies can be employed for nasal vaccine delivery. These can be split into two major types; particulate antigen delivery systems such as emulsions, liposomes, microspheres,

where the antigenic material is entrapped or presented on the surface of a particle, and solution systems, where the antigen is dissolved or suspended within a simple solution vehicle [Illum et al., 2001]. With nasal inoculation of liposome/DNA complexes, liposomes are trapped within the lung epithelium and the cationic lipid to DNA ratio is changed during transit through the lung epithelial cells [Tanaka et al., 2004]. Administration by nasal instillation of PEI–PEG/DNA complexes in mice resulted in significant levels of transgene expression [Kichler et al., 2002].

2.5.4 Transdermal delivery

The success of the transdermal approach has resulted in delivery of low-molecular weight drugs available in the market [Langer, 2004]. Transdermal delivery of large macromolecules is restricted due to low skin permeability. Thus, a main goal for transdermal delivery is increasing the permeability of the skin for transfer of therapeutic drugs into the body. Transdermal delivery can be achieved by using two different methods to render the skin permeable to drugs, namely physical and electrical forces. The three physical modes which have been adopted to enhance skin permeability for transdermal drug delivery include photoacoustic waves [Doukas and Kollias, 2004], low-frequency sonophoresis [Mitragotri and Kost, 2004], and microneedles [Prausnitz, 2004]. The electrical means of delivering drugs transdermally include iontophoresis [Kalia et al., 2004] and electroporation [Denet et al., 2004]. With success in delivery of drugs transdermally, the use of delivery vectors such as liposomes, transferosomes and nano/microparticles [Kohli and Alpar, 2004] has the potential to be used as a less destructive approach for gene therapy.

Currently, most pDNA delivery systems based on synthetic polymers are non-biodegradable and toxic both in cell culture and in animals *in vivo* at concentrations high enough to yield therapeutic effects. This therapeutic index is unacceptable for applications in humans, and hence alternative transdermal delivery options for non-viral gene transfer hold promise. A hydrogel formed by an aqueous based, thermosensitive, biodegradable and biocompatible triblock copolymer based on poly[ethylene glycol-b-(D,L-lactic acidco-glycol acid)-b-ethylene glycol] (PEG-

PLGA-PEG) could be a promising platform for non-viral delivery of pDNA for gene therapy in wound healing [Valenta and Auner, 2004].

There is a potential application for ultrasound as an enhancer for topical gene therapy [Cao et al., 2000]. Topical gene therapy requires penetration of the vector–gene complex to the target cells within the skin. With the identification of genes responsible for almost 100 diseases affecting the skin, the possible option of cutaneous gene therapy for treatment of diseases such as severe forms of particular genodermatoses (monogenic skin disorders), such as epidermolysis bullosa and ichthyosis is possible [Lavon and Kost, 2004].

The application of an electric field for electroporation dramatically enhances plasmid gene transfer *in vivo* [Wells, 2004]. Electroporation for the gene therapy of skin has also been employed for *in vivo* delivery of *lacZ* DNA to hairless mice. Three days after treatment, the skin was removed and stained with X-gal (a colorigenic substrate for the LacZ enzyme). Extensive expression of the *lacZ* gene was observed in the dermis, including the hair follicles confirming the use of electro oration for DNA vaccination [Banga and Prausnitz, 1998]. However, electroporation is particularly useful for delivery to more superficial tissues such as skin and muscle. The major limitation of electroporation is the invasive nature of delivery which results in cell damage.

Microneedle delivery of plasmid DNA encoding hepatitis B surface antigen induced stronger immune responses compared to hypodermic injection, requiring fewer immunizations for full seroconversion. Delivery of naked plasmid DNA into skin using coated microneedles [Gill and Prausnitz, 2007] was achieved by dipping arrays into a solution of DNA and scraping multiple times across the skin of mice *in vivo* to create microabrasions. The expression of a luciferase gene showed a 2800-fold increase using microneedles compared to topical application [Mikszta et al., 2002].

2.5.5 Ocular delivery

Although the defense mechanisms of the eye protect it against exogenous and endogenous pathogens, inflammatory and immune-mediated processes are still the

leading cause for blindness. The eye is easily accessible and occupies an "immune-privileged" site, offering opportunities for successful development of gene therapy. An additional advantage of using the eye for gene therapy is the possibility of assessing the success of the treatment in a non-invasive manner by directly measuring visual function. [Borras 2003; Andrieu-Soler et al., 2006]. Gene therapy has the potential to interfere with the immune response at different steps modulating the microenvironment of the eye [Pleyer and Ritter, 2003]. Naked DNA delivery to the cornea has the potential to alter the treatment of a wide variety of corneal and anterior segment diseases [Stechschulte et al., 2001]. Transfer of exogenous genes to the entire retina and other ocular structures is possible with a vascular route of gene delivery using a non-viral gene transfer method [Zhang et al., 2003]. *In vivo* delivery of exogenous genes to the eye has the potential of treating ocular diseases. Efficient and stable transfer of the functional gene was achieved with PEO-PPO-PEO polymeric micelles through topical delivery in mice and rabbits. These *in vivo* experiments indicate the possible potential use of block copolymers for DNA transfer [Liaw et al., 2001]. Non-viral gene therapy strategies open real therapeutic potential for the treatment of ocular diseases [Bloquel et al., 2006].

2.5.6 Pulmonary delivery

The pulmonary epithelium has been an important delivery route for gene therapy in the last decade. The overall structure of the respiratory tract constitutes the upper airways (larynx) and the lower airways (consisting of trachea, bronchi and alveoli), and are shown in Figure 2.4. The delivery of aerosol therapeutics into the pulmonary system is dependent on the aerosol particle size and target region in the respiratory tract. Inhaled aerosols are effective therapeutic carriers capable of non-invasive systemic delivery of therapeutics [Dalby and Suman, 2003; Sullivan et al., 2006]. The aerosol characteristics for targeted therapeutic delivery to the different regions of the lung during inhalation are shown in Table 2.4. Only delivery by breathing via the mouth is considered for aerosol dosage forms.

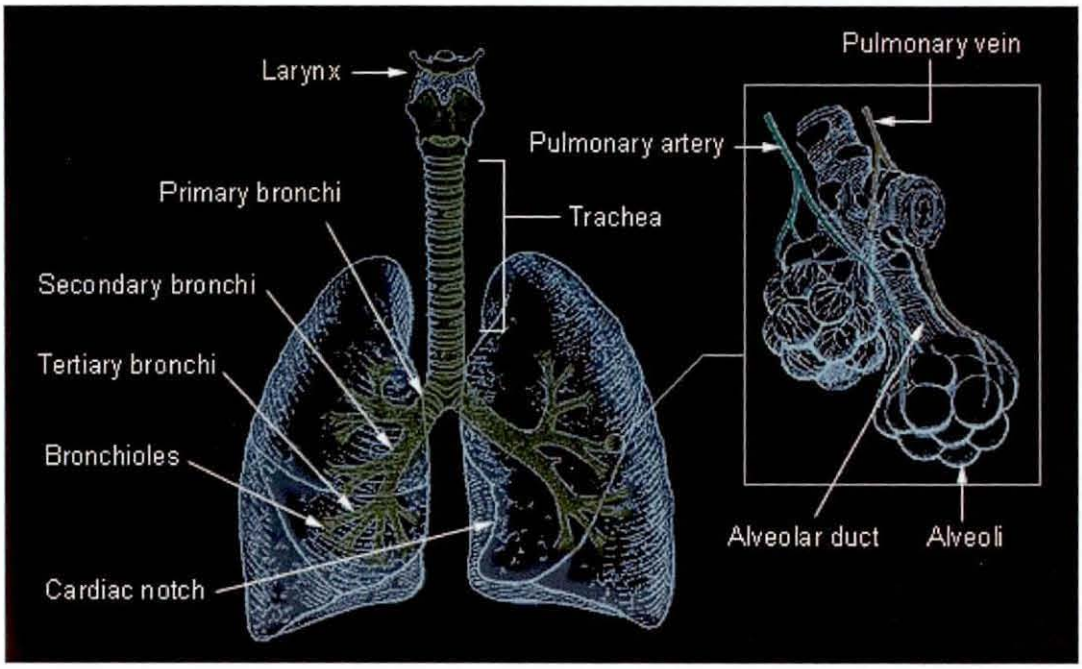

Figure 2.4: Human respiratory system showing anatomy of the lower airways comprising trachea, bronchi and alveoli.

Table 2.4: Targeting aerosols to the lung via inhalation [Hanes et al., 2003]

Target region	Particle diameter	Primary deposit mechanism	Inhalation method	Potential target diseases for gene therapy
Extrathoracic	> 8 μm	Impaction	High inspiratory flow velocity	Cancer
Tracheobronchial	4-8 μm	Impaction and sedimentation	Slow inspiratory flowrate	CF, COPD, cancer
Alveolar	2-5 μm	Sedimentation and diffusion	Slow inspiratory flowrate	Vaccines, cancer cytokine therapy
	0.02-0.05 μm	Diffusion		

Pulmonary gene therapy holds considerable promise for the treatment of many previously incurable lung diseases, such as cystic fibrosis [Davies, 2006]. DNA compacted with polycations has been used with good success in animal models, with minimal toxicity, and is currently being tested in human trials [Davis and Zaidy,

2003]. Cationic liposomes have been used successfully for DNA delivery to airway cells *in vitro* and are being tested in human clinical trials for their efficacy in cystic fibrosis transmembrane conductance regulator (CFTR) gene delivery in cystic fibrosis patients. However, liposomes are not as effective for gene delivery to human airway cells *in vivo* when compared with transfection of airway cells *in vitro*. The physiological barriers to gene delivery in cystic fibrosis lungs are the main reasons for the reduced expression levels [Baatz et al., 2001].

The main physiological barriers to gene delivery in the lungs [Vadolas et al., 2002] are mucus, pulmonary surfactant and alveolar macrophages. Mucus is the most frequently reported extracellular barrier to the delivery of genes to the cells of the upper respiratory tract. Respiratory mucus lines the luminal side of the tracheo-bronchial tree from the entrance of the trachea to the terminal bronchioles, humidifying inspired air and trapping small particles or microorganisms until they can be transported out of the lungs. Pulmonary surfactant synthesized by type II alveolar cells and non-ciliated epithelial cells is a surface-active material that reduces the surface tension in the lungs. The main components of surfactants are phospholipids, neutral lipids, serum proteins, and surfactant proteins. Surfactant proteins may reduce the efficiency of gene delivery when the DNA vectors contain carbohydrate moieties. Gene therapy targeted to the alveolar regions of the lung or to the systemic circulation via the alveoli may be limited by the actions of the alveolar macrophages [Hanes et al., 2003].

2.6 Devices used for pulmonary delivery

The three types of pulmonary delivery devices commonly used in the treatment of respiratory ailments such as asthma, COPD (chronic obstructive pulmonary disease) and cystic fibrosis, and delivery of anti-infectives include (i) pressurized metered dose inhalers (pMDI), (ii) dry powder inhalers (DPI) and (iii) nebulisers. The most important parameters that define the site of deposition of aerosol drugs within the respiratory tract are the particle characteristics of the aerosol. The nature of the aerosol droplets is dependent on its MMAD (mass median aerodynamic diameter), which is a function of particle size, shape and density. The aerodynamic size of aerosol particles generated by various inhalers is fundamental to lung delivery since only the fine

particle fraction (FPF) of approximately <5 μm diameter can potentially reach the target surface within the lung [Smith and Parry-Billings, 2003]. Pulmonary drug administration imposes stringent requirements on the delivery device, since particle size of the powder or droplet greatly influences the accessibility to the delivery site, and ultimately the degree of drug absorption from the lungs [Agu et al., 2001].

2.6.1 Pressurised metered dose inhalers

Pressurised metered dose inhalers (pMDIs) are the most popular vehicle for drug delivery into the lungs, and some 500 million units are manufactured each year. MDIs utilize propellants (chlorofluorocarbons and increasingly, hydrofluoroalkanes) to atomize the drug solution, which results in a uniform spray. Macromolecules are not soluble in pMDI propellants and have to be formulated as dispersed systems i.e., solid particles dispersed in propellants. Dornase-α and salmon calcitonin have been formulated in pMDI systems, demonstrating good retention of primary and secondary structures [Oliver et al., 2001]. However, such dispersed formulations have an affinity for aggregation and particle growth, resulting in some macromolecules with an intrinsic instability in the environment of the propellant formulations [Taylor and Gumbleton, 2004]. Research on the technology for producing drug nanoparticles for dispersion in HFA propellant for pulmonary gene therapy has been studied [Birchall, 2006].

2.6.2 Dry powder inhalers

The development of macromolecular formulations for dry powder inhaler (DPI) devices has been prompted due to the potential for longer product shelf-life. In the 1980s and 1990s, the passive systems were developed into Diskus (GSK, RTP, and NC) and Turbuhaler (Astra Zeneca) which are multi-dose, blister and reservoir systems, respectively. Recently, additional single dose devices such as the Aerolizer (Novartis, Basel, Switzerland) and the Handihaler (Boehringer Ingelheim, Germany) and mutidose devices like Clickhaler (Innovata Biomed, St. Albans, UK) have been approved [Dalby and Suman, 2003]. The Nektar Pulmonary Inhaler and Aspirair™

(Vectura) device are examples of active devices that rely upon hand-assisted compressed air for aerosol generation. Whilst dry powder formulations for DPIs have considerable potential for gene therapy in the lung, the issue of formulation remains a major obstacle to their practical use [Davies et al., 2005]. An inhaler and powder formulation developed by Nektar, Exubera® (human insulin of rDNA origin) insulin inhalation powder is approved in the US and EU for adults with Type 1 and Type 2 diabetes.

2.6.3 Nebulisers

An alternative to pMDIs and DPIs for delivery of biopharmaceuticals is the nebuliser, which can generate respirable aerosols from the liquid with less formulation requirements and a wider dose range. The types of nebulisers commonly used for respiratory drug delivery are Pneumatic or Jet nebulisers and Ultrasonic nebulisers [Barry, 2002; Le Brun et al., 2000]. The European Standard for Nebulising Systems [EN 13544-1:2001] specifies CEN (European Committee for Standardisation) methodology to measure aerosol output and aerosol particle size [Dennis and Pieron, 2004].

2.6.3.1 Jet nebuliser

The operation of a pneumatic nebuliser requires a pressurized gas supply as the driving force for liquid atomization [Hess, 2000]. Compressed gas is delivered through a jet, causing a region of negative pressure. The solution to be aerosolized is entrained into the gas stream and sheared into an unstable liquid film, which breaks into droplets because of surface tension forces. The aerosol is delivered into the inspiratory gas stream of the patient.

2.6.3.2 Ultrasonic nebuliser

The ultrasonic nebuliser uses a piezoelectric transducer to produce ultrasonic waves that pass through the solution and aerosolize it at the surface of the solution. The

frequency of the ultrasonic waves determines the size of the particles, with an inverse relationship between frequency and particle size. The conversion of ultrasonic energy to mechanical energy by the transducer produces heat, which is absorbed by the solution near the transducer. Small-volume ultrasonic nebulisers are commercially available for delivery of bronchodilators. Large-volume ultrasonic nebulisers are used to deliver inhaled antibiotics in patients with cystic fibrosis [Webb et al., 2004]. Ultrasonic nebulisers produce a large number of droplets per unit volume, which in the absence of air circulation through the nebuliser will tend to aggregate and settle in the case of a low velocity aerosol [Taylor and McCallion, 1997].

2.6.3.2.1 Conventional type

The conventional ultrasonic nebuliser with two tanks utilizes the cavitation effect of ultrasonic waves for nebulisation. The energy of ultrasonic vibration from an ultrasonic transducer is focused onto the surface of a solution through cooling water. The solution is nebulised by the effects of cavitation. The nebulisation volume can be adjusted by changing the amount of electric energy applied to the transducer. The nebulised medication is carried to a mouthpiece by airflow that is blown by a fan. Ultrasonic nebuliser resulted in inefficient delivery of liposomes compared to jet and mesh nebulisers [Elhissi and Taylor, 2005].

2.6.3.2.2 Mesh type

The mesh-type of ultrasonic nebuliser is seen as the next-generation of nebulisers. The liquid passes through a mesh with an array of hundreds or thousands of micron-sized holes. Mesh type nebulisers may be classified into two types based on their mode of vibration as active or passive vibrating mesh. An active vibrating mesh indicates the mesh itself is vibrated directly by a piezoelectric crystal. For a passive vibrating mesh, the vibrations of an ultrasonic horn force liquid through the mesh, which vibrates in sympathy with the horn [Newman and Gee-Turner, 2005]. The key mesh nebulisers either in development or on the market following regulatory approval [Knoch and Keller, 2005] include:

- Active vibrating mesh:

  (i) e-Flow® (PARI, Germany), Touchspray® (Odem, UK)

  (ii) AeroNeb®/ Aerodose® (Aerogen, USA),

- Passive vibrating mesh:

  (i) MicroAir® (Omron, Japan)

  (ii) Microflow™ (Pfeiffer, Germany)

The advantages of ultrasonic mesh nebulisers include little requirement for patient coordination necessary, small dead volume and quiet operation, aerosol accumulation during exhalation, high dosage delivery, no chlorofluorocarbon release and fast drug delivery. It has the potential for smaller volume fills, lower or no residual volumes of drug, higher lung deposition and shorter nebulisation times. The disadvantages which have limited their acceptance are that they are expensive, prone to electrical and mechanical breakdown, not recommended for all drug formulations available and requirement of drug preparation. Some ultrasonic nebulisers may be used with the solution to be nebulised placed directly over the transducer. The use of nebulisers to administer biopharmaceutical agents has many important limitations. Such drugs are often very unstable in aqueous solutions, and are easily hydrolyzed. In addition, the process of nebulisation exerts high shear stress on the labile compounds, which can lead to product denaturation or degradation. Other important characteristics of nebuliser performance include nebulisation time, cost, ease of use, and requirements for cleaning and sterilization. Technical profiles of the next-generation mesh nebulisers for pulmonary delivery and their regulatory/market status are compared and shown in Table 2.6.

2.6.4 Alternative aerosolisation methods

The alternative aerosolisation methods based on electro-mechanical and electro-hydodynamic principles shown in Table 2.5 are discussed in the next section.

Table 2.5: Technical specifications for next-generation mesh nebulisers

Nebuliser type/ driving force/ Company	**Trade Name (Status)**	**MMAD * (μm)**	**Aerosol Mass fraction < 5μm (%)**	**Aerosol Condition**	**Technical information**	**Ref.**
Vibrating mesh: OnQ technology **/Aerogen**	Aeroneb Pro *(Market)*	3.1	83	Nebulized medium – 0.083% Albuterol (3mL); Freq. 128 kHz	Adult % Dose deposited :13; Minimum vol. 0.3 mL; (Autoclaveable)	Aerogen website [1]
Vibrating mesh: Ultrasonic **/Odem**	Touch-spray *(NA)*	4.39 (1) 5.32 (2)	62.3 (1); 43.4 (2)	Nebulized medium – (1) - CC plasmid DNA & (2) - linear plasmid; Temp - 23°C; RH - 50%;	Intact DNA following aerosolization: (1) CC – 10% (2) CC – 50%; Minimum vol. 0.3 mL	Smart et al., 2002
Vibrating mesh: Ultrasonic / **Pari**	Pari eFlow *(Market)*	GSD 1.5	63	NA	Single pass; no recirculation; Minimum vol 0.73 mL	CF website [2]
Vibrating mesh: Ultrasonic / **Omron**	MicroAir *(Market)*	5.0	80	Temp – 10-40°C; RH – 30-85%; Freq. 180 kHz	Lung deposition (% vol fill): 18.1 (8.0); Minimum vol. 0.5 mL	Omron website [3]
Electro-Mechanical Extrusion / **Aradigm**	AERx *(NA)*	2.95	NA	Nebulized medium—Aq. Formul.	Dia -1μm; Unit dose; Minimum vol. 0.045 mL	Deshpande et al. 2002
Electro-Hydrody-namic device / **Battelle**	Mystic Inhalation device *(NA)*	2.85	90-95	Nebulized medium – NaCl in ethanol	Minimum vol. 0.02 mL	Battelle website [4]

* MMAD – Mass Median Aerodynamic diameter; NA – Not available

[1] - http://www.aerogen.com/uploads/File/pdf/scipres_aaaai_0504.pdf

[2] - http://www.sourcecf-crd.com/

[3] - http://www.omronhealthcare.com/enTouchCMS/FileUplFolder/NE-U22V-BR-3687.pdf

[4] - http://www.battelle.org/healthcare/pdf/mystic.pdf

2.6.4.1 Electro-mechanical device

An electro-mechanical extrusion device for aerosolisation of liquid is the AER$_x$® delivery device (Aradigm, USA). This device is not yet approved and essentially consists of a single-use nozzle contained in each disposable AER$_x$ Strip™ created as

a laser-machined array. The nozzle exit is approximately 1 μm in diameter with a uniform shape which is expected to deliver consistent, fine-particle dosing from the blister/strip containing 50 μl of medication. The aerosol is generated by extruding the formulation under pressure through an array of holes. Aerosolisation of unformulated plasmid DNA (pCMV-SEAP with an approx. size of 7.5 kb)has shown it is degraded upon passage through the AER_x nozzle system [Deshpande et al., 2002]. However, formulation of the plasmid DNA with cationic lipoplex has resulted in no damage to the sc structure on delivery. The AERx system has been used for the pulmonary delivery of small molecules such as morphine and fentanyl and proteins such as insulin (6 kDa) and recombinant human deoxyribonuclease I (rhDNase - 37 kDa) [Dennis 2004]. Aradigm's AER_x insulin Diabetes Management System (iDMS) has been licensed to Novo Nordisk for Phase 3 testing of Type 1 and Type 2 diabetes.

2.6.4.2 Electro-hydrodynamic device

The electro-hydrodynamic (EHD) process applies an electric field over a flowing conductive liquid. The electric field is generated by transferring high voltage DC (direct current) through an array of electrodes, creating a field of discharge ions in front of a multi-spray site nozzle. These cations induce an accumulation of charge at the liquid's surface causing a Taylor cone to form at each spray site [Taylor, 1964]. As the surface charge overcomes the surface tension of the liquid, a fine mist of nearly mono-dispersed droplets is formed. As the droplets pass through the field of ions, their charge is subsequently neutralized, causing the cloud to disperse into uniformly sized droplets. A device presently in its development using the electro-hydrodynamic technology (Ventaria, USA) has been reported to efficiently reproduce aerosol droplets in the 1-5 μm range [Williams, 2007]. Research on the aerosolisation of plasmid DNA using an EHD device is discussed in detail in Chapter 4.

2.6.5 Targeted gene delivery by magnetofection

In addition to the physical modes of gene transfer used for transdermal delivery, another approach based on the application of a magnetic field promises targeted non-invasive gene delivery. Magnetofection is the delivery of genes using magnetic forces and has been shown to enhance transfection efficiency of non-viral systems up to several-hundred-fold. Non-viral gene carriers, such as polyethylenimine (PEI), are associated with superpara-magnetic nanoparticles and complexed with plasmid DNA. Gene delivery is targeted by the application of a magnetic field leading to an accelerated sedimentation of magnetofectins on the cell surface and increase in contact time. They do not directly affect the intracellular uptake mechanism and could lead to efficient targeting of gene expression into the desired organ and tissue *in vivo* [Huth et al., 2004]. Magnetofection may overcome the fundamental limitations of non-viral gene transfer to the airways [Gersting et al., 2004]. The greatest potential for using magnetic nanoparticles to treat paediatric respiratory illness lies in the nanoparticle-facilitated delivery of therapeutic genes for cystic fibrosis [Dobson, 2007]. TransMAG^{PEI} (Chemicell, Germany), a PEI– coated iron oxide particle, complexed to Genzyme Lipid 67 (GL67) mixed with luciferase plasmid DNA was tested in mouse mammary epithelial cells. Although an increase in gene transfer *in vitro* was observed, there was no increase in the transfection efficiency *in vivo* [Xenariou et al., 2004]. Biocompatible magnetic nanoparticles for gene delivery show much promise for *in vitro* and *in vivo* transfection studies [Dobson, 2006].

2.7 Theory of aerosol generation from an ultrasonic nebuliser

In ultrasonic devices, the energy required to atomise a liquid comes from a piezoelectric crystal which vibrates at a high frequency. The base of the crystal is held firm such that the vibrations are transmitted from its front surface to the nebuliser fluid. During ultrasonic nebulisation, waves are formed on the surface of the solution. When the ultrasonic vibrations are sufficiently intense, a fountain of liquid is formed at the surface of the liquid in the nebulization chamber. It is observed that large droplets are emitted from the apex and a fog of small droplets is emitted from the lower part

[Topp, 1973]. Two theories have been developed which describe the mechanism of liquid disintegration and aerosol production in ultrasonic devices, namely (i) capillary theory and (ii) cavitation theory.

2.7.1 Capillary theory

The capillary wave theory depicts droplet formation as resulting from the production of capillary waves on the surface of the excited liquid. When the amplitude of the applied energy is sufficiently high, the crests of the capillary waves break off and droplets are formed. The rate of generation of capillary waves is dependent on the intensity of the ultrasonic vibration and the physicochemical properties of the liquid being atomized [Flament et al., 1999].

2.7.2 Cavitation theory

The cavitation theory postulates that liquid is atomized by hydraulic shocks produced by the implosion of cavitation bubbles near its surface [Niven et al., 1995]. The dependence of atomization on the cavitation phenomena was demonstrated for frequencies between 0.5 and 2 MHz. A combined approach of the above theory states that droplet formation results from capillary waves initiated and driven by cavitation bubbles.

2.8 Aerosol gene delivery

The field of aerosol gene delivery began to decline until it was discovered that polymers (PEI) resulted in far better transfection within the lungs than did lipids or naked DNA [Densmore, 2003]. A number of potential obstacles to the intrapulmonary delivery of genes via conventional jet nebulisation include shearing effects associated with nebulisation and requirements to produce aerosol droplet sizes appropriate for optimal delivery to the peripheral lung and to maximise the dose of DNA delivered to lung surfaces. Non-viral polyplexes are emerging as suitable candidates for use in

pulmonary inhalation gene therapy. PEI-based formulations appear to be good candidates for aerosol delivery of genes for the treatment of a variety of genetic pulmonary disorders, including lung tumors [Rudolph et al., 2005]. Polyelectrolyte complexes between DNA and PEG/PEI subjected to aerosolization in an ultrasonic nebuliser was milder than jet nebulization [Kleemann et al., 2004]. Aerosol-delivered PEI-based formulations are very effective in transfecting the lungs, but produce relatively low levels of transfection in the nasal passages of mice [Densmore, 2003]. Although the results from gene therapy clinical trials are expected soon, developing an aerosol gene delivery mechanism which would be as safe and effective as intravenous delivery will be a challenge to the healthcare industry.

2.9 Roadmap to non-viral gene therapy

The road map to non-viral gene therapy is shown in Figure 2.6. The essential steps required to deliver gene therapeutic grade plasmid DNA to the clinic includes (i) plasmid DNA formulation, (ii) delivery route and device, (iii) gene expression and (iv) clinical trials. As shown in the roadmap, different formulations have been attempted for the delivery of plasmid DNA, although each formulation has to be tested for a particular delivery route and device. The expression of the transgene to a large extent influences the choice of formulation. The barriers to gene expression limiting transfection may be biological or physiological. The former is primarily due to extracellular/ intracellular interactions with the transgene, while the latter due to the limitations in DNA delivery through the device or administration route. A number of gene therapy clinical trials are in progress for the treatment of cystic fibrosis, cancer, influenza and cardiovascular diseases.

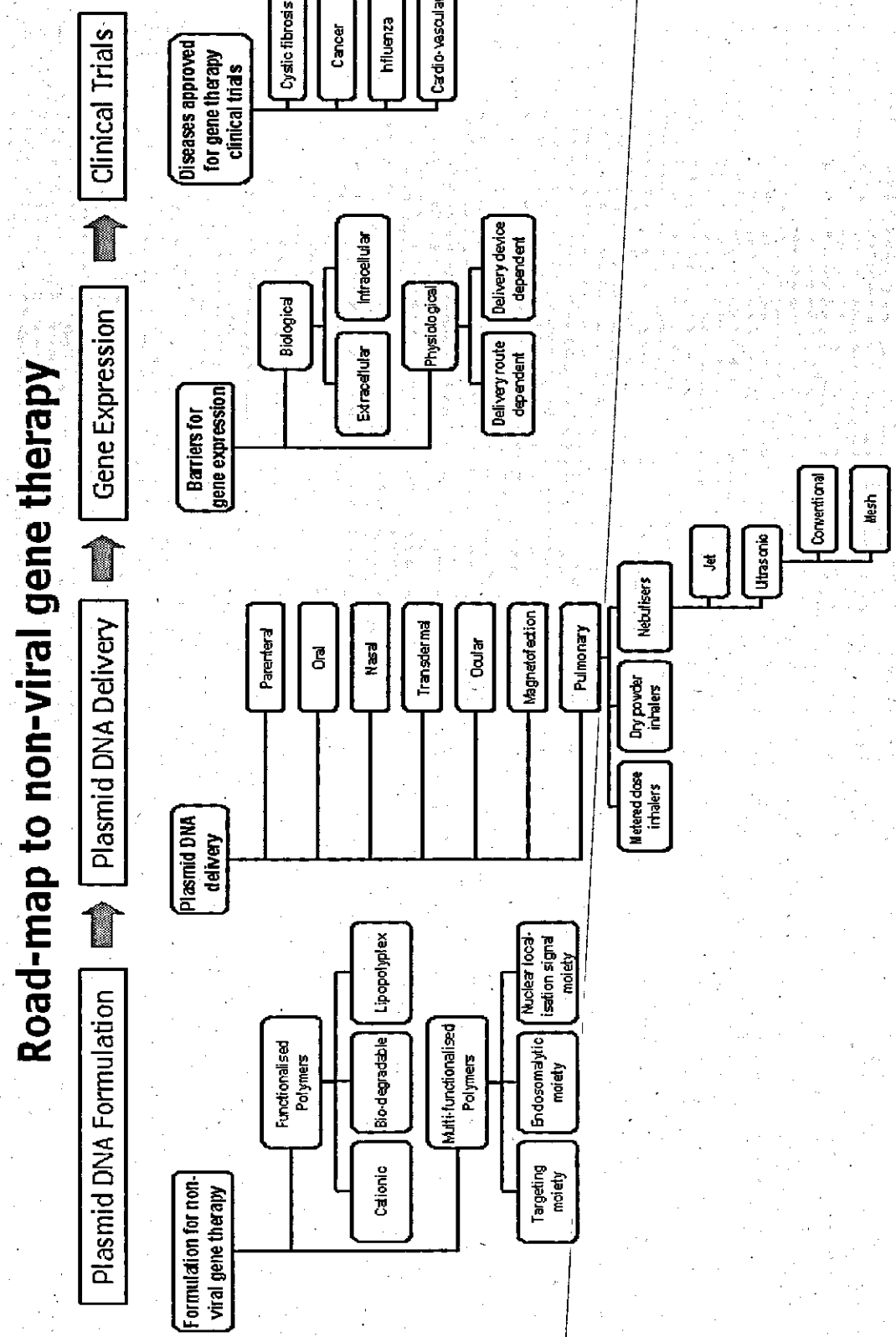

Figure 2.5: Roadmap to non-viral gene therapy

2.10 Conclusions

Gene therapy is gaining credibility and is an emerging area in medicine today. Plasmid-based gene therapy has been proven to be well-tolerated and safe for administration by a variety of routes (e.g., intramuscular, intratumoral, pulmonary, transdermal) but efficiency has often been limited with current technologies. A rational approach towards the design of synthetic gene delivery systems is necessary taking into account the route of administration and the targeted site at which gene expression is expected to take place. A major milestone in the efficiency of plasmid delivery for gene therapy will be the development of highly pure plasmid DNA formulations capable of safe passage through the delivery device and route. The use of a commercially available device for safe delivery of super-coiled structure of plasmid DNA provides a starting point that will ensure rapid adoption for the pre-clinical testing of genetic drugs. A mesh nebuliser promises to deliver respirable aerosols through the non-invasive route for the treatment of respiratory and systemic diseases. The utilisation and development of state-of-the-art delivery devices is of considerable importance for the success of plasmid-based medicines and vaccines as innovative therapies for the future. The next chapter of the thesis discusses the materials and methods adopted in this thesis.

CHAPTER 3. MATERIALS AND METHODOLOGY

3.1 Materials/ Equipment

This chapter discusses all the materials and equipment used for the experiments in this research thesis.

3.1.1 Chemicals

All the chemicals used in the experiments were purchased from Sigma chemicals, UK, unless specified. Solutions were made from deionised, bacteria-free water (of resistivity >18 MΩ.cm) from an Elgastat UHP (Elga Ltd., UK) system.

3.1.2 Delivery device

The delivery devices used for the aerosolisation of liquid solutions were U22 (MircoAIR® NE-U22) and U03 (U1 NE-U03) (both from Omron Healthcare, Japan) mesh nebulisers operated at frequencies of 175 kHz and 65 kHz as shown in Figures 3.1 and 3.2 respectively. Both the nebulisers are used for producing therapeutic aerosols of liquid solutions, while the U22 is a recently introduced nebuliser regarded as a promising device for the pulmonary delivery of liquid suspensions. The U03 mesh nebuliser and nebuliser mesh (496A) was provided by Omron Healthcare, Japan.

3.1.3 Plasmid DNA

The plasmids *gWIZ* (5.7kb) and *pQR150* (20 kb) were obtained by purification from *Escherichia coli* DH5α (Gibco-Life Technologies, Gaithersburg, MD) cells harvested from a fermentation batch and stored at -80°C. A plasmid purification kit (QIAgen) was used for the purification of the super-coiled plasmid DNA (pDNA). The quality of the supercoiled pDNA used for the aerosolisation experiments was checked to ensure it had an A_{260}/A_{280} ratio of 1.8-1.9 (discussed in section 3.2.7.1).

Figure 3.1: A U22 (MicroAIR® NE-U22) mesh nebuliser.

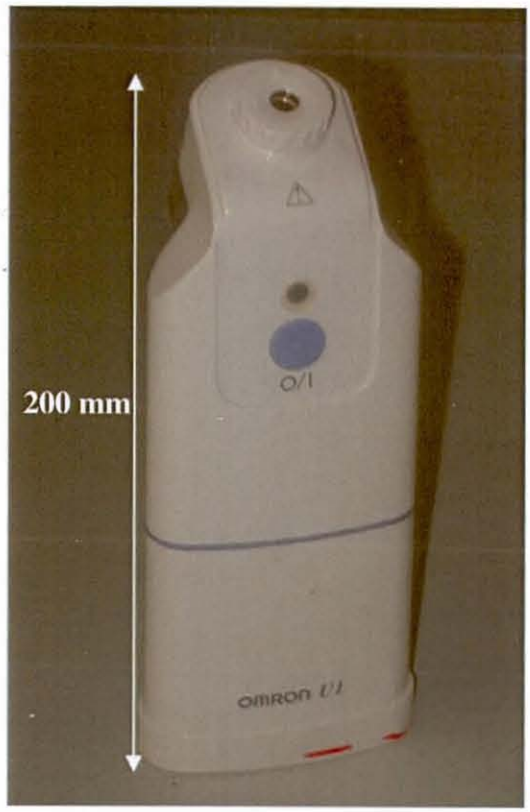

Figure 3.2: A U03 (U1 NE-U03) mesh nebuliser

3.1.4 Equipment used for the experiments

A summary of the equipment used for the research experiments is shown in Table 3.1.

Table 3.1: Equipment/software used for experiments

Experiment	**Objective of the experiment**	**Equipment/ software**	**Make/ Facility**
Nebulisation of plasmid DNA	Aerosolisation of plasmid DNA	Omron mesh nebuliser	Omron Healthcare, Japan
Aerosol characterisation	Particle size determination	Laser diffraction	Malvern Master sizer, UK
Collection of aerosols	Condensation and collection of aerosols	Fabricated glass apparatus	In-house fabrication
Dimensions of the mesh	Nozzle size	SEM (Leo 440)	Leo EM, UK
	Nozzle shape	Interferometer	Zygo, USA
	Mesh thickness	Optical Universal measuring machine	Societe Genevoise, Switzerland
	Nozzle details	Light microscope	Olympus, UK
Analysis of pDNA damage/ nanoparticles	Analysis of pDNA	GelDoc 2000 gel documentation	Biorad, UK
	A_{260}/A_{280} ratio	Biomate^3 Spectrophotometer	Genesys, UK
	PicoGreen assay	Tecan Safire^2 Microplate reader	Tecan UK
	Atomic force microscopy	Dimension 3100 SPM	Veeco Instruments, USA
Transfection of CHO-S cells with plasmid DNA	Growth of CHO-S cell line	Galaxy S CO_2 Incubator	Wolf Laboratories, UK
	Cell Viability/ cell count	Casy cell counter and analyser system	Scharfe System, Germany
	Transfection efficiency	Flow cytometer	Beckman Coulter UK
	Fluorescence determination	Tecan Safire^2 Microplate reader	Tecan UK
Aerosolisation from nebuliser	Frame speeds (1/s) of 4500/9000.	Kodak Ektapro high-speed camera	Kodak Ektapro
Computational fluid dynamics	Generation of grid for CFD domain	Gambit 2.1	Fluent, UK
	CFD simulations of flow through nozzle	Fluent 6.2	Fluent , UK
Design of experiments	Response surface method (RSM)	DesignExpert	Stat-Ease Inc., USA
	Factorial design of experiments	Minitab	Minitab, UK

3.2 Methodology

The methodology adopted for the experimentation is detailed below.

3.2.1 Operation of a U22 mesh nebuliser

The U22 mesh nebuliser is representative of the next-generation of pulmonary devices capable of delivering respirable aerosols with high throughput, high dosage handling capability, portability and ease of operation. The U22 mesh nebuliser operated at a frequency of 175 kHz (determined using a laser vibrometer). A schematic of the medication container of the U22 mesh nebuliser is shown in Figure 3.3.

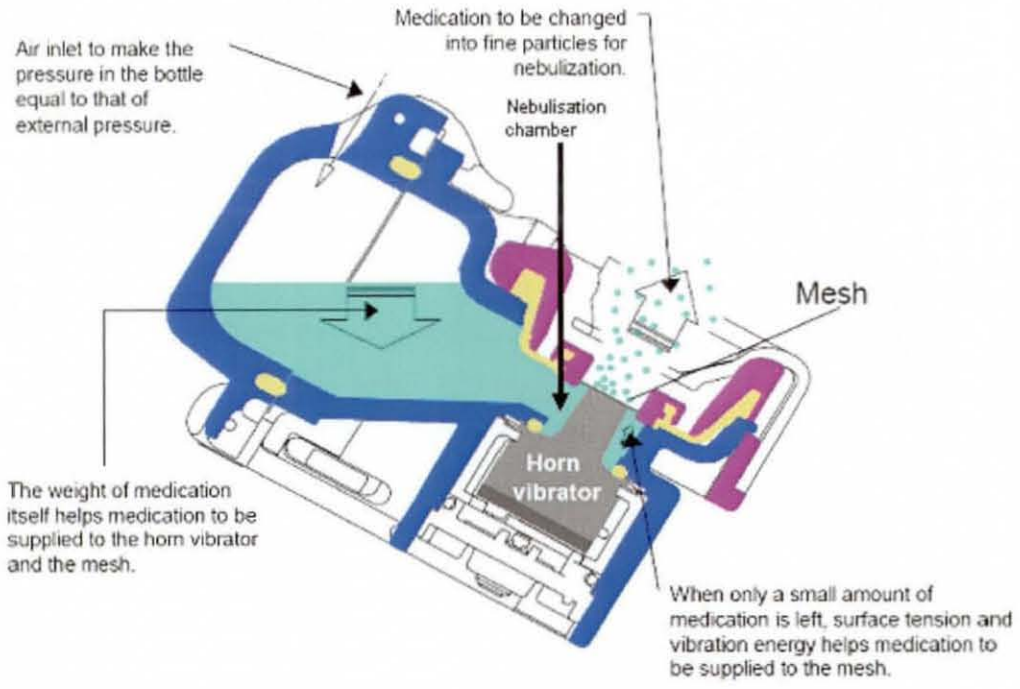

Figure 3.3: Principle of operation of the U22 mesh nebuliser [Kishida et al., 2003] showing the medication container and the mesh of the device; the vibrator horn is powered by a DC volt supply of 3V; plasmid DNA sample from the 'nebuliser chamber' is taken to check integrity of supercoiled (sc) structure.

3.2.2 Operation of a U03 mesh nebuliser

The U03 mesh nebuliser is a lower frequency device operating at 65 kHz compared to the U22 mesh nebuliser. The nozzle size of the U03 device was equal to that of the U22 device. A schematic of the nozzle and chamber of the U03 device is shown in Figure 3.4 (Yamamoto and Asai, 2004). The U03 mesh nebuliser operates with the same principle as the U22 device, except that liquid is drawn to the nozzle mesh by the annular section of vibrator horn (Figure 3.4).

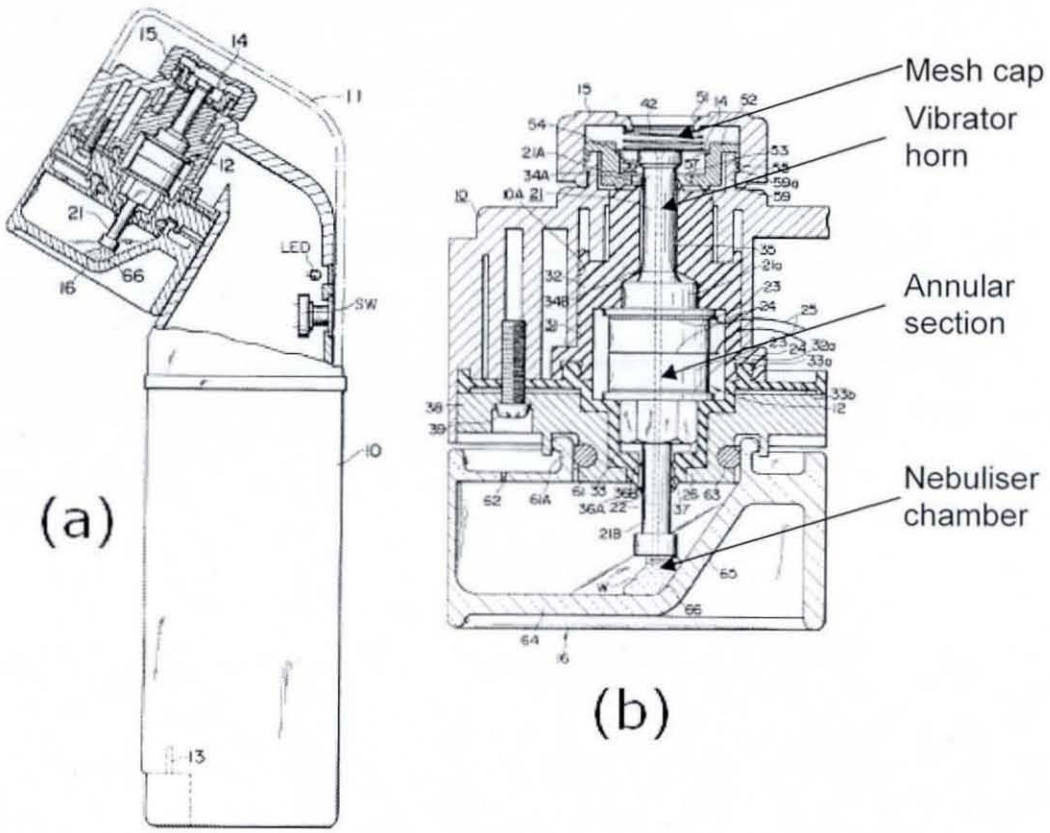

Figure 3.4: U03 mesh nebuliser: a) sketch of the device, b) schematic of medication container showing nozzle mesh and nebuliser chamber; liquid is drawn through the annular section and forced through the mesh resulting in generation of aerosols.

3.2.3 Characterisation of the mesh nebuliser

The mesh plate of the U22 mesh nebuliser was studied for the configuration and orientation of mesh holes using a Scanning Electron Microscope, a Zygo Interferometer, an Optical Comparator and a Light Microscope. A SEM was used for the determination of the nozzle dimensions and arrangement of nozzles on the mesh. A Zygo Interferometer is a three dimensional, surface structure analyzer, which provides graphic images and high resolution numerical analysis to accurately characterize the surface structure. The New View uses scanning white light interferometry to image and measure the microstructure and topology of the surfaces in three dimensions. An optical comparator (Type-214 B universal measuring machine) was used to measure the thickness of the mesh. The machine had accuracy in the μm range, suitable for the dimensions of the nebuliser mesh. A section of the nebuliser mesh was molded in epoxy resin and polished to observe the section of the nozzle under a light microscope.

3.2.4 Aerosol collection apparatus

A straight forward aerosol collection apparatus including USP (United States Pharmacopeia) throat geometry was fabricated in glass for collection of aerosols from the mesh nebuliser as shown in Figure 3.5. The aerosol collection strategy was designed based on a modification of the apparatus used for collection of nebulised proteins by Cipolla and Gonda [1994]. The aerosols from the nebuliser were allowed to pass through a fabricated glass USP throat [Zhang et al., 2004] and collected in a sterile test tube placed in a vacuum flask containing ice. In order to facilitate condensation of the aerosols suction was applied using a vacuum pump at the outlet of the vacuum flask. An optimum suction flow rate of 15-20 L/min resulted in maximum condensation of the aerosols in the test tube. Approximately 15-20% (v/v) of the aerosols with pDNA was recovered in the condensed form in the collection test tube after 5 min of nebulisation.

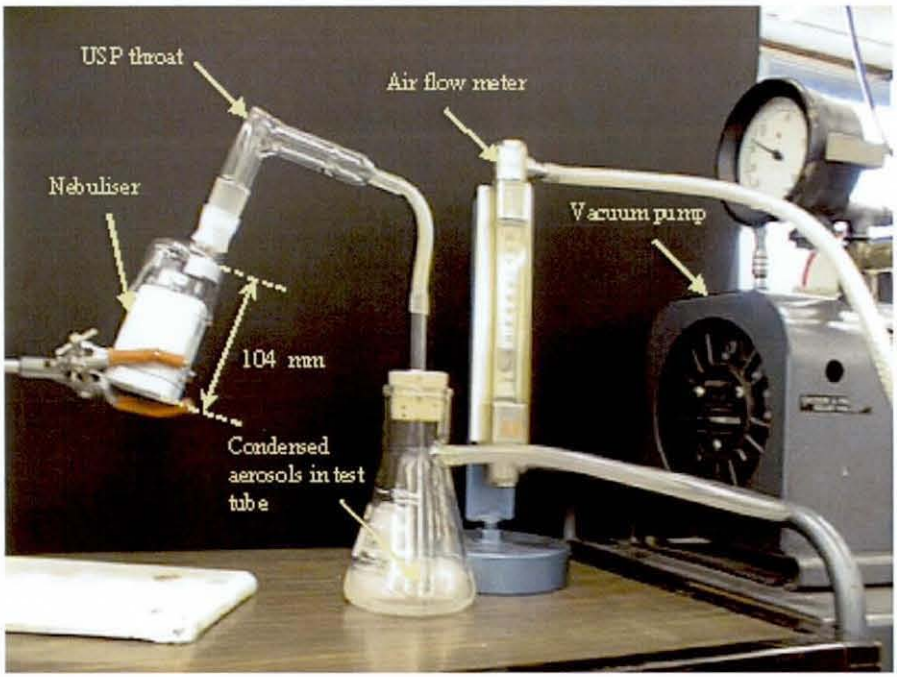

Figure 3.5: Aerosol collection apparatus from a U22 mesh nebuliser, same apparatus was used for the U03 mesh nebuliser.

3.2.5 High speed imaging of aerosolisation

High-speed imaging of aerosolisation from the vibrator horn with and without mesh was carried out for the U22 mesh nebuliser. For high speed imaging of the aerosolisation process, a buffered solution of PBS (Phosphate-buffered saline) was placed on the vibrator horn (Figure 3.6a). Aerosol formation was imaged using a high-speed video system based around a Kodak Ektapro motion analyser [Versteeg et al., 2005] at 4500 and 9000 frames per second to visualize aerosolisation with and without mesh. A schematic of the high speed imaging set-up is shown in Figure 3.6b. To gain optical access to the vibrating horn a section of the fluid container was removed in the tests without mesh. Consequently, instead of utilizing the fluid container to hold the formulation, 0.5 µl of formulation was pipetted directly onto the surface of the vibrator in both cases, to allow meaningful comparison of aerosolisation with and without mesh. At the chosen frame rate it is of course not possible to resolve flow events due to individual oscillations, but overall features of the aerosolisation process were captured adequately.

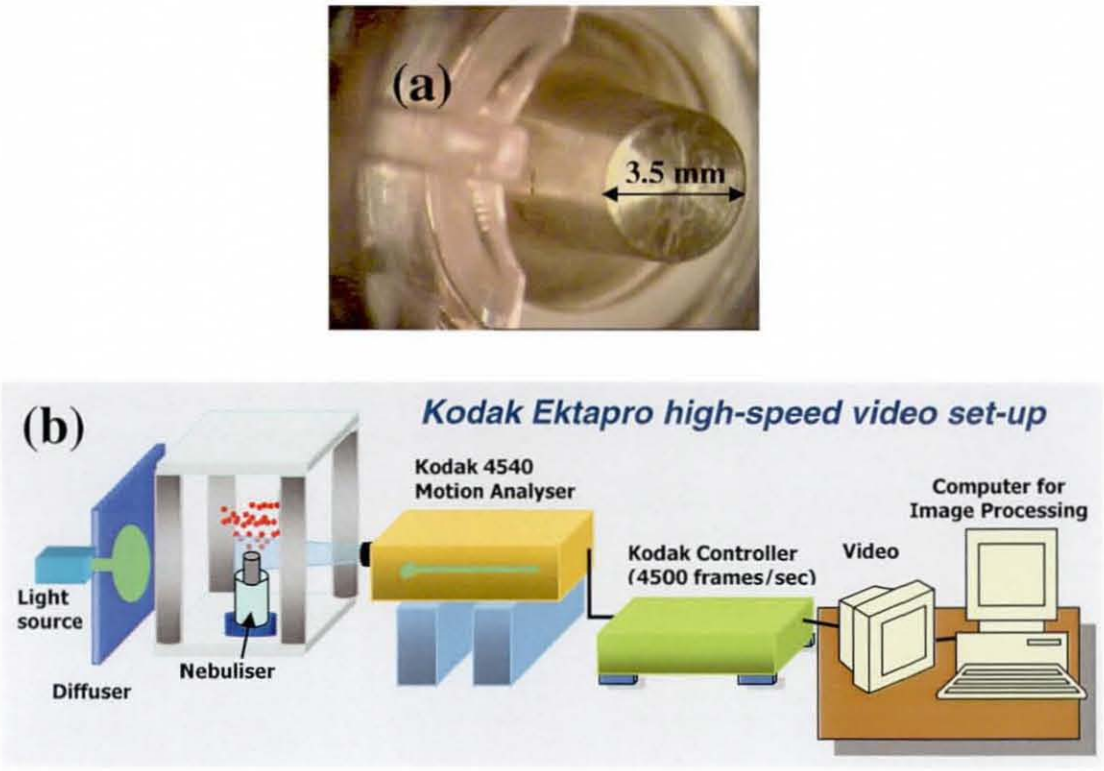

Figure 3.6: (a) Vibrator horn (diameter at the top of the horn is 3.5 mm) of the U22 mesh nebuliser, (b) schematic of a high speed imaging set-up.

3.2.6 Purification of plasmid DNA from cells

Escherichia coli (DH5 α) cells containing the plasmid (pQR150) of size 20 kb was grown in a pilot fermenter and harvested from the fermentation broth. The cell paste of the 5.7 kb plasmid prepared from an earlier fermentation batch was used for plasmid purification and nebulisation. The QIAprep mini/maxi-prep kits were used for the purification of plasmid DNA [Qiagen, 2004] as detailed below. The general procedure consists of three basic steps: (i) preparation and clearing of bacterial lysate, (ii) adsorption of DNA onto the QIAprep membrane and (iii) washing and elution of plasmid DNA.

The procedure for miniprep plasmid DNA purification is described. Firstly, the *E.coli* cell paste was made up to a uniform cell suspension using 0.9% (w/v) NaCl solution to achieve an optical density at 600 nm of 10-12.5. One mL of the cell

suspension was then centrifuged at 4000 rpm for 10 min. The pelleted bacterial cells were resuspended in 250 µl of resuspension buffer (P1) and transferred to a micro centrifuge tube. Care was taken to avoid any visible cell clumps after resuspension of the pellet. To the micro centrifuge tube with cell suspension in P1 buffer, 250 µl lysis buffer (P2) was added and gently inverted 4–6 times to mix. However, the lysis reaction was not allowed to proceed for more than 5 min. To the lysate in the micro centrifuge tube, 350 µl neutralisation buffer (N3) was added and inverted immediately but gently 4–6 times. The neutralized lysate was then centrifuged at 13,000 rpm (~17,900 x *g*) in a table-top micro centrifuge for 10 min. A compact white pellet was formed. The supernatants from step 4 were then transferred to the QIAprep spin column by decanting. Centrifugation was done at 13,000 rpm (~17,900 x *g*) in a table-top micro centrifuge for 30–60 s. The flow-through was discarded. The QIAprep spin column was washed by adding 0.5 ml plasmid binding buffer (PB) and centrifuging at 13,000 rpm (~17,900 x *g*) in a table-top micro centrifuge for 30–60 s. The flow-through was discarded. This step was necessary to remove any trace nuclease activity exhibited by the strains. The QIAprep spin column was washed by adding 0.75 ml plasmid elution buffer (PE) and centrifuging at 13,000 rpm (~17,900 x *g*) in a table-top micro centrifuge for 30–60 s. The flow-through was discarded, and centrifuged again for an additional 1 min to remove any trace of residual wash buffer, in order to avoid the residual ethanol from PE buffer to inhibit subsequent enzymatic reactions. The QIAprep column was placed in a clean 1.5 ml micro centrifuge tube. To elute DNA, 50 µl equalisation buffer (10 mM Tris·Cl, pH 8.5) or TE buffer was added to the centre of each QIAprep spin column, let stand for 1 min, and centrifuged at 13,000 rpm (~17,900 x *g*) in a table-top micro centrifuge for 1 min.

3.2.7 Analysis of plasmid DNA

The analysis of plasmid DNA in the samples after purification, formulation and nebulisation were carried out by absorbance measurements of DNA concentration and purity, agarose gel electrophoresis and a PicoGreen assay.

3.2.7.1 DNA concentration and purity measurements

The purified plasmid solution was quantified using UV spectroscopy. A sample of the plasmid solution was resuspended in 1X TE buffer (the dilution was done to achieve an absorbance within the linear range of 0.1-1.0 AU). The Biomate^3 UV-Visible Spectrophotometer is programmed to measure the absorbance readings at A_{260} (maximum absorbance for DNA), A_{280} (maximum absorbance for RNA) and A_{260}/A_{280} ratio (plasmid DNA purity). A ratio of A_{260}/A_{280} reveals information on the plasmid purity, with a DNA ratio of 1.8-1.95 required for plasmid DNA preparations used in gene therapy experiments. The spectrophotometric analysis of A_{260}/A_{280} ratio between 1.8-1.95 served as a functional test to determine the purity of plasmid DNA for gene therapy applications [Schleef, 2005].

3.2.7.2 Agarose gel electrophoresis

Electrophoresis refers to the movement of charged particles in a gel when subjected to an electric field. This method uses an electromotive force to pull charged molecules through a gel matrix to achieve separation based on mass-charge ratio. Nucleic acids are negatively charged due to their ionized phosphate groups. As the size of the nucleic acid increases, charge also increases so the mass-charge ratio remains constant. The electrophoretic separation of compounds is almost entirely based on size and is achieved by the sieving effect of the gel matrix. Ethidium bromide, an intercalating dye that binds to ds DNA, ssDNA and RNA is added. It is useful to visualise different conformations of the plasmid (namely supercoiled, open-circular and nicked). Fragments of linear DNA migrate through agarose gels with a mobility that is inversely proportional to the $\log_{10}$ of their molecular weight. As a quality check, for a plot of migration distance of linear DNA fragments (Lambda HindIII DNA marker) from the well against the $\log_{10}$ of either their molecular weights or number of base pairs, an approximate straight line is obtained.

3.2.7.2.1 Preparation of buffers and agarose gel

The recipe for preparation of TBE buffer (5X) is (i) Tris Base (Tris hydroxymethylmethyamine, M_r=121.13) - 54.43 g, (ii) Boric acid - 27.78 g, (iii) EDTA - 1.85 g, which are dissolved in 800 mL of ultrapure water and volume adjusted to 1L. In order to make 0.5X TBE Buffer for the gel, the prepared 5X TBE buffer was diluted with ultrapure water.

For agarose gel electrophoresis, 0.8% (w/v) agarose gel was prepared using the standard procedure. The open edges of an electrophoresis tray were sealed with an autoclave tape to form a mould. In order to prepare 130 mL of 0.8% (w/v) agarose solution, 1.04 g of powdered agarose was taken in 130 mL of 0.5X TBE Buffer in a clean Erlenmeyer flask. The flask containing buffer solution with agarose was heated in a microwave oven for time intervals of 1 min with constant swirling, till the agarose was completely dissolved and the solution was clear. The solution was then cooled to 60°C. Using a 1 mL Gibson pipette, the edges of the electrophoresis tray were sealed to form a mould with a small quantity of agarose solution. The gel comb was positioned in the mould of the gel tray. The agarose solution was then transferred to an Erlenmeyer labelled "ethidium bromide" in a fume chamber used for handling Ethidium bromide (EtBr). EtBr solution was then added from the stock solution to achieve a final concentration of 0.06 μg/mL. The flask was swirled gently in order to mix the ethidium bromide. The warm agarose solution was then poured into the mould. Any air bubbles formed during the transfer were pricked with a pipette tip. The agarose gel was then allowed to set at room temperature for 45 min and then the comb was carefully removed. The gel was wrapped in a cling-film and placed in a flat-bottomed container in a refrigerator at 4°C until further use.

3.2.7.2.2 Loading of DNA samples in the agarose gel

The DNA samples required to be run on the gel were first prepared and the following procedure adopted for loading DNA samples in the gel. The loading buffer and the DNA sample were added in the ratio of 1:1. The number of eppendorfs required to

prepare the DNA samples and the marker were placed on the eppendorf rack. The DNA samples (5 to 15 µl) and marker (5µl) were added to the labelled eppendorfs on the rack. The loading buffer (5µl) was added to the eppendorf labelled as marker (Lambda HindIII) and 10µl to the remaining eppendorfs containing DNA samples. The eppendorfs were then spun in a bench micro centrifuge at 13000 rpm for 30 s. The eppendorfs were then placed in the rack. Prior to preparation of the DNA samples, the agarose gel was unwrapped and the sealed autoclave tape taken from the edges of electrophoresis tray. The agarose gel with the electrophoresis tray was then placed in the central compartment of the electrophoresis box. The position of the well in the gel was checked to make sure that the DNA ran through the gel towards the anode. 0.5X TBE buffer was then poured into the gel box at both ends until the buffer just covered the top of the gel. The contents of each eppendorf were then carefully pipetted into the wells of the agarose gel, taking care not to spill the samples or push air into the wells. The top of the gel box is then replaced and the power pack controls set to 40-80 V for 2-8 hours. The gel was then run till the required separation was achieved.

3.2.7.2.3 Quantification of agarose gel

For quantification of DNA in the agarose gel, the electrophoresed gel was removed from its container and slid carefully into the transilluminator. The hood of the transilluminator was closed and UV light switched on. The focus of the camera and lighting was adjusted. When the gel was out of the frame, the position of the gel was adjusted in order to capture the image of the gel and save it on a disk for future reference. The UV light was turned off and hood opened. A piece of foil was slid under the gel and removed from the transilluminator. The gel was wrapped in a cling-film and foil and placed in its container and stored at 4°C. The percentage damage to the plasmid DNA was calculated from an analysis of the band intensity observed in the agarose gel by densitometry using Geldoc QuantityOne® (BioRad software) by comparing pre- and post-nebulisation samples. The density of the DNA band before nebulisation was taken as the reference to determine the percentage damage during nebulisation. In order to account for the differential binding of ethidium bromide to the different plasmid structures, a correction factor of 1.36 was applied to the sc structure.

3.2.7.3 PicoGreen assay

The PicoGreen assay uses the well-established principle of DNA denaturation in alkali for molecules with increased single stranded nicks. PicoGreen (Molecular Probes, Paisley, UK), a dsDNA binding fluorescent dye, binds selectively to double-stranded (ds) DNA. The microplate-based fluorescence assay was based on the protocol reported by Rock et al. [2003]. The DNA concentration used for the assay was 200-300 ng/mL. Two aliquots of 50µl of plasmid DNA were combined with 50 µl of PicoGreen (1/200) and taken in the wells of a microplate (Sarstedt, Leicester, UK). The microplate was incubated for 5 minutes and the fluorescence signal was measured using a Safire$^{2\ TM}$ (Tecan, UK) Microplate reader. To one well, 0.075M NaOH was added and mixed well to increase the pH to 12.4. The decrease in fluorescence was monitored due to the release of the fluorescent dye denaturation of DNA by alkali. The relative fluorescence which is a ratio of the fluorescence signal at pH 12.4 to the fluorescence at pH 8 was computed. The damage to the supercoiled structure in the samples of the 5.7 kb plasmid and the PEI/DNA formulations of the 20 kb plasmid was analysed and the relative fluorescence computed. An XFluor^{TM} software was used for direct control from Excel and reporting the results of the assay.

3.2.7.4 Atomic force microscopy

AFM imaging for visualisation of pDNA was carried out in a Dimension 3100 Scanning Probe Microscope (SPM) (Vecco Instruments, Santa Barbara, CA, USA). TappingMode^{TM} etched silicon probes (TESP) cantilever tips used for AFM imaging in air were purchased from Veeco Instruments (Veeco Instruments, Dourdan, France). AFM provides the two-dimensional conformation of the sc structure of the plasmid by immobilization of the DNA molecules on a flat mica surface. Being an atomically flat surface with negative charge, mica cannot bind the negatively charged DNA molecules without cationic treatment to the surface. A freshly cleaved mica disc (diameter - 20 mm) was coated with 100 µl of 10 mM $NiCl_2$ to render the mica surface cationic for the adsorption of anionic pDNA [Hansma and Laney, 1996]. The pDNA was frozen and stored in a deep freezer at -4°C prior to imaging in AFM. 5µl of pDNA

solution were diluted to a concentration of 1 µg/mL and pipetted onto the mica surface. After 1 min, the mica disc was washed with sterile, filtered water and dried prior to AFM imaging. For samples of formulated plasmid DNA with PEI, no surface treatment of the mica disc was necessary due to the positive charge of the formulating agent. The AFM imaging was carried out in TappingMode™ in air at room temperature with a TESP probe using a Dimension 3100 SPM (Veeco Instruments, Santa Barbara, CA). TappingMode™ imaging allows high resolution topographic imaging of sample surfaces that are loosely held to their substrate, or otherwise difficult to image by other AFM techniques. The AFM images were flattened for better clarity using a Nanoscope IV controller.

3.2.8 Formulation of plasmid DNA

The purified plasmid DNA with an A_{260}/A_{280} ratio greater than 1.8 was formulated prior to nebulisation using the mesh nebuliser. Formulation of the plasmid DNA was carried out using ionic buffers and cationic substrates. The ionic buffers used were NaCl solution (150-300 mM), PBS and HEPES. The cationic substrates used were liposomes, DEAE-dextran and PEI.

3.2.8.1 Formulation using liposomes

The formulation of liposomes was carried out according a protocol described in the Megafectin™ Opti kit application manual (Qbiogene, USA). An initial DNA concentration of the 20 kb plasmid used for the preparation of the cationic liposomes was 67 µg/mL. A stock solution of the liposomes, DOTAP/DOPE and DOTAP/Cholesterol was prepared by suspension of the lyophilized lipids in 200 µl of sterile 20 mM HEPES buffer. The final concentration of the cationic lipid is 1 mM. In order to make a formulation of cationic liposomes with DNA to cationic lipid ratio of 0.5 (recommended), the plasmid DNA solution was mixed with liposomes and HEPES in the following ratio: liposomes:HEPES:Plasmid DNA = 2:3:5. The formulations prepared were incubated for 15 min at room temperature and protected from light. A final DNA concentration in the cationic liposome formulation was 33 µg/mL. An

unformulated control with a plasmid DNA concentration of 33 µg/mL was also prepared.

3.2.8.2 Formulation using DEAE-dextran

DEAE-dextran (DD) is a cationic polyelectrolyte used for complexing plasmid DNA. A sample of DEAE-dextran was procured from PK Chemicals, Denmark. According to the manufacturer's product specifications, the nitrogen content in DEAE-dextran is 3.2% (1.1 nmol nitrogen per µg). DNA contains 3 nmol of phosphate per µg. A stock solution of 0.1% (w/v) DD in 0.01M PBS was prepared and filter sterilized using a 0.2 µm filter. Formulations of plasmid DNA with DD were prepared with nitrogen to phosphate ratios of 0.1, 0.2 and 0.4. The formulations were incubated at room temperature for 30 min and then stored at 4°C.

3.2.8.3 Formulation using PEI

A stock solution of PEI (0.9 mg/ml) was prepared in deionised water and the pH was adjusted to 7.2 with HCl followed by filter sterilization and then stored at room temperature (RT). Plasmid DNA (20 kb) was mixed with PEI to achieve a PEI nitrogen:DNA phosphorus ratio of 10:1 [Densmore et al, 2000]. The solution was allowed to incubate at RT for 15 min prior to use for aerosolisation studies.

3.2.9 Transfection studies

Transfection studies were carried out using suspension-adapted Chinese Hamster Ovary Cells and are described below in detail.

3.2.9.1 Chinese hamster ovary cells

The cell line used in this study was CHO-S suspension-adapted cells (Invitrogen/Gibco, La Jolla, USA). All cells were stored in liquid nitrogen in the growth medium added with 10 % DMSO. For experimental studies, cells were thawed rapidly and centrifuged at 150 g for 3 minutes. After removal of the supernatant, the cells were re-suspended in 10 mL of growth medium and incubated in a Galaxy S™ incubator (Wolf Laboratories, UK) set at standard conditions (37 °C, 5 % CO_2).

3.2.9.2 Maintenance of CHO-S cells

After recovery from cryopreservation, cultures were maintained in CHO-S Serum Free Medium II (CHO-SFM II, Invitrogen/Gibco, La Jolla, USA), at viable cell densities between 2 x 10^5 – 3 x 10^6 viable cells per mL. Cells were cultured in 250 mL Corning® cell culture flasks (50 - 100 mL working volume) at 120 rpm (orbital shaker) in a Galaxy S™ incubator (Wolf Laboratories, UK) set at standard conditions (37 °C, 5 % CO_2). Cells were maintained as described, and used for experiments up to 25 passages.

3.2.9.3 Preparation of PEI-pDNA complexes using 5.7 kb plasmid

A stock solution of 0.9 mg mL^{-1} polyethyleneimine (PEI 25 kDa; branched) was prepared in deionised water, neutralized to pH 7.0 with HCl and filter sterilised. Stock solutions were stored at room temperature. The DNA samples of the 5.7 kb plasmid at a concentration of 20 µg mL^{-1} were used for nebulisation experiments. In order to prepare formulated PEI/pDNA for nebulisation, the 5.7 kb plasmid was mixed with PEI to achieve a PEI nitrogen:DNA phosphorus ratio of 10:1. The formulated PEI/pDNA complex was nebulised in the U22 mesh nebuliser, and samples before and after nebulisation used for transfection studies. To prepare PEI-pDNA complexes with nebulisation samples of the 5.7 kb plasmid, the before and after nebulisation pDNA samples were mixed with PEI to achieve a PEI nitrogen:DNA phosphorus ratio of 10:1. The solution was allowed to incubate at RT for 15 min prior to transfection.

3.2.9.4 PEI-pDNA transfection of CHO-S cells

Transfection experiments were performed in Corning® ultra low-binding (ULB) 24-well plates (Sigma, UK) to ensure that the cells remained in suspension according to a protocol described in Tait [2006]. CHO-S cells were grown in CHO-S SFM II medium and used for transfection with the before and after nebulisation formulated samples. CHO-S cells were taken from mid-exponential growth phase culture (age 24 hours) and centrifuged in a Beckman GS-6 centrifuge to pellet $6.3*10^6$ cells.mL^{-1}. The cells were resuspended in 30 mL CHO-S SFM II medium to achieve a cell density of $2.1*10^5$ cells.mL^{-1}. 950 µl of this cell suspension was aliquoted into the wells of the 24-well plate. The wells were loaded with 50 µl of the formulated pDNA samples before and after nebulisation samples in triplicate, allowing duplication for sampling at 24 and 48 hours after transfection. Control untransfected wells were loaded with 50 µl of medium. The 24-well plate was covered with Breathe Easy™ membranes (Diversified Biotech, Boston, MA, U.S.A.) to ensure even gaseous exchange and evaporation from all wells. The plate was incubated in a Galaxy S™ incubator (Wolf Laboratories, UK) set at standard conditions (37°C, 5% CO_2). The initial cell density used for transfection was determined. After 24 hours, the membrane was cut down the middle and the 24 hour transfected samples collected in sterile eppendorfs. The cell density was determined for each of the transfected samples. In order to measure fluorescence of the transfected samples on a microplate reader, 500 µl of the transfected and untransfected 24 hour samples were spun in an Eppendorf® centrifuge (Model 5415 R) at 1000 rpm for 3 min. The pellet was resuspended in 100 µl of PBS solution and the fluorescence measured in the dark using a Safire^{2TM} microplate reader. Similar analysis was performed for the 48 hour transfected and untransfected (control) samples.

3.2.9.5 Determination of viable cell density and percentage viability

Viable cell density and cell viability were determined by either haemocytometer cell counting (trypan blue exclusion) or the CASY® technology using a cell counter and analyser model TTC (Scharfe System, Germany). The principle for the CASY

system is based on pulse area analysis by electric sensing zone method. Similar to trypan blue exclusion method where the trypan blue dye stains the dead cells by entering the ruptured cell membrane and not intact cells, the CASY technology detects the viable, dead and total cell count by pulse area analysis and can detect minuscule changes in membrane integrity. The cells suspended in Casyton® colourless isotonic saline solution and aspirated through a precision measuring pore of diameter 150 µm. The cells passing through the measuring pore are scanned at a frequency of 1 million measurements per second in a low voltage field. The resulting signal of every individual cell is analyzed in area, height and width, and time course.

3.2.9.6 Flow cytometric analysis

The transfection efficiency was determined by flow cytometry using a Coulter Epics XL MCL flow cytometer (Beckman Coulter UK Ltd, Bucks, UK) equipped with EXPO 32™ ADC software. CHO-S cells were transfected with eGFP gWiz™ plasmid DNA as described in section 3.2.7.4. Cells were harvested by centrifugation (1000 rpm, 3 min), washed once with 5 mL of PBS, fixed in 5 mL of 4% (v/v) paraformaldehyde (PFA) and incubated at -20°C for 15 min. Cells were then washed twice with PBS and stored in PBS at 4°C. Transfection efficiencies (defined as the percentage of eGFP positive cells i.e., the cells expressing the GFP protein resulting in fluorescence in a transfected population) were determined by excitation of eGFP with an Argon laser at 488 nm, with emission measured at 510-530 nm. The QC for the fluorescence measurement was carried out using flow check fluorospheres, which are 10 µm latex particles fluorescent on all wavelengths detected by XL.

3.3 Summary

This chapter highlighted the materials/equipment and methodology used to carry out the experiments on the purification and nebulisation of plasmid DNA. The operation of the mesh nebulisers used in this research investigation, the techniques used for analysis of plasmid DNA damage and the transfection protocol are discussed. Chapter 4 discusses on the purification of plasmid DNA from host *Escherichia coli* cells and its nebulisation using a mesh nebuliser.

CHAPTER 4. PURIFICATION AND NEBULISATION OF PLASMID DNA

4.1 Introduction

The objective of the work reported in this chapter was to produce pure supercoiled plasmid DNA in the form recommended for gene therapy and study the extent of damage to the fragile sc structure of different plasmid sizes upon aerosol delivery using a mesh nebuliser. Purification of plasmid DNA for non-viral gene therapy is a critical process in the production of plasmid DNA based therapeutics. During the purification of plasmid DNA it is possible that the fragile sc structure may be disintegrated into the open-circular and linear forms of the plasmid. It is essential to produce purified plasmid DNA in the supercoiled form to the necessary quality standards required for gene therapy experiments. The plasmid specifications and test method guidelines [Schleef, 2005] for gene therapy trials stipulate a number of assays pertaining to the purity of plasmid DNA and DNA homogeneity. The recommendations for the purity and DNA homogeneity suggest an A_{260}/A_{280} ratio of 1.8-2.0 and >95% supercoiled form (using agarose gel electrophoresis) respectively. Nebulisers are the common respiratory devices for aerosol delivery of liquid formulations and have the advantages of large dosage handing capability, ease of operation and low formulation requirements. Aerosol delivery of plasmid DNA in the intact sc form using a nebuliser remains a challenge to be surmounted for the success of the non-invasive respiratory route as an approach for administration of gene therapeutics.

This chapter is structured into three main sections, namely: (i) purification of plasmid DNA of sizes from 5.7 to 20 kb, (ii) characterisation of U22 and U03 mesh nebulisers and (iii) nebulisation of plasmid DNA in a U22 and U03 mesh nebuliser.

4.2 Purification of plasmid DNA

In this research investigation, *Escherichia coli* cell paste harbouring plasmids of size 5.7 kb and 20 kb, produced separately from UCL pilot plant trials were purified using plasmid purification protocols [Qiagen Ltd, UK]. A single colony of *E.coli* cells each containing plasmids of size 8.7 kb and 13 kb (received from Dr. John Ward, Molecular Biology Department of UCL) were cultured in shake-flasks by fermentation to achieve the cell-density required for plasmid purification. The fermentation and purification of plasmid DNA and the protocols are described in Chapter 3.

4.2.1 5.7 kb and 20 kb plasmids

The purity of *gWIZ*^{TM} GFP (5.7 kb) and *pQR150* (20 kb) plasmid DNA in buffer purified using plasmid purification protocol was assessed by determination of (i) A_{260}/A_{280} ratio (*Table 4.1*) and (ii) DNA homogeneity (*Figure 4.1*).

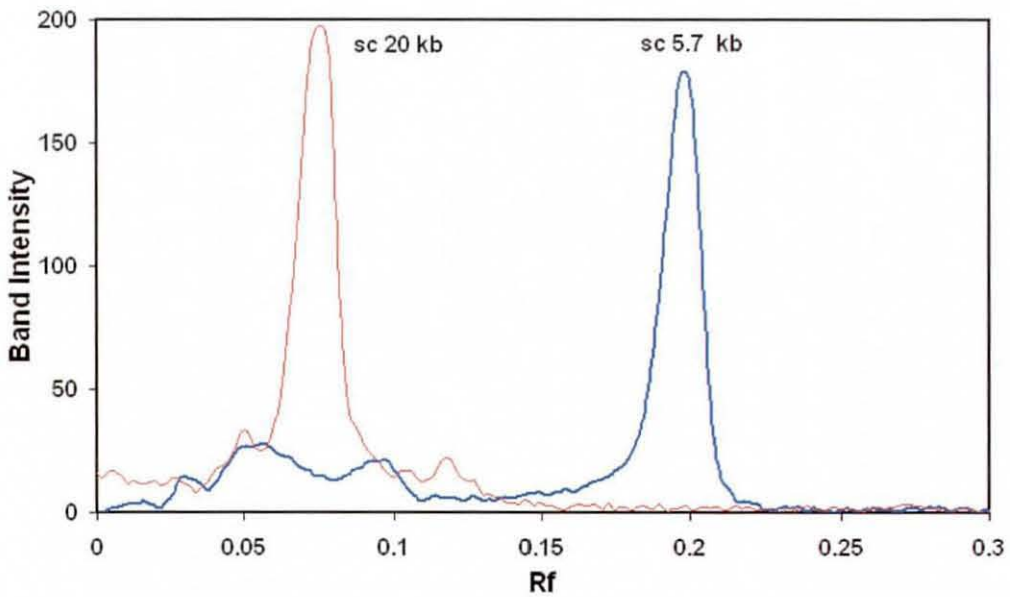

Figure 4.1: DNA homogeneity of purified supercoiled 5.7 kb and 20 kb plasmids determined by densitometric scan of an agarose gel; *sc 5.7 kb – 96.57%, sc 20 kb – 96.61%* (an ethidium bromide correction factor of 1.36 was applied to the sc structure).

Table 4.1: Plasmid DNA purity for 5.7 kb and 20 kb plasmids by A_{260}/A_{280} ratio (n=6)

Plasmid DNA	**A_{260}**	**A_{280}**	**A_{260}/A_{280}**
5.7 kb	0.521 ± 0.12	0.269 ± 0.06	1.93 ± 0.02
20 kb	0.496 ± 0.14	0.255 ± 0.08	1.95 ± 0.02

Figure 4.1 shows the DNA homogeneity determined from the densitometric scan of an agarose gel from the peak values of the band intensity for the sc structure compared to the open-circular and linear forms of the plasmid. A correction factor of 1.36 was applied to the sc structure to account for the differential binding of ethidium bromide to the sc structure. DNA homogeneity of ≥ 95% for the sc structure indicated a high percentage of sc plasmid as per the requirements for non-viral gene therapy.

4.2.2 8.7 kb and 13 kb plasmids

The production of *Escherichia coli* Top10 and *Escherichia coli* JM107 cells from a single colony harbouring *pQR492* (8.7 kb) and *pQR186* (13 kb) plasmids respectively, was carried out using shake-flask fermentation. The fermentation process consisted of an inoculum development stage and a cell mass production stage. The operating conditions for the shake-flask fermentation are presented in Chapter III. The cell mass from the fermentation process was used as input for plasmid purification using the QIAgen Maxi-prep purification kit. The purity of supercoiled plasmid DNA as output was assessed by determination of (i) A_{260}/A_{280} ratio (*Table 4.2*) and (ii) DNA homogeneity using a densitometric scan of an agarose gel (*Figure 4.2*). From Table 4.2, the purity of 8.7 and 13 kb plasmids are assessed by A_{260}/A_{280} ratio between 1.8 and 1.95.

Table 4.2: Plasmid DNA purity for 8.7 kb and 13 kb plasmids by A_{260}/A_{280} ratio

Plasmid DNA	**A_{260}**	**A_{280}**	**A_{260}/A_{280}**
8.7 kb	0.686 ± 0.14	0.367 ± 0.08	1.87 ± 0.003 (n=4)
13 kb	0.358	0.196 ± 0.002	1.824 ± 0.01 (n=2)

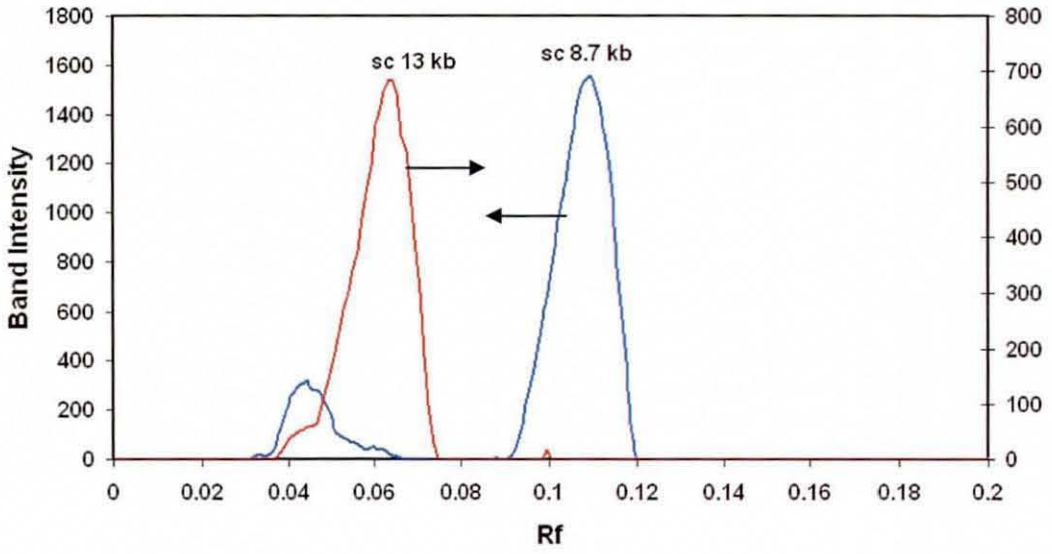

Figure 4.2: DNA homogeneity of purified supercoiled 8.7 kb and 13 kb plasmids determined by densitometric scan of agarose gel; *sc 8.7 kb – 96.34%, sc 13 kb – 96.9%* (an ethidium bromide correction factor of 1.36 was applied to the sc structure).

4.3 Characterisation of a U22 mesh nebuliser

The characterisation of the nebuliser was carried out to determine the dimensions of the nebuliser mesh, the aerosol particle size distribution and the nebulisation rate from the U22 mesh nebuliser.

4.3.1 Dimensions of the nebuliser mesh

The nebuliser mesh was observed in a SEM to determine the size of the nozzle and the distance between the nozzles. The magnification required to observe the nozzle size was 10,000X, while that required to determine the distance between the nozzles was 2,000X (Figure 4.3). The dimensions of the nozzle are reported in Table 4.3.

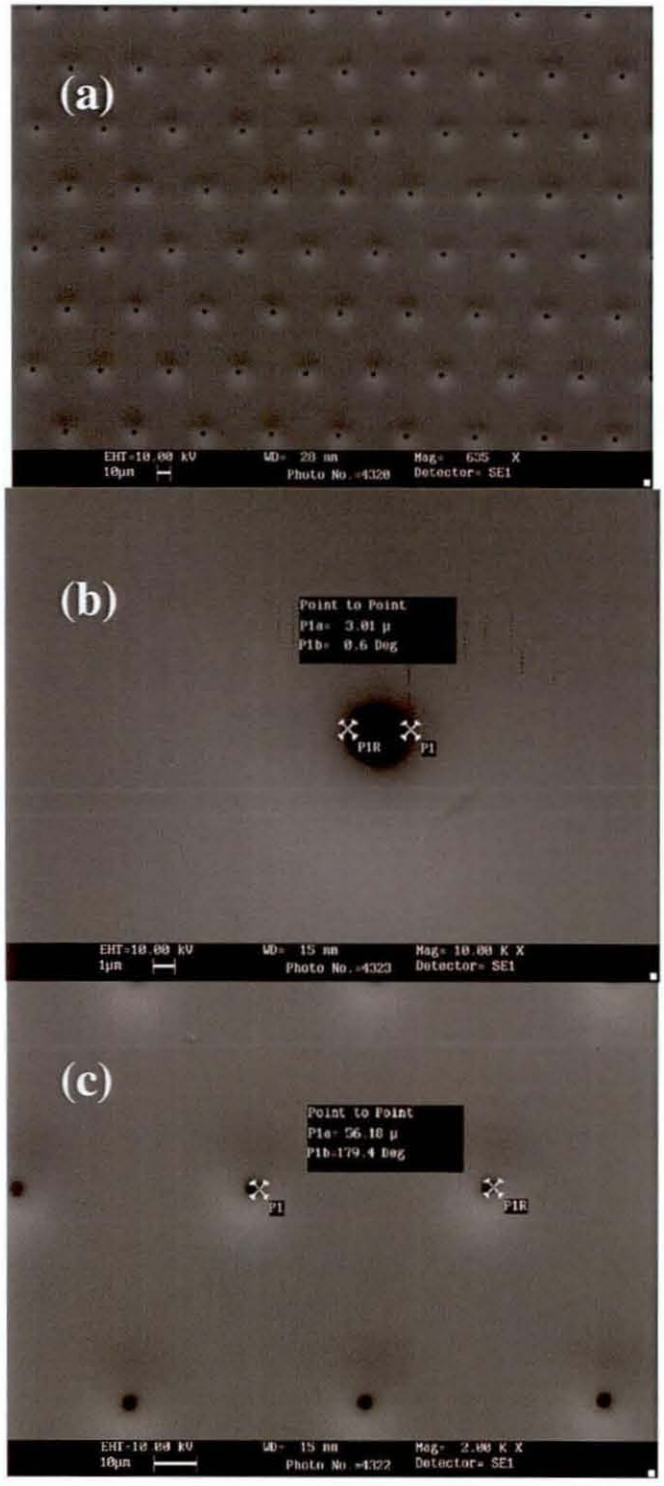

Figure 4.3: Scanning electron micrograph of the mesh of a U22 nebuliser showing (a) arrangement of nozzles on the mesh, (b) single nozzle and (c) distance between nozzles.

A section of the nebuliser mesh was molded in epoxy resin (section 3.2.3) and the images of the nozzle were captured using a light microscope to determine the dimensions against a calibrated image of a scale bar. A cross-section of the nebuliser mesh is shown in Figure 4.4 below.

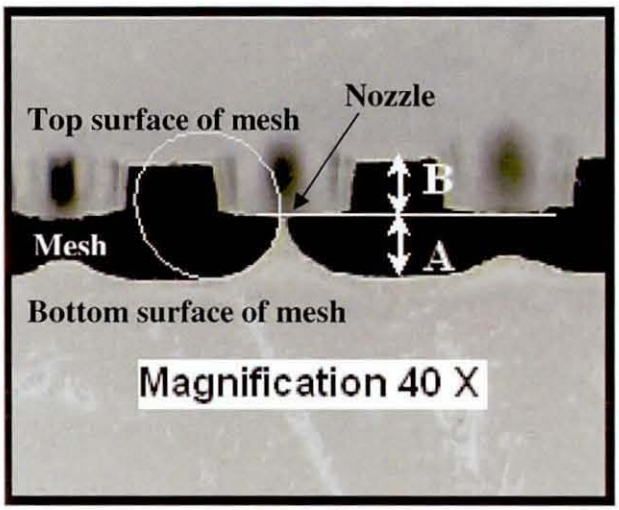

Figure 4.4: Cross-section of a nebuliser mesh of the U22 mesh nebuliser; A and B represent total mesh thickness

The dimensions of the U22 nebuliser mesh determined using Scanning Electron Microscope, Zygo Interferometer and Optical comparator are shown in Table 4.3.

Table 4.3: Dimensions of mesh of the U22 nebuliser mesh

Dimension details	**Tool used for determination (μm) (n=2)**			
	SEM	**ZI**	**OC**	**Computed**
Diameter of the mesh nozzle	3.0 ± 0.01	3.0 ± 0.8	-	
Distance between mesh nozzles	56 ± 0.2			
Mesh plate thickness (A)	-	12.2 ± 1.0	13.0 ± 0.05	-
Mesh plate thickness (B)	-	-	13.0 ± 0.05	-
Mesh plate thickness (A+B)			26.0 ± 0.05	
Internal arc radius of the nozzle				15.6

4.3.2 Aerosol particle size distribution

The aerosol particle size was determined using a Malvern Mastersizer Z Laser Diffraction Instrument at a distance of 25 mm from the receiver lens and height of 20 mm from nebuliser. Figure 4.5 shows the average particle size distribution of distilled water aerosols from the mesh nebuliser sampled during the nebulisation process. The fine particle fraction (1-5μm) of the aerosols was observed to be 35-40%.

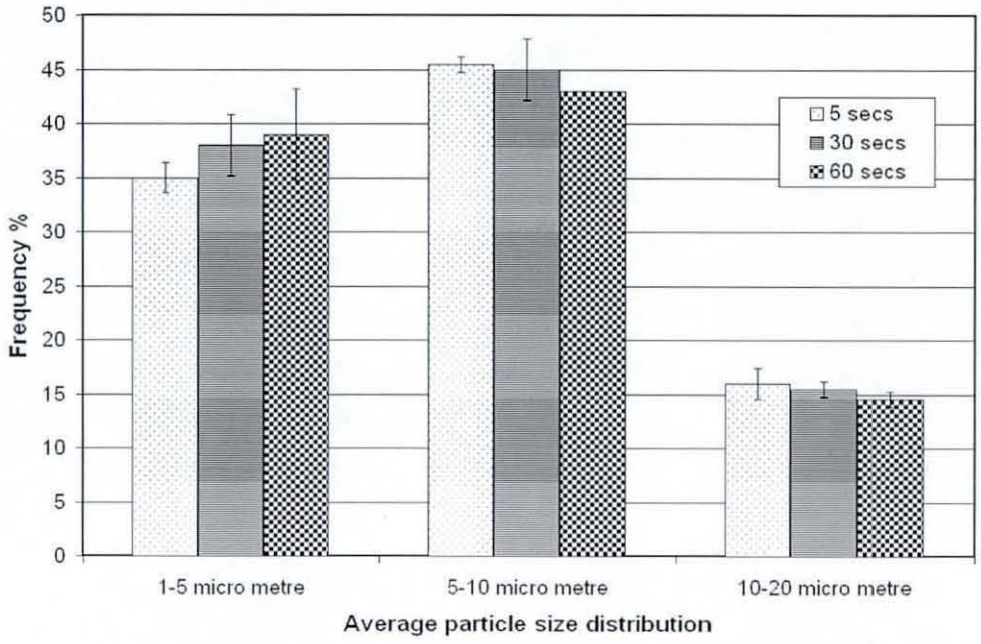

Figure 4.5: Average particle size distribution of aerosols during nebulisation from U22 mesh nebuliser (n=3).

4.3.3 Nebulisation rate

The nebulisation rate of aerosols from the U22 mesh nebuliser is shown in figures 4.6a & b. As shown in the figure, the nebulisation rate was found to be ~0.45 mL/min for the U22 mesh nebuliser.

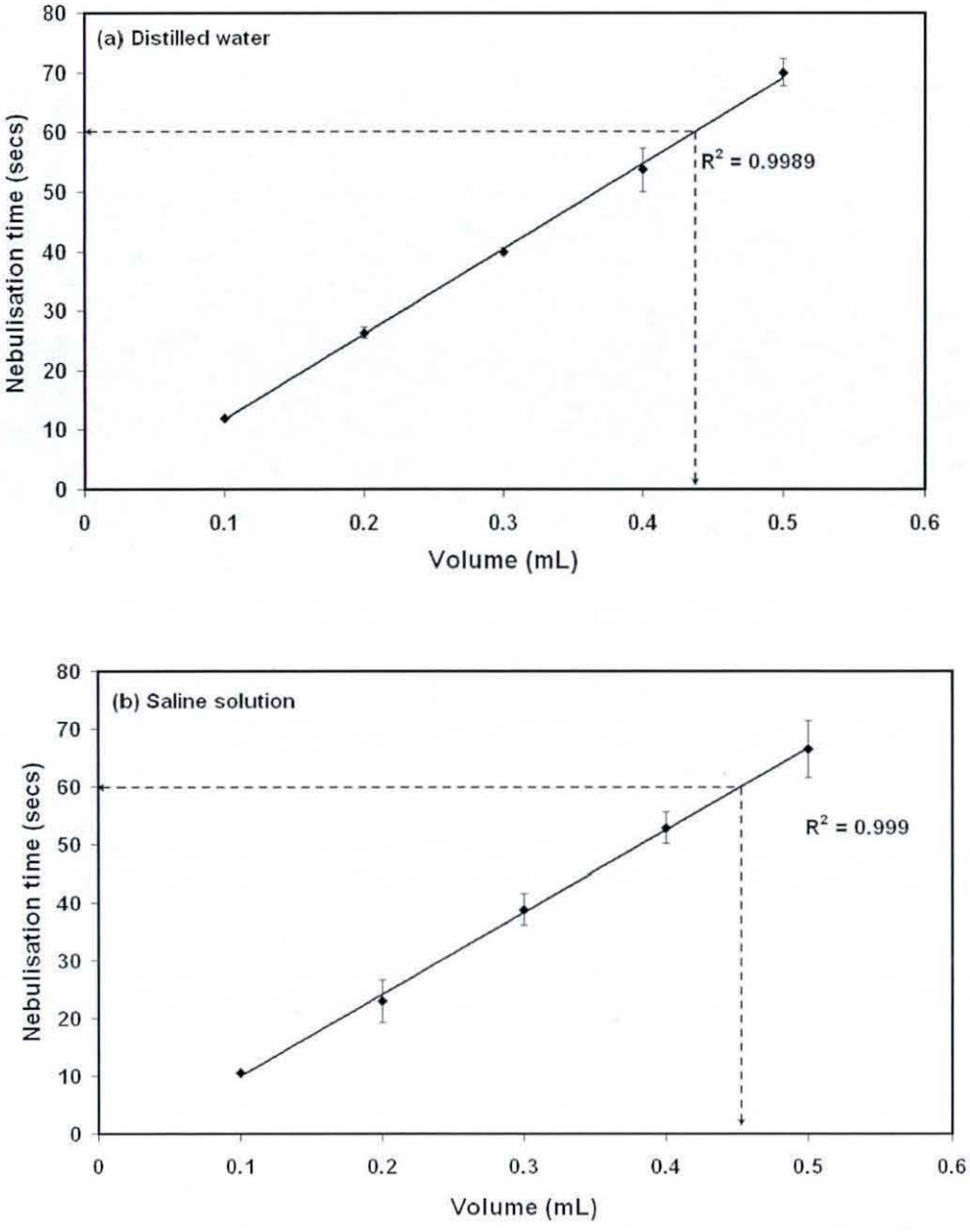

Figure 4.6: Nebulisation rate in the U22 mesh nebuliser (a) distilled water – 0.44 mL/min, (b) saline solution – 0.45 mL/min (n=4).

4.4 Characterisation of a U03 mesh nebuliser

The characterisation of a U03 mesh nebuliser was carried out to determine the nozzle dimension of the nebuliser mesh and the nebulisation rate. Limited analysis and

experimentation was carried out due to the non-availability of this mesh and device in the market. The U03 mesh nebuliser used for the experiments had a mesh with a nozzle size of 3 μm, which was determined using a high-resolution light microscope. The nebulisation rate of saline solution in the U03 mesh nebuliser was 0.2 ± 0.01 mL/min

4.5 Aerosol delivery of plasmid DNA

As has been already indicated, aerosol delivery of plasmid DNA holds considerable promise for the treatment of many demanding respiratory diseases, such as cystic fibrosis, influenza or lung cancer. The delivery of plasmid constructs in the size range of 5 to 20 kb is particularly challenging. The retention of the supercoiled structure (sc) of the plasmid during aerosol delivery is essential for its use as a genetic drug and to comply with regulatory requirements on product quality. In order to ensure maximum retention of the supercoiled content in the aerosols, plasmid DNA in liquid formulation was used for aerosolisation. Although plasmid DNA has been used in liquid aerosolisation devices, damage to the sc structure has been reported and is summarised below.

Studies on liquid aerosolisation devices have shown that aerosolisation can result in damage to the sc structure of the pDNA in the aerosols due to shear effects (Table 4.3). In order to assess the level of damage due to the aerosolisation process, the integrity of the supercoiled structure was compared in the chamber before aerosolisation and in the aerosols after aerosolisation. As seen in Table 4.3, jet nebulisation resulted in damage to a 5 kb and 9.8 kb plasmid, the loss of the sc content being possibly due to hydrodynamic shear and shock waves [Lentz et al., 2005]. Damage to a small plasmid of size 4.8 kb in the aerosols of a jet nebuliser was reported by Kleemann et al. [2004] due to the shearing effects of aerosolisation. Ultrasonic nebulisation of plasmid DNA resulted in no damage to a 5 kb plasmid in the nebuliser chamber [Lentz et al., 2006a]. Aerosolisation based on electrohydrodynamic (EHD) delivery did not damage supercoiled pDNA. Although there is no damage to the sc structure of the plasmid in the aerosols, the EHD device is yet to be commercialized for pulmonary delivery in

the clinic [Davies et al., 2005]. A press release from Ventaria Pharmaceuticals [dated March 21, 2006] stated the device based on EHD technology (Mystic™) is in the manufacturing stage with Nypro Inc., a medical device manufacturing company [Ventaria website]. A commercial mesh-based nebuliser (eFlow®) has also been reported to damage extensively plasmid DNA [Smart et al., 2002]. However, the aerosol delivery of a naked gWiz™ Luc plasmid has resulted in an intact supercoiled structure in the aerosols using a miniaturized nebulisation catheter device [Koping-Hoggard et al., 2005]. The results of the experiments on the nebulisation of plasmid DNA in a mesh nebuliser is discussed in the next section.

Table 4.4: Damage to sc pDNA in the aerosols and nebuliser chamber of some reported aerosolisation devices

Aerosolisation device ***(clinical status)***	**Plasmid size (kb)**	**Percentage damage to sc DNA**		**Reference**
		Aerosols	**Nebuliser chamber**	
Jet nebuliser *(approved)*	5.0	40%	NA	Lentz et al., 2005
	9.8	90%	NA	
	4.8	> 75%	NA	Kleemann et al., 2004
	4.6	NA	*After 4 min*: 50%	Davies et al., 2005
	7.1	NA	90%	
	9.2	NA	100%	
Ultrasonic nebuliser *(approved)*	5.0	NA	*After 9 min*: Nil	Lentz et al., 2006
	9.8	NA	50%	
	4.6	NA	*After 4 min*: 70%	Davies et al., 2005
	7.1	NA	80%	
	9.2	NA	90%	
EHD device *(in trials)*	4.6, 9.2, 15.3	No damage		Davies et al., 2005
Mesh nebuliser *(approved)*	4.5	50%	NA	Smart et al., 2002
	11.0	90%	NA	
Nebulisation catheter device *(preclinical trials)*	6.7	No damage		Koping-Hoggard et al., 2005

NA – Data not available

4.6 Nebulisation of plasmid DNA in a U22 mesh nebuliser

The objective of this experiment was to investigate the use of a commercially available mesh nebuliser (MicroAIR® NE-U22) for nebulisation of plasmids of size from 5.7 to 20 kb. Aerosols of plasmid DNA from nebulisation using the U22 mesh nebuliser in a Bio-safety cabinet were condensed and collected in a sterile aerosol collection apparatus (shown in Chapter 3) and assessed for damage to the sc structure. In order to determine the extent of damage to the plasmid DNA in the nebuliser chamber, the nebuliser was switched off during the middle of the nebulisation process and a sample taken from the nebuliser chamber as shown in figure 3.3.

In order to assess the extent of damage to the supercoiled structure of plasmid DNA upon aerosolisation in the mesh nebuliser, the plasmids were formulated in a suitable biological buffer including TE (Tris-EDTA), phosphate-buffered saline (PBS) and N-2-Hydroxyethylpiperazine-N'-2-ethanesulfonic acid (HEPES). The sc structure of the plasmid has been reported to be condensed in the presence of an ionic salt solution [Levy et al., 1999] and this was adopted to reduce size of the sc structure and consequently damage during nebulisation. The ionic salt solution used in this investigation was 150 mM and 300 mM NaCl. In the following section, nebulisation of the plasmids in the U22 mesh nebuliser are discussed and the results are reported.

4.6.1 Assessment of pDNA damage

The assessment of damage to the sc structure during nebulisation was determined by agarose gel electrophoresis, atomic force microscopy and PicoGreen assay, and the methodology for these is described in Chapter 3.

4.6.1.1 Agarose gel electrophoresis for pDNA damage

The damage to the plasmids of size from 5.7 to 20 kb during nebulisation in the U22 mesh nebuliser was quantified using agarose gel electrophoresis.

4.6.1.1.1 5.7 kb plasmid

Nebulisation of the 5.7 kb plasmid formulated in buffers with and without ionic strength due to NaCl were carried out using the U22 mesh nebuliser. In order to ascertain the extent of damage to the sc structure during and after nebulisation, the commonly used technique is an agarose gel electrophoresis (AGE). AGE is a qualitative tool to determine the extent of plasmid DNA damage. However, a densitometric scan of the agarose gel provides a quantitative estimate of the plasmid forms based on the band density. Figure 4.7 shows agarose gel electrophoresis of the samples of 5.7 kb plasmid formulated in TE buffer taken during and after the nebulisation process. A sample was taken from the nebuliser chamber (NC) mid-way through the nebulisation process. Aerosols of plasmid DNA were condensed and collected after nebulisation (AN) using an aerosol collection apparatus as discussed in Chapter 3.

Negative control samples of the buffer before and after nebulisation (lanes 2 & 3) were carried out prior to nebulisation of 5.7 kb plasmid, to ensure the absence of DNA in the nebuliser from previous use. As observed in lanes 5 and 6 of Fig. 4.7a, sc structure of the plasmid was intact in the nebuliser chamber and in the aerosols, respectively. Smears of damaged DNA in lane 6 of Fig. 4.7a and lane 3 of Fig. 4.7b are likely to be a result of fragmentation of the open circular to linear forms. These results suggest that the sc structure of the 5.7 kb plasmid is able to withstand the forces due to aerosolisation, while the larger and less compact open-circular forms are degraded during nebulisation.

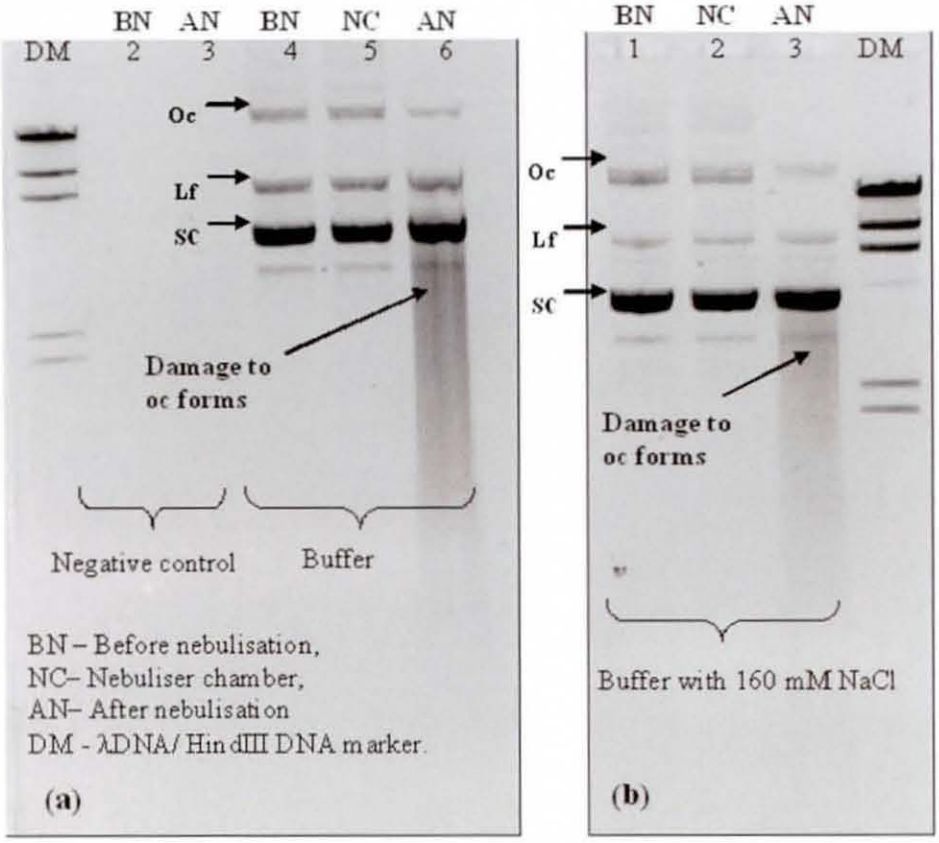

Figure 4.7: Agarose gel electrophoresis of nebulisation of 5.7 kb plasmid: a) TE buffer; lanes 2 and 3: BN and AN samples in TE buffer; lanes 3, 4 and 5: BN, NC and AN samples in TE buffer showing open-circular (oc), linear form (Lf) and supercoiled (sc) forms of the plasmid; b) TE buffer with 160 mM NaCl; lanes 1, 2 and 3: BN, NC and AN samples in TE buffer with 160mM NaCl showing oc, Lf and sc forms of the plasmid.

The densitometer scans corresponding to the agarose gels in Figures 4.7a and 4.7b are shown in Figures 4.7c and 4.7d respectively. The bulk of the sc 5.7 kb plasmid is intact (>98%) after nebulisation, while a major portion of the oc (30-60%) is damaged. The plasmid formulated in 160 mM NaCl also showed a similar degradation of the oc and linear isoforms of the sc plasmid (Figure 4.4d) in the aerosols after nebulisation.

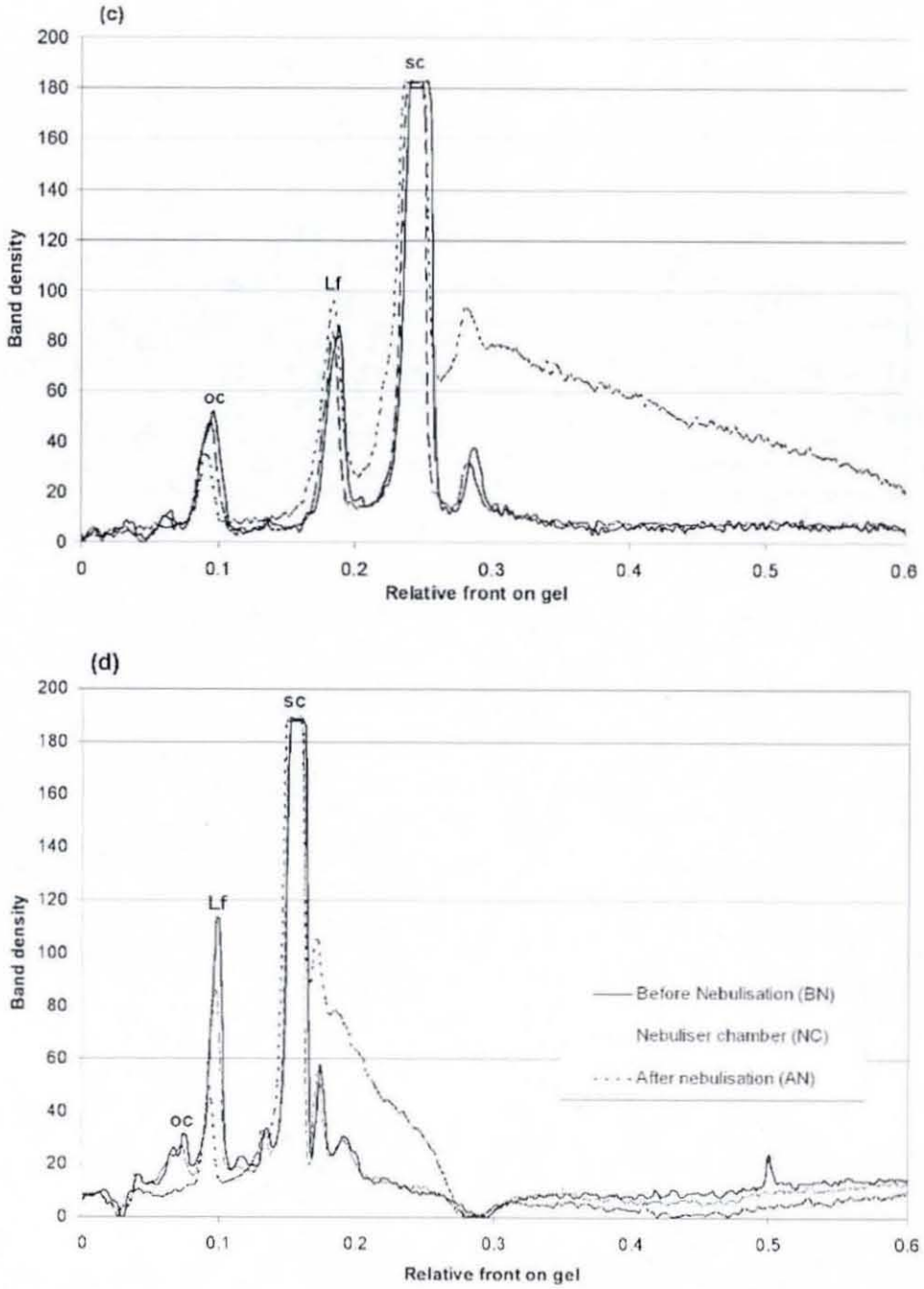

Figure 4.7 c) & d): Agarose gel electrophoresis of nebulisation of 5.7 kb plasmid: c) and d) densitometer scans showing peaks of open-circular (oc), linear form (lf) and supercoiled (sc) of Figure 4.7 a) and b) respectively resulting in less than 5% damage to the sc form in both cases.

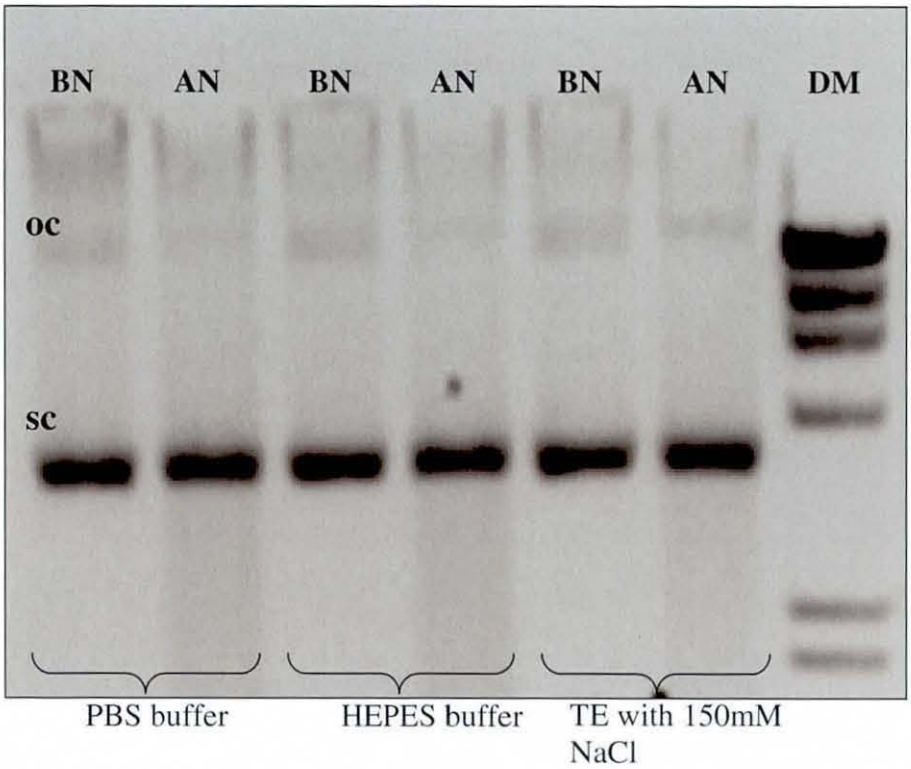

Figure 4.8: Agarose gel electrophoresis of nebulisation of 5.7 kb plasmid: a) PBS buffer: BN and AN samples; b) HEPES buffer: BN and AN samples; c) TE with 150mM NaCl: BN and AN samples; open-circular (oc) form of the 5.7 kb plasmid is damaged in the AN samples; DM – DNA marker.

Agarose gel electrophoresis of the nebulised 5.7 kb plasmid formulated in common biological buffers such as phosphate-buffered saline (PBS) and N-2-Hydroxyethylpiperazine-N'-2-ethanesulfonic acid (HEPES) resulted in no damage to the sc structure (Figure 4.8). However, a smear of linear DNA fragments in the after nebulisation samples suggested partial fragmentation of the open circular forms of the plasmid. Densitometric scans of the agarose gel revealed damage of < 2% to sc structure of the 5.7 kb plasmid formulated in the above buffers. In order to investigate the influence of plasmid size on damage to supercoiled structure upon nebulisation in the mesh nebuliser, plasmids of size 8.7, 13 and 20 kb were used for the experiments.

4.6.1.1.2 8.7 kb plasmid

Nebulisation of 8.7 kb plasmid formulated in TE buffer resulted in damage to the sc structure of the plasmid was observed in an agarose gel. In order to reduce the size of the sc structure, the plasmid was formulated in TE buffer with 150mM NaCl. However, the sc structure was less damaged when observed in an agarose gel. Densitometric scans provide a better representation of the damage to sc structure compared to an agarose gel (please refer Appendix) and are shown in Figure 4.9.

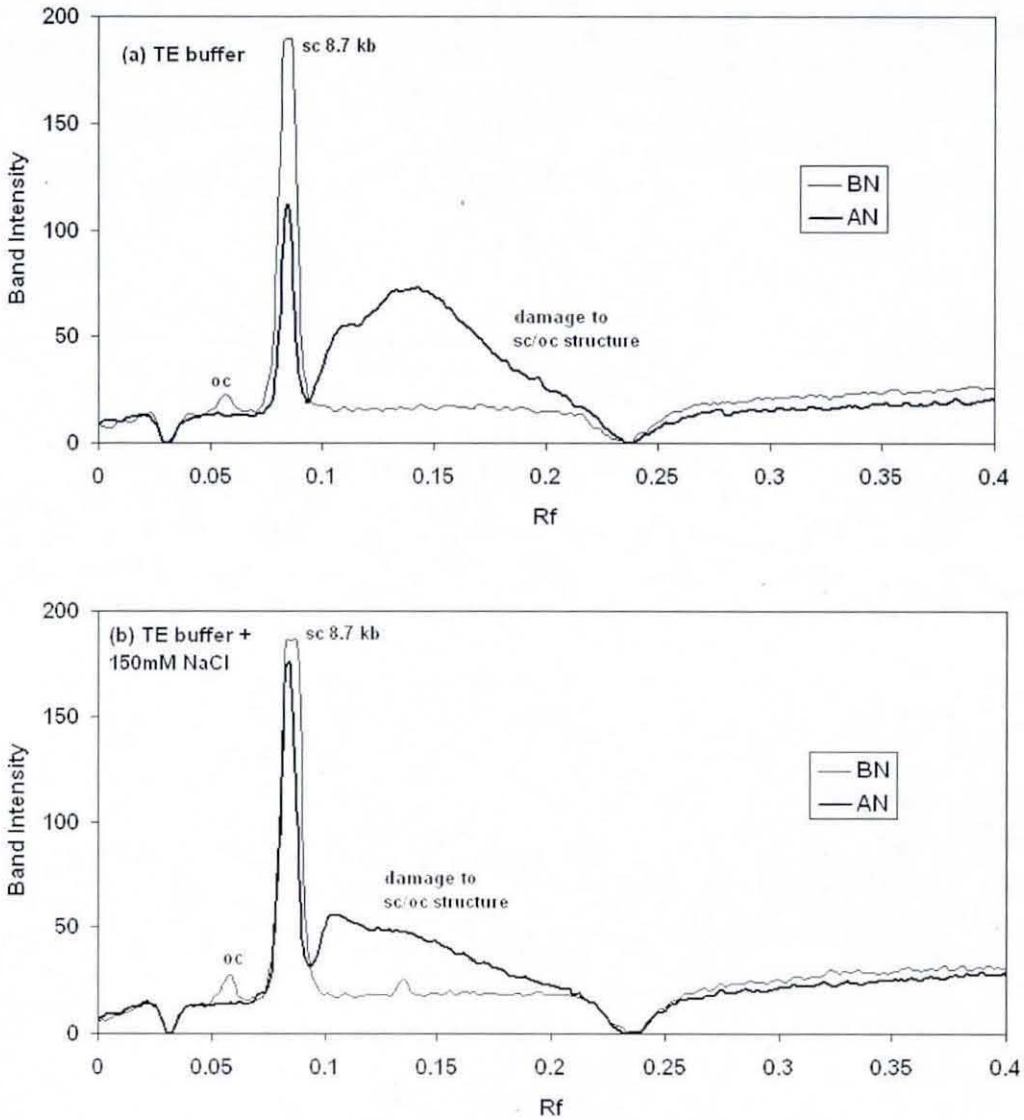

Figure 4.9: Densitometric scans of agarose gel from nebulisation of 8.7 kb plasmid formulated in: a) TE buffer, b) TE buffer with 150 mM NaCl; % damage to sc structure in a) 45% and b) 6.5%; BN – before nebulisation, AN – after nebulisation.

From Figures 4.9a and 4.9b, densitometric scans of the agarose gel indicate that nebulisation resulted in partial damage (47.64 ± 6.05%) and slight damage (6.5%) to the sc structure of the 8.7 kb plasmid formulated in TE buffer, and TE buffer with 150 mM NaCl respectively. Formulation of the 8.7 kb plasmid in buffer with ionic strength (150 mM NaCl) enabled condensation of the sc structure to a smaller size, thereby resulting in less damage. The scans also revealed complete damage to the oc structure resulting in a smear of linear DNA fragments. In order to examine the influence of plasmid size on damage to its sc structure when nebulised in the mesh nebuliser, a 20 kb plasmid was used for the experiments and the results are presented in the following section.

4.6.1.1.3 20 kb plasmid

Nebulisation of 20 kb plasmid formulated in TE buffer with and without ionic strength due to NaCl was carried out using the U22 mesh nebuliser. Ionic strength using 150 mM or 300 mM NaCl was used to condense the large sc structure in order to avoid damage. Figure 4.10 shows gel electrophoresis of the samples of 20 kb plasmid formulated in TE buffer (lanes 2 to 4) and in TE buffer with 160mM NaCl (lanes 5 to 7). As observed in Fig. 4.10, the sc structure of the 20 kb plasmid remained intact in the nebuliser chamber (lane 3), while the sc structure was completely degraded in the aerosols (lane 4). The smear of DNA in lanes 4 and 7 indicate that after aerosolisation the pDNA was completely degraded into smaller fragments. Formulation of the 20 kb plasmid in TE buffer with 160 or 300 mM NaCl did not stabilize the sc structure during aerosolisation. Lanes 3 and 6 sampled from the nebulisation chamber showed, however, that no damage to the 20 kb plasmid occurs in the chamber. This suggests that DNA damage primarily occurs during the passage of the solution through the mesh or when the aerosol is formed just above the mesh. The size distribution of the sheared fragments after nebulisation shown in Figure 4.11 was obtained by densitometric analysis of Fig.4.10. The 20 kb plasmid was disintegrated into smaller fragments ranging from about 5 kb to less than 0.5 kb. A major proportion (~90%) of the fragments were in the size range of 0.5-2 kb and 2-4.3 kb, quantified based on the molecular weight of the marker DNA.

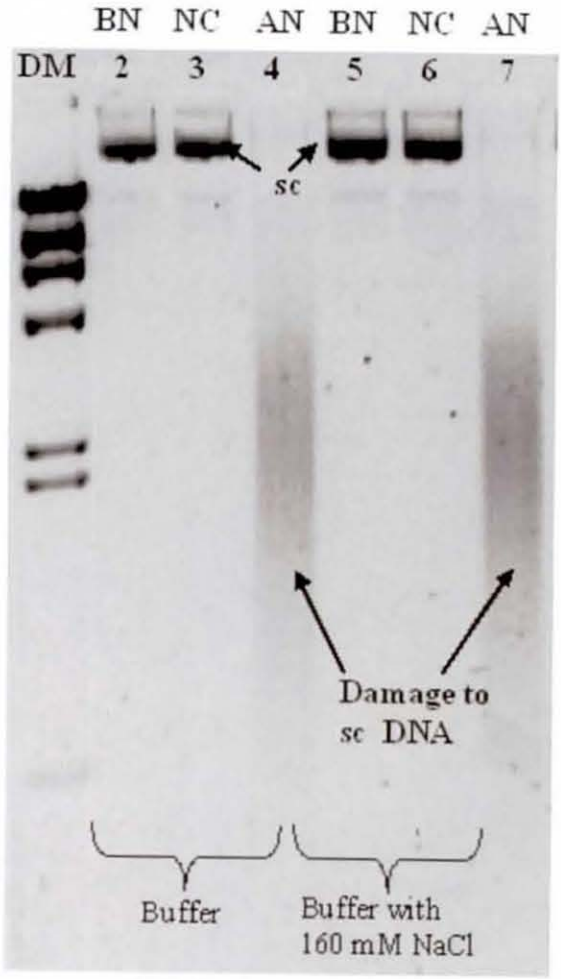

Figure 4.10: Agarose gel electrophoresis study of nebulisation of 20 kb plasmid: lanes 2, 3 and 4: BN, NC and AN samples in TE buffer; lanes 5, 6 and 7: BN, NC and AN samples in TE buffer with 160mM NaCl showing supercoiled (sc) form of the plasmid.

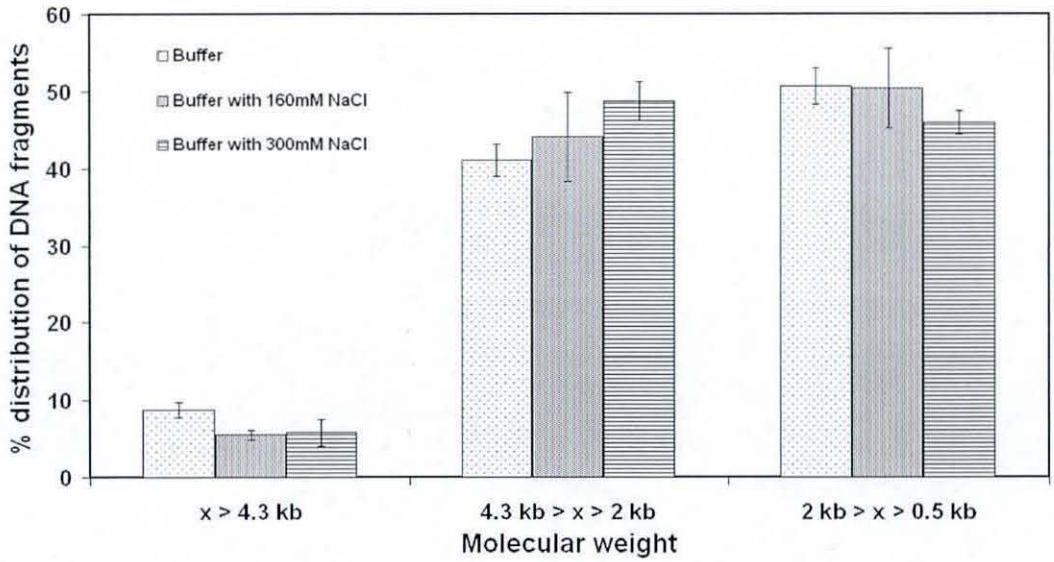

Figure 4.11: Distribution of sheared DNA fragments after nebulisation of the 20 kb plasmid generated from the densitometric scans of agarose gel (n=2); 'x' is the DNA molecular size in kb determined from DNA marker as a reference.

4.6.1.2 Atomic force microscopy for plasmid DNA imaging

In order to visually examine the damage to sc structure of the plasmid, AFM imaging in air was carried out using a Scanning Probe Microscope. The methodology adopted for preparation of the samples for AFM imaging is detailed in Chapter 3.

4.6.1.2.1 5.7 kb plasmid

In order to visualise the extent of damage to the isoforms of 5.7 kb plasmid, nano-scale characterisation of the plasmid was carried out using an atomic force microscope (AFM). AFM imaging of the 5.7 kb plasmid before nebulisation (Figure 4.12a) indicated a molecular size of approximately 330 nm for a single sc structure. Imaging an after nebulisation sample (Figure 4.12b) showed the sc structure with the presence of a small number of DNA fragments from the open circular isoforms. This observation was in agreement with the results from agarose gel electrophoresis reported in earlier. To identify the plasmid isoform which resulted in generation of

DNA fragments upon nebulisation, an assay based on PicoGreen dsDNA binding dye was performed and is reported in the next section.

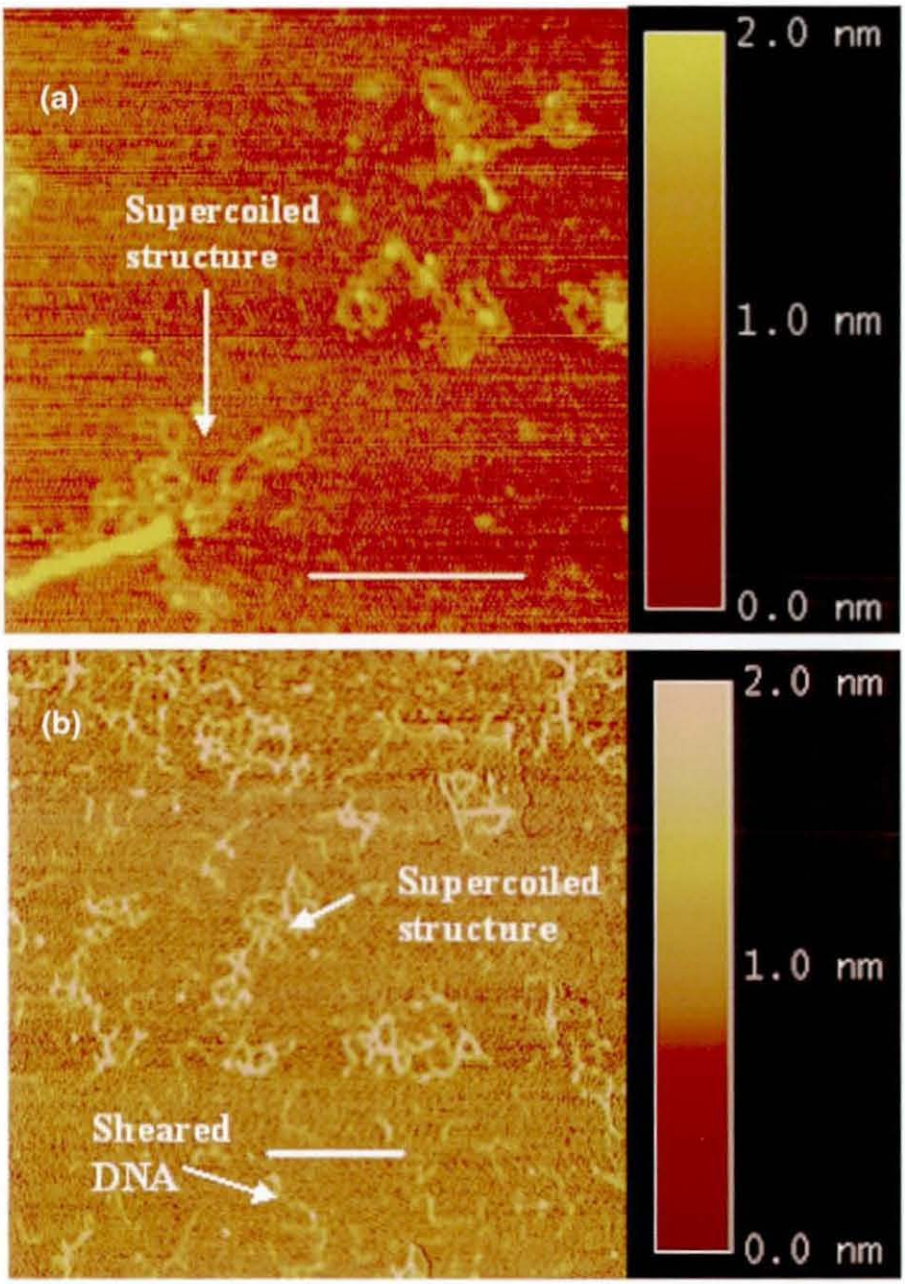

Figure 4.12: Structural analysis of sc structure of 5.7 kb plasmid DNA by AFM imaging in air: a) before nebulisation, scan size of 0.75 x 0.75 μm, scale bar – 250 nm; b) after nebulisation showing sc structure and sheared fragments of 5.7 kb, scan size of 2.5 x 2.5 μm, scale bar – 500 nm.

4.6.1.2.2 20 kb plasmid

The size of the sc structure of the 20 kb plasmid in TE buffer (Figure 4.13a) was observed to be approximately 1250 nm, about four times the size of a 5.7 kb plasmid. Upon nebulisation, the 20 kb plasmid was completely disintegrated into spaghetti-like fragments (Figure 4.13b). The disintegration of the sc structure into such fragments of molecular size less than one-fifth of the original size is probably caused by shear experienced by the plasmid upon passing through the nozzles of the nebuliser mesh.

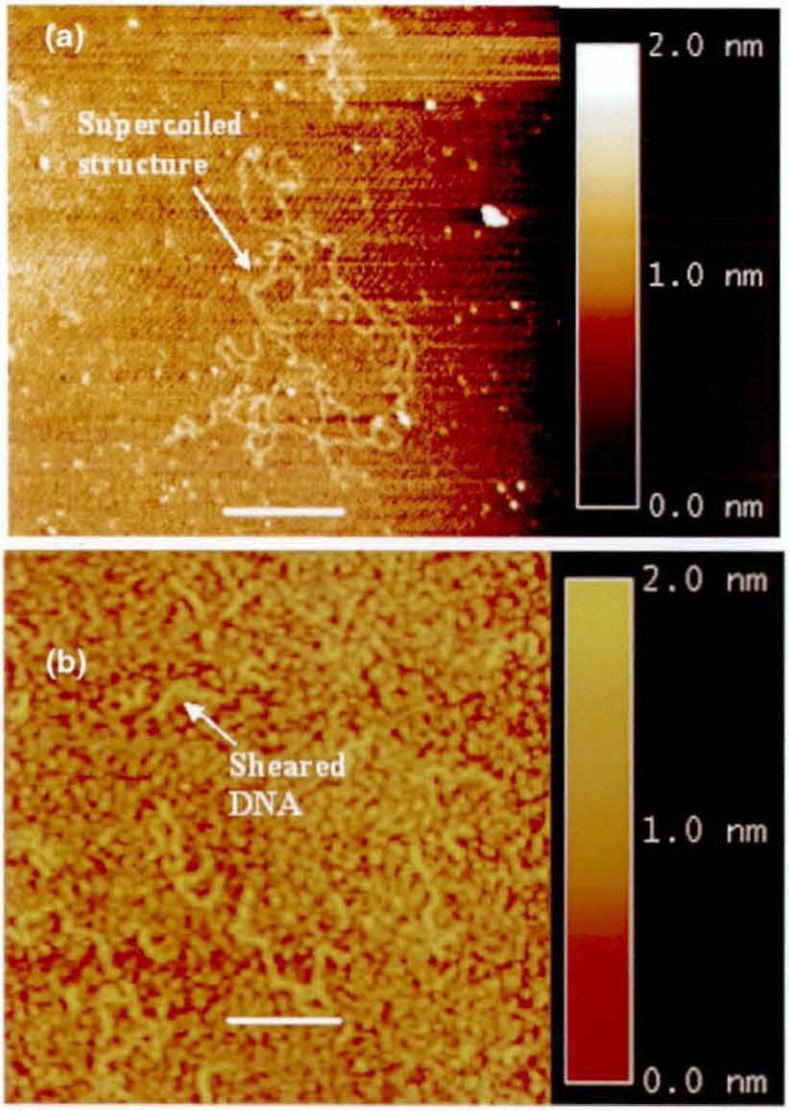

Figure 4.13: Structural analysis of sc structure of 20 kb plasmid DNA by AFM imaging in air: a) before nebulisation; b) after nebulisation showing sheared fragments of 5.7 kb, scan size of 2.5 x 2.5 μm, scale bar – 500 nm for both images.

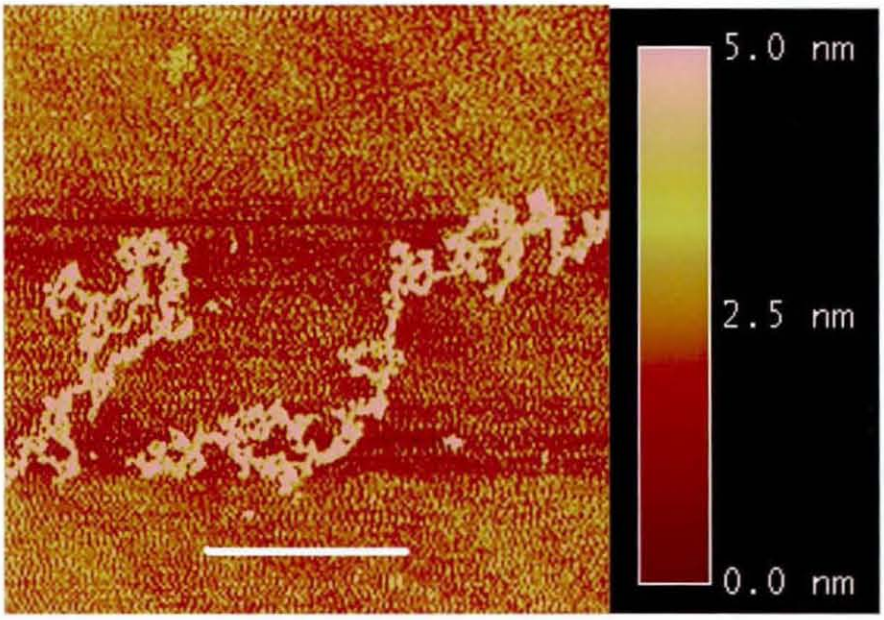

Figure 4.14: Structural analysis of sc structure of condensed 20 kb plasmid DNA; scan size of 7.5 x 7.5 μm, scale bar – 2500 nm.

From figure 4.14, a condensed 20 kb plasmid in ionic buffer exhibited a large molecular configuration possibly due to the agglomeration of two or more plasmids. Although the presence of ionic buffer resulted in a tightly twisted geometry, damage to the sc structure was observed to be the same as that without an ionic buffer as shown in Figure 4.10. A PicoGreen assay was performed to identify the damage to the sc structure of the plasmid and is discussed in the next section.

4.6.1.3 PicoGreen assay for analysis of DNA damage

PicoGreen is a fluorescent dye that selectively binds only to double-stranded DNA. Damage to the linear, oc or sc plasmid DNA after nebulisation is shown by a change in fluorescence due to differential dsDNA binding of the PicoGreen dye. The relative fluorescence of the sample is directly proportional to the concentration of double-stranded DNA (X) available to the PicoGreen dye [Georgiou and Papapostolou, 2006] and is given by equation 4.1, where k is the DNA binding constant.

$$RFU = k * X \quad \text{.....Equation 4.1}$$

The DNA binding constant (k) is determined from the slope of the RFU vs plasmid DNA concentration plots for before and after nebulisation or degradation. The DNA binding constant ratio (k_{ratio}) is determined from the ratio of k_{BN} or k_{BD} before nebulisation or degradation to k_{AN} or k_{AD} that after nebulisation or degradation and provides an insight into the extent of damage to the plasmid forms. If $k_{ratio} = 1$, there should be no degradation to the plasmid DNA sample. If $k_{ratio} > 1$, a decrease in the fluorescence after nebulisation/degradation suggests dissociation of linear double stranded (ds) DNA to single stranded (ss) DNA. If $k_{ratio} < 1$, an increase in the fluorescence after nebulisation/degradation suggests dissociation of oc/sc DNA to linear dsDNA.

Assessment of DNA damage to the plasmid forms is crucial for the ultimately successful aerosol delivery using the mesh nebuliser. It is essential to determine whether the shear to the plasmid forms observed using the agarose gel is a result of damage to the sc structure or other forms of the plasmid. Although densitometric scans from agarose gel provide valuable information on damage to the sc structure, they depend to a large extent on the migration of the different plasmid forms on the agarose gel. Besides, the differential binding of the Ethidium Bromide dye to the sc structure also suggests that the results from agarose gel can provide complimentary information on damage to the plasmid forms. However, the PicoGreen assay provides a highly sensitive approach for selective binding of the dye to dsDNA at DNA concentrations in the picogram range.

4.6.1.3.1 5.7 kb plasmid

A standard graph of fluorescence against DNA concentration for the 5.7 kb plasmid exposed to PicoGreen dye for high and low concentration range is shown in Figure 4.15. A linear relationship was observed between relative fluorescence units (RFU) and plasmid DNA concentration.

In order to understand the extent of degradation to the isoforms of 5.7 kb plasmid, the plasmid was exposed to alkaline denaturation at pH 12 and the dsDNA quantified using PicoGreen assay. As shown in Figure 4.16, a decrease in the fluorescence on exposure to alkaline pH suggested possible disintegration of the linear dsDNA plasmid

form due to alkaline denaturation. As observed from the figure, the RFU vs DNA concentration graph was observed to be linear. The ratio of the slopes of trend lines of the fluorescence vs DNA concentration plot at pH 8 to pH 12 (k_{ratio}) was found to be 1.43. A k_{ratio} value >1 suggested damage to the linear forms of the ds plasmid DNA to ssDNA.

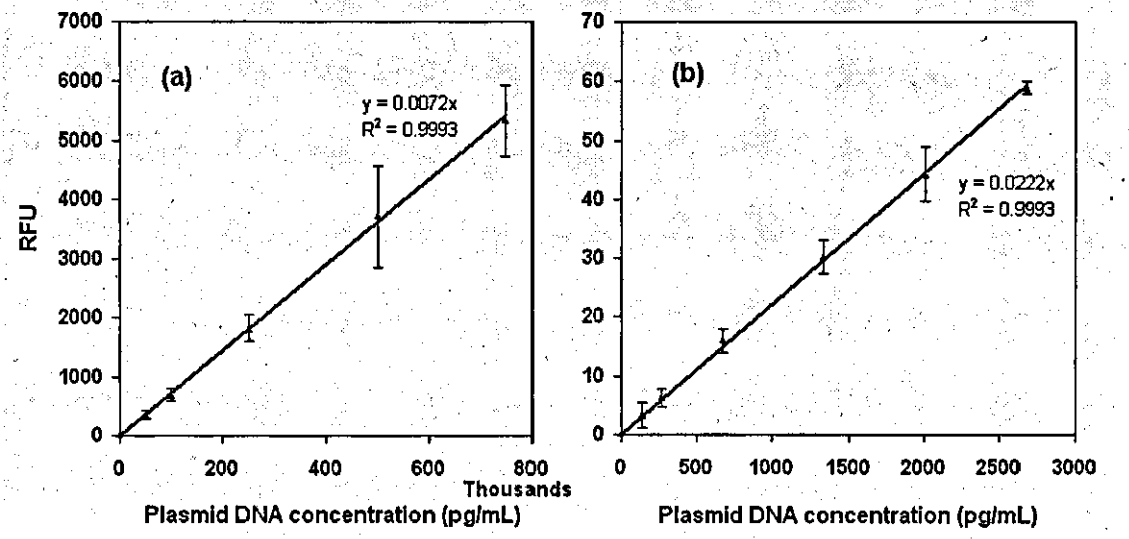

Figure 4.15: A standard DNA fluorescence graph using PicoGreen assay for 5.7 kb plasmid at a) high concentration (0-800 ng/mL), b) low concentration (0-3 ng/mL) range (n=3).

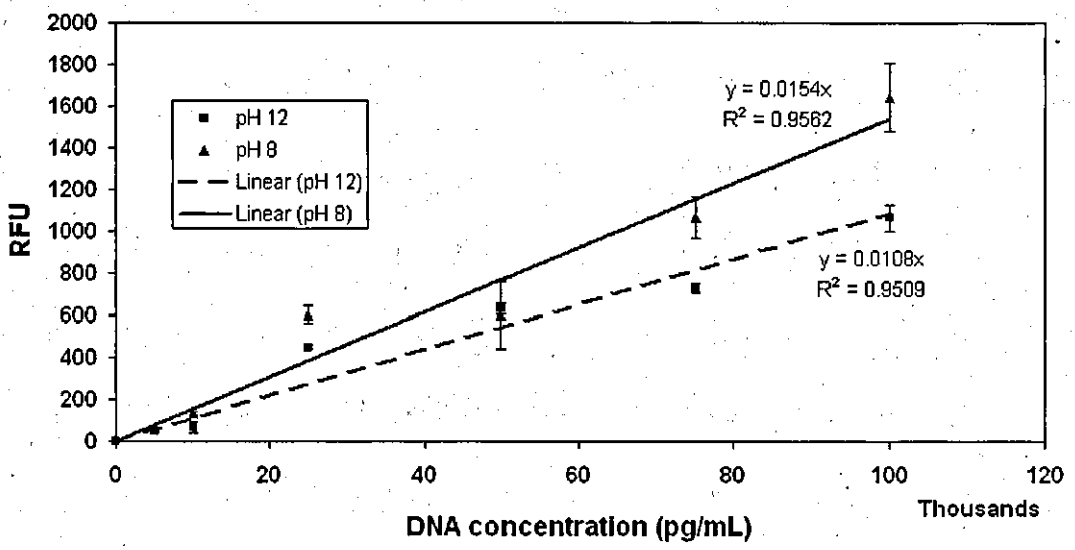

Figure 4.16: PicoGreen assay for 5.7 kb plasmid exposed to alkaline denaturation at pH 12; k_{BD} = 0.0154, k_{AD} = 0.0108, k_{ratio} = 1.43 (n=3).

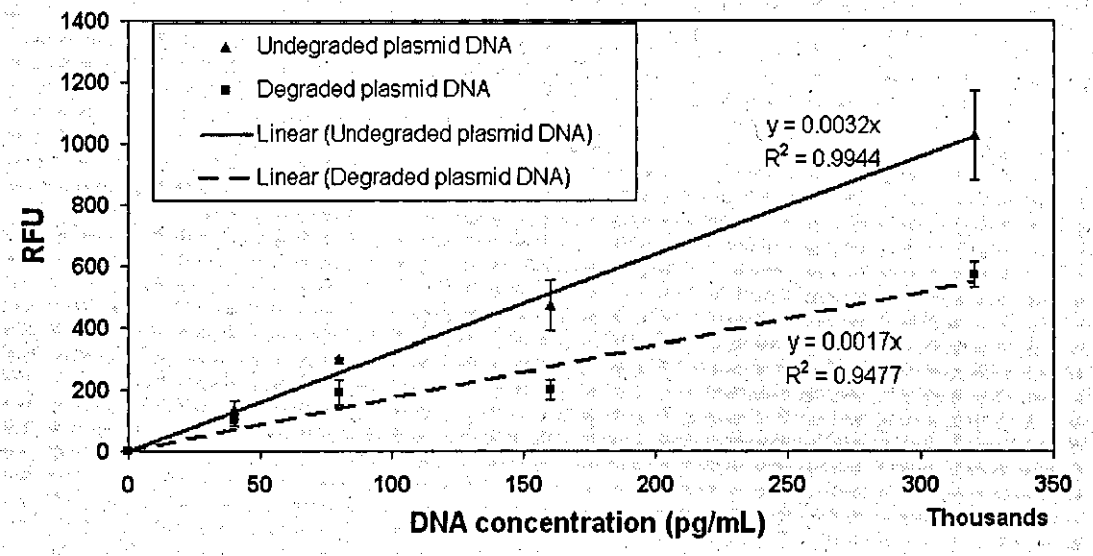

Figure 4.17: PicoGreen assay for 5.7 kb plasmid exposed to chemical degradation at 60°C for 24 hours; $k_{BD} = 0.0032$, $k_{AD} = 0.0017$, $k_{ratio} = 1.88$ (n=3).

In order to assess the extent of damage to sc structure of the 5.7 kb plasmid due to chemical degradation, a PicoGreen assay was carried out. The 5.7 kb plasmid was exposed to chemical degradation by incubating at 60°C for 24 hours. As shown in Figure 4.17, the fluorescence of the plasmid exposed to chemical degradation was lower than the undegraded plasmid, suggesting a possible degradation of the linear dsDNA to ssDNA. Consequently, k_{ratio} was found to be higher at 1.88.

Incubation of the 5.7 kb plasmid at 60°C for an additional 24 hours, led to an increased fluorescence of the degraded sample (Figure 4.18) for DNA concentrations >500 ng/mL. This increase in fluorescence of the degraded plasmid sample is a result of increased degradation to the oc and sc forms of the plasmid into linear dsDNA. The formation of linear dsDNA led to an increased binding of the fluorescent dye resulting in higher fluorescence and consequently lower k_{ratio}. The lower value of R^2 for the degraded plasmid DNA suggested that the relationship between RFU and DNA concentration was non-linear for concentrations >500 ng/mL.

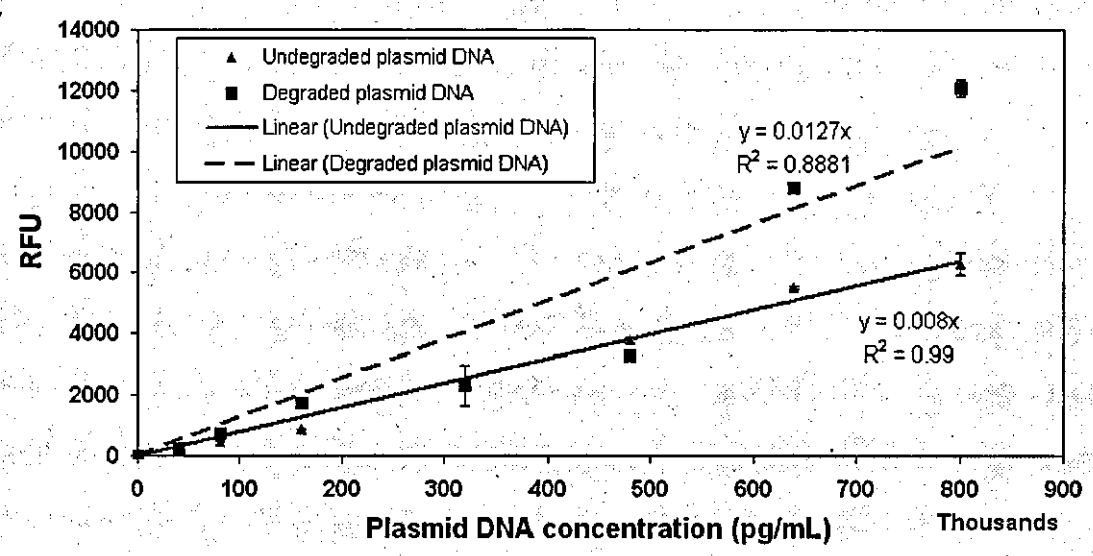

Figure 4.18: PicoGreen assay for 5.7 kb plasmid exposed to chemical degradation at 60°C for 48 hours; $k_{BD} = 0.008$, $k_{AD} = 0.0127$, $k_{ratio} = 0.63$ (n=2).

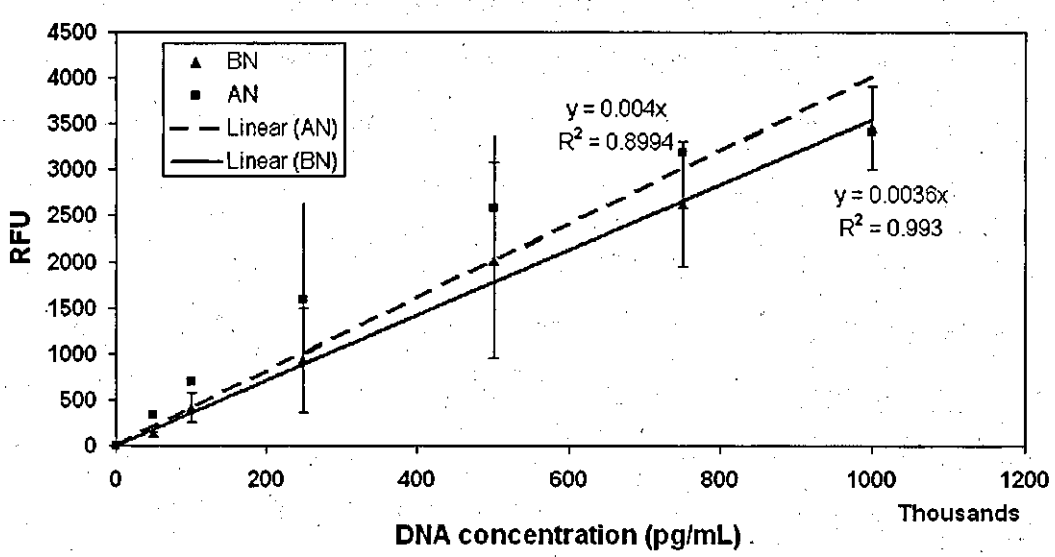

Figure 4.19: PicoGreen assay for 5.7 kb plasmid exposed to nebulisation; $k_{BN} = 0.0036$, $k_{AN} = 0.004$, $k_{ratio} = 0.9$ (n=3).

The fluorescence of 5.7 kb plasmid after nebulisation was observed to be slightly higher than before nebulisation (Figure 4.19). This is due to the increased binding of

PicoGreen dye to linear dsDNA which was formed by degradation of either the oc or sc structure of the plasmid. The binding constant ratio, k_{ratio} = 0.9, closer to unity, suggested that the linear dsDNA generated after nebulisation resulted primarily from the oc structure of the plasmid. The densitometric scans of agarose gel as shown in Figure 4.7 c confirmed the above findings that the smear of linear DNA fragments did originate from the damage to the oc structure of the plasmid. A summary of the results from the PicoGreen assay on the nebulisation/ degradation of the sc structure of the 5.7 kb plasmid are shown in Table 4.5.

Table 4.5: Summary of PicoGreen results on damage to 5.7 kb plasmid

PG assay for 5.7 kb plasmid in the range	***RFU = k*X* (X in pg/mL)**	**k_{ratio} = k_{BN}/k_{AN}**	**Inference to pDNA damage**
5.7 kb plasmid			
0 to 800 ng/mL	*Y = 0.0072*X*		pDNA standard (Figure 4.15)
0 to 3000 pg/mL	*Y = 0.0222*X*		
pDNA at pH 8			Damage to linear pDNA (Figure 4.16)
0 to 100 ng/mL	*Y = 0.0154*X*		
pDNA denaturation at pH 12			
0 to 100 ng/mL	*Y = 0.0108*X*	1.43	
pDNA (before degradation)			Damage to linear pDNA (Figure 4.17)
0 to 300 ng/mL	*Y = 0.0032*X*		
pDNA degradation (24 hours)			
0 to 300 ng/mL	*Y = 0.0017*X*	1.88	
pDNA (before degradation)			Damage to sc/oc pDNA (Figure 4.18)
0 to 800 ng/mL	Y = 0.008*X		
pDNA degradation (48 hours)			
0 to 800 ng/mL	Y = 0.0127*X	0.63	
pDNA (before nebulisation)	Y = 0.0036*X		Damage to oc pDNA (Figure 4.19)
pDNA (after nebulisation)	Y = 0.004*X	0.90	

The above results suggest that the PG assay could serve as a rapid technique to detect damage to the isoforms of the 5.7 kb plasmid during formulation and delivery as a non-viral gene therapeutic. The high sensitivity of detection with the PicoGreen dye promises efficient quantification of dsDNA in the plasmid isoforms. In the next section, nebulisation of the 8.7 kb plasmid is discussed and the results are presented.

4.6.1.3.2 20 kb plasmid

A standard graph of fluorescence versus plasmid DNA concentration for 20 kb plasmid using PicoGreen reagent was plotted as shown in Figure 4.20. A PicoGreen assay was carried out for nebulisation samples of 20 kb plasmid exposed to alkaline denaturation at pH 12 (Figure 4.21). An increase in fluorescence of the after nebulisation sample at pH 8, suggested an increase in dsDNA due to the almost complete degradation of the large sc structure. An increase in DNA concentration in the after nebulisation sample based on A_{260} measurement (Table 4.6) was confirmed with the increase in DNA concentration due to increased fluorescence. Incubation in alkaline pH of the before nebulisation and nebuliser chamber sample resulted in no significant change in fluorescence due to the non-degradation of the compact sc structure. However, incubation of the after nebulisation sample in alkaline pH resulted in decreased fluorescence due to the degradation of the linear dsDNA into ssDNA. Agarose gel electrophoresis also confirmed the almost complete degradation of the sc structure of the 20 kb plasmid on nebulisation.

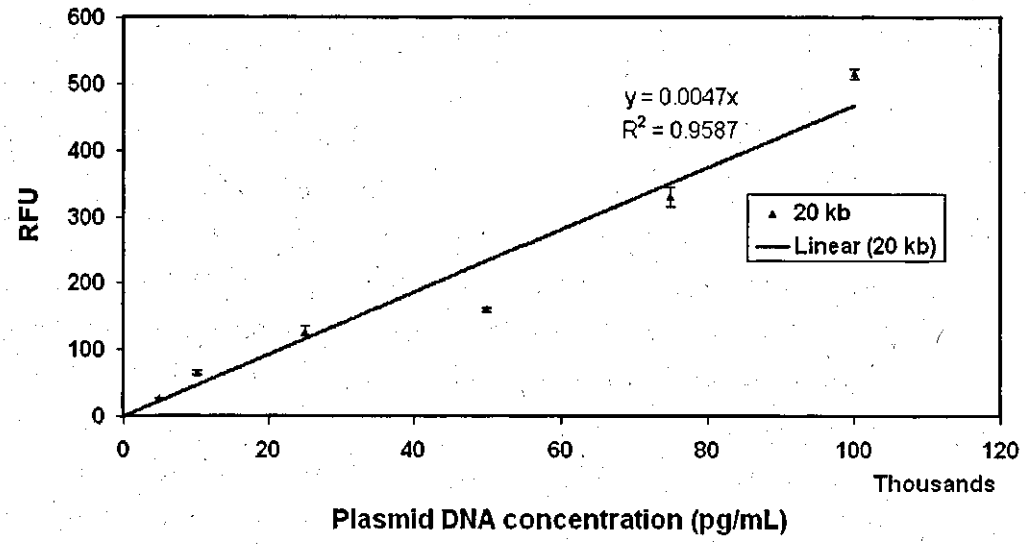

Figure 4.20: A standard graph using PG assay for a 20 kb plasmid (n=3).

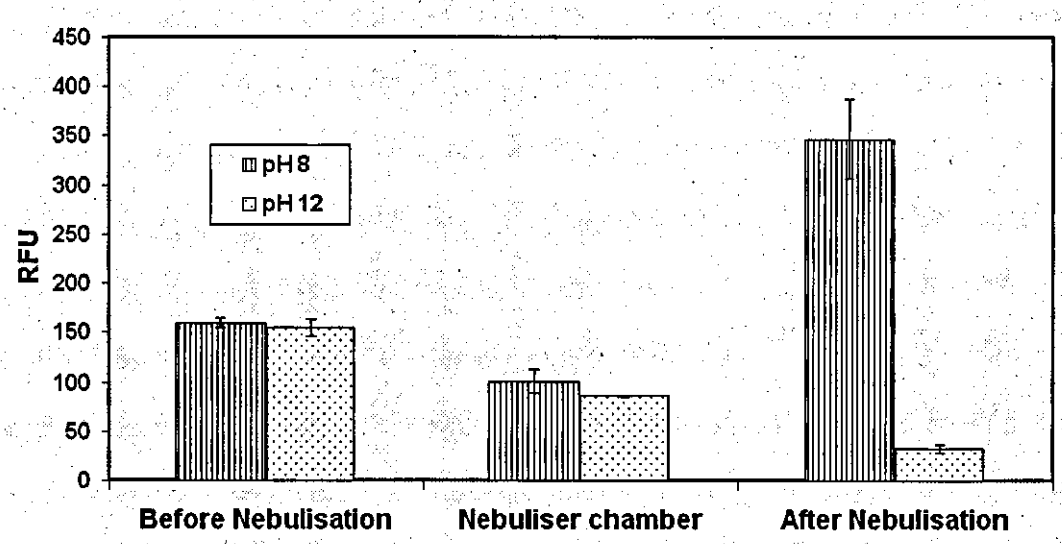

Figure 4.21: PicoGreen assay of nebulisation samples of 20 kb plasmid exposed to alkaline denaturation (n=3).

Table 4.6: Absorbance measurements of nebulisation samples of 20 kb plasmid (n=2)

20 kb plasmid sample	**A_{260}**	**A_{280}**	**A_{260}/A_{280}**	**DNA conc (μg/mL)**
Before Nebulisation (BN)	0.367 ± 0.01	0.194 ± 0.002	1.895 ± 0.082	16.13 ± 0.77
Nebuliser chamber (NC)	0.34 ± 0.029	0.165 ± 0.03	2.077 ± 0.19	15.44 ± 0.79
After Nebulisation (AN)	0.599 ± 0.18	0.324 ± 0.09	1.843 ± 0.053	26.04 ± 8.22

4.6.2 Summary of pDNA nebulisation in a U22 mesh nebuliser

Plasmids of size 5.7, 8.7, 13 and 20 kb were used for nebulisation studies in the U22 mesh nebuliser. From Table 4.7, a 5.7 kb plasmid formulated in a buffer with ionic strength due to NaCl can be nebulised with no significant damage to the sc structure. However, the sc structures of plasmids of size 8.7, 13 and 20 kb were observed to be damaged on nebulisation. The extent of damage to the sc structure for plasmids of size >5.7 kb was observed to be higher with increasing plasmid size for the experimental parameters studied here upon aerosolisation in the U22 mesh nebuliser.

Table 4.7: Summary of plasmid DNA nebulisation in a U22 mesh nebuliser

Plasmid size	**DNA concentration/ buffer conditions**	**% damage to sc plasmid DNA (n=2 minimum)**	**Tools to detect pDNA damage**
5.7 kb	DNA - 20μg/mL, TE buffer	5.52	Agarose gel electrophoresis (AGE), PicoGreen assay, Concentration based on A_{260}, Atomic force microscopy (AFM)
	DNA - 20μg/mL, TE buffer + 150mM NaCl	0.55	
	DNA - 20μg/mL, TE buffer + 300mM NaCl	0.41	
	DNA - 20μg/mL, PBS buffer	0.54	
	DNA - 20μg/mL, HEPES buffer	1.27	
8.7 kb	DNA - 20μg/mL, TE buffer	47.64	Agarose gel electrophoresis
	DNA - 20μg/mL, TE buffer + 150mM NaCl	6.45	
13 kb	DNA - 20μg/mL, TE buffer	70.68	
20 kb	DNA - 20μg/mL, TE buffer	96.15	AGE, PicoGreen assay, Concentration based on A_{260}, AFM
	DNA - 20μg/mL, TE buffer + 150mM NaCl	92.27	
	DNA - 20μg/mL, TE buffer + 300mM NaCl	96.45	

4.7 Nebulisation of plasmid DNA in a U03 mesh nebuliser

Nebulisation of 5.7, 8.7 and 20 kb plasmids were carried out in a U03 mesh nebuliser to determine the extent of damage to the sc structure. Densitometric scans of agarose gel for nebulisation samples of 5.7, 8.7 and 20 kb plasmids are shown in Figure 4.22.

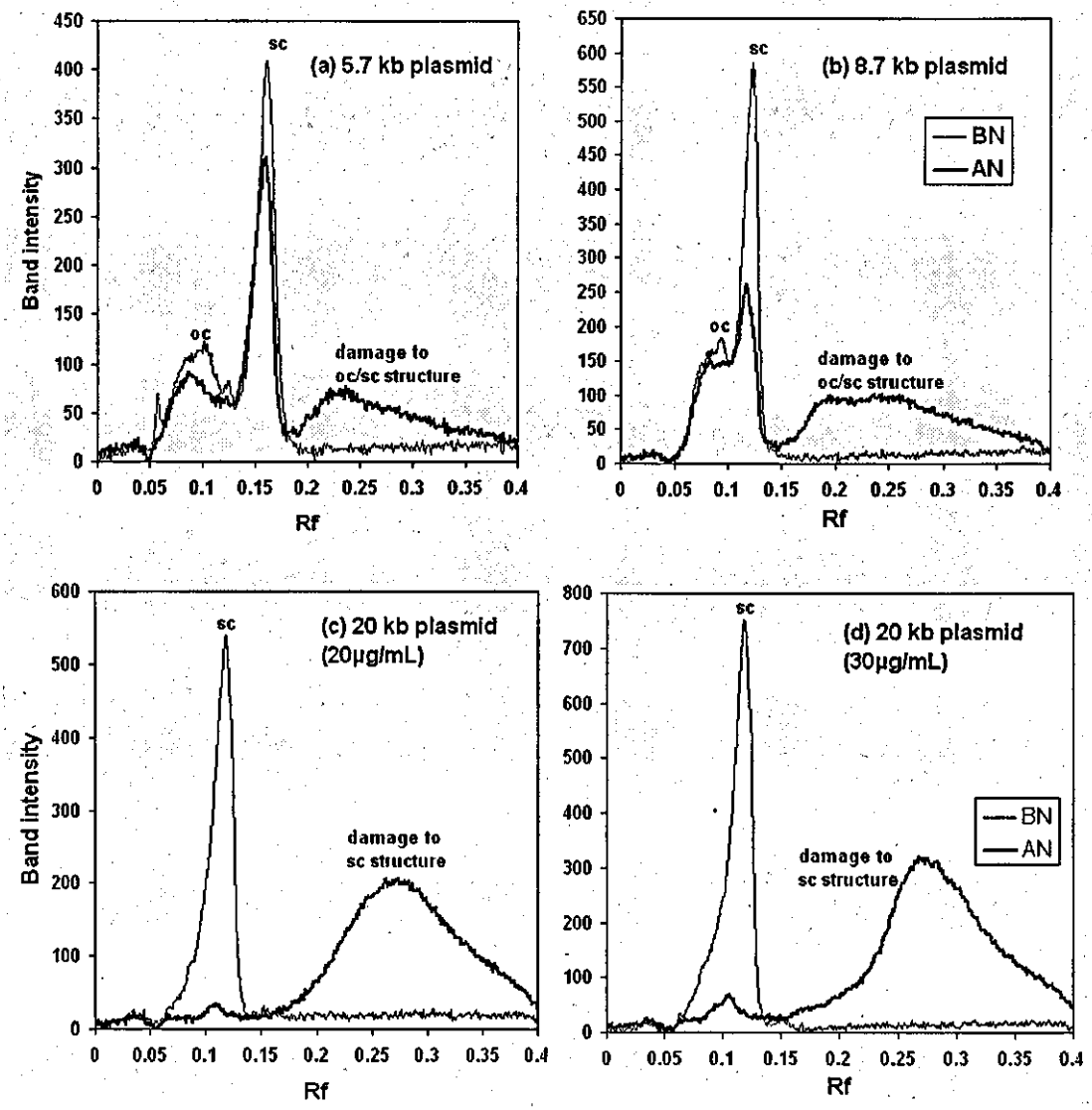

Figure 4.22: Densitometric scans of agarose gel electrophoresis of nebulisation of plasmids in U03 nebuliser: a) 5.7 kb, b) 8.7 kb, c) 20 kb (20 µg/mL), d) 20 kb (30 µg/mL); % damage to sc structure after nebulisation in a) 24.3%, b) 55.9%, c) 92.5%, d) 90.7%.

The sc structure of *all* the plasmids was observed to be damaged after nebulisation. This contrasts with the higher frequency U22 device which was able to safely deliver the 5.7 kb plasmid. The damage to the 5.7 kb plasmid in the U03 device may be due to the increased residence time of the plasmid in the nebuliser chamber.

4.8 Discussion

Studies on the quality of purified plasmid DNA shown in Figures 4.1 and 4.2 and Tables 4.1 and 4.2, suggest plasmid formulations were suitable for non-viral gene therapy. In addition to DNA homogeneity from Figures 4.1 & 4.2, the agarose gel also confirmed the absence of chromosomal DNA and RNA [Schleef, 2005]. Research in the aerosol delivery of pDNA is being pursued in many existing pulmonary devices. The emerging generation of mesh nebulisers are claimed to have greater aerosolisation efficiency, precision and consistency of drug delivery to the lungs than conventional jet or ultrasonic nebulisers [Dhand, 2003].

The characterisation of the U22 and U03 mesh nebulisers enabled determination of the nozzle size, nebulisation rate and aerosol particle size distribution. The nozzle size of 3 μm was same for the two nebulisers studied. However, the nebulisation rate for the U03 nebuliser was less than half of the U22 mesh nebuliser. This was due to the low frequency of the U03 device compared to the U22 device. Since the U22 device is available in the market, while the U03 device is an earlier version of the U22 and is not currently available, majority of the plasmid DNA nebulisation experiments were carried out using the U22 mesh nebuliser.

In order to evaluate a device for the aerosol delivery of pDNA, it is of utmost importance to check the integrity of the sc structure of the plasmid in the aerosols. Nebulisation of 5.7 kb plasmid was carried out to study the effect of aerosolisation on the integrity of sc structure of the plasmid. The 5.7 kb plasmid after nebulisation showed a smear of the open-circular structure in the aerosols, suggesting disintegration into linear fragments. The plasmid formulated in 160 mM NaCl also showed a similar degradation of the oc and linear isoforms of the sc plasmid (Figure 4.7b) in the aerosols after nebulisation. The densitometer scans corresponding to the gel (Figure 4.7d) showed that the bulk of the sc plasmid remains intact (>98%), while a major portion of the oc (30-60%) is damaged. The formulation of 5.7 kb plasmid in suitable ionic strength buffers such as PBS, HEPES was carried out to check the effect of buffer on nebulisation. As shown in Figure 4.8 and confirmed with densitometric scans of the agarose gel (data not shown), the sc structure of the plasmid was intact (<1.5% damage) after nebulisation.

The isoforms of a plasmid (linear and open-circular) are more susceptible to damage than the sc form due to their length when exposed to large hydrodynamic forces [Lengsfeld and Anchordoquy, 2002]. For instance, the multimeric forms of a 5.2 kb plasmid were observed to be degraded on plasmid purification [Chowdhury and Akaike, 2005]. Past work has also shown that the damage potential to the sc structure was observed to be greater with larger sized plasmids when using different aerosolisation devices as illustrated by Table 4.4. Attempts by Smart et al. [2002] to deliver a 4.6 kb and 11 kb plasmid using a mesh nebuliser with a vibrating membrane resulted in 50% and 90% degradation respectively to closed circular structures, and a 3 kb and 11 kb linear DNA subjected to 50% degradation upon nebulisation. It was suggested by the authors that torsional stress could be responsible for the damage to the closed circular plasmid.

AFM imaging has been reported to assess the damage to pDNA as a result of irradiation [Murakami et al., 2000]. Visualisation of the pDNA using AFM is a valuable tool to quantify the size of the plasmid and evaluate the extent of damage upon nebulisation. AFM imaging by tapping mode in air had been reported for plasmids of size 1.2 kb and 9.7 kb in order to measure the contour length [Podesta et al., 2004]. Although the exact hydrodynamic conformation of the pDNA in solution is not known, a two dimensional conformation is likely to provide a reasonable assessment of the size of such large shear sensitive sc structures. The absence of damage to sc 5.7 kb plasmid after nebulisation suggested that at a size of 330 nm (Figure 4.12b), it can easily pass through the 3 μm diameter nozzle of the mesh nebuliser with little adverse effect on the supercoiled structure. The presence of almost intact sc structure in the aerosols of the 5.7 kb plasmid indicated that the mesh nebuliser could be used for the aerosol delivery of such plasmids. Unsuccessful delivery using some nebulisers could be attributed to the different operating conditions of the device, namely vibration frequency, mesh nozzle size, etc.

Nebulisation of 8.7 kb plasmid in TE buffer and TE buffer with 150 mM NaCl using U22 mesh nebuliser resulted in damage to the sc structure. As shown in Figure 4.6, sc structure of the plasmid in TE buffer was partially damaged (45% damage), while in TE buffer with 150 mM NaCl damage was marginal (6.5% damage). Condensation of the sc structure of 8.7 kb plasmid in buffer with ionic strength protected the fragile

structure from significant damage. Aerosolisation of a larger plasmid of size 20 kb using the same nebuliser resulted in fragmentation of the sc structure (>90%) of the naked 20 kb plasmid in the aerosols after nebulisation (Table 4.7). However, absence of damage to the sc structure in the nebuliser chamber and damage in the aerosols suggested shear experienced during aerosol formation from the mesh nebuliser as the cause of the fragmentation. The size distribution of the DNA fragments in the aerosols ranging from about 5 to 0.5 kb (Figure 4.11) was possibly due to the effects of high hydrodynamic forces, similar to that experienced when DNA was subjected to hydrodynamic shear using a Point-sink Shearer device [Thorstenson et al., 1998]. This device uses a syringe pump to create hydrodynamic shear forces by pushing a DNA sample through a small abrupt contraction, to generate short linear fragments for DNA sequencing. The DNA fragments generated were in a tight size range with the size of the largest fragments to be twice as that of the smallest. The size distribution of the fragments observed after nebulisation of the 20 kb plasmid in the aerosols also resulted in a similar distribution. Although sc plasmid DNA in higher ionic strength buffers has been reported to have a tightly twisted geometry [Levy et al., 1999], it was ineffective in withstanding the shearing effects of aerosolisation as observed in the results.

Naked supercoiled 20 kb plasmid in a two-dimensional conformation was found by AFM imaging to have a molecular length of 1250 nm, which is almost half the nozzle size for the devices under study. This suggested that the plasmid would be highly susceptible to the forces associated with its passage through the nozzles of the nebuliser mesh. Ionic strength due to NaCl resulted in a more condensed structure to the plasmid [Lyubchenko and Shylakhtenko, 1997]. AFM imaging of the condensed sc plasmid in NaCl showed evidence of a larger molecular size (Figure 4.14) possibly resulting from the agglomeration of two or more sc structures. Hence, nebulisation produced destruction of the sc structure into spaghetti-like fragments shown in Figure 4.13b. This may have been accompanied by the size of the plasmid molecule and release of torsional strain from the sc structure of the plasmid.

To assess the extent of degradation to the isoforms of 5.7 kb plasmid, a fluorescence based assay was performed using PicoGreen reagent for double-stranded DNA quantification. Levy et al. [2000] have reported the quantification of sc content in plasmid DNA solutions using a fluorescence-based method. The linear concentration

range for DNA quantification extends over four orders of magnitude - 25 pg/mL to 1 μg/mL, with a single dye concentration [Singer et al., 1997]. A linear standard graph of relative fluorescence units versus DNA concentration was obtained for high and low concentration ranges of 5.7 kb plasmid (Figure 4.15). In order to understand the damage to the plasmid isoforms, the 5.7 kb plasmid was exposed to (i) alkaline denaturation (pH 12) and (ii) chemical degradation (60°C for 24 and 48 hours), and the double-stranded DNA quantified using PG assay. From Figure 4.16, the decrease in fluorescence at alkaline pH is due to degradation of the isoforms of linear dsDNA into ssDNA. The binding constant (k) is dependent on the dsDNA concentration available for the PicoGreen dye. Based on the ratio of the binding constant (k_{ratio}) before and after alkaline denaturation, it is possible to infer whether damage to the isoforms of plasmid is due to linear or oc/sc isoforms. Alkaline denaturation of the 5.7 kb plasmid with a k_{ratio} of 1.43, suggested damage is predominantly due to linear isoforms. Under controlled alkaline conditions, the degree of denaturation of dsDNA molecules is known to increase with increasing number of breaks and alkaline labile sites (i.e. depurinated sites) [Rock et al., 2003]. Chemical degradation (24 hours incubation) of the 5.7 kb plasmid resulted in a similar damage with a k_{ratio} of 1.88 (Figure 4.17). However, chemical degradation for 48 hours resulted in an increased fluorescence and low k_{ratio} (0.63) as shown in Figure 4.18, possibly due to the predominant damage of oc/sc dsDNA into linear dsDNA. A slight increase in fluorescence and a k_{ratio} close to 1 (0.9) for the after nebulisation sample of 5.7 kb plasmid (Figure 4.19), suggested possible damage to the oc dsDNA, as confirmed by agarose gel electrophoresis (Figure 4.7).

A linear standard graph of fluorescence versus DNA concentration based on PicoGreen assay for 20 kb plasmid is shown in Figure 4.20. A PicoGreen assay of alkaline denaturation of the nebulisation samples of 20 kb plasmid (Figure 4.21) showed no increase in fluorescence confirming no damage to the sc structure in the nebuliser chamber as also evident from agarose gel electrophoresis. However, an increase in fluorescence of the after nebulisation sample suggested damage to the sc structure due to the formation of linear dsDNA. Alkaline denaturation of the after nebulisation sample resulted in decreased fluorescence possibly due to the damage of linear dsDNA leading to ssDNA. This shows that the PicoGreen assay could serve as a useful technique for quick assessment of damage to plasmid DNA during nebulisation.

Absorbance measurements at 260 nm as shown in Table 4.6 revealed a higher DNA concentration in after nebulisation sample, resulting from degradation of the sc structure into linear DNA fragments.

The U03 mesh nebuliser operating at a lower frequency was chosen to investigate the extent of damage to the sc structure of plasmid DNA due to the driving force for aerosolisation. Nebulisation of plasmids of size 5.7, 8.7 and 20 kb using the U03 nebuliser showed significant damage to the sc structure (Figure 4.22). The damage to the sc structure of the 5.7 kb plasmid using the U03 device may be due to the increased residence time in the device. The aerosol droplet size generated during ultrasonic atomization is reported to be inversely proportional to the device frequency [Yule and Al-Suleimani, 1999]. The larger droplet size due to the lower frequency of the U03 device may have resulted in the generation of high shear forces near the nozzle exit also leading to damage of the sc structure of the 5.7 kb plasmid.

4.9 Conclusion

Purification of plasmid DNA in its supercoiled form from recombinant *Escherichia coli* cells as per the specifications for gene therapeutics is crucial for its application in non-viral gene therapy clinical trials. Aerosol delivery of plasmid DNA has potential applications for the treatment of acute respiratory diseases such as cystic fibrosis, influenza and SARs. Here typical plasmids of size from 5.7 to 20 kb were purified in the supercoiled form and the formulations of plasmid DNA aerosolised using a commercially available, clinically approved U22 mesh nebuliser. In order to facilitate quick adoption of a potential plasmid DNA based genetic drug, the U22 mesh nebuliser was chosen for this research investigation. Nebulisation of the 5.7 kb plasmid resulted in safe aerosol delivery of the sc structure. However, damage to the oc structure of the 5.7 kb plasmid and sc structure of 8.7, 13 and 20 kb plasmids were detected using gel electrophoresis, atomic force microscopy and the PicoGreen assay using the U22 mesh nebuliser. Safe delivery of sc structure of the 5.7 kb plasmid using the U22 mesh nebuliser suggested that damage is dependent on the size of the molecular sc structure. Further experiments based on a DOE to predict the influence of nozzle size, ionic and DNA concentrations on damage to the sc structure of the 20 kb

plasmid were attempted to provide valuable information for formulation of the 20 kb plasmid. The experimental design adopted for the DOE and the results are reported in the next chapter.

CHAPTER 5. NEBULISATION OF PLASMID DNA: DESIGN OF EXPERIMENTS

5.1 Introduction to Design of Experiments (DOE)

The aim of the design of experiments (DOE) was to study the influence of formulation and device factors on damage to the sc structure of 20 kb plasmid upon nebulisation and predict a relationship between the response and variables. A design of experiments based on the response surface method (RSM) was adopted to investigate the significant variables affecting delivery of 20 kb plasmid using the U22 mesh nebuliser. The RSM is used when only a few significant factors are involved in the optimisation [Ragonese et al., 2002]. RSM is a collection of statistical and mathematical techniques useful for developing, improving, and optimizing processes, based on a graphical perspective of the problem environment [Myers & Montgomery, 2002].

A response surface is the geometric representation obtained when a response variable is plotted as a function of one or more quantitative factors, while a contour plot is a series of lines or curves that identify values of the factors for which the response is constant [Mason et al., 2003]. The experimental design adopted for the RSM optimization was Box-Behnken design. A Box-Behnken design is an independent, rotatable or nearly rotatable quadratic design, in which the experimental combinations are at the midpoints of the edges of the process space and at the centre [Box and Behnken, 1960; Zidan et al., 2007; Ferreira et al., 2007]. Box-Behnken design can be used when performing non-sequential experiments and allow efficient estimation of the first- and second-order coefficients. In addition, Box-Behnken designs have fewer design points than central composite designs for the same number of factors and ensure all factors are never set at their high levels simultaneously [Design-Expert Manual, Stat-Ease Inc., USA].

5.2 Nebulisation of 20 kb plasmid – Response surface method

As observed in Chapter 4, the size of the 20 kb plasmid is of the order of a nozzle size, and significant damage to plasmids of increasing size, suggested nozzle size as an important variable for further experimentation. Since the size of the plasmid DNA can be condensed in the presence of ionic salts such as NaCl, DNA and NaCl concentrations were chosen as the other two variables to study the effect of interaction on damage to plasmid DNA. The main objective of this chapter is to discuss the effect of chosen variables such as nozzle size, DNA concentration and NaCl concentration on damage to the sc structure of 20 kb plasmid upon nebulisation based on a three-dimensional optimization using the DoE approach.

Nebulisation of 20 kb plasmid in the U22 mesh nebuliser was carried out based on the experimental design involving chosen variables and levels as discussed in section 5.1.1 below. The response identified was percentage damage to the sc structure of the plasmid after nebulisation, quantified using densitometric scans of the agarose gel. The densitometric scan measurements were obtained from two or more agarose gels, and the average value used as an actual response to determine the response function using Design-Expert® software.

5.2.1 Choice of variables and levels

Nebulisation experiments in Chapter 4 enabled identification of the key variables influencing damage to the sc structure of the plasmid. Nebulisation of different sized plasmids showed maximum damage to the sc structure of the 20 kb plasmid with the standard 3 μm nozzle of U22 mesh nebuliser. The safe delivery of the 5.7 kb plasmid using the same device and nozzle size suggested damage could be dependent on the relative size of the plasmid compared with the mesh nozzle. Hence, nebulisation of 20 kb plasmid at mesh nozzle sizes of 4 and 5 μm (provided by Omron Healthcare, Japan) was attempted to study the effect of nozzle size on damage to the sc structure. The plasmid DNA concentration reported to be used for transfection studies [Tachibana et al., 2002] was 20 μg/mL. DNA concentrations of 10, 20 and 30 μg/mL were therefore chosen for the study, in order to investigate their influence on damage to the sc structure after nebulisation. In order to understand the effect of ionic concentration on

pDNA formulations in ionic buffer and its impact on pDNA damage, the concentration levels used for the experimental design were 0, 150 and 300 mM NaCl. The variables and levels chosen for the experimental design are summarised in Table 5.1.

Table 5.1: Variables and levels chosen for experimental design

Variables	**Levels**		
	-	**0**	**+**
Nozzle size (μm)	3.0	4.0	5.0
DNA concentration (μg/mL)	10	20	30
NaCl concentration (mM)	0	150	300

5.2.2 Experimental design

The experimental design chosen for the response surface method was a Box-Behnken design. Box-Behnken design has the advantage of performing limited experimental runs (12 + 3 centre points) compared to a full factorial design ($3^3 = 27$) for a three variable experimental design with three evenly spaced levels. The experimental design with the levels of the variables and response of % damage to the sc structure from average values of densitometric scans of agarose gels is shown in Table 5.2.

The statistical analysis, diagnostic plots, contour plots and response surface plots were used for choosing the model, checking the adequacy and interpreting the response.

Table 5.2: Box-Behnken experimental design and experimental response

Run	Nozzle size X_{nozzle} (µm)	DNA conc C_{DNA} (µg/mL)	NaCl conc C_{NaCl} (mM)	Experimental Response* (% damage to sc structure)
1	4	20	150	28.00
2	4	10	0	45.94
3	4	10	300	18.16
4	5	10	150	30.11
5	3	10	150	95.96
6	4	20	150	21.74
7	5	30	150	23.28
8	5	20	300	22.95
9	3	20	0	96.36
10	4	30	0	35.75
11	3	20	300	93.57
12	4	20	150	28.67
13	4	30	300	29.91
14	3	30	150	98.18
15	5	20	0	30.38

* - (n=3) Average measurements from densitometer scans of triplicate gels.

5.2.3 Statistical analysis of Box-Behnken design

The results of the Box-Behnken design using Design-Expert® 7.2 (Stat-Ease, Inc., Minneapolis, USA) software are reported. The statistical analysis of the model is shown in Tables 5.3, 5.4 and 5.5. Statistical analysis based on 'Sequential Model Sum of Squares' (SMSS) as shown in Table 5.3 compares the three models: linear, 2FI (Two factor interaction) and quadratic. The table suggests that the linear and quadratic models are significant, since the p-value is <0.05. However, the lack of fit tests shown

in Table 5.4 suggests that the quadratic model fits well compared to the linear model, as evident from the insignificance of lack of fit tests. The insignificance of lack of fit is good since the objective of the model is to fit the response.

Table 5.3: Statistical analysis of Box-Behnken design based on SMSS

Source	Sum of squares	Degrees of freedom (df)	Mean square	F value	p-value (Prob >F)	Significance
Linear	9856.78	3	3285.59	8.95	0.0018	
2FI	146.20	3	48.73	0.11	0.9551	
Quadratic	4521.27	3	1507.09	100.31	<0.0001	Significant

Table 5.4: Lack of Fit Tests for Box-Behnken design

Source	Sum of squares	df	Mean square	F value	p-value	Significance
Linear	4742.82	9	526.98	70.69	0.0005	
2FI	4596.62	6	766.10	102.77	0.0002	
Quadratic	75.36	3	25.12	3.37	0.1356	Insignificant

Table 5.5: Model summary statistics for Box-Behnken design

Source	Standard deviation	R^2	Adjusted R^2	Predicted R^2	PRESS	Suggestions
Linear	19.16	0.6738	0.5985	0.4256	8402.48	
2FI	21.51	0.6838	0.4940	-0.1736	17168.70	
Quadratic	3.88	0.9928	0.9836	0.9144	1252.29	Significant

PRESS – Predicted Residual Sum of Squares

Table 5.5 provides the overall summary of the model statistics and indicates that the coefficient of determination R^2 and adjusted R^2 values for the quadratic model agree well, suggesting good predictability (Predicted R^2) of the response function.

The ANOVA for the response surface quadratic model is given in Table 5.6.

Table 5.6: Analysis of Variance (ANOVA)

Source	Sum of squares	df	Mean square	F value	p-value	Suggestions
Model	14524.25	9	1613.81	107.41	<0.0001	Significant
X_{nozzle} - Nozzle size	9615.38	1	9615.38	639.96	<0.0001	Significant
C_{DNA} – DNA conc	1.16	1	1.16	0.077	0.7889	
C_{NaCl} – NaCl conc	240.24	1	240.24	15.99	0.0052	Significant
X_{nozzle}* C_{DNA}	20.48	1	20.48	1.36	0.2813	
X_{nozzle}* C_{NaCl}	5.38	1	5.38	0.36	0.5683	
C_{DNA}* C_{NaCl}	120.34	1	120.34	8.01	0.0254	Significant
X_{nozzle}* X_{nozzle}	4314.21	1	4314.21	287.14	<0.0001	Significant
C_{DNA} * C_{DNA}	55.63	1	55.63	3.70	0.0957	
C_{NaCl} * C_{NaCl}	27.75	1	27.75	1.85	0.2163	
Residual	105.17	7	15.02			
Lack of Fit	75.36	3	25.12	3.37	0.1356	Insignificant
Pure Error	29.82	4	7.45			
Cor Total	14629.42	16				

Table 5.6 implies that the Model F-value of 107.41 is significant, with only 0.01% chance that a "Model F-value" this large could occur due to noise. The significant variables of the model were nozzle size (X_{nozzle}), NaCl concentration (C_{NaCl}) and the interaction between DNA and NaCl concentration (C_{DNA}*C_{NaCl}). The model equation used to predict the damage to sc structure of the 20 kb plasmid is given by the

quadratic polynomial equation shown below, with the nozzle size in μm, DNA concentration in μg/mL and NaCl concentration in mM.

$$Damage_{sc} = +688.647 - (285.062 * X_{nozzle}) - (1.135 * C_{DNA}) - (0.113 * C_{NaCl}) - (0.226 * X_{nozzle} * C_{DNA}) - (7.733E\text{-}3 * X_{nozzle} * C_{NaCl}) + (3.656E\text{-}3 * C_{DNA} * C_{NaCl}) + (32.009 * X_{nozzle}^2) + (0.036 * C_{DNA}^2) + (1.141E\text{-}4 * C_{NaCl}^2) \quad \text{Equation (5.1)}$$

The next section will analyse the diagnostic plots to check the adequacy of the model.

5.2.4 Model Diagnostic plots

The normal probability plot shown in Figure 5.1a indicated that the residuals followed a normal distribution, which indicated that the model satisfied the assumptions of the analysis of variance. The predicted versus actual response values shown in Figure 5.1b showed good correlation as confirmed by the predicted R^2 = 0.9144 (Table 5.5).

5.2.5 Model predictions: Contour and Response surface plots

The model predictions for all three levels of the three variables were studied in order to check the relevance of the model predictions and derive useful information from the contour and response surface plots generated using Design-Expert 7.2.

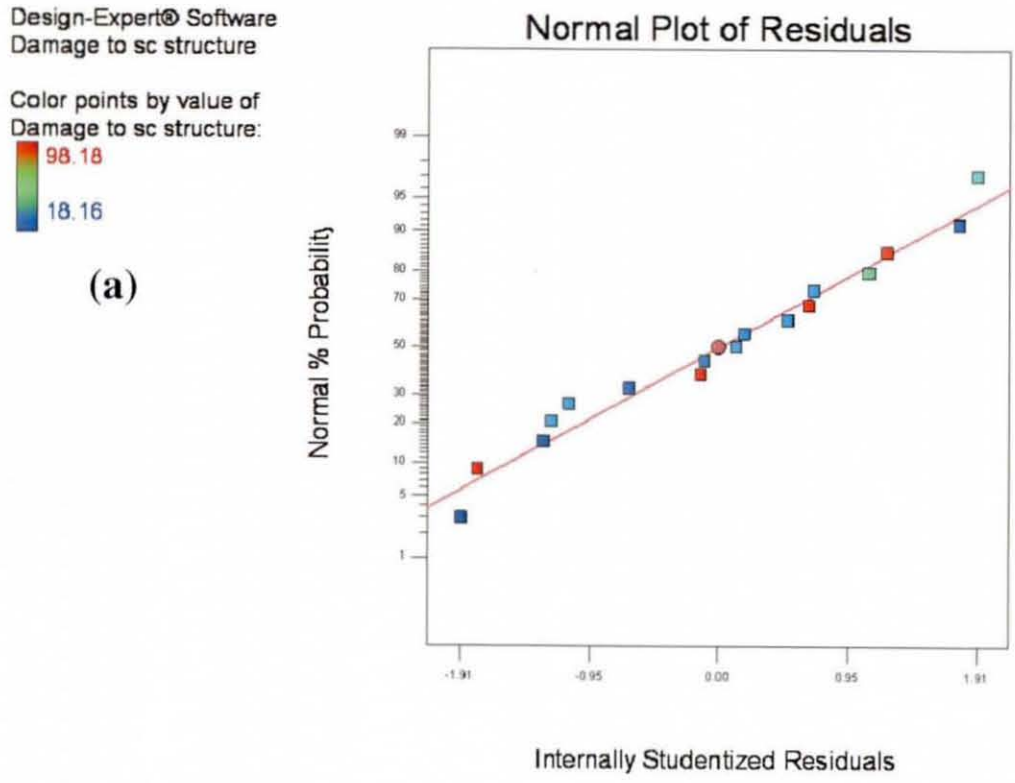

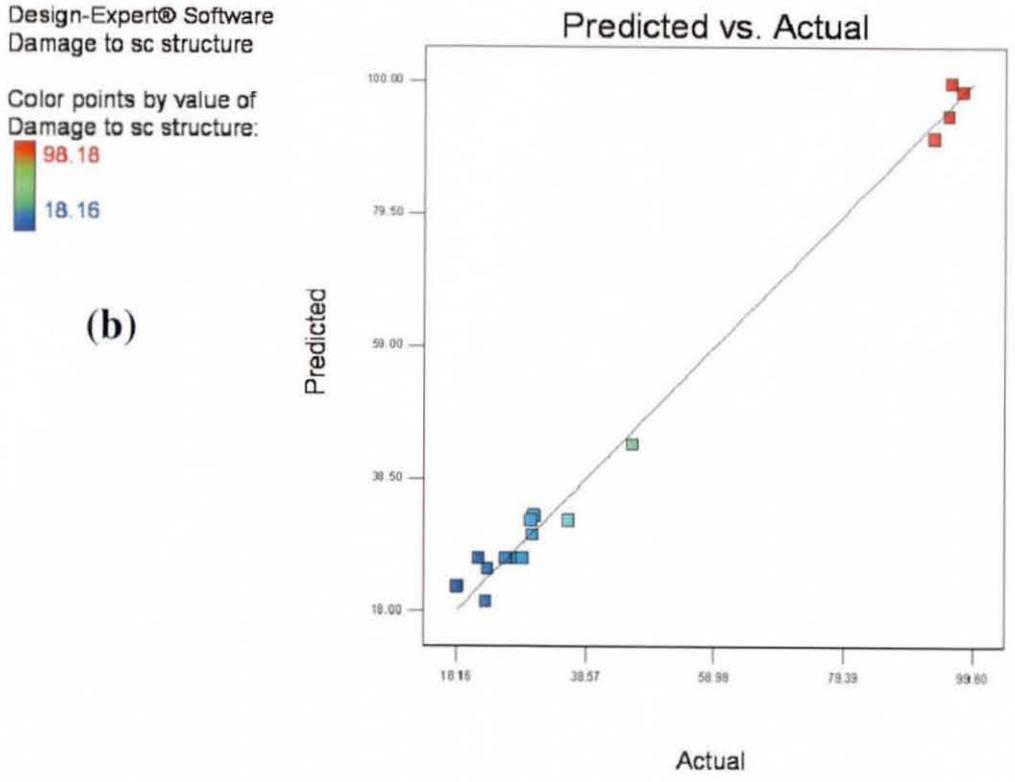

Figure 5.1: Diagnostic plot: a) Normal probability; b) Actual versus Predicted response.

5.2.5.1 Effect of Nozzle size

5.2.5.1.1 Nozzle size 3 μm

As shown in Figure 5.2, the sc structure of the 20 kb plasmid is predicted to be damaged (> 85%) on nebulisation with 3 μm nozzle of the mesh nebuliser. Maximum damage (>95%) to the sc structure was observed up to DNA and NaCl concentrations of 15 μg/mL and 100 mM respectively. Condensation of the sc structure with NaCl, resulted in 85-90% damage at NaCl and DNA concentrations >200 mM and <20 μg/mL respectively. However, at DNA concentrations >25 μg/mL damage to the sc structure was more pronounced due to inefficient condensation in limiting concentrations of the ionic buffer.

5.2.5.1.2 Nozzle size 4 μm

Damage to sc structure of the 20 kb plasmid was significantly lower than that in the 3 μm nozzle (Figure 5.3), possibly due to increased nozzle size. Damage levels of 30-40% were predicted with an ionic concentration less than 150 mM and DNA concentrations less than 20 μg/mL. However, at >150 mM NaCl and 20-25 μg/mL DNA concentrations, damage was predicted to be minimum, possibly due to the effective condensation of sc structure at high ionic strength. At DNA concentration 30 μg/mL, damage was marginally higher due to inefficient condensation of the sc structure.

5.2.5.1.3 Nozzle size 5 μm

Damage to sc structure of the 20 kb plasmid (Figure 5.4) was similar to the 4 μm nozzle. As observed in Figure 5.4, damage levels of around 25-40 % were observed with ionic concentration <200 mM NaCl and DNA concentration up to 30 μg/mL. These predicted damage levels compared to the 4 μm nozzle are probably lower due to the increased nozzle diameter. However, at NaCl concentrations >200 mM, damage to sc structure was predicted to be <25%. This is probably due to the effective condensation of sc structure to a molecular size leading to less damage when passing through the 5 μm nozzle.

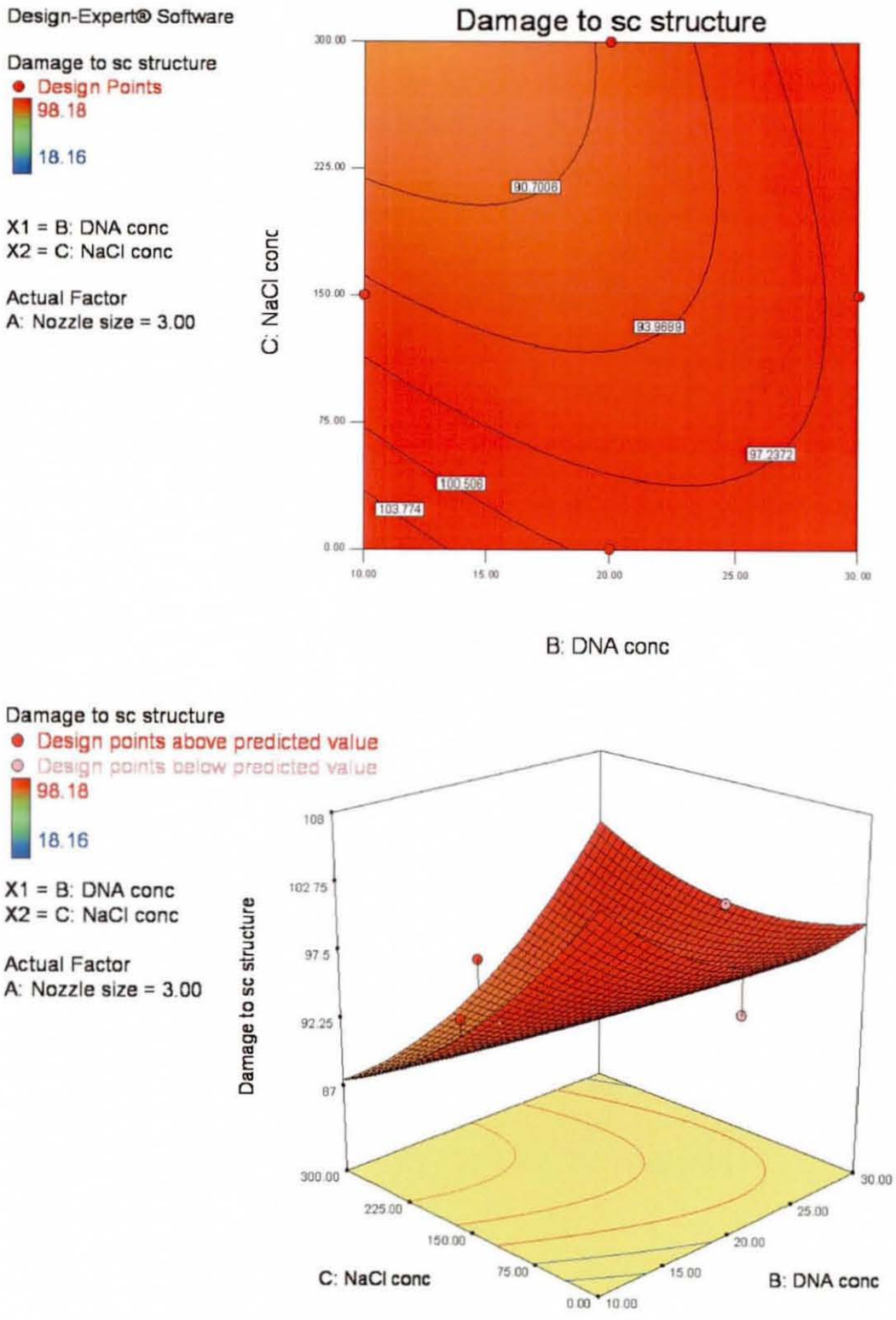

Figure 5.2: Response surface contour and 3D plots of the effect of 3 μm nozzle on damage to the sc structure of 20 kb plasmid

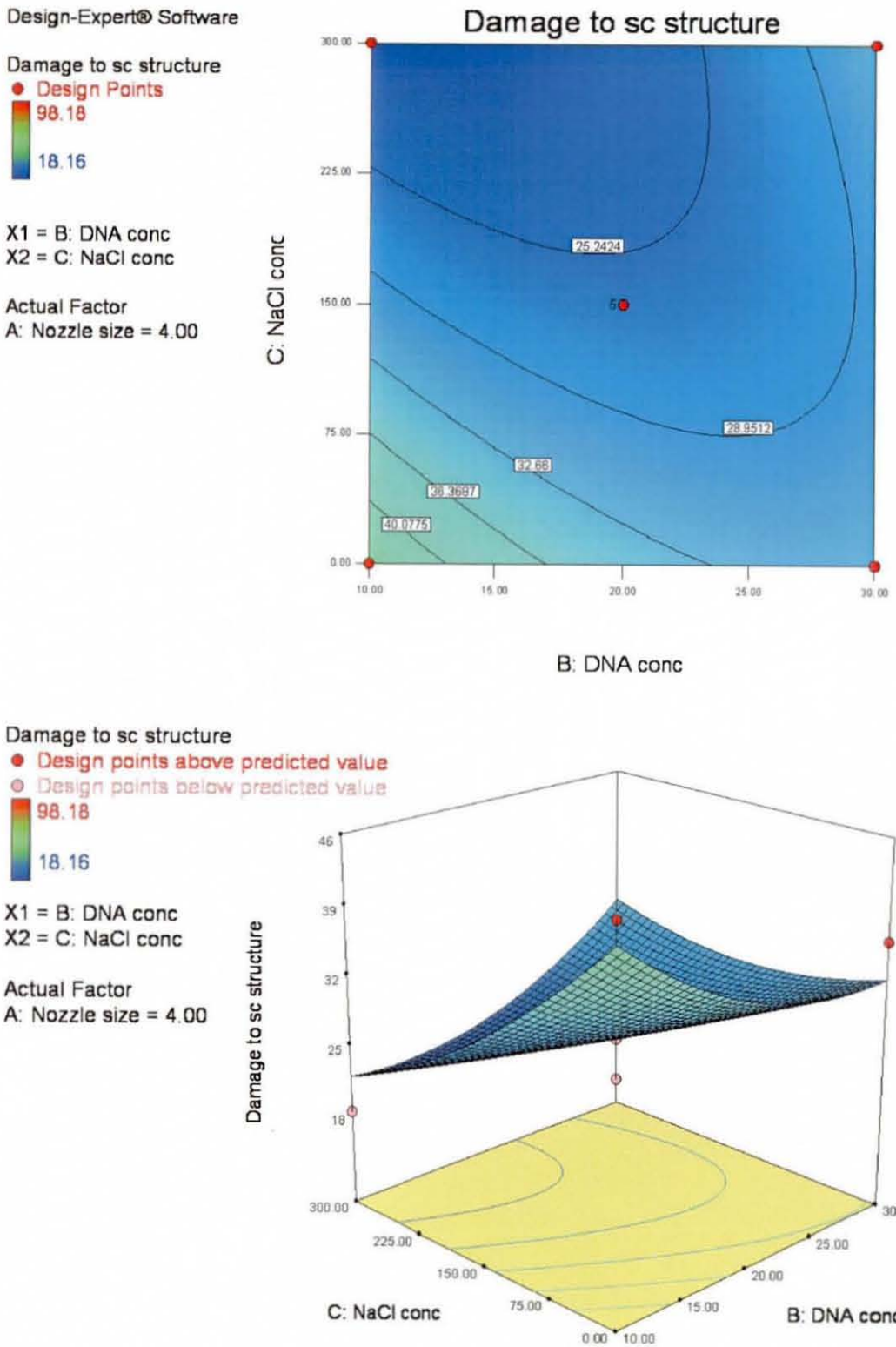

Figure 5.3: Response surface contour and 3D plots of the effect of 4 μm nozzle size on the damage to the sc structure of 20 kb plasmid

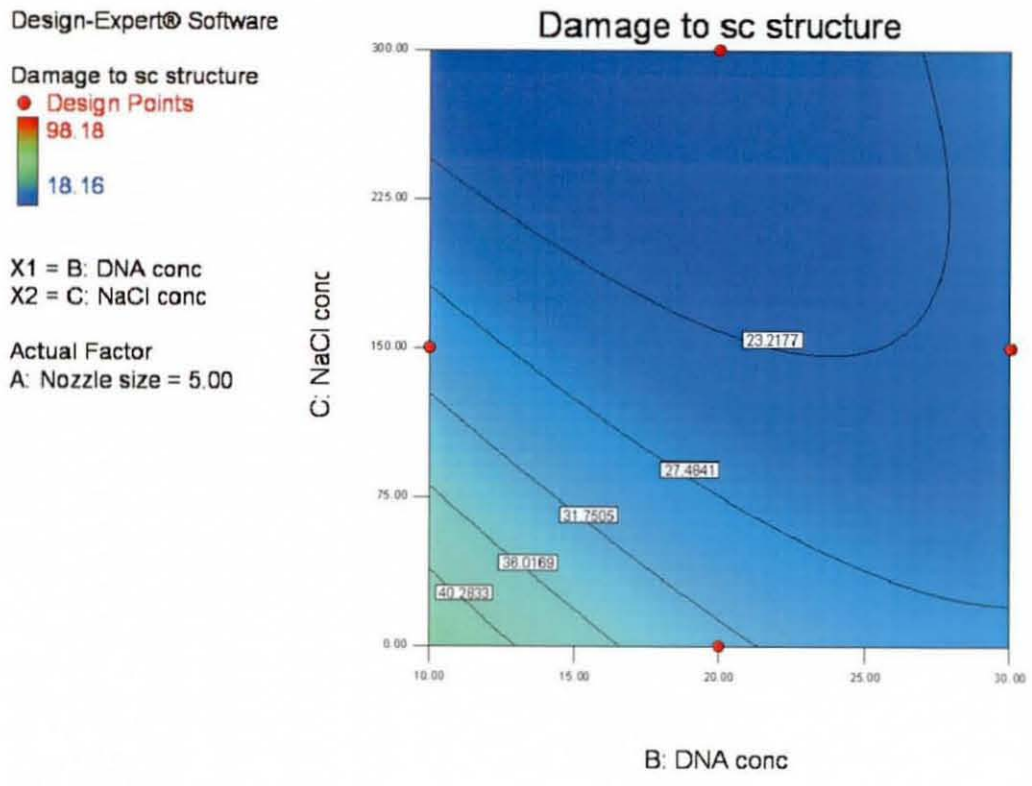

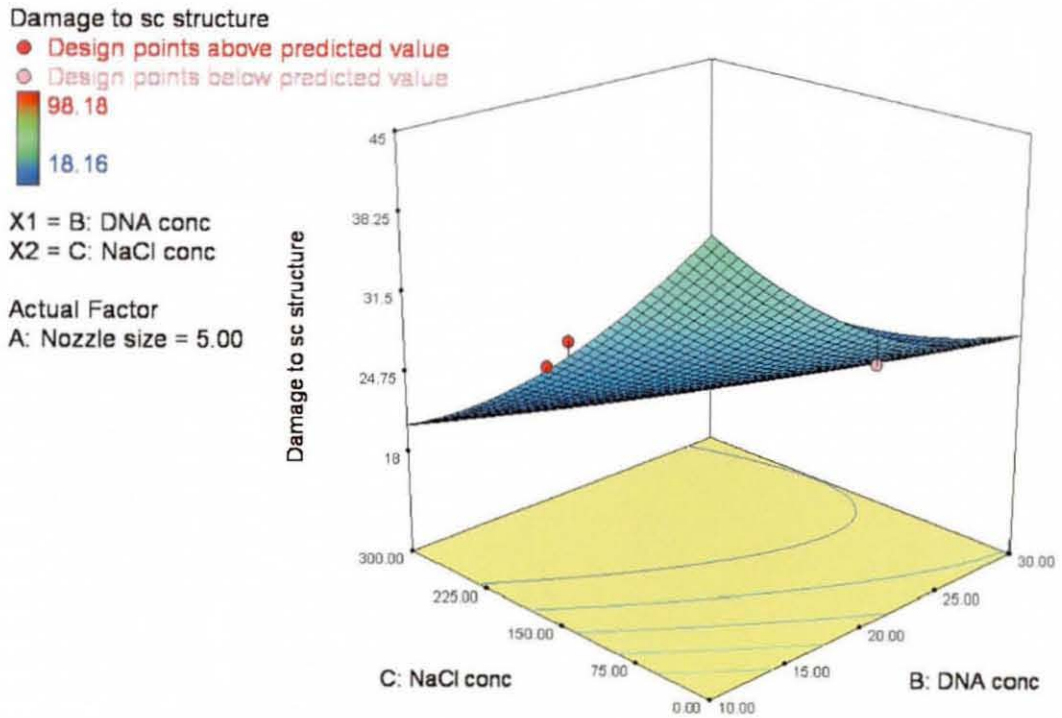

Figure 5.4: Response surface contour and 3D plots of the effect of 5 μm nozzle size on damage to the sc structure of 20 kb plasmid.

5.2.5.2 Effect of DNA concentration

The effect of DNA concentration on the damage to the sc structure was studied in the predicted contour and response surface plots as shown below.

5.2.5.2.1 DNA concentration 10 μg/mL

Damage to the sc structure of the plasmid at 10 μg/mL DNA concentration was predicted to be high at lower nozzle size as shown in Figure 5.5. At a nozzle size of 3 μm, sc structural damage was observed to be higher at ionic concentration <150 mM, possibly due to the inefficient condensation of the sc molecules at low ionic strength. Structural damage (80-85%) to the sc plasmid was predicted for the 3 μm nozzle at NaCl concentrations >150 mM. With an increase in nozzle size up to 4 μm, less damage to the sc structure was observed with increasing ionic concentration. For nozzles of size between 4 μm and 5 μm, the extent of damage to the sc structure indicated by the model was similar with lower damage at high ionic strength. The model predicted a region of minimal damage to the sc structure at a NaCl concentration >150 mM.

5.2.5.2.2 DNA concentration 20 μg/mL

For a DNA concentration of 20 μg/mL, the damage to the sc structure of the plasmid was predicted to be >80% for the 3 μm nozzle (Figure 5.6). There was no decrease in damage to the sc structure due to the presence of ionic strength with the 3 μm nozzle, suggesting that the size of the condensed supercoiled molecule may be of the order of the nozzle size. However, for nozzle sizes from 3 μm to 4 μm, the model predicted a low damage to the sc structure at NaCl concentration >150 mM, similar to that predicted at 10 μg/mL DNA concentration. For the 4 μm nozzle, the damage level was predicted to be the same at different ionic concentrations, suggesting no effect of condensation of the sc structure with increase in ionic concentration. For a nozzle size between 4 μm and 5 μm, the model predicted a region of minimal damage to the sc structure at NaCl concentration ≥100 mM, suggesting that a minimum NaCl concentration of 100-150 mM is required to condense the sc molecule at 20 μg/mL DNA concentration.

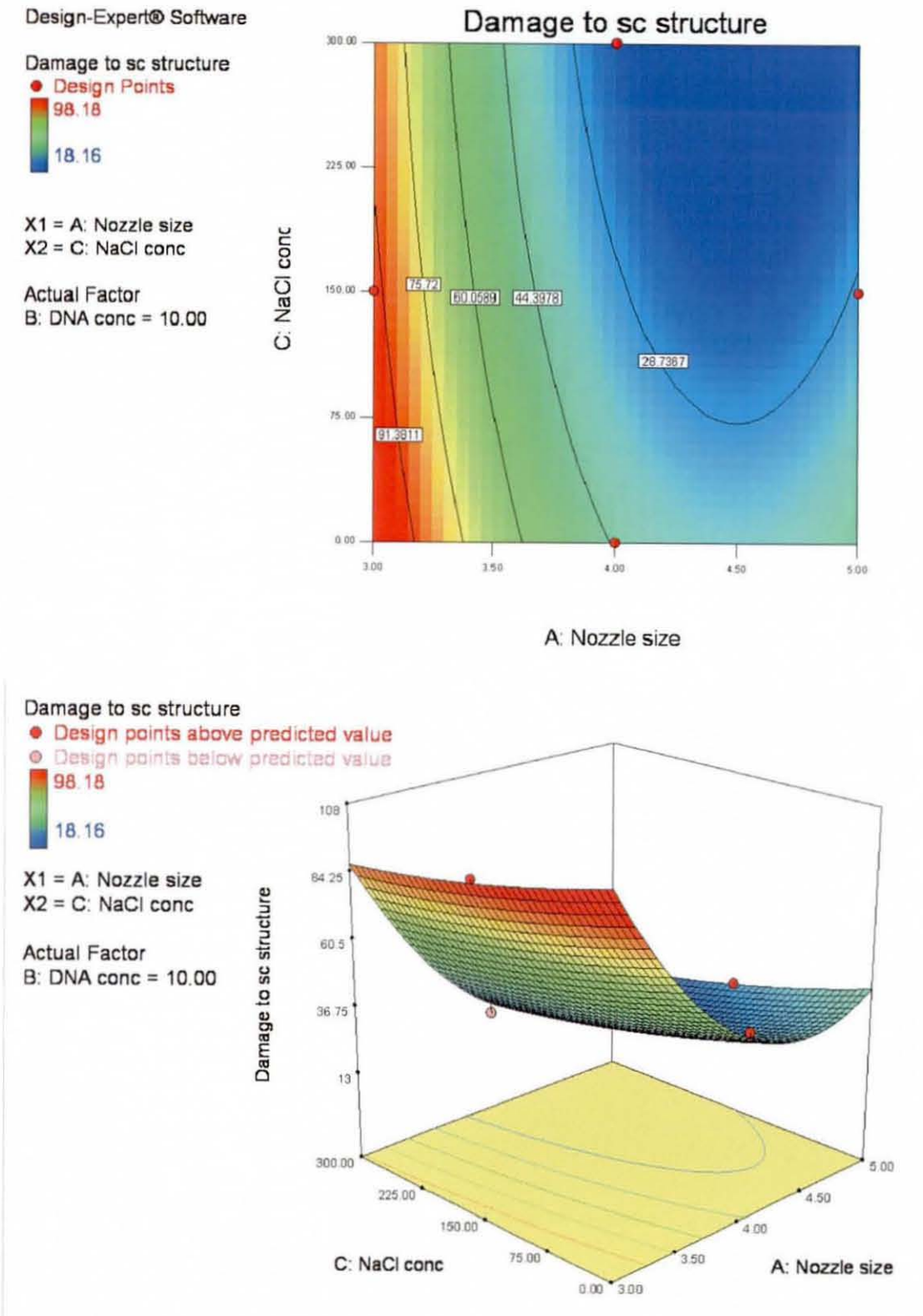

Figure 5.5: Response surface contour and 3D plots of the effect of 10 μg/mL DNA concentration on damage to the sc structure of 20 kb plasmid.

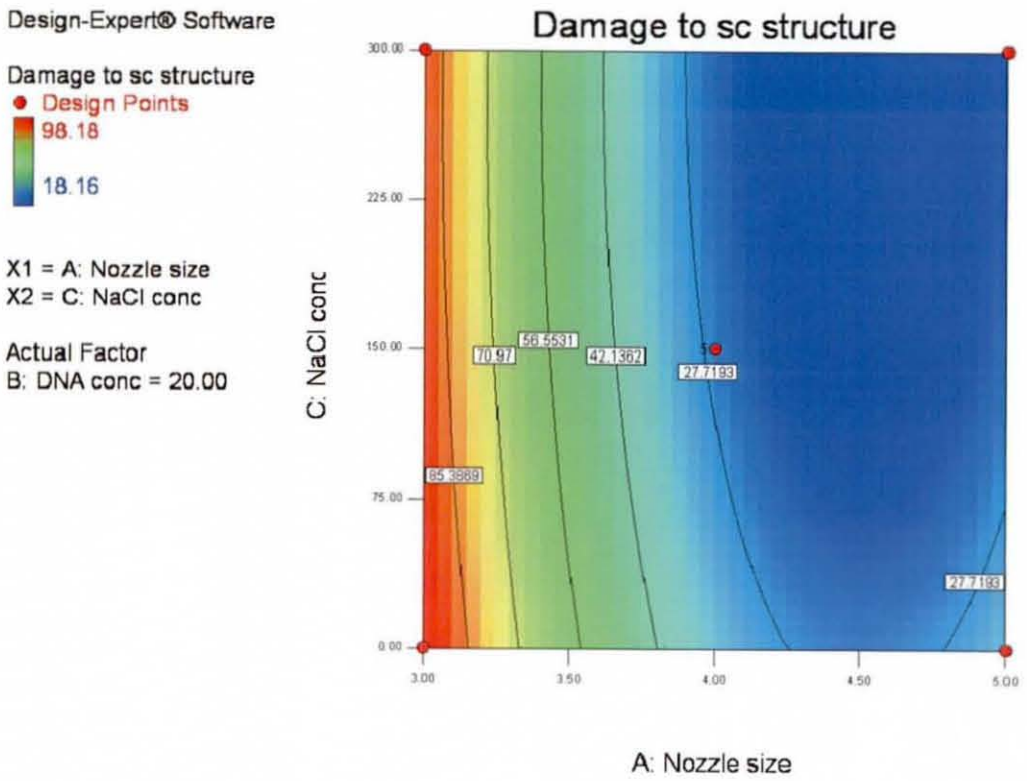

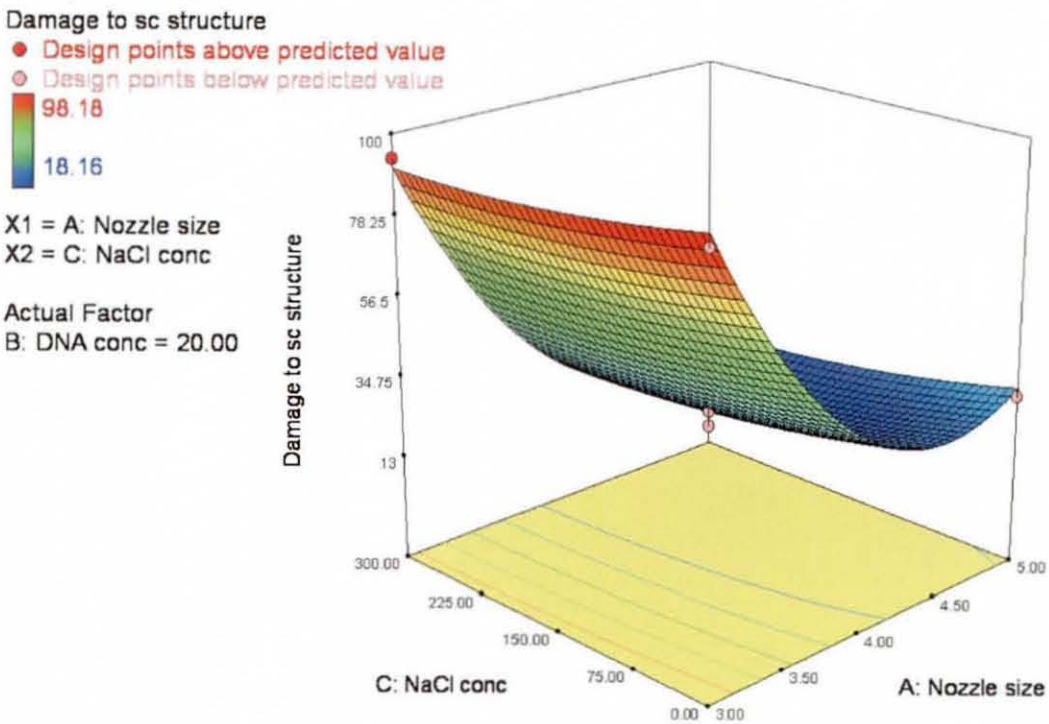

Figure 5.6: Response surface contour and 3D plots of the effect of 20 μg/mL DNA concentration on damage to the sc structure of 20 kb plasmid.

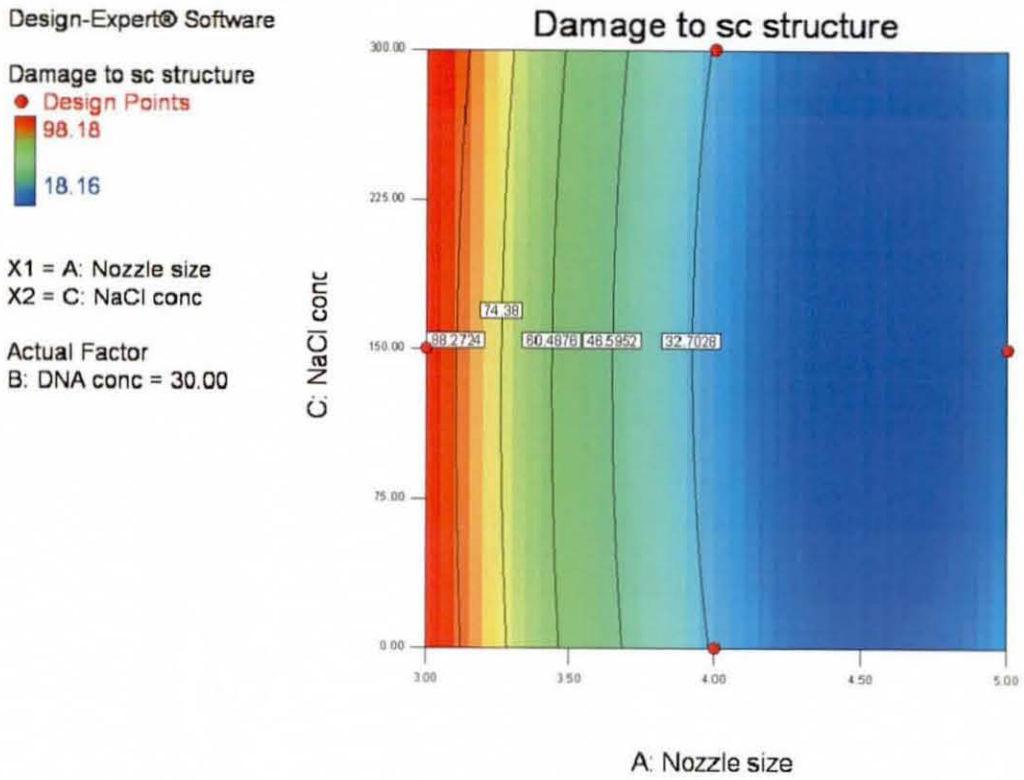

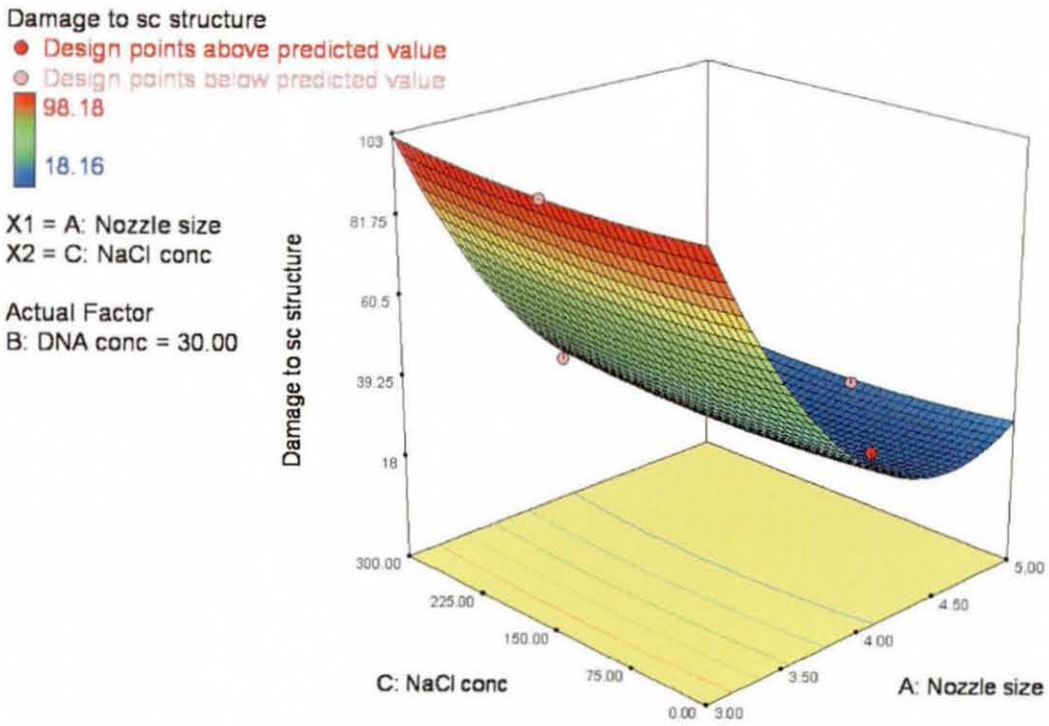

Figure 5.7: Response surface contour and 3D plots of the effect of 30 μg/mL DNA concentration on the damage to the sc structure of 20 kb plasmid.

5.2.5.2.3 DNA concentration 30 μg/mL

As shown in Figure 5.7, damage to the sc structure of the plasmid was predicted to be > 95% for the 3 μm nozzle. For nozzle sizes between 3 μm and 4 μm, damage to the sc structure was predicted to be independent of NaCl concentration. This could be due to the inefficient condensation of the sc structure with NaCl at high DNA concentration. For a 4 μm nozzle, damage level was similar to that observed at 20 μg/mL DNA concentration, suggesting no effect of condensation of the sc structure with increase in nozzle size. For a nozzle size between 4 μm and 5 μm, the model predicted minimal damage to the sc structure.

5.2.5.3 Effect of NaCl concentration

Theoretically, the sc structure of the plasmid is susceptible to maximum damage when formulated in buffer with no ionic concentration. The predicted response for the three ionic concentrations is discussed below.

5.2.5.3.1 0 mM NaCl

The model predicted the sc structure to be more damaged in the 3 μm nozzle than in 4 μm and 5 μm nozzles (Figure 5.8), suggesting size as a significant parameter for damage to the sc structure. Maximum damage (>80%) was predicted at the 3 μm nozzle for all DNA concentrations. Damage levels from 40-80% were predicted for nozzle sizes between 3 μm and 4 μm. The model predicted that at a nozzle size >4 μm, the damage was less than that at smaller nozzle size. Low levels of damage (20-40%) were predicted between 4 μm and 5 μm nozzle sizes suggesting that the uncondensed sc structure experienced less degradation forces at increasing nozzle size.

5.2.5.3.2 150 mM NaCl

Nebulisation of the 20 kb plasmid in 150 mM NaCl resulted in a compact sc structure of smaller molecular size, as evident by the somewhat lower damage to the

sc structure, when compared to that without ionic concentration at the 3 μm nozzle (Figure 5.9). Damage to the sc structure was also predicted to be less for nozzles of size from 3 - 4 μm. A region of minimal damage to the sc structure was predicted between 4 μm and 5 μm nozzle sizes, suggesting that the reduced size of the sc structure was primarily due to condensation in the presence of ionic concentration. The extent of damage to the sc structure in the presence of 150 mM NaCl was predicted to be lower than that without NaCl concentration. The significance of NaCl concentration ($p<0.05$) in the model suggested damage to the sc structure during nebulisation can be protected by ionic concentration.

5.2.5.3.3 300 mM NaCl

The increase in ionic concentration to 300 mM NaCl has perhaps resulted in efficient condensation of the sc structure leading to lower damage as predicted in Figure 5.10 than with an ionic strength of 150 mM NaCl. At the 3 μm nozzle, for DNA concentration <20 μg/mL less damage to the sc structure was predicted. This is likely to be due to a reduction in molecular size. However, for higher DNA concentration the damage levels were similar to those observed at 150 mM NaCl. Damage was also predicted to be similar at 150 mM NaCl between 3 μm and 4 μm nozzle sizes. For nozzle sizes between 4 μm and 5 μm, prediction of minimal damage regime widened perhaps due to better condensation of the sc structure to a smaller molecular size at DNA concentrations <25 μg/mL. However, at 30 μg/mL DNA concentration, damage was predicted to be slightly higher due to the inefficient condensation of sc structure in high DNA concentrations, resulting in larger molecular size.

From the response surface and contour plots, it is clear that the model is capturing the effect of the variables in a statistical way allowing prediction at intermediate levels of the variables. As predicted by the model statistics, the variables of nozzle size and NaCl concentration and interaction between variables of DNA and NaCl concentrations had a significant effect on damage to the sc structure of the 20 kb plasmid.

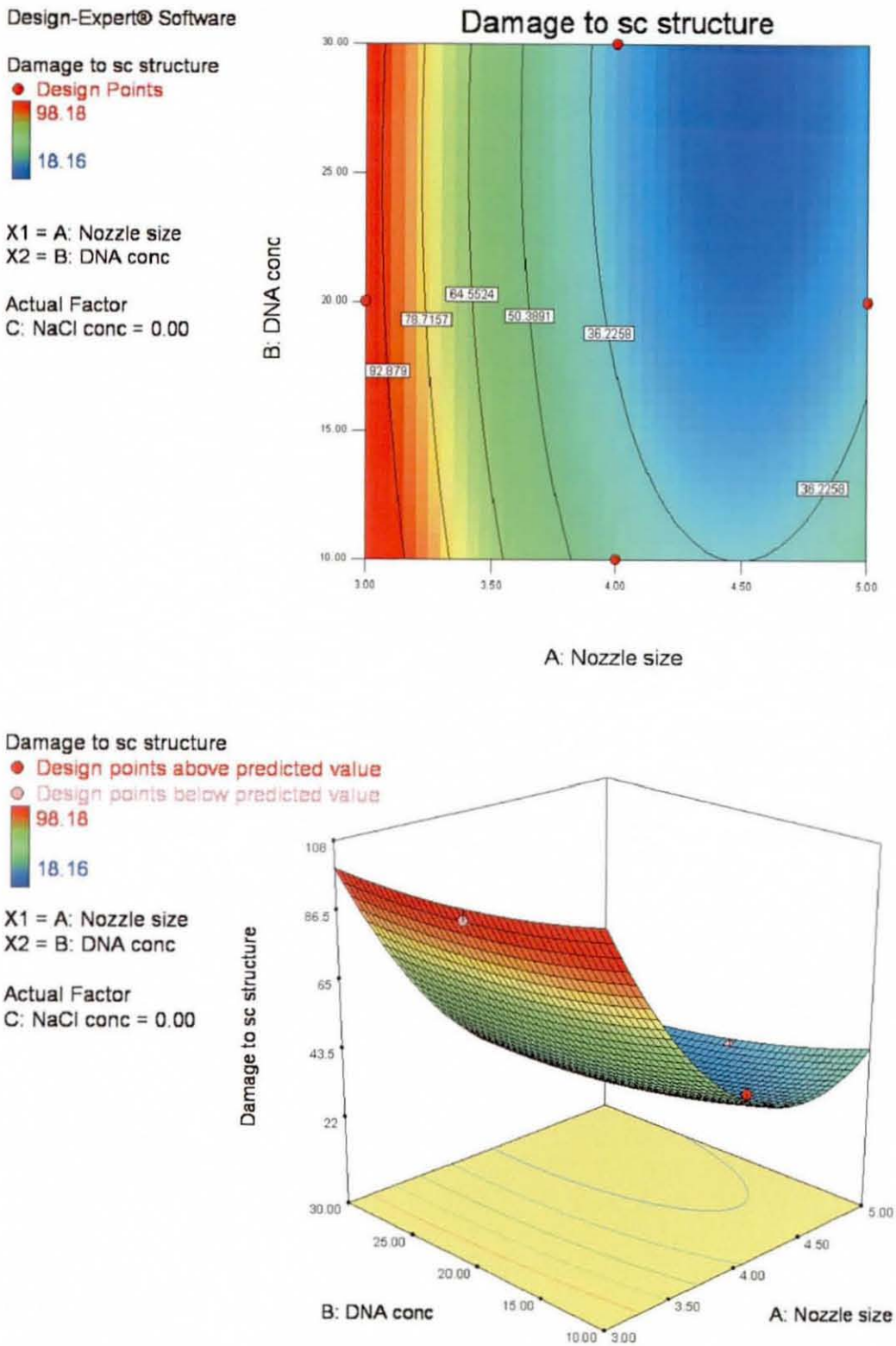

Figure 5.8: Response surface contour and 3D plots of the effect of 0 mM NaCl concentration on damage to the sc structure of 20 kb plasmid.

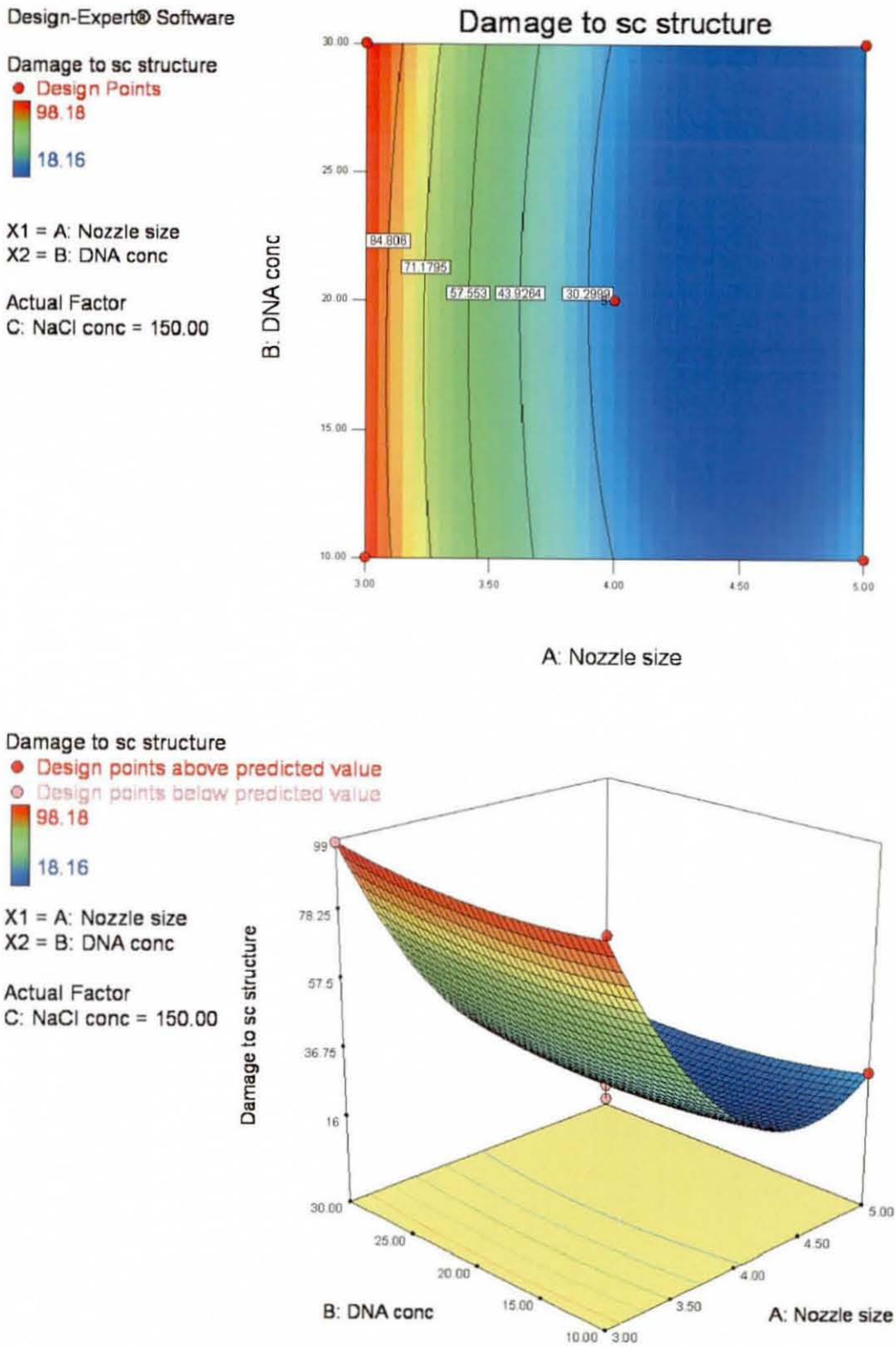

Figure 5.9: Response surface contour and 3D plots of the effect of 150 mM NaCl concentration on the damage to the sc structure of 20 kb plasmid.

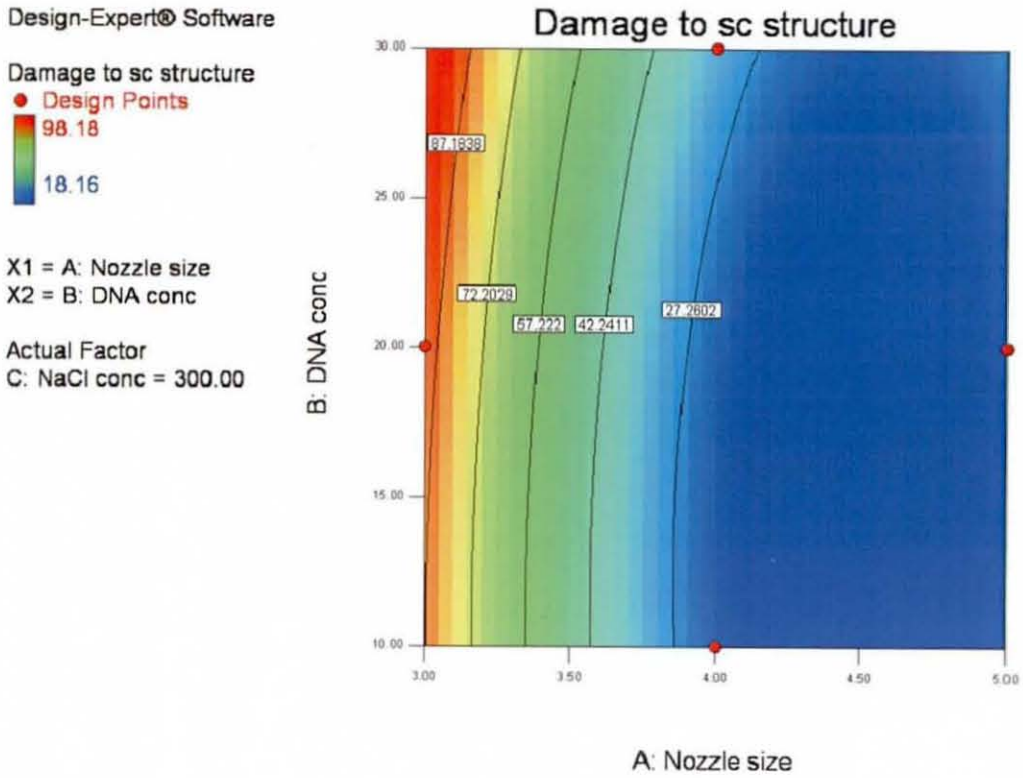

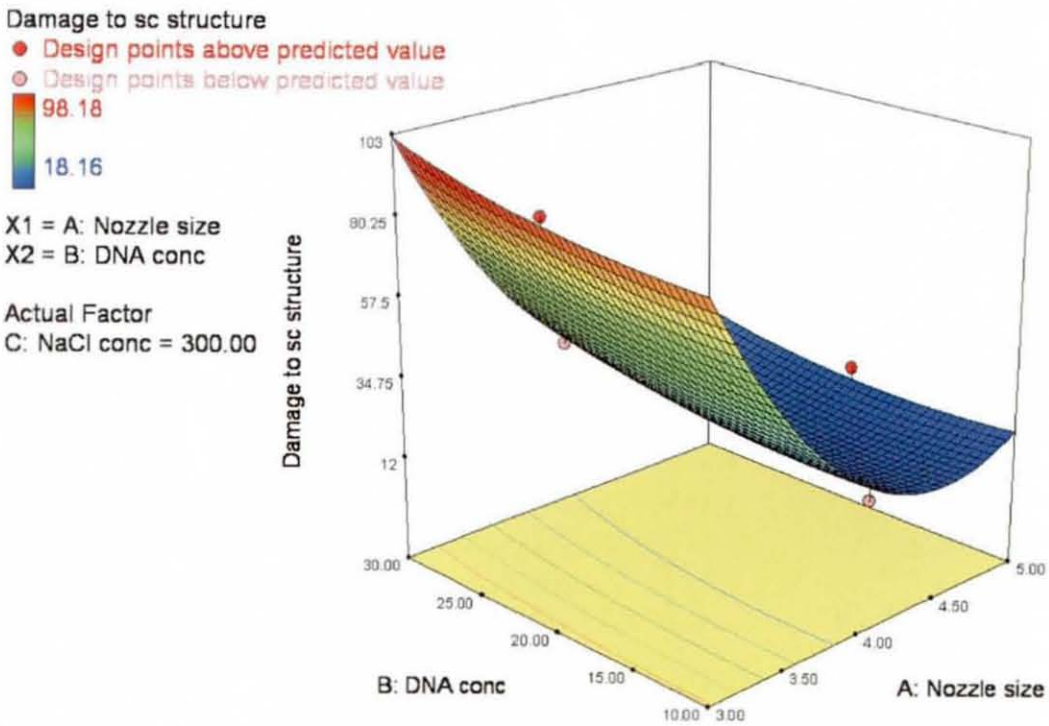

Figure 5.10: Response surface contour and 3D plots of the effect of 300 mM NaCl concentration on the damage to the sc structure of 20 kb plasmid.

5.2.5.4 Response from model predictions

From the model equation 5.1, the predicted response showing the effect of NaCl and DNA concentration on minimum damage to the sc structure for different nozzle sizes are shown in Figure 5.11. As reported in the contour and response surface plots, damage to the sc structure of the 20 kb plasmid at the 3 μm nozzle was observed to be the maximum without NaCl concentration. However, a decrease in damage was observed with NaCl concentration. For nozzles of size 4 μm and 5 μm, damage was lower than that at the 3 μm nozzle. This study showed that nozzle size is a significant parameter in the damage to the sc structure of the 20 kb plasmid. In order to relate nozzle size with aerosol particle size, aerosol characterisation from the nozzles was carried out and is reported in the following section.

5.3 Aerosol characterisation from the U22 mesh nebuliser

The characterisation of aerosols from the mesh nebuliser with 3 μm and 4 μm nozzles is shown in Table 5.7. The aerosol particle size was determined using a laser diffraction instrument (Malvern Master Sizer®, Malvern Instruments, UK). The diameter of the aerosols using the 3 μm mesh was observed to be 4 to 5 times higher than that with a 4 μm mesh. Large liquid droplets were generated using the 5 μm mesh and hence the aerosol particle size was not characterised.

Table 5.7: Characterisation of distilled water aerosols from the U22 nebuliser with 3 μm and 4 μm nozzle sizes

Nozzle size (μm)	$D_{(4,3)}$ (μm)	$D_{(3,2)}$ (μm)	$D_{(v,\,0.5)}$ (μm)
3	9.29 ± 0.17	5.40 ± 0.39	7.54 ± 0.06
	CV 1.79%	7.18%	0.82%
4	45.06 ± 3.60	21.73 ± 1.50	36.02 ± 2.55
	CV 7.98%	6.90%	7.08%
5	Droplet size not determined		

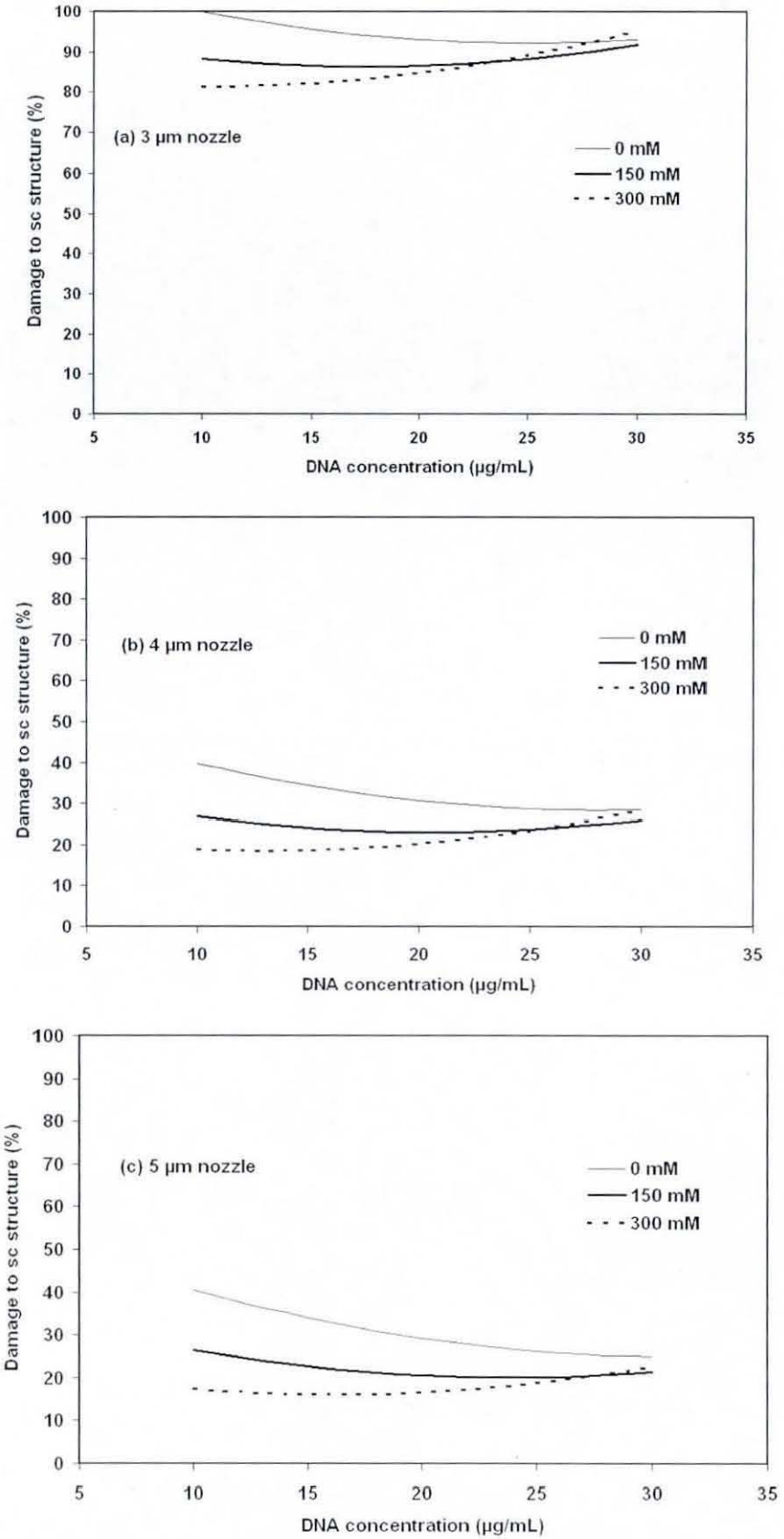

Figure 5.11: Minimum predicted damage to sc structure of 20 kb plasmid for DNA and NaCl concentrations at nozzle sizes of: a) 3 µm, b) 4 µm, c) 5 µm.

5.4 Discussion

The micron-sized nozzle of the mesh nebuliser permits generation of uniform aerosols. The size of the aerosols generated is dependent on the nozzle size. The 3 μm nozzle of the commercially available U22 mesh nebuliser results in the generation of respirable aerosols. In order to investigate the damage to the sc structure at varying nozzle size, a 4 μm and 5 μm nozzle mesh were used for the experiments. Aerosol characterisation from the 4 μm nozzle mesh using laser diffraction resulted in aerosols of size up to 4 times higher than the 3 μm nozzle. Only a spray of liquid droplets was generated from the 5 μm nozzle mesh. However, the effect of nozzle size is an important variable; nozzles of size 3, 4 and 5 μm in the experimental design provide an insight into the influence of nozzle size on damage to the sc structure of the 20 kb plasmid.

Earlier experiments (Chapter 4) on the nebulisation of plasmid DNA had shown that damage to the sc structure varied with the concentration of plasmid DNA used. The main purpose of the experimental design here was to further examine the influence of factors responsible for damage to the sc structure of plasmid DNA. Based on the screening experiments, the concentrations of plasmid DNA at 10, 20 and 30 μg/mL was employed as a second variable to assess its effect on damage to the sc structure.

Persistence length is the length in which DNA can bend for half a turn at energy of 1 k_BT, where k_B is the Boltzmann constant, T is the temperature. Persistence length (l_p) of DNA that indicates the stiffness of a polymer in good solvent and is characteristic of a semi-rigid polymer. DNA has been reported to have a shorter persistence length (~50 nm) in ionic concentrations [Lasic 2000]. The positive effect of NaCl concentration on damage to the sc structure of the plasmid has been observed for the 5.7 kb plasmid (Chapter 4). In order to understand the effect of NaCl concentration on large sized plasmids, it was chosen as the third variable for the experimental design at concentrations of 0, 150 and 300 mM. The concentration of 0 mM NaCl served as a control to enhance the model of damage in the presence of 150 and 300 mM NaCl.

The statistical analysis of Box-Behnken experimental design suggested the quadratic and linear model as significant (Table 5.3). However, the lack of fit tests showed (Table 5.4) insignificance for the quadratic model, suggesting the model fitted well.

This result from the lack of fit test was confirmed from the model summary statistics shown in Table 5.5. A predicted R^2 value of 0.914 agreed reasonably with the adjusted R^2 value of 0.983.

The model F value of 107.41 determined from ANOVA (Table 5.6) implied that the model was significant. The p-value < 0.05 for nozzle size, NaCl concentration and interaction between NaCl and DNA concentration, suggested these terms as significant for the model. The model diagnostic plots of normal probability plot and actual versus predicted response shown in Figure 5.1 suggested adequacy of the model.

The predicted damage to sc structure for the significant variables of the model i.e. Nozzle size and NaCl concentration is summarised in Figure 5.11. As shown in Figure 5.11a, at 3 μm nozzle size, significant damage to the sc structure of 20 kb plasmid was predicted without NaCl concentration. However, at 150 and 300 mM NaCl concentrations damage was predicted to be lower. In comparison at the 4 μm and 5 μm nozzle, damage was predicted to be somewhat similar, at lower levels of damage than with the 3 μm nozzle. A reduction in damage level was predicted for all the three nozzle sizes with increasing NaCl concentration, suggesting a positive influence of the significant interaction between NaCl and DNA concentrations (Table 5.6) towards damage to the sc structure. However, DNA concentration was not found to significantly influence damage to the sc structure.

To summarise, the results of DoE on nebulisation of 20 kb plasmid confirm "size" as an important parameter influencing aerosol delivery of plasmid DNA. In order to understand the relationship between the variables of nozzle size and plasmid size, a 2^2 factorial experiment was performed as discussed in chapter 7.

5.5 Conclusions

A design of experiments based on a Box-Behnken design identified the significant variables affecting the sc structure on nebulisation using the U22 mesh nebuliser. The model predicted the actual response well and enabled better understanding of the

damage to the sc structure upon nebulisation. Low damage to sc structure of 20 kb plasmid was predicted at nozzle sizes >3 μm. However, the requirement to use a nozzle size >3 μm to render inhalable aerosols for respiratory delivery suggests that 20 kb plasmid needs to be further condensed by formulation in order to circumvent damage. From the model predictions and analysis, it is concluded that the size of 20 kb plasmid remains the main bottleneck for aerosol delivery of the sc structure. Engineering studies on the mechanism of fluid flow through the nozzle of the mesh nebuliser using high-speed imaging and computational fluid dynamics in the next chapter are discussed to provide a detailed understanding of the phenomenon of aerosolisation and the hydrodynamic force responsible for damage of the sc structure.

CHAPTER 6. ENGINEERING ANALYSIS ON NEBULISATION OF PLASMID DNA

6.1 Introduction

Earlier results on the nebulisation of plasmid DNA and the influence of design variables on nebulisation in Chapters 4 and 5 respectively suggested the nozzle size of the mesh nebuliser as a bottleneck for safe aerosol delivery of large plasmids. In this chapter engineering analysis of the nebulisation of plasmid DNA was carried out to study more closely the factors which damage the sc structure upon aerosolisation and predict the forces responsible for causing damage to the sc structure. In order to provide an understanding of the droplet generation from the vibrator horn, the factors responsible for droplet size and strain rates are discussed. High speed imaging of aerosol generation was performed to determine the influence of the mesh on aerosol generation and subsequent damage to sc structure of 20 kb plasmid. Modelling of fluid flow through the nozzle of the mesh nebuliser using computational fluid dynamics predicted the hydrodynamic forces responsible for damage to the sc structure. Estimation of plasmid DNA size for safe delivery of the supercoiled structure in the mesh nebuliser was attempted from the plasmid DNA degradation kinetics based on molecular size. In order to perform engineering analysis of the nebulisation of plasmid DNA, it was essential to understand the mechanism of degradation of sc structure, and evaluate the molecular relaxation time and timescales associated with fluid/ particle flow through the device.

6.2 Droplet formation from capillary waves

The purpose of this analysis is to examine, using capillary theory, the importance of various physical effects on droplet generation in the mesh nebuliser chosen for the research. The mean droplet size generated from thin layers is proportional to the capillary wavelength on the liquid surface [Topp, 1973]. The droplet diameter (D) can

be expressed in terms of capillary wavelength (λ) with a dimensionless empirical factor by the following equation:

$$D = 0.34\lambda \quad \text{.....Equation 6.1}$$

The capillary wavelength can be represented by the Kelvin equation [Yule and Al-Suleimani, 2000] as given below:

$$\lambda = \left(\frac{8\pi\gamma}{\rho f^2}\right)^{1/3} \quad \text{.....Equation 6.2}$$

where γ is the surface tension in N/m, ρ is the density in kg/m^3 and f is the frequency in cycles/s. The droplet diameter can be determined by substitution of the result of the above equation into Equation 6.2.

The threshold amplitude for generation of capillary waves is given by [Taylor and McCallion, 1997]:

$$a_{th} = \frac{4\upsilon}{f\lambda} \quad \text{.....Equation 6.3}$$

where a_{th} is the threshold amplitude, υ is the kinematic viscosity of the liquid, f is the acoustic frequency and λ is the capillary wavelength.

The typical amplitude a in nebulisers can be determined from the threshold amplitude and is given by:

$$a = 4\,a_{th} \quad \text{.....Equation 6.4}$$

Assuming the vibrator horn transducer vibrates in a sinusoidal motion, the displacement of transducer is given by:

$$y(t) = a\,\sin(\omega t) \quad \text{.....Equation 6.5}$$

where $\omega = 2\pi f$ = angular frequency (rad.s^{-1}).

Differentiation of equation 6.5, yields the velocity of the transducer which is represented by:

$V(t) = dy/dt = a\omega \cos(\omega t)$ .....Equation 6.6

The root mean square (RMS) velocity is given by:

$$V_{rms} = \frac{a\omega}{\sqrt{2}}$$ .....Equation 6.7

The strain rate ($\dot{\gamma}$) is represented as a ratio of the root mean square velocity and the droplet diameter and is given by:

$$\dot{\gamma} = O\left(\frac{V_{rms}}{D}\right)$$ .....Equation 6.8

In order to understand the influence of device parameters such as frequency and physical properties such as viscosity, surface tension, density on droplet diameter and strain rate, equations 2.2 to 2.9 were used for the computation and are tabulated in Table 2.7. Assuming the physical properties of fluid (water) are surface tension = 0.073 Nm^{-1}, density = 1000 kgm^{-3}, and viscosity = 0.001 $kgm^{-1}sec^{-1}$.

As shown in Table 6.1, aerosolisation at a higher frequency results in the generation of smaller droplets and higher strain rates than at the operating condition of the device at 175 kHz. No effect on droplet size was observed with a change in viscosity, but the strain rate is found to vary linearly with viscosity. An increase in droplet size was observed at higher surface tension than at 0.073 $kg.s^{-2}$, but a decrease in strain rate was observed. At higher density the droplet size and strain rate decreased when compared with that at 1000 $kg.m^{-3}$. Theoretical models of the effect of frequency and fluid physical properties on droplet diameter and strain rate provided useful information prior to high-speed imaging of aerosol generation from the mesh nebuliser.

Table 6.1: Theoretical predictions of the effect of frequency and physical properties on droplet size and strain rate in a mesh nebuliser

Effect of parameter	**-**	**Operating condition**	**+**	**Increase in parameter**
Effect of Frequency				
Frequency (kHz)	*75*	*175*	*1750*	
Droplet size (μm)	17.1	9.8	2.1	Decreases
Strain rate (s^{-1})	$> 0.6x10^5$	$> 1.8x10^5$	$> 40x10^5$	Increases
Effect of Viscosity				
Viscosity ($kg.m^{-1}s^{-1}$)	*0.0001*	*0.001*	*0.01*	
Droplet size (μm)	9.9	9.9	9.9	No effect
Strain rate (s^{-1})	$> 0.18x10^5$	$> 1.8x10^5$	$> 18x10^5$	Increases
Effect of Surface tension				
Surface tension ($kg.s^{-2}$)	*0.0073*	*0.073*	*0.73*	
Droplet size (μm)	4.6	9.9	21.4	Increases
Strain rate (s^{-1})	$> 8.3x10^5$	$> 1.8x10^5$	$> 0.4x10^5$	Decreases
Effect of Density				
Density ($kg.m^{-3}$)	*500*	*1000*	*1500*	
Droplet size (μm)	12.5	9.9	8.7	Decreases
Strain rate (s^{-1})	$> 2.3x10^5$	$> 1.8x10^5$	$> 1.6x10^5$	Decreases

6.3 High-speed imaging of aerosolisation

6.3.1 Introduction

High-speed imaging studies of aerosol generation from the mesh nebulisers provide an improved understanding of the underlying phenomena and the timescales involved in aerosolisation. A high speed video was used to capture aerosol generation from a U22 mesh nebuliser to visualise events at small timescales and help identify mechanisms with the potential to damage plasmid DNA during nebulisation.

6.3.2 Aerosolisation using the U22 mesh nebuliser

The vibrator horn represents the heart of the nebulisation device. High speed imaging of aerosolisation of the liquid from the vibrator horn without mesh provides

an insight into time and velocity profiles occurring at millisecond time intervals. The liquid chosen for the aerosolisation studies was phosphate-buffered saline (PBS). The experimental set-up for the high speed imaging has been discussed in detail in section 3.2.5 of Chapter 3. In order to mimic the presence of a liquid film on the surface of the vibrator horn between the horn and the mesh, aerosol generation from the vibrator horn was studied for a 0.5µl liquid droplet. Aerosol generation for an initial 5µl droplet was studied in order to understand the size of the droplet generation with reducing liquid film on the surface of the vibrator horn without mesh.

6.3.2.1 Aerosolisation from 5 µl droplet without mesh

High speed imaging of the aerosolisation events from the vibrator horn of a 5µl droplet without the mesh was carried out. The vibrator horn vibrates at a frequency of 175 kHz. The mesh of the nebuliser with micron-sized nozzles is passive with respect to the vibrating horn. To understand the vibration-induced atomisation without the mesh, high speed imaging of droplets generated from 5 µl PBS pipetted onto the surface of the vibrator was performed. Frame sequences at the early-, mid- and late-aerosolisation phases in Fig.6.1, show fine particle aerosols in the late phase, possibly due to shorter surface wavelengths (λ) [Yule and Al-Suleimani, 2000] from the reducing thickness of liquid film.

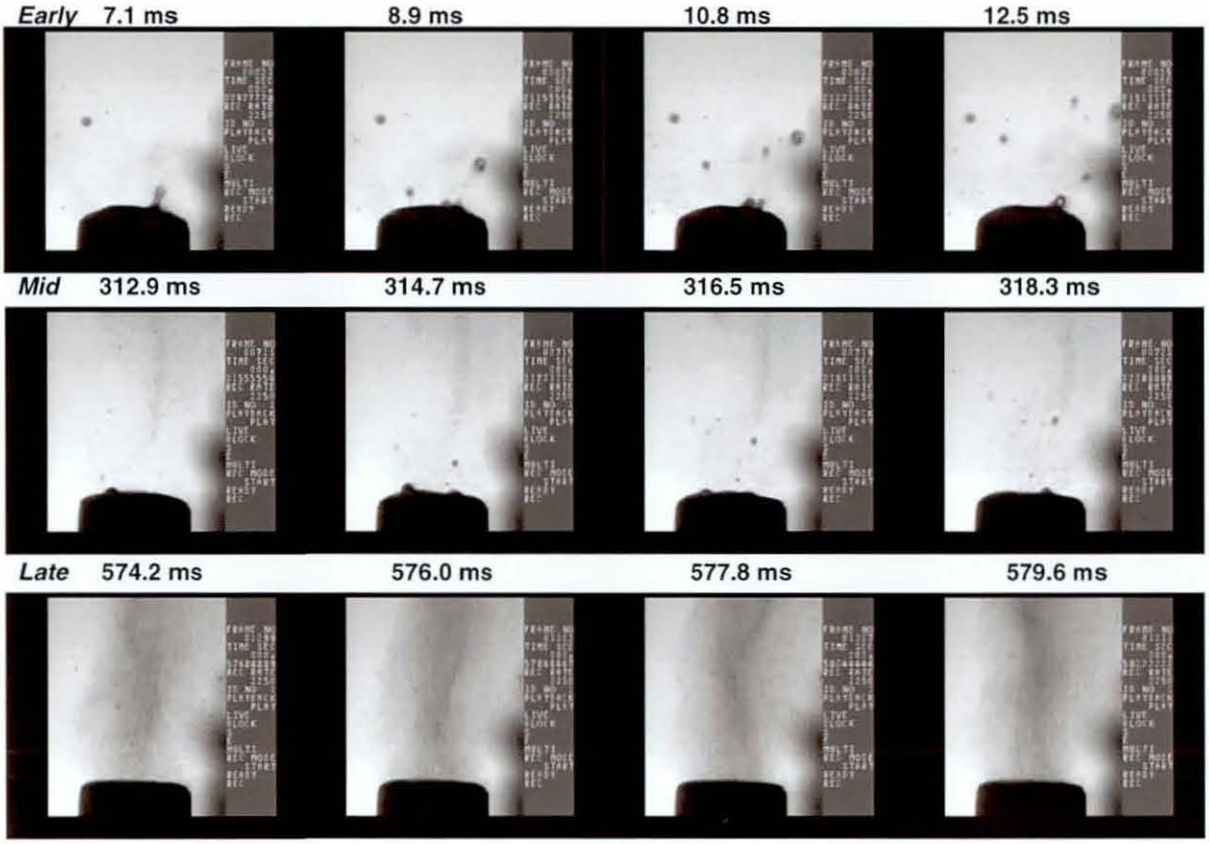

Figure 6.1: Imaging of aerosols from 5µl droplet on vibrator without mesh.

6.3.2.2 Aerosolisation of 0.5 µl liquid film without and with mesh

The position of the mesh and vibrator in the device during nebulisation is likely to result in the formation of a thin liquid film. To mimic the presence of a liquid film without a mesh, a 0.5 µl initial volume of solution was used. Visualisations of transient nebulisation of 0.5 µl of PBS solution without the mesh and with the mesh are shown in Figures 6.2a and 6.2b respectively. Aerosolisation without mesh resulted in an aerosol cloud with maximum density after 4.5 ms, whereupon liquid depletion causes a reduction of the density of the cloud and gives it a more focused appearance along the axis of the transducer. Aerosol formation with the mesh resulted in a continuous stream of very fine droplets (average size reported as 4.4 µm [Kishida et al., 2003]), with decrease in cloud density due to depletion of liquid after about 30 ms. The aerosol production ceases after 60 ms, while it takes 80 ms for complete aerosolisation with mesh. Analysis of the images of aerosolisation without mesh yielded droplet size estimates of around 10 µm.

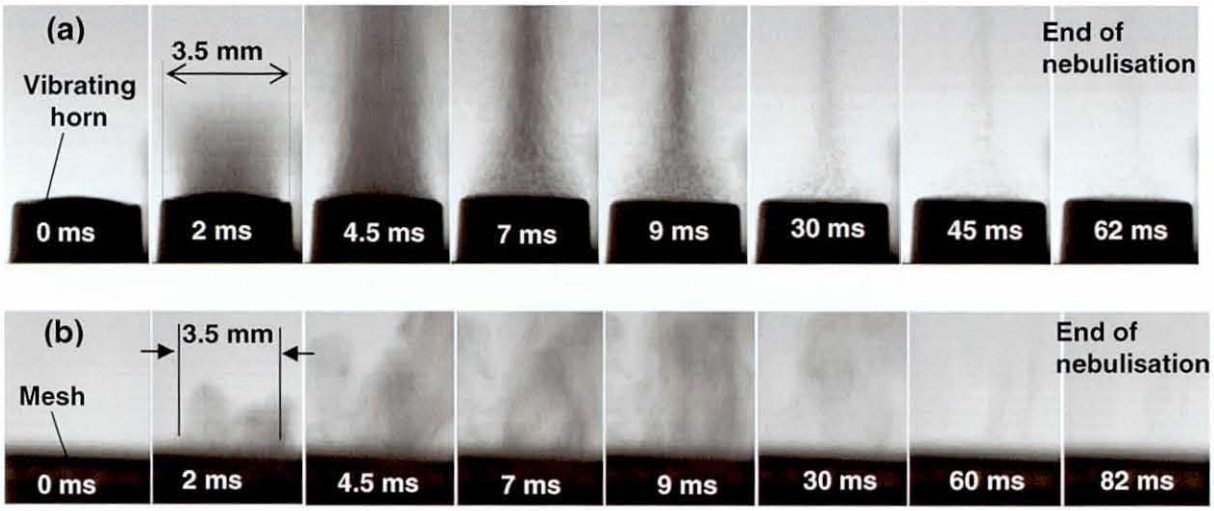

Figure 6.2: High speed imaging of PBS solution aerosols generated by the mesh nebuliser (a) without mesh and (b) with mesh in place.

6.3.2.3 Nebulisation of plasmid DNA without and with mesh

Agarose gel electrophoresis analysis of recovered aerosols (Figure 6.3) from nebulisation of a 20 kb plasmid with the U22 mesh nebuliser with the mesh in place showed no damage to the super-coiled (sc) DNA in the nebuliser chamber (lane 2), but almost complete damage (95.1% damage) in the aerosols (lane 3). Nebulisation of 20 kb plasmid DNA without the mesh in place showed partial damage to the sc DNA in the nebulisation chamber (lane 6) and in the recovered aerosols (lane 7). Densitometric scans of the agarose gel revealed partial damage in the nebuliser chamber and recovered aerosols of 46.1 and 48.0% respectively. Since the 20 kb fluid does not pass through the mesh holes, another damage mechanism must therefore occur. In the following section further analysis was carried out to determine the influence of cavitation on damage to the sc structure in the nebuliser chamber.

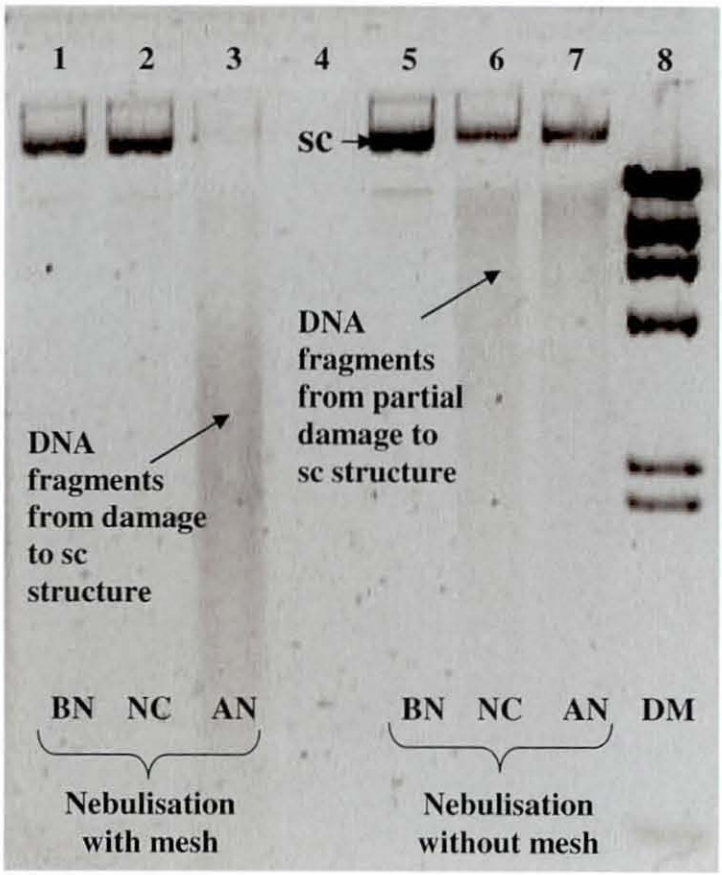

Figure 6.3: Nebulisation of 20 kb plasmid with and without mesh. Lanes 1,5 – before nebulisation (BN), lanes 2,6 – nebuliser chamber (NC), lanes 3,7 – after nebulisation (AN), DM - λHindIII DNA marker.

6.3.2.4 Analysis of high-speed imaging

Analysis of high speed images on aerosolisation from the vibrator horn with and without mesh suggested a slightly longer aerosolisation time with the mesh. For aerosolisation from the vibrator horn without mesh, the acceleration amplitude of the horn can be determined by the following equation [Bassett and Bright, 1976].

Acceleration amplitude $a = \frac{2\beta\omega}{\rho c}$ .....Equation 6.9

In equation 6.9, β is the pressure amplitude (in Pa), ω is the angular frequency (in rad/sec) given by $2\pi f$, with f as the frequency of the vibrator horn (in Hz), ρ is the density of the liquid (in kg/m^3) and c is the velocity of sound (in m/sec).

In order to determine the pressure amplitude, the acceleration amplitude (a) was first computed. The velocity V of the vibrator horn is subjected to sinusoidal oscillations due to ultrasonic vibrations from the transducer and is given by the following equation:

$V = \overline{V} Sin\omega t$ .....Equation 6.10

Differentiating equation 6.10 to obtain the acceleration, the above equation is modified to

$a = \overline{a} Cos\omega t$ .....Equation 6.11

In equation 6.11, ($\overline{a}$) is the acceleration amplitude and can be represented by the constant of differentiation, $\overline{V}\omega$. The value of $\overline{V}$ = 0.6 m/sec was determined from laser vibrometry measurements. The angular frequency (ω) for a frequency of 175 kHz = 1.09×10^6 $rad.s^{-1}$. From the values of $\overline{V}$ and ω, an acceleration amplitude ($\overline{a}$) of 6×10^5 m/s^2 was obtained. Substituting the value of acceleration oscillation amplitude in equation 6.9, the pressure amplitude (β) generated without the mesh was 2.3 bar.

For aerosolisation with mesh, a 10 fold increase in acceleration amplitude was observed, resulting in pressure amplitude of ~ 40 bar. At pressure amplitudes >2 bar for a bubble radius of O(μm), transient acoustic cavitation is reported at a frequency of 20 kHz [Young, 1999]. From this study, it could be interpreted that, at a frequency of 175 kHz, partial damage to the sc structure on aerosolisation without mesh is a result of transient acoustic cavitation.

6.3.3 Discussion

The formation of sprays from a liquid film on a vibrating surface is generally explained by the formation of droplets from the apexes of an orderly pattern of standing capillary waves, with a wavelength that can be related to vibration frequency by stability analysis. However, this assumption is challenged by the fact that, after droplet formation commences, the orderliness of the standing-wave pattern is lost due to one or more secondary instability phenomena. These phenomena, which lead to disorderliness were investigated by using high-speed imaging techniques and a low-frequency vibrating film to model the high-frequency case, because of the difficulty of penetrating clouds of small droplets in the latter case.

The droplet-formation processes from a film on a vibrating wall have been examined at frequencies less than 1 kHz [Yule and Al-Suleimani, 2000]. Although, droplets are formed from capillary waves, the organized, generally orthogonal, standing-wave pattern found before atomization inception becomes disorganized during atomization. Variability of the droplet-formation process is observed, which leads to the range of droplet sizes typically found for ultrasonic atomization. This variability can include multiple droplet formation from single ligaments; variation in ligament orientation, length and diameter; and emergence of a fully formed droplet from the crater formed at the lower limit of the vibration of a wave, the so-called volcano mode. Initial droplet angles of flight and velocities exhibit wide ranges of values, and individual wave cells eject droplets intermittently, with a variable number of cycles between ejections. Reasons for this disorder may include irregularity caused by the rapid backflow of wave crests from which droplets have formed; asymmetry of inflow into wave cells during ligament formation when surrounding waves have formed droplets in a previous cycle; and recovery from depletion of liquid from wave cells due to droplet formation.

In order to physically scale-up the atomization process, it is necessary to maintain similar values of important dimensionless parameters for the small-scale, high-frequency and the large-scale, low-frequency cases. The parameters from the point of view of instability (in the order of decreased importance) are

$$We = \frac{\rho_L U^2 h}{\sigma}, \quad Re = \frac{\rho_L U h}{\eta}, \quad Fr = \frac{U^2}{ga}, \quad \frac{h}{a}, \quad \frac{\rho_L}{\rho_g} \quad \text{.....Equation 6.12}$$

where We is the Weber number, U is the velocity scale given by $f\,a$, which was reported to be 1 ms^{-1} [Barrero and Loscertales, 2007]. The values of the units considered were σ is the surface tension in Nm^{-1}, η is the dynamic viscosity in kg m^{-1} s^{-1}, ρ is the density in kg m^{-3}, f is the frequency in kHz, h is the film thickness in m, a is the amplitude in m.

The droplet size estimate of 10 μm for aerosolisation without the mesh corresponds with Yule and Al-Suleimani's theoretical estimate for droplet size from a vibrating liquid surface [Yule and Al-Suleimani, 2000] using the operating parameters of the nebuliser. Using Bassett and Bright's theory and laser vibrometry measurements of the horn acceleration, typical pressure amplitudes of 2-40 bar in the liquid were computed. Cavitation is likely under such pressure amplitude conditions and is known to initiate drop formation from vibrating liquid surfaces [Topp, 1973]. The above high speed imaging study strongly suggests cavitation as a candidate damage mechanism. Damage to the sc structure of a 9.8 kb plasmid was also observed in the nebuliser chamber of a conventional ultrasonic nebuliser and attributed to cavitation [Lentz et al., 2005]. The occurrence of partial damage to the plasmid DNA in the nebuliser chamber without the mesh and no damage with the mesh suggests that in the latter case, the effects of cavitation may be experienced only by the liquid film between the horn and the mesh during the short residence time just prior to aerosolisation.

6.4 Background to engineering analysis

Experiments on nebulisation of plasmid DNA have shown the sc structure of the 20 kb plasmid to be almost completely degraded into linear fragments of size varying from 4 to 0.5 kb. In order to understand the mechanism of damage to the sc structure, chemical degradation of the sc structure of a 5.7 kb plasmid has been attempted. Levy et al. [2000b] compared damage to the sc structure based on chemical degradation with that due to high shear rates. Further reversible transition of the plasmid isoforms (sc, oc and linear forms) during exposure to strain rates during

flow has been reported [Meacle et al., 2006]. It is crucial to understand the timescales associated with the transition of the plasmid isoforms. In this work, knowledge of the relaxation times and time scales involved in the aerosolisation has been determined to provide insights into the duration of exposure to strain rates capable of causing damage to the sc structure.

6.4.1 Mechanism of degradation of supercoiled plasmid DNA

In order to understand the mechanism of degradation of a supercoiled plasmid DNA, the sc structure of a 5.7 kb plasmid was nebulised and then subjected to chemical degradation. Figure 6.4 shows a comparison of results of agarose gel electrophoresis of nebulised only, and nebulised and subsequently chemically degraded 5.7 kb plasmid DNA. As shown in the agarose gel (Figure 6.4), nebulisation of 5.7 kb plasmid in TE buffer and TE buffer with 150 mM NaCl resulted in damage to the open-circular (oc) forms of the plasmid, showing a smear of fragmented DNA below the sc structure. The reasoning for damage to the oc structure and no damage to the sc structure is due to exposure of loose oc structure to shear forces during the aerosolisation process. In order to induce chemical degradation, the nebulisation samples were exposed to high temperature. As shown in Figure 6.4, the sc structure of plasmid in TE buffer (lanes 6, 7) was completely degraded to oc and linear forms. Due to efficient condensation of sc structure in ionic strength buffer, chemical degradation resulted in less damage to sc structure (lanes 8, 9).

The densitometric scans of the agarose gel (Figure 6.4) are shown in Figure 6.5. The sc structure of plasmid in TE buffer upon chemical degradation at high temperature (95°C for 10 min) is almost completely damaged as shown in Figure 6.5a. However, condensation of the sc structure in ionic strength has resulted in retention of a sc structure (Figure 6.5b). The results of this study suggest that chemical degradation to sc plasmid DNA follows an irreversible transition from sc → oc form with the formation of a nick or breakage in DNA strands, and then further breakage of oc → linear forms. The linear double-stranded (ds) DNA fragments are susceptible to degradation to yield single-stranded (ss) DNA fragments, as reported in Chapter 4. Hence, the mechanism of sc plasmid DNA degradation can be represented as: sc →

oc → linear dsDNA → ssDNA. However, depending on the size of the sc molecule and nature of forces, degradation of the sc structure to linear dsDNA is possible as observed for a 20 kb plasmid in Chapter 4. A notable aspect of the above study is the encouraging information on the stability of sc structure of plasmid in ionic strength even at high temperature. This is important for stabilisation of the sc structure in ionic buffers at high temperature. The next section deals with the timescales involved in damage to the sc structure during nebulisation.

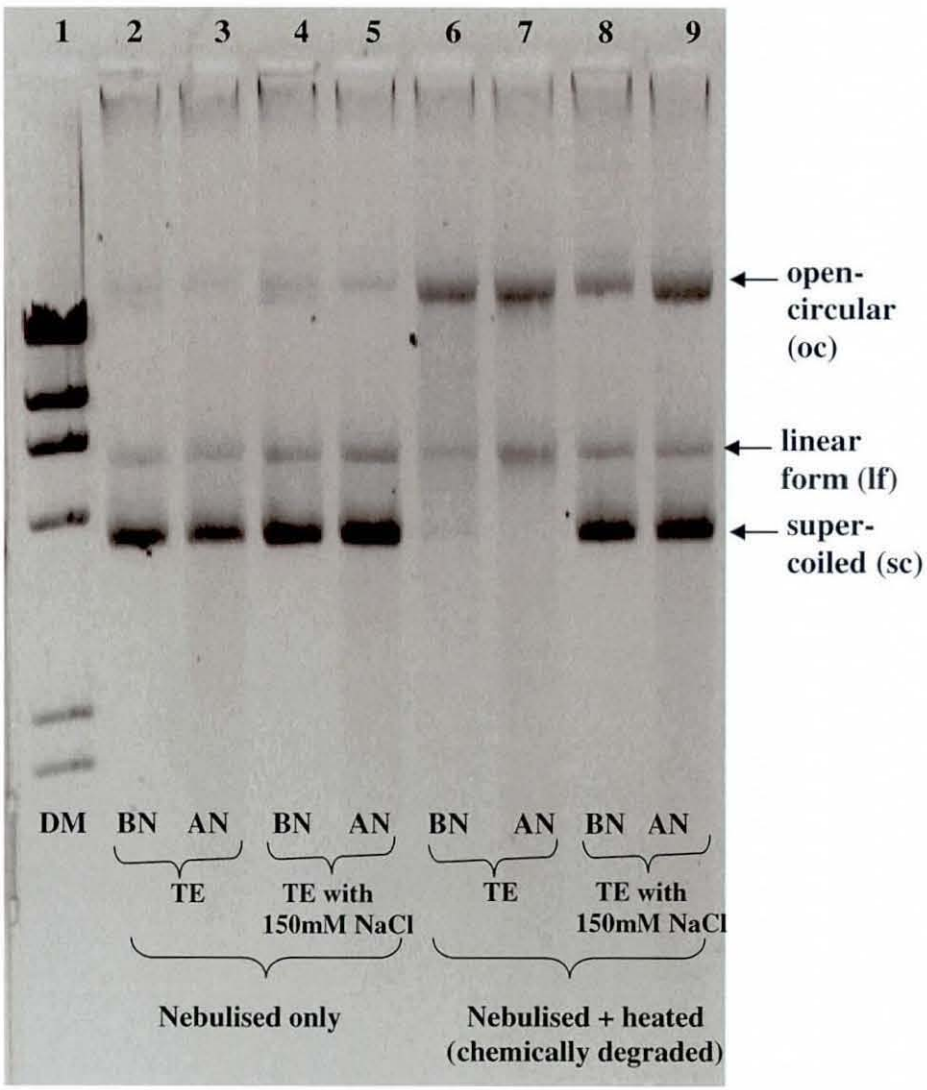

Figure 6.4: Agarose gel electrophoresis of nebulisation of 5.7 kb plasmid in TE buffer (lanes 2,3) and TE buffer with 150 mM NaCl (lanes 4,5); Chemical degradation of nebulisation samples (lanes 6 to 9); DM – DNA marker, BN – before nebulisation, AN – after nebulisation.

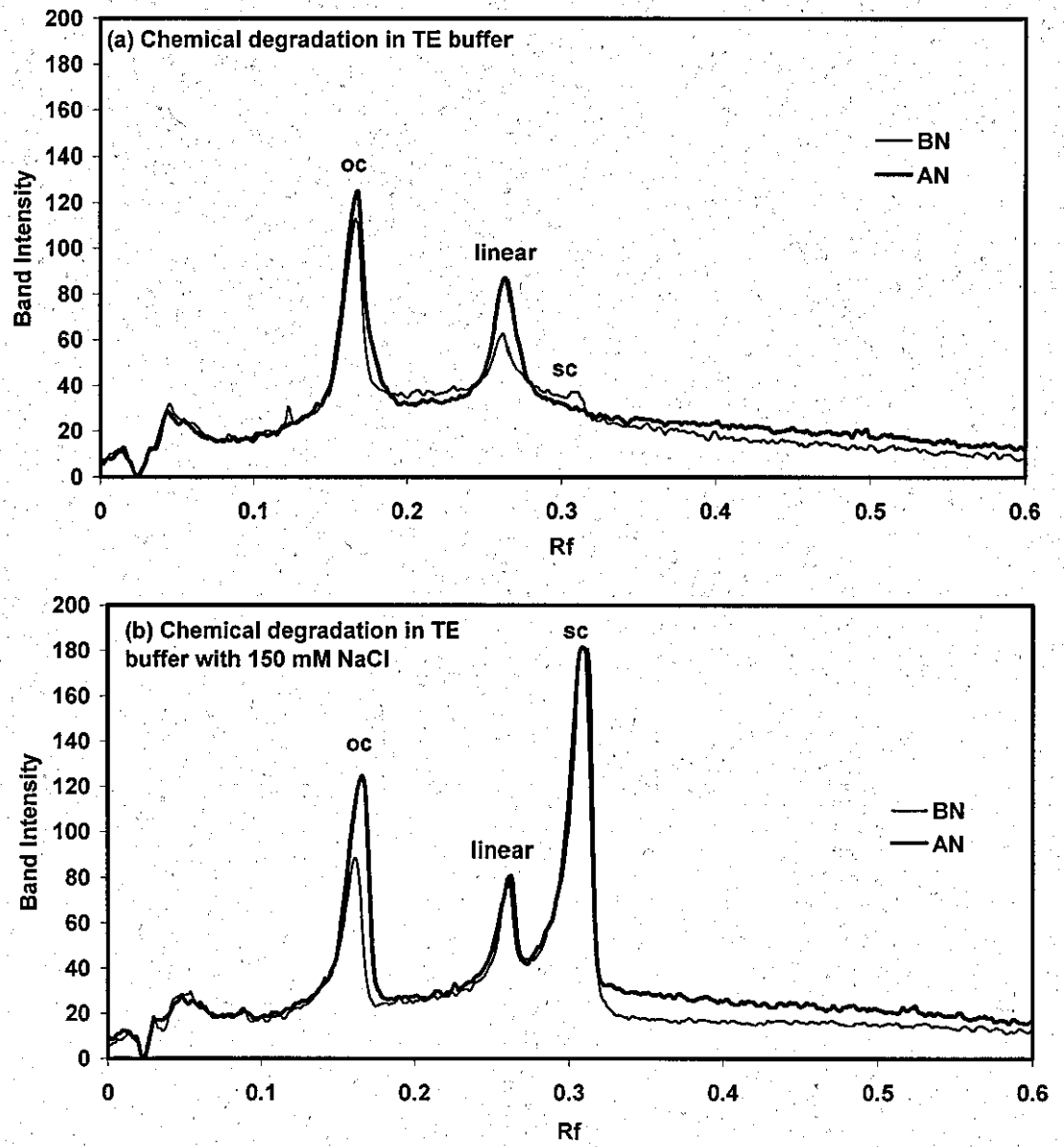

Figure 6.5: Densitometric scans of agarose gel (shown in Figure 6.4) of chemical degradation of nebulisation samples (lanes 6 to 9).

6.4.2 Time scales involved in process

Understanding of the time scales involved in the aerosolisation process could provide useful information on damage to the DNA sc structure. DNA being a flexible biopolymer, the time scales involved in the nebulisation provide clues whether relaxation of the DNA strands could lead to structural transition between the plasmid isoforms. In homogenous extensional flow, theory predicts that a coil-stretch transition occurs when the Deborah number (*De*), the product of the longest

relaxation time and the strain rate of the flow exceeds a critical value [Larson and Magda, 1989]. While the relaxation time provides a time scale for the time required for a stretched polymer to recoil back to natural equilibrium, the strain rate is a time scale for the speed of the fluid that is deforming the molecules. The ratio between these two time scales provides a critical value in determining the stretching of the molecule [Wong et al., 2003]. Meachem et al. [2005] reported the timescales for droplet formation and ejection processes by accounting for key fluid mechanical features of the phenomena from a basic understanding of the governing physics gained through careful visualization and scaling. Relaxation times are significant parameters in polymer solution dynamics and indicate the time required for the stretched polymer to regain its equilibrium position. They take into account the size of the molecule and hydrodynamic properties of the solution and are discussed below

6.4.2.1 DNA relaxation time scales

Relaxation of the plasmid DNA could occur in the regions close to the nozzle mesh experiencing a combination of elongational and shear flow. For the behaviour of buffered DNA in solution as a flexible coil, the relaxation time can be calculated from the Rouse model. The Rouse model predicts the distribution of polymer relaxation times based on freely draining theory [Larson, 1999]. This theory assumes the solvent drag on each part of the polymer molecule is the same as it would be if the other part of the polymer was not present, neglecting the effect of hydrodynamic interactions. The Rouse relaxation time for the flow of DNA in microfluidic devices are represented as a function of intrinsic viscosity $[\eta]$, solvent viscosity (η_s), molecular weight of the DNA (M), the gas constant (R) and temperature (T) [Shrewsbury et al., 2001] by the following equation.

$$\text{Relaxation time } (\tau_r) = \frac{[\eta]\eta_s M}{RT} \quad \text{.....Equation 6.13}$$

For a flexible polymer in a solvent with dominant hydrodynamic interactions, the intrinsic viscosity can be determined from universal hydrodynamic constant [Larson, 1999] using the following equation:

$$[\eta] = K_\theta M^{1/2} \quad \text{.....Equation 6.14}$$

In equation 6.14, the hydrodynamic coefficient $K_\theta = \Phi[\langle R^2 \rangle / M]^{3/2}$ and depends on the chemical make-up of the polymer and can be calculated from the elementary structural properties of the polymer, $R_{rms} \cong \langle R^2 \rangle^{1/2}$ is the root mean square separation of the ends of the molecule and Φ is the universal hydrodynamic constant $= 2.5*10^{21}$ dl cm^{-3} mol^{-1}.

For a 5.7 kb plasmid, assuming $R_{rms} = 330*10^{-9}$ m (the diameter determined from AFM imaging) $= 330*10^{-7}$ cm, $M = 3.55*10^6$ gm/mole (1 base pair – 623 gm/mole), K_θ coefficient = 0.013 dl g^{-1} $(g/mol)^{-1/2}$ = 1.3 cm^3 g^{-1} $(g/mol)^{-1/2}$, the intrinsic viscosity $[\eta]$ = 2449 cm^3/g, the relaxation time (τ_r) for a 5.7 kb plasmid is 3 ms. Similarly, for a 20 kb plasmid of molecular weight $M = 12.46*10^6$ gm/mole, the relaxation time (τ_r) is 23 ms.

Hydrodynamic interactions are disturbances in the solvent velocity field created by the motion of one part of a polymer chain that then affect the drag exerted by the solvent on other parts of the same chain [Larson, 1999; p132]. Hydrodynamic interactions influence both linear and nonlinear rheological properties of dilute solutions. The linear properties of dilute chains affected by hydrodynamic interactions are intrinsic viscosity, relaxation time and diffusivity.

The Rouse model is regarded as inappropriate in dilute solutions and hence the dynamics of a flexible polymer in dilute solution with hydrodynamic interaction is represented by the Zimm model [Doi and Edwards, 1986]. The chain relaxation time according to the Zimm model is given by the following equation:

$$\tau_{r_{Zimm}} = \frac{0.61[\eta]\eta_s M}{RT} \quad \text{.....Equation 6.15}$$

where $[\eta]$ is the intrinsic viscosity, η_s is the solvent viscosity, M is the molecular weight of plasmid. The computed chain relaxation times based on the Zimm model for the 5.7 kb and 20 kb plasmids are 1.83 ms and 14.83 ms respectively.

Experimental studies on the nebulisation of plasmid DNA using a mesh nebuliser discussed in Chapter 4, showed the sc structure of a 5.7 kb plasmid is not degraded, while that of a 20 kb plasmid is degraded. With the lack of data in literature on DNA damage and relaxation time scales of DNA using such devices, comparison of the relaxation time with the timescales based on the particle/fluid flow through the device may provide information on damage to large sized plasmids. Timescales based on parameters such as particle size, frequency, inertia, capillary and viscous properties are discussed below.

6.4.2.2 Process time scale

The periodicity of the aerosols generated from the vibrator horn is dependent mainly on the oscillation frequency. The inverse of driving frequency can be used as a parameter to define the characteristic time scale for the aerosolisation process. The process time scale (τ_f) for a mesh nebuliser operating with a frequency (f) of 175 kHz can be determined by

$$\tau_f = \frac{1}{f} \quad \text{.....Equation 6.16}$$

The process time scale is therefore of the order of 5 microseconds.

6.4.2.3 Inertial time scale

The inertial time scale (τ_u) characterizes the impetus for fluid motion and is defined as the ratio of the characteristic length scale (r_o) and the ejection velocity (U) of the droplets. The minimum velocity (U_{min}) of ejected droplets was computed from a product of radius of the orifice (r_o) and device frequency (f). U_{min} was observed to be one-fourth of the droplet ejection velocity (U) of 1 m/s, determined from frequency and volumetric flow rate measurements.

Inertial time scale $\tau_u = \frac{r_o}{U}$ .....Equation 6.17

For an inertial time scale of 1.5 μs, the validity of the ejection law [Meachem et al., 2005] holds since $\tau_u < \tau_f$ and ejection takes place.

6.4.2.4 Particle relaxation time scale

The particle relaxation time based on Stokes number [Finlay, 2001] is given by

$$\tau_{St} = \frac{\rho_p d^2}{18\eta} \quad \text{.....Equation 6.18}$$

In the above equation, d is the diameter of the plasmid particle, ρ_p is the particle density (assuming 500 kg.m^{-3}) and η is the viscosity of the buffer with plasmid DNA. Incorporating in equation 6.9, for a 5.7 kb plasmid, when d = 330 nm, τ_{St} = 2.82 nano second and for 20 kb plasmid, when d = 1250 nm, τ_{St} = 0.04 micro second.

These two timescales indicate that the plasmid DNA particle motion adjusts itself easily to the imposed process and inertial timescales, so the particle motion is effectively quasi-steady.

6.4.2.5 Capillary time scale

The capillary time scale is the time scale at which the surface tension acts at the interface. This gives a measure of the time constant that defines the dynamics of the interface deformation. Capillary time scale is a function of the surface tension (γ), the characteristic length scale (r_o), and the fluid density (ρ) and is represented by the following expression:

$$\text{Capillary time scale } \tau_\sigma = \sqrt{\frac{\rho r_o^{\,3}}{\gamma}} \quad \text{.....Equation 6.19}$$

Using $\rho = 10^3$ kg.m^{-3}, $\gamma = 0.072$ N.m^{-1} and $r_o = 1.5\text{x}10^{-6}$ m, this yields the capillary timescale $\tau_\sigma = 2.15 \text{ x } 10^{-7}$ s = 0.21 μs. The validity of the ejection law [Meachem et al., 2005] holds since $\tau_\sigma < \tau_f$ and droplet ejection takes place.

6.4.2.6 Viscous time scale

The viscous time scale characterizes fluid relaxation via viscous forces induced by the fluid motion and is defined as the square of the characteristic length scale divided by the viscous diffusivity (η/ρ) and is represented by the following expression:

Viscous time scale $\tau_\mu = \frac{\rho r_o^{\,2}}{\eta}$ .....Equation 6.20

The viscous time scale (2.25 μs) was observed to be comparable to other time scales.

6.4.2.7 Summary of time scales

The values of time scales discussed above for 5.7 and 20 kb plasmids related to DNA dynamics, relaxation, and aerosolisation process are summarised in Table 6.2. The relaxation timescales for the plasmids were observed to be slower than all the flow timescales. This observation suggests that the flow changes so fast that the DNA configuration is effectively frozen. However, the Stokes relaxation timescales for the plasmids are observed to be faster than all other flow timescales. In such a situation, the motion of the plasmid DNA particle as a whole is quasi-steady; i.e. the particle effectively immediately adjusts itself to local flow. The next section deals with the mechanics of fluid flow through the nozzle of the mesh nebuliser and predicts the hydrodynamic force responsible for damage to the DNA sc structure.

Table 6.2: Computed time scales studied for aerosolisation of 5.7 and 20 kb plasmids

Timescales studied	Time	5.7 kb plasmid	20 kb plasmid
DNA/ polymer models	Relaxation time	1.83 ms	14.83 ms
DNA particle size	Stokes relaxation time	2.82 ns	0.04 μs
Fluid flow though device	Process time	5 μs	
	Inertial time	1.5 μs	
	Capillary time	0.21 μs	
	Viscous time	2.25 μs	

6.5 Mechanics of fluid flow through nebuliser

A computational fluid dynamics study was carried out to assess the flow of fluid through the nozzles of an ultrasonically driven mesh nebuliser in order to examine if it is possible to predict the potential degradation of a genetic drug within the device. Typical strain/deformation rates through the nozzle of the mesh during the nebulisation process were determined to understand the deformation/degradation of the therapeutic. A knowledge of the strain rates and size of the sc structure determined using atomic force microscopy enabled prediction of the hydrodynamic force responsible for damage to the sc structure.

6.5.1 CFD methodology

The CFD approach was aimed at modelling the flow of fluid through a nozzle of the mesh nebuliser to estimate the level of strain rates prevalent in the flow conditions. Literature on the dynamics of flow through the micro-scale domain provides no information on the level of strain rates responsible for the damage of shear-sensitive materials in mesh type nebulisers. The assumptions within the model include:

1. The fluid has the physical properties of water and the flow is laminar,
2. The motion of the fluid relative to the mesh nozzle was examined in a frame of reference that was attached to the moving mesh wall,
3. The relative fluid motion was simulated by means of a linear (steady-state) and sinusoidal (unsteady-state) velocity inlet,
4. Axisymmetric flow and friction between fluid and air is neglected.

6.5.1.1 Model geometry and boundary conditions

A cross-section of the nebuliser mesh of the U22 device and an axi-symmetric domain chosen for the flow of fluid through a single nozzle with boundary conditions is shown in Figure 6.6.

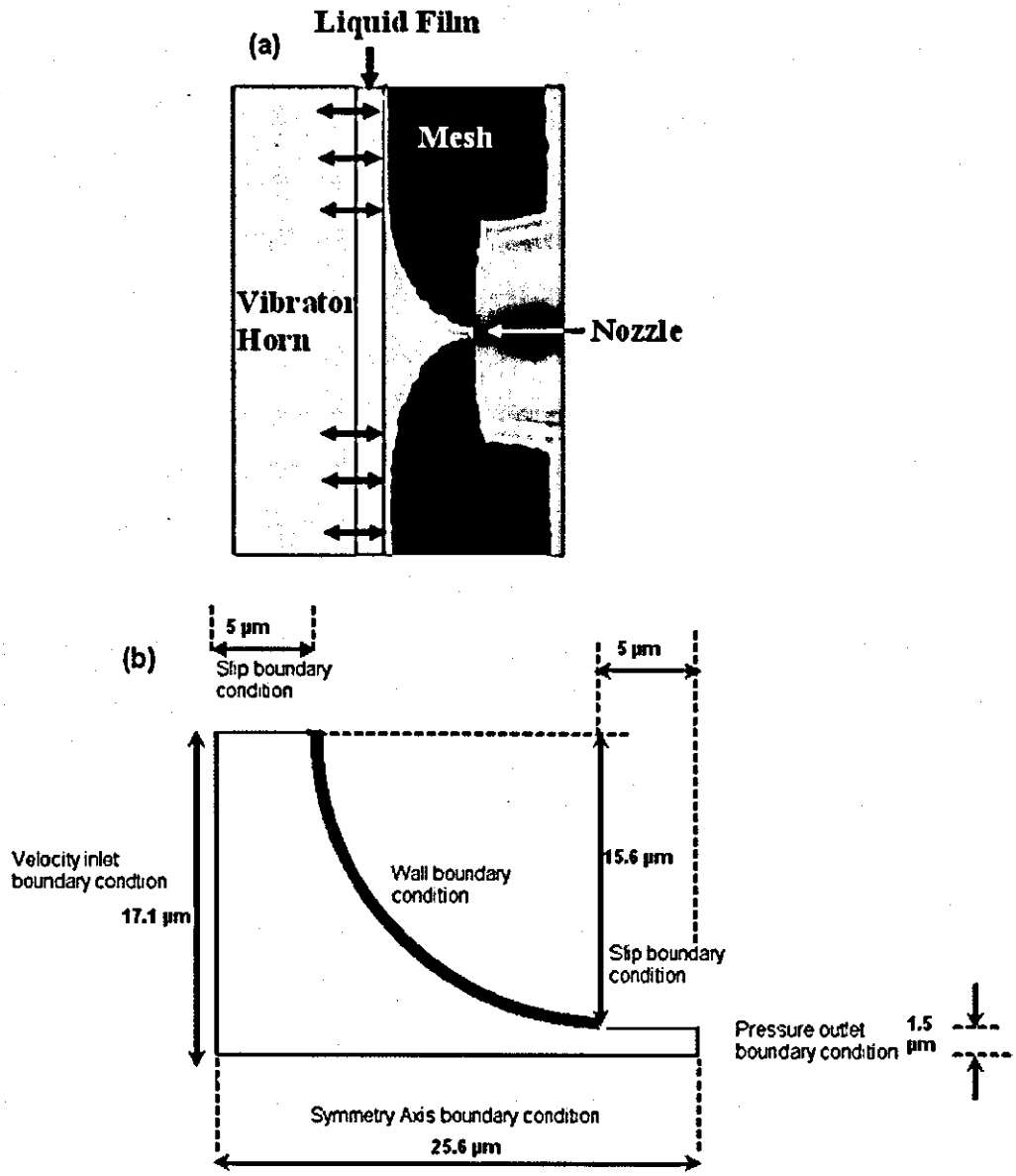

Figure 6.6: a) Section of a nozzle of the mesh used in the U22 mesh nebuliser; diameter of the nozzle – 3µm; frequency of the vibrator horn – 175 kHz. b) Dimensions and boundary conditions for the axi-symmetric domain of a nozzle of the nebuliser mesh; boundary conditions - velocity inlet at the vibrator horn, pressure outlet at the nozzle exit; wall at the nozzle wall; slip adjacent to the nozzle wall; symmetry axis at the axis of the nozzle.

The nozzles in the mesh have a diameter of 3 µm and a radius of 15.6 µm at the inlet. The dimensions of the mesh for a single nozzle are also shown in Figure 6.6. The

dimensions and boundary conditions for the domain are discussed in Chapter 3. A slip boundary condition was introduced beyond the nozzle exit in order to simulate the formation of a liquid jet surrounded by air in the region near the nozzle exit. A fine grid of 78,983 triangular cells created in Gambit was used to generate the results presented here. Steady-state and transient flow simulations were carried out using the commercial CFD code, Fluent 6.2. In the latter case, a sinusoidal velocity component, which fluctuated at a frequency of 175 kHz and with assumed amplitude of 10% of the inlet velocity, was added to the inlet velocity. Flow through the nozzle is laminar (Reynolds number ~ 3) for the domain and the solution algorithm adopted was SIMPLE pressure-velocity coupling [Versteeg and Malalasekera, 1995] along with second-order discretisation for pressure and third-order MUSCL (Monotone Upstream-Centred Schemes for Conservation Laws) momentum discretisation. The strain rates based on elongational and shear strain determined from CFD were used to calculate the maximum hydrodynamic force from the elongational and shear-induced elongational strain rate components respectively. Grid dependency studies using triangular and quadrilateral meshes (discussed in section 6.3.1.3) with parameters of pressure drop and average strain rate at the nozzle exit were carried out to establish if a mesh was refined in sufficient detail to reveal the velocity gradients.

6.5.1.2 CFD simulation for fluid flow though nozzle

In order to determine the dominant strain effects and the magnitude of the strain rates in the fluid flow, a CFD model was developed of the flow through a single axi-symmetric nozzle as shown in Figure 6.6b. The flow of fluid through the mesh nozzle of the nebuliser possibly results in the following strains on the fluid near the nozzle: (i) shear strain due to friction between the nozzle wall and the fluid, (ii) elongational strain due to reduction in area as the fluid passes through the nozzle and (iii) compressional strain as the fluid leaves the nozzle due to the change from solid/liquid to gas/liquid boundary conditions and the associated rapid redistribution of the velocity profile. A contour plot of streamlines for steady-state simulation is shown in Figure 6.7. The streamlines exhibited by the fluid flow through the nozzle suggested that the computational grid has been refined well to characterize the effect of strain fields for the domain. The steady state simulations revealed the general trends of the

shear strain rate and compressional/ elongational strain rate profile calculated by Fluent in the vicinity of the nozzle exit.

Transient simulations yielded similar levels of strain rates near the nozzle. The highest strain rate occurred near the nozzle exit and due to the constriction at the nozzle of the nebuliser mesh. Theoretically, the maximum strain rates at the nozzle exit determined by 'v/d' ratio (defined by ratio of velocity of fluid at nozzle to the diameter of the nozzle) are in the order of 10^6 s^{-1}. Plasmid DNA is susceptible to elongation and shear due to its fragile molecular structure and hence elongational and shear strain rates were used to predict the maximum hydrodynamic force. The resulting elongational and shear strain rates computed from the flow field are shown in Figure 6.7.

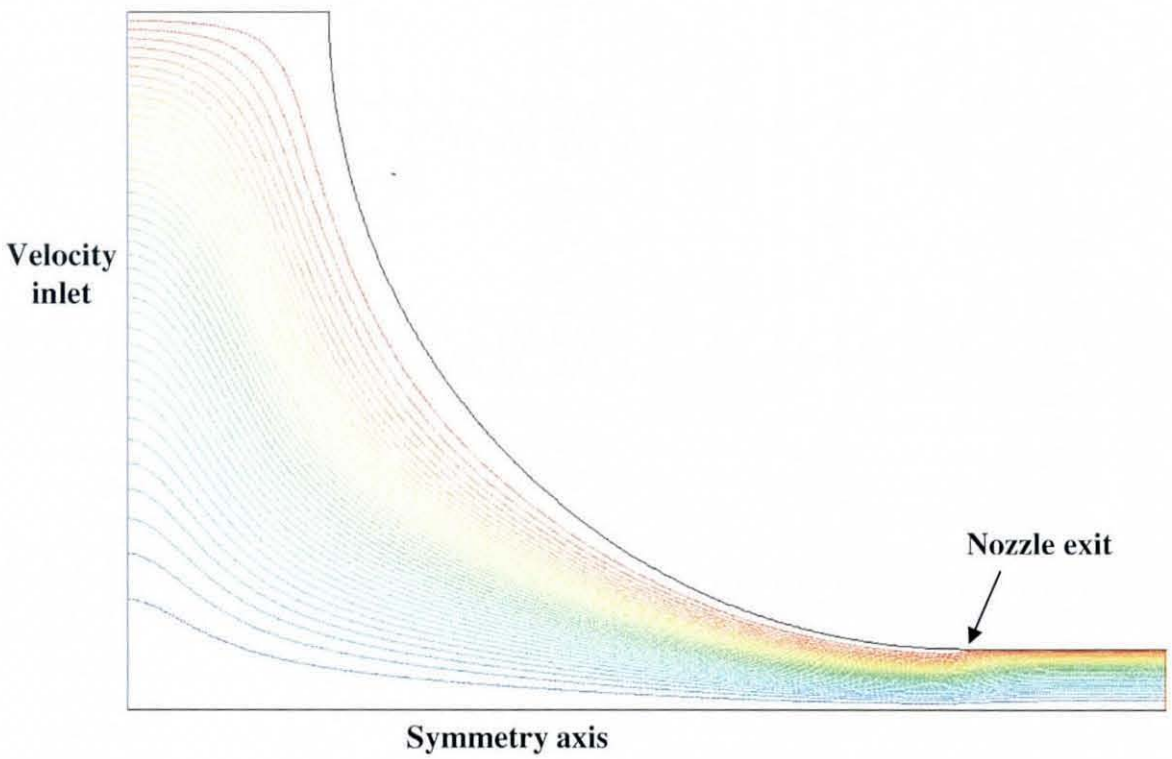

Figure 6.7: Contours of velocity stream lines for steady state simulation of the flow of fluid through the nozzle of the mesh nebuliser.

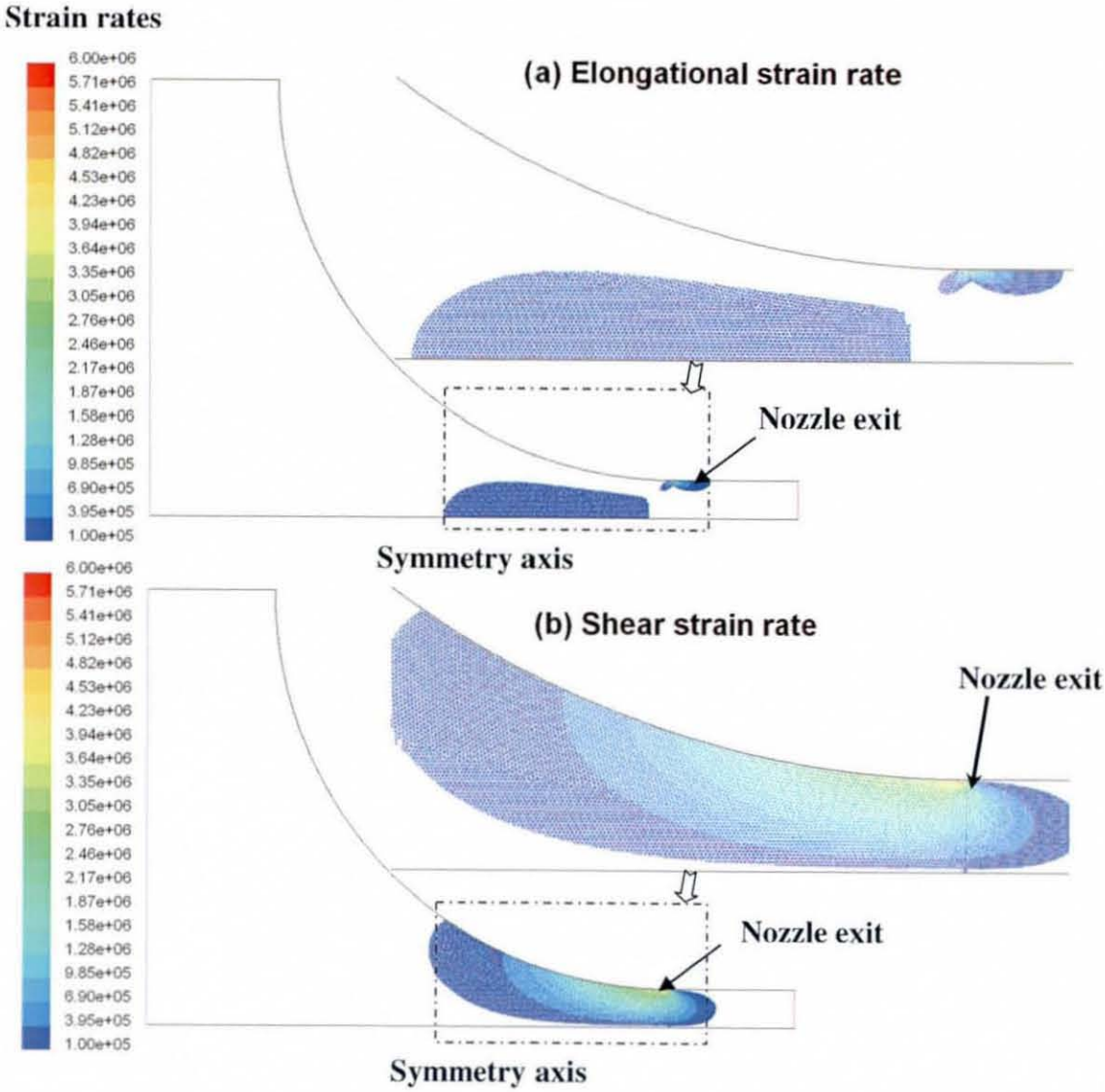

Figure 6.8: CFD simulations of strain rates (in s^{-1}) used to determine the maximum hydrodynamic force near the nozzle of the mesh nebuliser (a) elongational strain rate and (b) shear strain rate; Inset shows the strain rates in the nozzle exit.

6.5.1.3 Grid dependency studies

In order to check the accuracy of the strain rate predictions from the CFD simulations, grid dependency studies were carried out. Grid refinement was carried out using triangular and quadrilateral meshes. Table 6.3 compares the results of the CFD simulation for different mesh sizes using triangular and quadrilateral meshes.

Table 6.3: Grid dependency studies with triangular and quadrilateral meshes

Results with triangular mesh				
Mesh cells	Average velocity at nozzle (m/s)	Pressure drop between inlet and nozzle (kPa)	Average strain rate at nozzle ($x10^6$ 1/s)	% Error between triangular & quadrilateral mesh (strain rate)
15,840	1.319	19.75	1.84	
20,771	1.319	19.82	1.85	
42,121	1.318	19.97	1.87	1.60
78,983	1.316	20.04	1.95	0.10
Results with quadrilateral mesh				
Mesh cells	Average velocity at nozzle (m/s)	Pressure drop between inlet and nozzle (kPa)	Average strain rate at nozzle ($x10^6$ 1/s)	% Error between triangular & quadrilateral mesh (press drop)
2,570	1.322	19.80	1.90	
10,280	1.318	19.98	1.95	0.05
41,200	1.317	20.01	1.95	0.15

From Figures 6.9 (a) & (b), it is seen that the average strain rates, pressure drop and average velocity are sufficiently resolved for the domain. The results with the boundary layer mesh showed similar levels of strain rates. The strain rates have been reported for the CFD domain based on 78,983 cells corresponding to unit mesh length of 37.5nm.

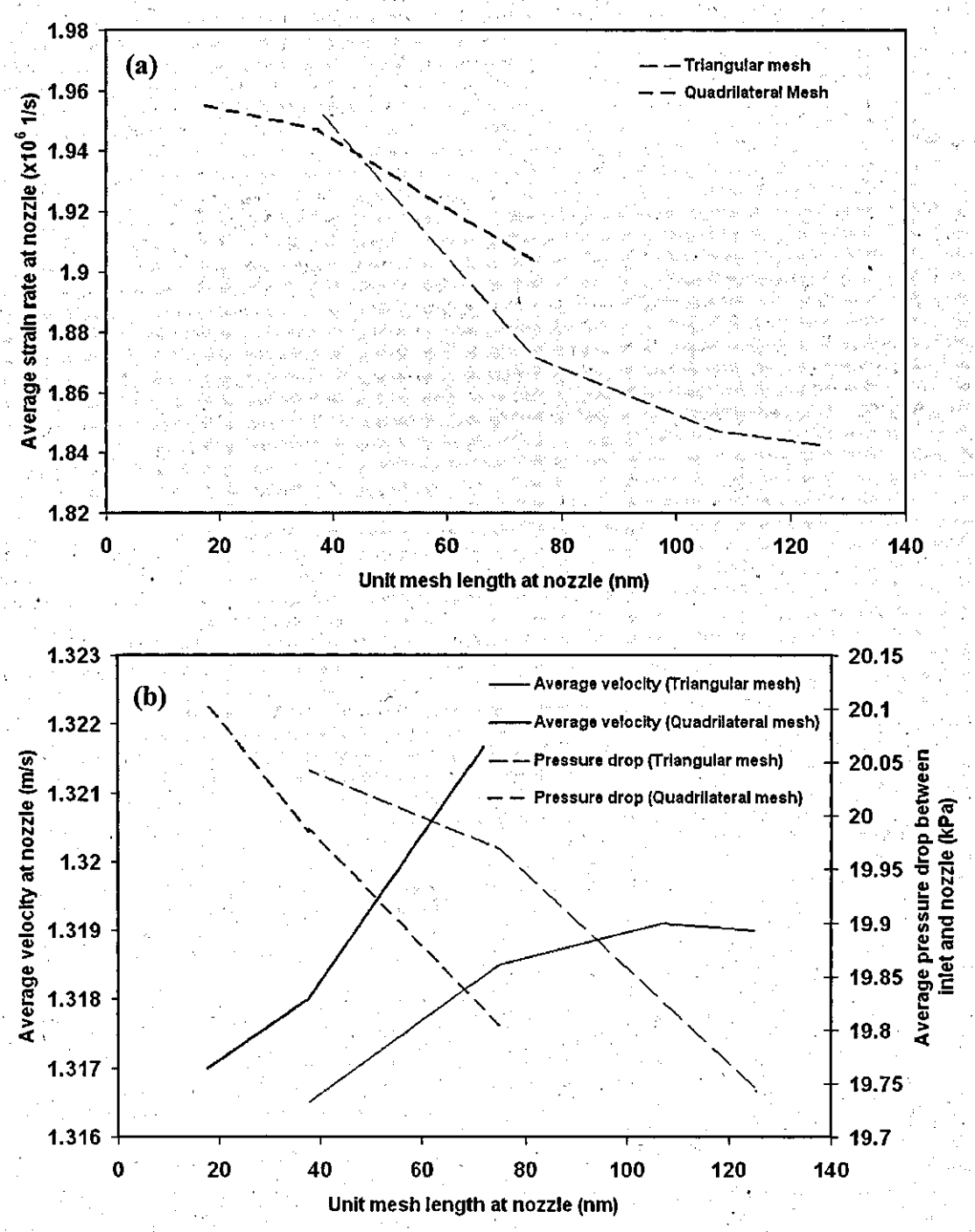

Figure 6.9: Grid dependency studies for triangular and quadrilateral meshes (a) average strain rate at nozzle, (b) Average velocity at nozzle and average pressure drop between inlet and nozzle for triangular and quadrilateral meshes.

6.5.1.4 Estimated hydrodynamic force on pDNA from strain rates

The strain rates experienced by the fluid in the nebuliser domain are fixed by the operating conditions of the device and can be used to estimate the hydrodynamic force on the fragile plasmid particles in the fluid. Lengsfeld and Anchordoquy [2002] reported the DNA molecule to assume a completely extended configuration resulting in maximum L, when the applied forces are greatest and most likely to break covalent bonds. Lentz et al. [2005] shows that the hydrodynamic force (F) on the sc structure of a plasmid is proportional to the length (L) of DNA molecule squared and the strain rate ($\dot{\gamma}$).

The magnitude of the hydrodynamic force can be estimated using Ryskin [1987] who showed that the magnitude of the stretching force at the midpoint of the chain is given by,

$$F_{max} = k\eta\dot{\gamma}L^2 \quad \text{.....Equation 6.21}$$

where F_{max} is the maximum hydrodynamic force, k is a dimensionless constant (given by equation 6.10), η is the viscosity, $\dot{\gamma}$ is the elongational strain rate and L is the length scale.

$$k = \frac{1}{2}\pi\frac{1}{\ln(5\pi/2c[\eta])} \quad \text{.....Equation 6.22}$$

where c is the concentration in g/cm^3 and $[\eta]$ is the intrinsic viscosity in cm^3/gm. For a DNA concentration of 20x10^{-6} g/cm^3 and an intrinsic viscosity of ~2450 cm^3/gm, the dimensionless constant k value was determined to be 0.3.

As shown in section 6.3.2.4, the small size of a pDNA molecule can be expected to move with the local flow velocity. The hydrodynamic force experienced by the molecule is caused by local velocity gradients. To first order in linear dimensions the velocity gradient tensor for an incompressible fluid can be regarded as a superposition of a pure straining motion and a rigid body rotation [Batchelor, 1967]. The latter cannot cause structural damage. A pDNA particle will experience variable stretching forces, which *can* lead to structural damage. The stretching strain rates are as follows if u is the axial flow velocity:

(i) $\partial u/\partial z$ is the elongational strain rate experienced when a molecule is aligned with local streamlines, and,

(ii) $0.5\partial u/\partial r$ is the elongational strain rate experienced by molecules in a pure shear flow that are oriented at 45° to the streamlines, where, $\partial u/\partial r$ is the shear strain rate.

The rotation of the molecule will cause the orientation to vary during its travel through the nebuliser mesh holes, so the elongational strain rate $\dot{\gamma}$ in Equation (6.21) must be computed as the maximum along each streamline of the flow field of the elongational strain rates due to the superposed strain and shear fields:

$$\dot{\gamma} = \max\left(\frac{\partial u}{\partial z}, 0.5\frac{\partial u}{\partial r}\right) \quad \text{.....Equation 6.23}$$

The evaluation of the hydrodynamic force (equation 6.21) requires a great deal of care since the force experienced by a pDNA molecule depends on its unknown configuration. Naked plasmid DNA behaves like a random coil, making it difficult to measure the supercoiled length. Moreover, the length scale changes as the particle distorts due to the flow forces. In order to define a realistic length scale for estimation of hydrodynamic force, the pDNA length scale was assumed as L_{AFM} (determined from AFM), where the DNA molecule forms a geometric projection from 3D to 2D [Valle et al., 2005] of its free, unstretched state. Furthermore, a theoretical estimate of the maximum plasmid size based on the molecular weight (M in kb) is given by the following equation [Kong et al., 2006].

$$L_{sc} = 0.4 \times 0.34M \quad \text{.....Equation 6.24}$$

In equation 6.24, the estimated supercoiled length (L_{sc}) is 40% of the contour length. For a 5.7 and 20 kb plasmid, the estimated L_{sc} is 775 nm and 2720 nm respectively. The average molecular dimensions determined using AFM (L_{AFM}) for the 5.7 and 20 kb plasmids were 330 nm and 1250 nm respectively. Hydrodynamic force estimates based on both these length scales, L_{sc} and L_{AFM} will be computed for unformulated plasmid. For a formulated plasmid, the estimate is based on L_{AFM} only, since L_{sc} for a compacted formulated plasmid cannot be determined.

Plasmid DNA molecules were assumed to be uniformly distributed throughout the fluid at the inlet plane and to have random orientation on entry to the nozzle. It is possible that each particle executes at least a 90 degree rotation upon its passage through the nozzle. Equation (6.21) was evaluated at several axial locations along all the streamlines that pass through the mesh points in the nozzle exit plane to yield estimates of the maximum hydrodynamic force experienced by pDNA particles. The amount of flow, and hence the number of pDNA molecules, associated with any given mesh point is proportional to the radius of its location. These estimates were subsequently sorted in order of size of the hydrodynamic force for the purposes of reporting in Figure 6.10 as a cumulative percentage of pDNA particles experiencing a hydrodynamic force equal to or smaller than a certain magnitude. Assuming the pDNA to be uniformly distributed throughout the flow, this can be interpreted as a fraction of the pDNA particles that experience a given force level at some instant in time during its passage through the nozzle.

In order to gauge the levels of maximum hydrodynamic force comparable to the bond strength it is necessary to estimate the force required to stretch and damage the plasmid DNA molecule. Double-stranded DNA breakages have been studied extensively theoretically and experimentally over the last 10 years by means of stretching loads. Table 6.4 summarizes the forces acting and the structural response of DNA. The stretching forces (30-300 pN) have a reversible elastic behaviour, while at higher forces (300-600 pN) strand separation and nick formation occur resulting in an irreversible transition, even before the limiting forces to break a covalent bond (1600 - 5000 pN) are reached. This work compares computational estimates of the stretching forces experienced by pDNA molecules during flow through the nebuliser mesh with the above estimates of maximum stretching loads.

Table 6.4: Summary of forces reported for stretching/damaging DNA

Force level	Effect of force on DNA	Reference	Force defining region
10 - 30 pN	Tensional forces for (i) Positively supercoiled DNA transition from plateau to extension state	Bustamante et al., 2003	DNA stretching region (Reversible transition)
< 65 pN	(ii) Nicked DNA transition from plateau to extension state		
65 - 110 pN	(iii) Positively supercoiled DNA in the extension state		
165 pN	Breakage of intermolecular structure based on non-covalent bonding	Lavery et al., 2002	
220 pN	Rotation of basepairs relative to phosphodiester backbone	Konrad and Bolonick, 1996	
300 pN	Shearing of bulk DNA in flowing buffer	Bustamante et al., 2000	DNA structural deformation region (Irreversible transition)
480 pN	The breaking of double strands reported to occur	Bensimon et al., 1995	
500 pN	Breakage of double stranded DNA based on retreating meniscus	Lebrun and Lavery, 1996	
600 pN	Mechanical separation of DNA strands	Konrad and Bolonick, 1996	
1600 pN	Force required to break a covalent bond	Lavery et al., 2002	
5000 pN	Force needed to cause bond scission in DNA according to Bond potential theory	Bustamante et al., 2000	

The basis for the calculation of magnitude of the hydrodynamic force acting on the plasmid DNA is as per formulae given by equations 6.21 & 6.22, which primarily depends on the strain rate and molecular length. Figure 6.10 provides information relating to the flow environment experienced by a typical pDNA molecule expressed as the percentage of the nozzle exit cross section area that is subject to a particular value of computed hydrodynamic force. Figures 6.10a-c shows estimates of the hydrodynamic stretching forces experienced by pDNA particles upon passage through the nebuliser mesh nozzle. The results are displayed as a cumulative distribution, where the vertical axis indicates the percentage of particles that experience a value less than or equal to a particular stretching force. These values are compiled by assuming a uniform distribution of the particles in the nebuliser fluid and displayed in the form of a histogram for any given cross-sectional plane in the vicinity of the nozzle exit.

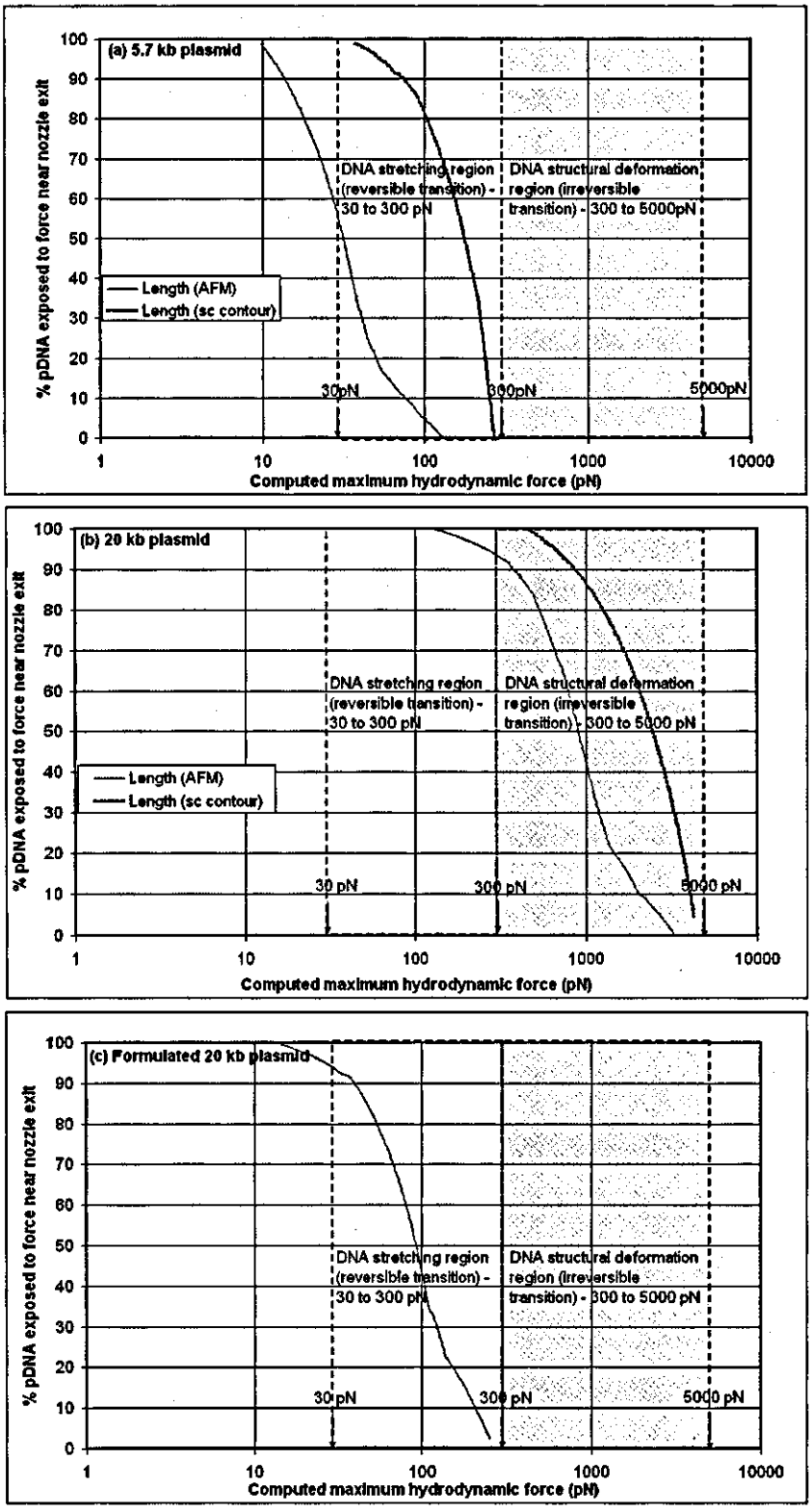

Figure 6.10: Percentage of plasmid DNA exposed to computed hydrodynamic shear force upon passage through nozzle exit of mesh nebuliser (a) 5.7 kb plasmid, (b) 20 kb plasmid, (c) formulated 20 kb plasmid; Arrows indicate the forces defining the DNA stretching and deformation region as given in Table 6.4.

6.5.2 Discussion

In order to determine the flow patterns experienced by biological macromolecules through micro-devices, a flow of lambda DNA through a microchannel is examined. A microflow composed of biological macromolecules constitutes a multifaceted problem, with a combination of elongational/ compressional flow and shear flow [Shrewsbury et al., 2001]. The relaxation time scales through such a microchannel for λ DNA in a buffered solvent at a viscosity of 0.904 cP is 0.041 second. Relaxation times are reported as the key parameters for polymer solution dynamics since they directly correlate different modes of molecule motion and the hydrodynamic properties of the solution [Wong et al., 2003]. Wong et al. studied the dynamics of single DNA molecules (T2 DNA with a size of 164 kb) under extensional flow through a microchannel for hydrodynamic focussing and observed a relaxation time of 0.63 second. The measured longest relaxation time for T7 DNA (size ~40 kb) was reported to be 50 ms [Resse and Zimm, 1990]. DNA intrinsic time scale is an upper bound estimate. It is likely that there will be shorter time scales associated with short ranging structural re-arrangements.

Scaling analysis of ejection physics enabled characterisation of droplet formation process based on timescales [Meachem et al., 2005]. The generation of aerosols from the nozzle of the ultrasonically driven mesh nebuliser is analogous to the ejection of droplets from an ultrasonic droplet ejector driven by a piezoelectric transducer. As a first step, for any ejection to occur, the comparison between inertial time scale and process time scale i.e, $\tau_u < \tau_f$ provides a quick estimate. This condition is satisfied for the nebuliser device. Secondly, the specific mode of ejection is determined by the relationship between process time scale and capillary time scale. Due to the oscillatory motion of the ultrasonic transducer, a positive and negative pressure gradient within the chamber results in a "push-pull" phenomenon of the flow. When $\tau_\sigma < \tau_f$, surface tension reacts more quickly than the positive pressure gradient, resulting in a disruption of the unstable neck of wavy jet near the orifice. This leads to the formation and ejection of an individual droplet. This condition is also satisfied for the nebuliser device and conforms to the release of aerosols during nebulisation.

Analysis based on time scales provides an insight into the physics of the process. It provides information on the nature of the relative fluid flow motion, namely: (i) relaxation times are slow, so the particle has a frozen orientation in the changing flow, (ii) the particle translates by following the mean flow and (iii) DNA particles experience flow forces or moments due to local strains. The residence time of the particle in the nozzle is too short for the slow upper bound relaxation time for DNA.

The time scale for damage of a 20 kb plasmid based on steady shear rate experiment is reported to be 2 μs at a shear rate of 4.8×10^5 s^{-1} [Levy et al., 1999]. Time scales associated with the device parameters and physical properties of fluid other than relaxation timescales are of the order of microseconds, suggesting damage is more likely for the 20 kb plasmid. However with lack of information on time scale for a 5.7 kb plasmid, it is observed that the upper time scale limit is slow compared with the other time scales. In the event of shorter internal time scales compared to relaxation time scales, it can be assumed that the DNA behaves just as an ordinary particle. Stokes relaxation time and capillary time scale are an order-of-magnitude shorter than the time scales associated with flow motions. This implies that the DNA particles are likely to follow the streamlines of flow, as discussed in the later section on computational fluid dynamics.

CFD simulations of fluid flow through the nozzle of mesh predicted strain rates in the vicinity of the nozzle exit. During the passage of plasmid DNA through the nozzle, the sc structure is exposed to elongational strain rates along the axis of the nozzle and then further exposed to shear strain rates just before the nozzle exit. As shown in Figure 6.4, shear and elongational strain rates were estimated to be greater than 10^5 s^{-1}. A maximum shear strain rate (γ_{shear}) of 6×10^6 s^{-1} and elongation strain rate (γ_{elong}) of 1×10^6 s^{-1} was localized to a very small region of the nozzle exit. Levy et al. [1999a] reported 90% damage to naked sc structure of the 20 kb plasmid on exposure to a shear rate of 1.2×10^6 s^{-1} for a period of 5-10 secs. The susceptibility of plasmid DNA to hydrodynamic shear has been reported in a homogeniser, centrifuge and atomizers at strain rates in the range of 10^4 - 10^6 s^{-1} [Lengsfeld and Anchordoquy, 1999].

Estimates of the hydrodynamic force on the unformulated 5.7 and 20 kb plasmids based on both the lower and upper limits of molecular length are shown as two distributions labeled Length (AFM) and Length (sc contour) in Figures 6.10a and

6.10b. Comparison showed that both cumulative distributions for L(AFM) and L(sc contour) were within the region of reversible stretching for 5.7 kb pDNA (Fig 6.10a). Equation (6.21) shows that the hydrodynamic forces will scale as the square of the particle size. Thus, naked 20 kb pDNA with a particle size of around four times that of a 5.7 kb pDNA is estimated to experience stretching forces that will be larger by a factor of 16. Figure 6.10b indicated that forces on the 20 kb plasmid would be within the range where irreversible structural deformation was expected for approximately 90% of the particles exposed to forces >300 pN. Formulation of the 20 kb plasmid in PEI produced a compact molecule of size roughly the same as that of an unformulated 5.7 kb, with forces in the reversible stretching region (Figure 6.10c).

The hydrodynamic force on the plasmid varies with the flow and molecular parameters. The flow parameter characterised by the strain rate ($\dot{\gamma}$) is the same for any particular device, where as the molecular parameter characterised by the molecular length of the plasmid varies with the molecular weight of the plasmid. Lengsfeld and Anchordoquy [2002] reported the DNA molecule to assume a completely extended configuration resulting in maximum L, when the applied forces are greatest and most likely to cause damage. This length scale configuration changes as the particle distorts due to the flow forces. AFM enables determination of the molecular length of the sc structure, enabling prediction of realistic hydrodynamic force. Lentz et al. [2006a] and Kong et al. [2006] reported the theoretical supercoiled length of the plasmid as proportional to the molecular weight of the plasmid. The length determined by AFM was found to be half of the theoretical supercoiled length and can be used as a lower and upper limit for the determination of the hydrodynamic force acting on plasmid DNA.

From figure 6.10a, the sc 5.7 kb plasmid is in the DNA extension/ stretching region, such levels of hydrodynamic force (<300 pN) on the compact sc structure of 5.7 kb plasmid are not likely to result in damage. The absence of damage to the 5.7 kb plasmid after nebulisation suggested that at a size of 330 nm, it can easily pass through the 3 μm diameter nozzle of the mesh nebuliser without much adverse effect on the supercoiled structure. However, ~95% of the 20 kb plasmid was exposed to forces greater than the 300 pN (Figure 6.10b) resulting in irreversible damage to the sc structure as confirmed by gel electrophoresis of the nebulised plasmid. The naked

supercoiled 20 kb plasmid had a molecular length of 1250 nm, almost one-third of the nozzle size. Although the ionic strength due to NaCl resulted in a more condensed structure [see also Lyubchenko and Shylakhtenko, 1997], nebulisation produced destruction of the sc structure into linear fragments. The damage to the sc structure resulted in the release of torsional strain from the molecule, as evident from the spaghetti-like fragments observed in the AFM.

CFD results suggest damage to the sc structure of 20 kb plasmid is likely to be due to high hydrodynamic forces experienced by a large fraction of the pDNA particles upon their passage through the nozzle of the nebuliser mesh. Shear rates of the order $>10^6$ s^{-1} have previously been found to cause damage to 20 and 29 kb plasmids during processing [Levy et al., 1999]. The fragmentation of DNA in a hydrodynamic shear testing device [Thorstenson et al., 1998] suggested that the velocity gradient at the orifice resulted in stretching of the DNA beyond its breaking point. It is suggested that the mechanism of sc pDNA degradation during aerosolisation proceeds via the formation of first an open-circular form (extension and breakage at the mid-point of a chain) followed by subsequent disintegration of the nicked plasmid to linear fragments (exposed to hydrodynamic forces > 300 pN).

The Ryskin equation used for the determination of magnitude of the hydrodynamic force as given by equation 6.21 suggested that breakage initiated at the mid-point of the polymer chain or DNA molecule. Figure 6.11 shows the distribution of the DNA fragments based on molecular size after nebulisation of the 20 kb plasmid as observed in an agarose gel electrophoresis. The peak of the DNA fragments after nebulisation was observed to be around 2.5 kb. The maximum amplitude of the peak of degradation products after nebulisation was observed to be almost half of the peak of undegraded supercoiled 20 kb plasmid (band density of 224.4 corrected with a sc factor of 1.36 for Ethidium bromide binding to sc DNA). This result based on amplitude of the band intensity coupled with the distribution of the fragmented molecules confirmed the assumption used for determination of hydrodynamic force that breakage to the plasmid sc structure occurred at the midpoint of the molecule.

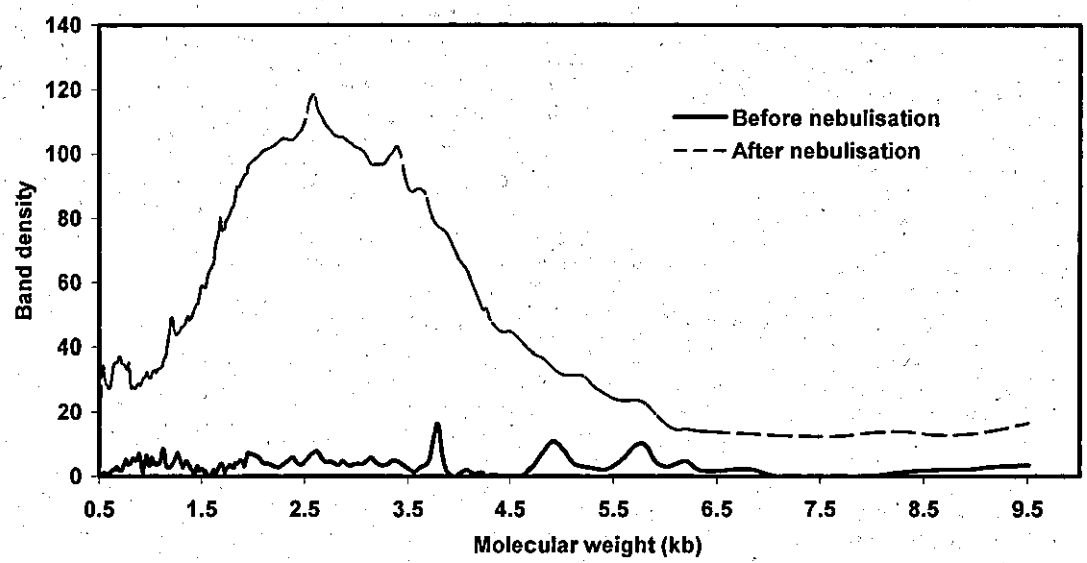

Figure 6.11: Distribution of DNA fragments of 20 kb plasmid based on molecular size after nebulisation as observed in agarose gel electrophoresis.

Zimm and Resse [1990] studied the flow-induced degradation of T7 DNA through an orifice and showed that the extensional flow leads to a broad distribution of DNA scission products. A schematic for the degradation of sc structure of a 20 kb plasmid is shown in Figure 6.12. If damage of the sc structure of the 20 kb plasmid were to occur at the mid-point of the polymer chain, a minimum of eight scissions on the molecule are required to generate DNA fragments of size 2.5 kb. In order to generate fragments of size from 0.5 to 5.5 kb, the number of scissions is higher for smaller fragments and four for fragments of size ~5 kb. The uniform distribution of DNA fragments of size from 0.5 to 5.5 kb is possibly due to exposure to hydrodynamic forces based on extensional strain rates along the axis of the nozzle, followed by forces due to shear strain rates near the nozzle exit. The shear to the open-circular forms of the 5.7 kb plasmid also indicates the susceptibility of more damage to the large open-circular forms present in the initial preparation. Hence, hydrodynamic forces present a realistic estimate of the chances of safe delivery of large sized plasmids and inform formulation for reduction of size of the sc structure.

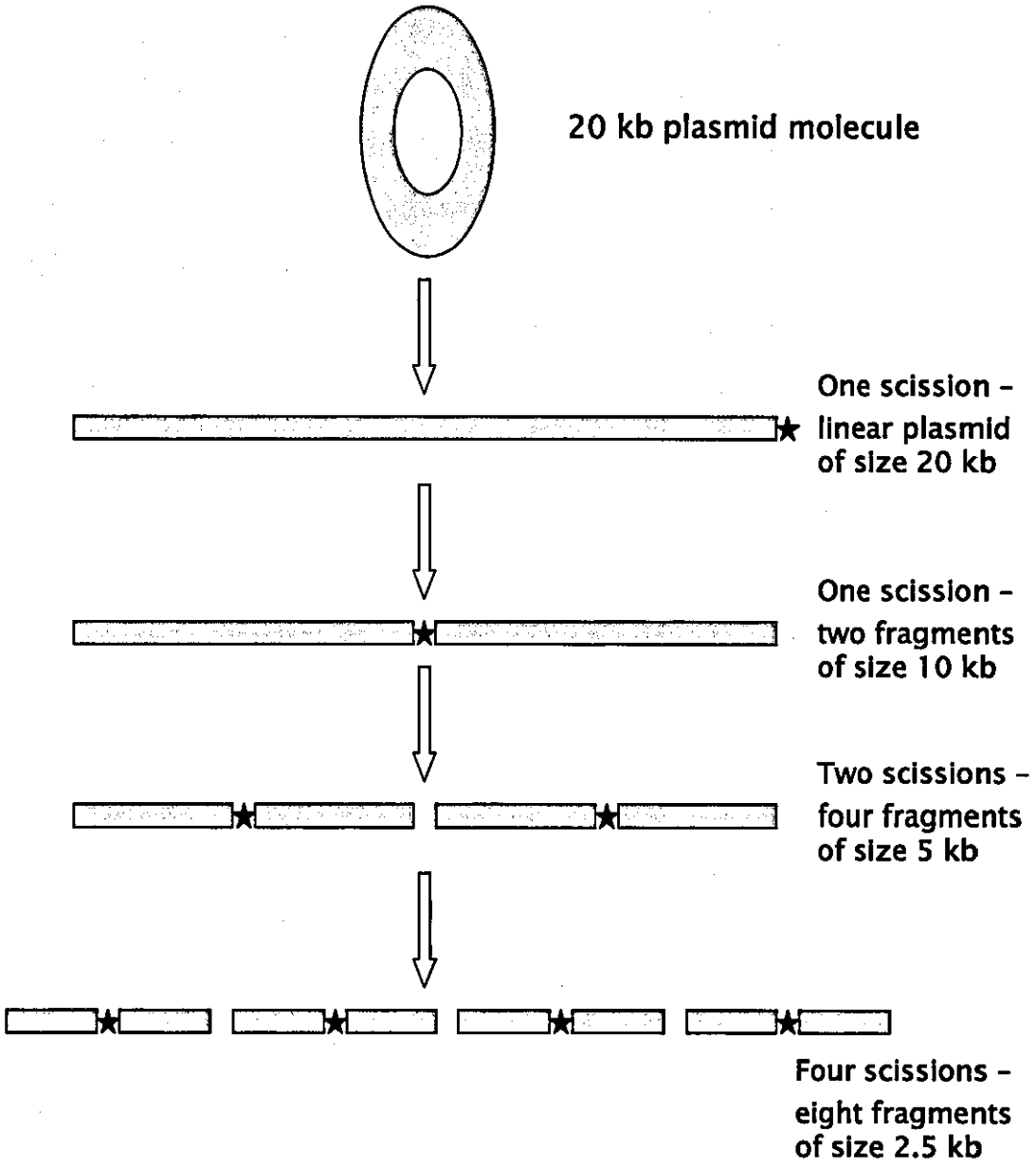

Figure 6.12: A schematic for generation of DNA fragments from degradation of 20 kb plasmid; a total of eight scissions are required to generate fragments of size 2.5 kb with the star symbol representing a scission.

Although engineering analysis has provided information on the hydrodynamic forces responsible for damage and attributed the limited influence of transient cavitation on plasmid DNA damage, it is essential to predict the limiting size of the plasmid for

safe delivery in the nebuliser. In the next section, plasmid DNA degradation in the mesh nebuliser is studied to determine the plasmid size for safe passage of the sc structure on aerosolisation.

6.6 Prediction of plasmid DNA size for safe delivery

In order to predict the size of plasmid DNA for safe aerosol delivery in a mesh nebuliser, the relative damage to the sc structure of the plasmids was studied. Experiments on the nebulisation of different sized plasmids using the U22 and U03 nebuliser devices are reported in Chapter 4. From these results, the ratio of intact sc plasmid DNA before nebulisation (C_o) to the intact sc plasmid DNA after nebulisation (C) was determined for different sized plasmids. A natural logarithm of (C_o/C) was plotted against the plasmid DNA molecular size to extrapolate the limiting size for safe delivery of sc structure of plasmid through the mesh nebuliser.

6.6.1 Degradation of plasmid DNA in a U22 mesh nebuliser

Figure 6.13 shows the plot for the degradation profile of plasmid DNA in a U22 mesh nebuliser. Extrapolation of the data from the plot, estimated that a plasmid size <6.7 kb can be safely delivered in the U22 mesh nebuliser operating at a device frequency of 175 kHz.

6.6.2 Degradation of plasmid DNA in a U03 mesh nebuliser

Figure 6.14 shows the plot for the degradation profile of plasmid DNA in a U03 mesh nebuliser. Extrapolation of the data from the plot, estimated a plasmid size < 3.8 kb can be safely delivered in the U03 mesh nebuliser operating at a device frequency of 65 kHz. The influence of device parameters like frequency of the vibrator horn on damage to the sc structure of the plasmid is discussed in the next chapter.

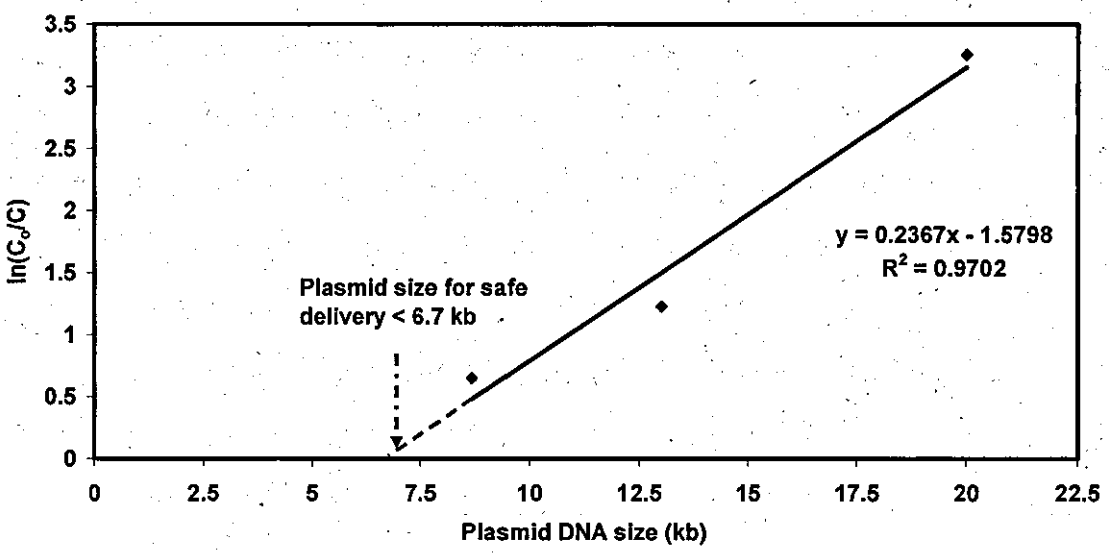

Figure 6.13: Limiting size for safe aerosol delivery of supercoiled plasmid DNA in the U22 mesh nebuliser (% damage data taken from Table 4.7).

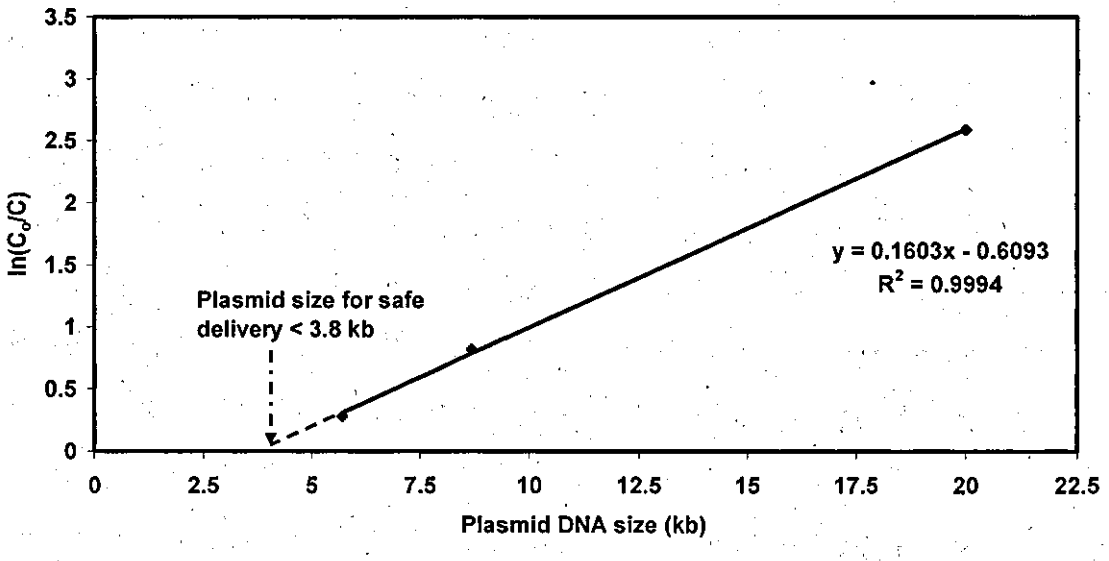

Figure 6.14: Limiting size for safe aerosol delivery of supercoiled plasmid DNA in the U03 mesh nebuliser (% damage data taken from Figure 4.22).

6.6.3 Discussion

Plasmid DNA degradation in a mesh nebuliser was observed to follow a linear profile based on the molecular size of the plasmid. Meacle et al. [2006] have shown the sc plasmid DNA degradation within a capillary device to be a first order process. Odell et al. [1988] have modelled flow-induced fracture as a rate process in which the energy barrier for bond breakage is lowered by mechanical forces exerted on the polymer by the flow. Lentz et al. [2005] studied the degradation of plasmid DNA in a jet nebuliser and suggested a minimum shear force must be exceeded before the hydrodynamic degradation rate constant becomes non-zero and therefore a molecular length scale exists below which degradation does not occur. No improvement in degradation rate is realised regardless of how far below this size one compacts DNA. However, Lentz et al did not provide any relationship to predict the size for safe delivery of plasmid DNA using a nebuliser device.

From figures 6.13 and 6.14, the limiting size of plasmid DNA for safe delivery upon nebulisation is estimated by extrapolation of the relationship between ratio of the sc plasmid before nebulisation to the intact sc structure after nebulisation and the plasmid size. Nebulisation in the U22 and U03 mesh nebulisers enables safe passage to plasmids of size less than 6.7 kb and 3.8 kb respectively. Damage to plasmids of smaller size using the U03 device at low frequency was perhaps due to effects of cavitation, as a result of increased residence time (low nebulisation rate) in the device. These figures are helpful in a practical sense to determine the limiting size for the safe delivery of the sc structure.

6.7 Conclusions

Engineering analysis of the nebulisation of plasmid DNA has provided data on the hydrodynamic force required for damage to the supercoiled structure of plasmid DNA. Damage to sc of the 20 kb plasmid and safe delivery of 5.7 kb plasmid is explained on the basis of estimated hydrodynamic force computed from the strain rates predicted using CFD modelling and sizing of sc structure using AFM imaging. Determination of hydrodynamic force levels to damage DNA in micro-scale flow environments has not yet been reported in the literature. This technique for

estimation of hydrodynamic force promises to provide information on the degradation of shear-sensitive therapeutics in such drug-delivery device combinations.

In addition to hydrodynamic force levels, high-speed imaging provided an insight on damage to the sc structure as a result of the motion of the ultrasonic vibrator horn. Partial damage to the sc structure without the mesh, suggested the influence of cavitation due to the oscillatory motion of the horn. Aerosolisation without mesh is a result of multiple vibrations of the vibrator horn. The out-of-phase vibrations of the horn and mesh result in a single-pass droplet generation through the mesh nozzle. A linear plot of plasmid DNA degradation against molecular size enabled estimation of the limiting size for safe passage of the sc structure upon aerosolisation in the mesh nebuliser. An unformulated plasmid of size less than 6.7 kb and 3.8 kb was estimated for safe delivery of the sc structure using the U22 and U03 mesh nebulisers respectively.

The influence of hydrodynamic force on damage to sc structure was observed to be a significant parameter affecting delivery and reduction of the size of sc structure ensured lower levels of hydrodynamic force and consequently safe aerosol delivery. The method of estimating limiting plasmid DNA size for safe delivery in a mesh nebuliser provides data for the design of plasmid DNA based gene therapeutics. From the engineering analysis on the nebulisation of plasmid DNA, it is observed that the device parameters such as nozzle size and frequency are crucial for the safe aerosol delivery of the sc structure of plasmids. The influence of these two parameters on plasmid DNA damage for different plasmid sizes is discussed in the next chapter.

CHAPTER 7. DEVICE PARAMETERS INFLUENCING PLASMID DNA DAMAGE

7.1 Introduction

Engineering studies on the nebulisation of plasmid DNA in a mesh nebuliser have shown damage to be dependent on the size of the sc structure of plasmid. Results from the univariate analysis in chapter 4 suggest that in addition to plasmid size and nozzle size, device frequency may also influence damage to sc structure of the plasmid. Device frequency imparts the driving force responsible for aerosolisation of the liquid and hence experiments on the effect of driving frequency and plasmid size are expected to provide information on damage to the sc structure. Factorial designs of experiments were carried out to investigate the influence of size and frequency on damage to the sc structure of plasmids upon nebulisation. Two multivariate two-level full factorial designs were performed with the following variables: (i) plasmid size and nozzle size, and (ii) plasmid size and device frequency. The 2^2 factorial design was used to check the significance, main effects and interactions of the variables involved.

7.2 Influence of size on damage: DOE using factorial design

As discussed in the earlier chapter, nozzle size of the mesh nebuliser is a crucial factor limiting the plasmid size for safe aerosol delivery of the sc structure. DoE using factorial design was carried out to understand the influence of nozzle size on damage to the sc structure of different plasmid sizes.

7.2.1 Choice of variables and levels

The variables for the 2^2 factorial design chosen were plasmid DNA size and nozzle size and the response was damage to the sc structure of the plasmid after nebulisation. To study the response and its interactions across a range of plasmid and nozzle sizes, a

plasmid size at the lower limit (8.7 kb) and higher limit (20 kb) was chosen for the study. Similarly, nozzle sizes at the lower (3 μm) and higher (5 μm) limit were employed. The variables and levels chosen for the experimental design are shown in Table 7.1.

Table 7.1: Variables and levels chosen for factorial design of experiments

Variables	**Levels**	
	-	+
Plasmid size (kb)	8.7	20
Nozzle size (μm)	3.0	5.0

7.2.2 Experimental design

The experimental design chosen was a full factorial design ($2^2 = 4$) for a two variable experimental design with two levels. The experimental design consisting of 4 runs with the levels of the variables is shown in Table 7.2.

Table 7.2: A 2^2 factorial experimental design for plasmid and nozzle sizes as variables

Run	**Plasmid size (kb) (Coded units)**	**Nozzle size (μm) (Coded units)**
1	8.7 (-)	5 (+)
2	20 (+)	3 (-)
3	20 (+)	5 (+)
4	8.7 (-)	3 (-)

The response of % damage to the sc structure was determined from average values of triplicate measurements from the densitometric scans of separate agarose gels.

7.2.3 Analysis of factorial experimental design

The analysis of 2^2 factorial design was done using Minitab® 15.1 (Stat-Ease, Inc., Minneapolis, USA), and the results from the statistical analysis, model diagnostic plots, contour plots and response surface plots are reported.

The results of the factorial fit for % damage to sc structure versus plasmid size and nozzle size are given in Tables 7.3 & 7.4. The estimated effects and coefficients for % damage are shown in Table 7.3. This table indicates the coefficient of determination R^2 and adjusted R^2 values for this model are good with a predictable response.

Table 7.3: Estimated effects and coefficients for % damage in coded units

Term	Effect	Coefficient	SE Coefficient	T	P
Constant		44.46	1.021	43.53	0.000
Plasmid size (kb)	35.60	17.80	1.021	17.43	0.000
Nozzle size (μm)	-52.60	-26.30	1.021	-25.75	0.000
Plasmid size (kb) * Nozzle size (μm)	-17.38	-8.69	1.021	-8.51	0.001
S (Standard deviation) = 2.88897					
PRESS (Predicted Residual Sum of Squares) = 133.538					
R^2 (Coefficient of determination) = 99.62%					
R^2 (Predicted) = 98.47%					
R^2 (Adjusted) = 99.33%					

Table 7.4 shows the results of analysis of variance (ANOVA) for % damage to the sc structure. Significant interactions for the main effects and two way interactions are predicted.

Table 7.4: Analysis of variance (ANOVA)

Source	Degrees of freedom (df)	Sequential Sum of Squares	Adjusted Sum of Squares	Adjusted Mean Sum of Squares	F value	p-value (Prob >F)
Main effects	2	8068.24	8068.24	4034.12	483.35	0.000
2-Way interactions	1	604.13	604.13	604.13	72.38	0.001
Residual error	4	33.38	33.38	8.35		

The significant variables of the model are plasmid size, nozzle size, and interaction between plasmid and nozzle size. The response equation for % damage to sc structure in terms of estimated coefficients (determined using data in uncoded units) and variables is given in equation 7.1.

$$Damage_{sc} = 16.1719 + (9.3026 * X_{plasmid}) - (4.2289 * X_{nozzle}) - (1.5380 * X_{plasmid} * X_{nozzle})$$

.....Equation 7.1

The next section will analyse the contour and response surface plots, and check the significance of the variables predicted in the model.

7.2.4 Model adequacy plots

The adequacy of the model and significance of the variables are discussed in Figures 7.1 and 7.2. Figure 7.1 shows the normal plot of the standardized effects in the model. In confirmation of the results in the earlier section, the main variables and interactions were predicted to have a significant effect on the model. As shown in the figure, plasmid size was predicted to have a positive effect resulting in increased damage to the sc structure. However, nozzle size was predicted to have a reverse effect with decreased damage to sc structure. As observed in the figure, the interaction between the two variables had a significant effect on the response.

The Pareto chart of standardized effects shown in Figure 7.2 also showed similar results as in Figure 7.1. However, nozzle size was predicted to have a greater influence on damage when compared to plasmid size. Although the effect of interaction between the variables was less than the main effects, it was still predicted to be significant.

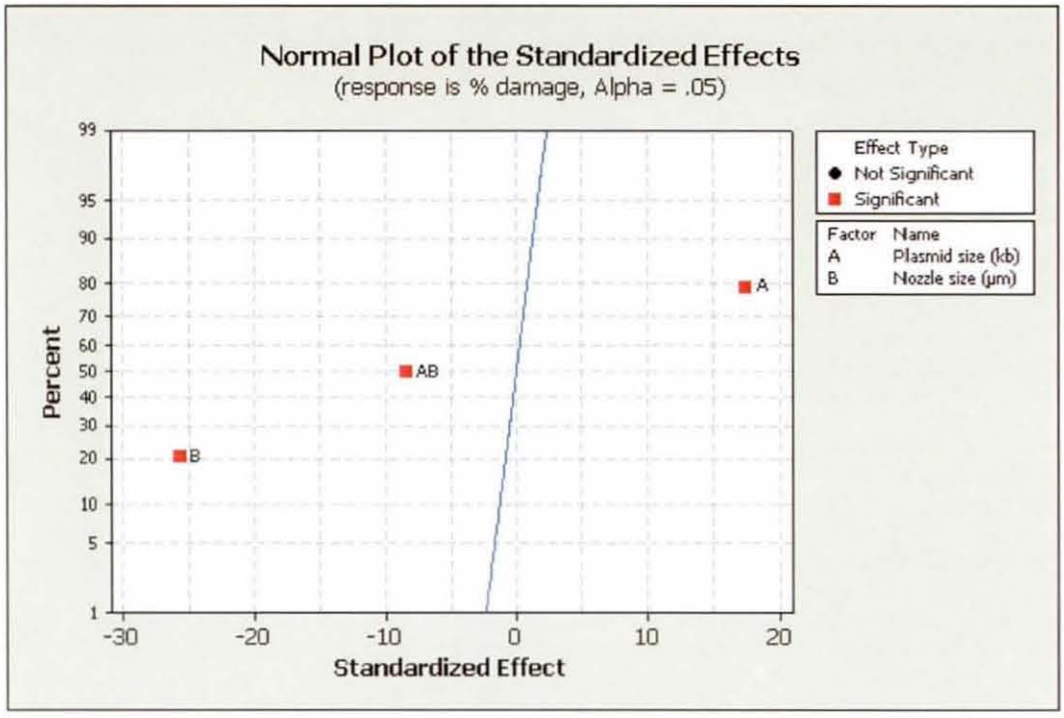

Figure 7.1: Normal plot of standardised effects for plasmid and nozzle sizes

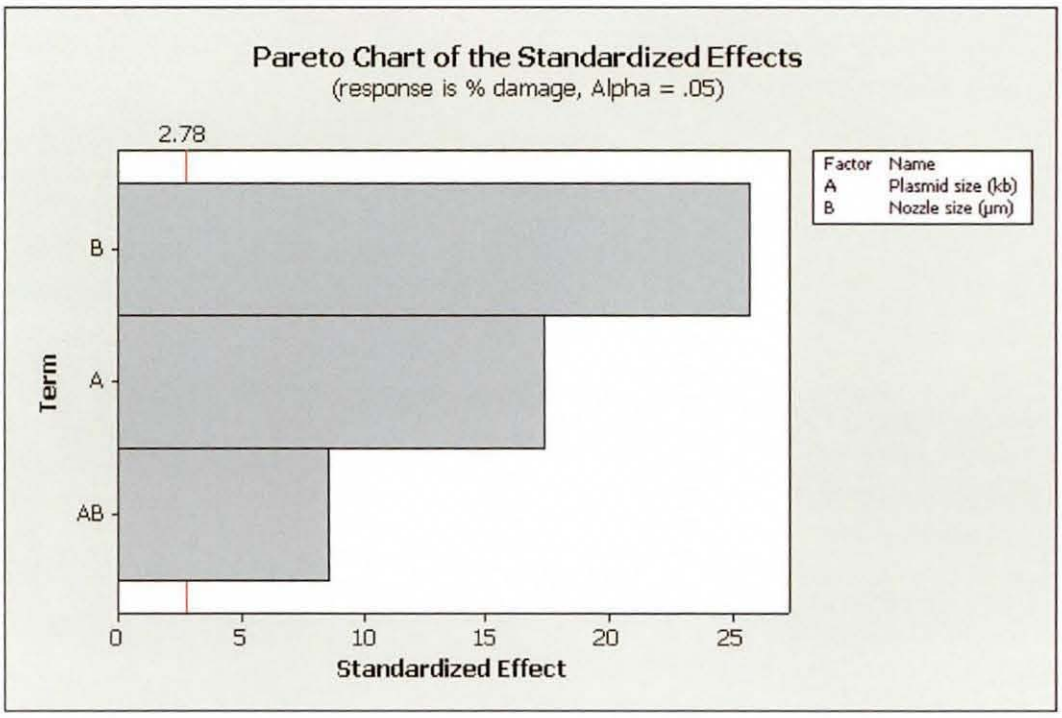

Figure 7.2: Pareto chart of standardised effects for plasmid and nozzle sizes.

7.2.5 Model predictions: Main effects and interaction plots

The main effects and interaction plots for damage to sc structure of plasmids is shown in Figures 7.3 and 7.4 respectively. The main effects plot shows the magnitude of the effects of each variable. As confirmed in Figures 7.1 and 7.2, the main effects plot shows the significance of the nozzle size. Interaction plots are useful for judging the presence of interactions. As shown in Figure 7.4, non-parallel lines in the interaction plots suggest the presence of interaction between the variables.

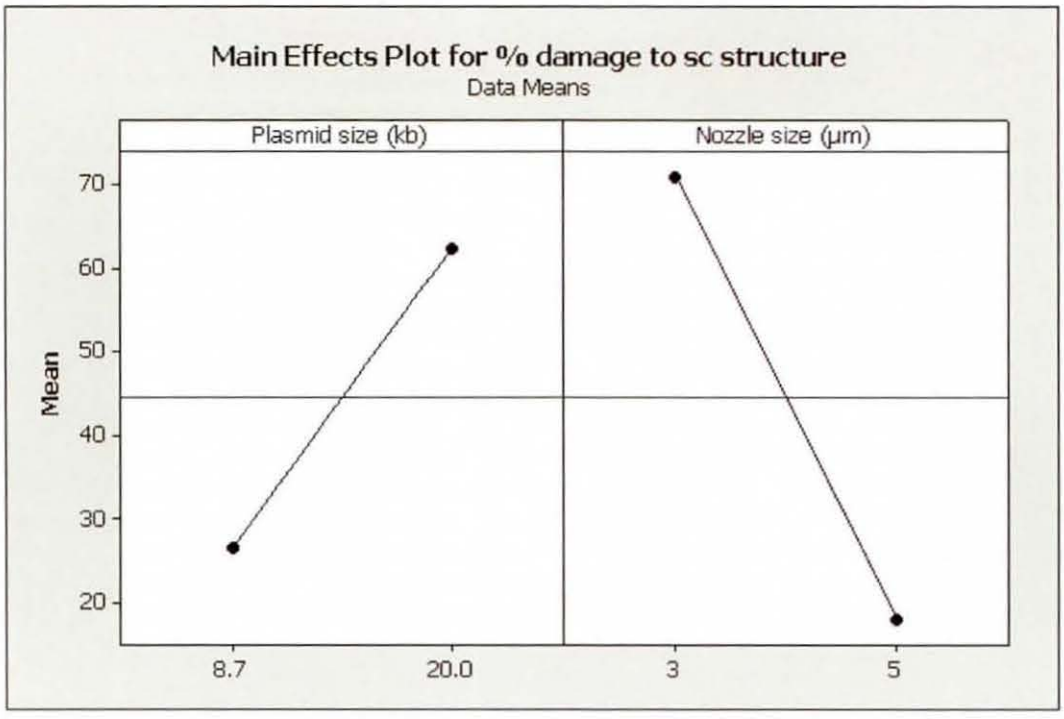

Figure 7.3: Main effects plot of plasmid and nozzle sizes for % damage to sc structure.

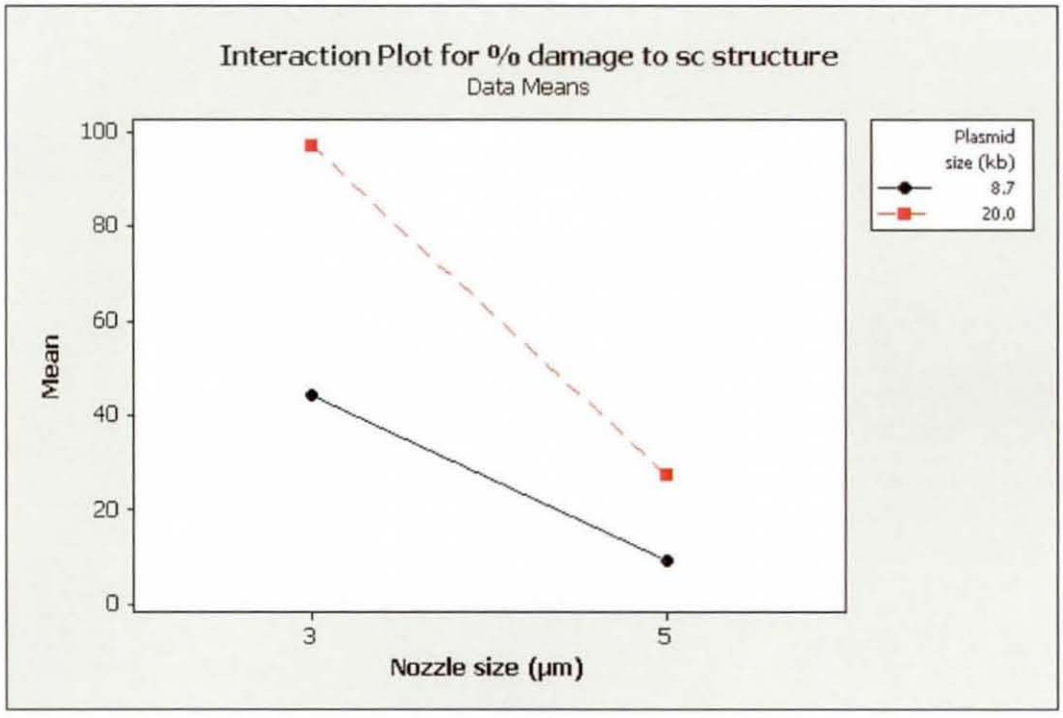

Figure 7.4: Interactions plot of plasmid and nozzle sizes for % damage to sc structure.

7.2.6 Model predictions: Contour and surface plots

The contour plots and surface plots predicted % damage to sc structure of plasmids from 8.7 kb to 20 kb for nozzle sizes from 3 μm to 5 μm as shown in Figure 7.5. The % damage to sc structure of a plasmid of intermediate size such as 13 kb for an intermediate nozzle size of 4 μm was predicted to be 40-60%. The experimental value of % damage was observed to be 62.1%. Although, the contour predictions did not exactly match the actual value, it does provide useful information on the levels of damage.

7.2.7 Discussion

Box-Behnken based DOE experiments on nebulisation of 20 kb plasmid using different nozzle sizes predicted damage to sc structure was more pronounced for a 3 μm nozzle than for 4 μm or 5 μm nozzles. Results from the statistical analysis, shown in Table 7.3 revealed plasmid size, nozzle size and their interaction to have a significant effect on the damage to sc structure of the plasmid. Similar results are shown by the normal plot of standardized effects (Figure 7.1) and Pareto chart of standardized effects (Figure 7.2).

The contour plot shown in Figure 7.5 predicted the damage levels to the sc structure of plasmids of size 8.7 kb to 20 kb for nozzles of size from 3 μm to 5 μm. For the 3 μm nozzle, predicted damage levels were about 40-60% for the 8.7 kb plasmid and >95% for the 20 kb plasmid. The actual damage at the 3 μm nozzle matched the predicted values well. With increase in nozzle size, the predicted damage levels decreased. At a nozzle size of 4 μm, predicted damage levels were 20-40% for the 8.7 kb plasmid and 40-60% for the 20 kb plasmid. Actual damage to the sc structure of 8.7 kb and 20 kb plasmid for the 4 μm nozzle were 15.5% and 35.8% respectively. For the 5 μm nozzle, predicted damage levels for the 8.7 kb and 20 kb plasmids were <20% and 20-40% respectively, which coincided with the actual values. The predictions for % damage to the sc structure from the contour plot were within the range of experimental values.

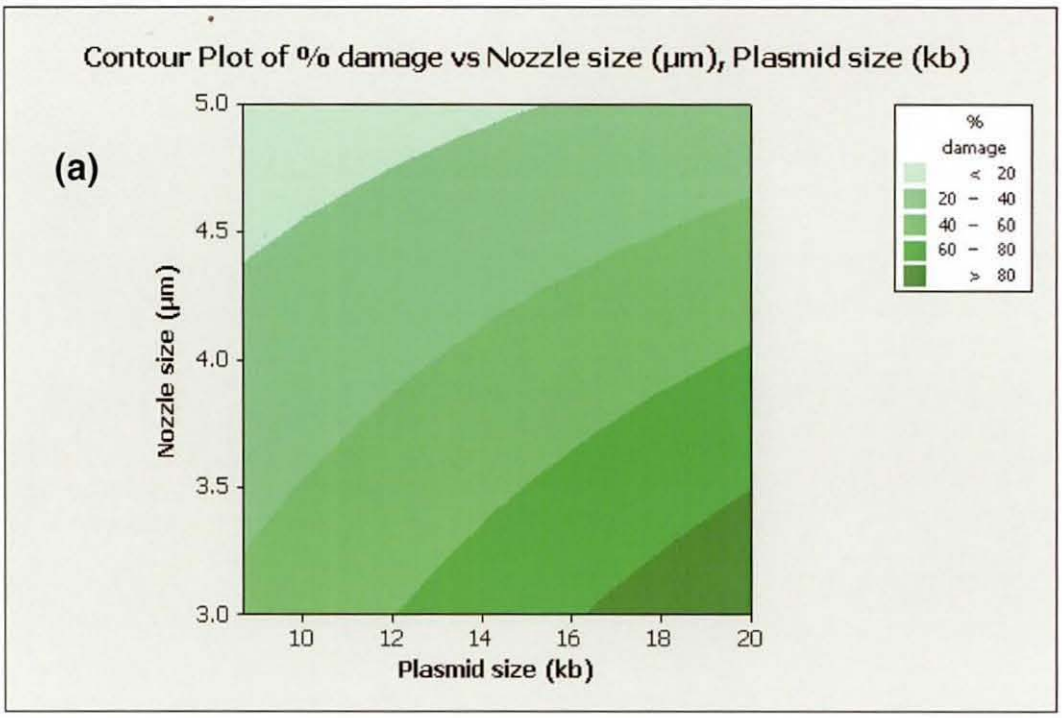

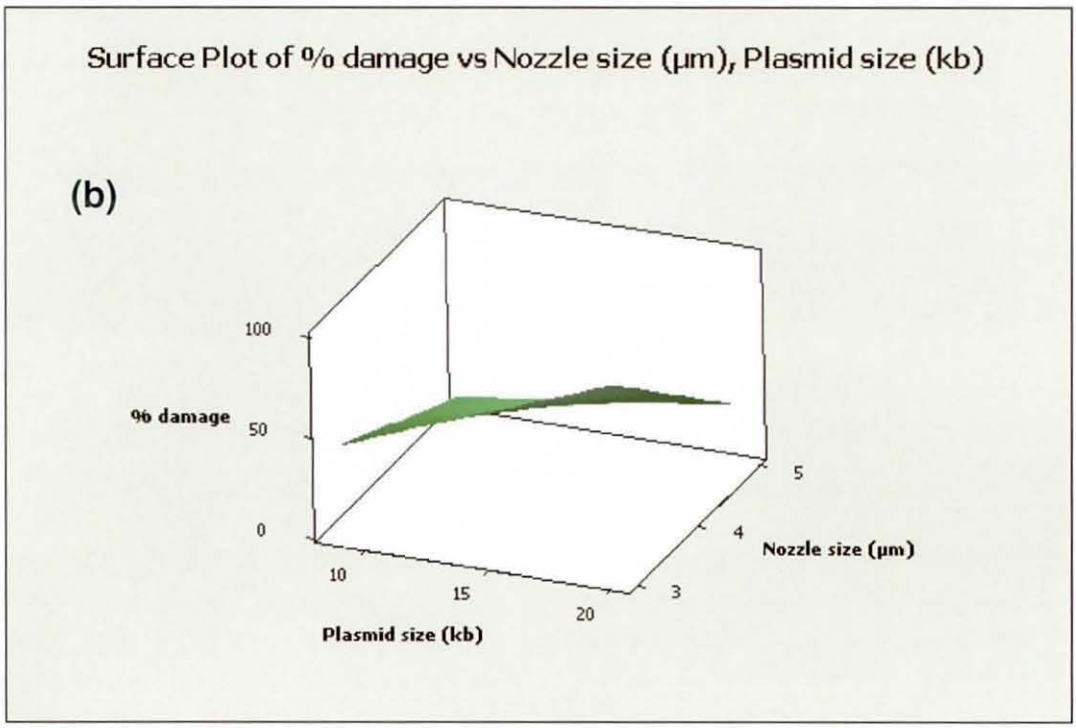

Figure 7.5: Model predictions from factorial design of plasmid and nozzle sizes: a) contour and b) surface plots of damage to sc structure of the plasmid

7.2.8 Summary

The contour plot for the percentage damage to sc structure of plasmids of size from 8.7 kb to 20 kb using different sized nozzles in the U22 mesh nebuliser provides an insight into the potential for damage to the sc structure. This approach is useful for assessing the damage to plasmids of different sizes aerosolised using different nozzle sizes and provides information for formulation of plasmid DNA and device design.

7.3 Influence of frequency on damage: DOE using factorial design

The frequency of the vibrator horn is at the core of the function of the nebuliser device. It generates the driving force required for aerosolisation of the liquid. Engineering studies in the earlier chapter (section 6.2) have shown the aerosol droplet size to be dependent on the device frequency. Hence, the influence of device frequency and plasmid size on damage to sc structure of plasmid DNA using factorial design of experiments is expected to provide useful information for device design and plasmid DNA formulation.

7.3.1 Choice of variables and levels

The variables for 2^2 factorial design chosen were plasmid DNA size and device frequency and the response was damage to the sc structure of the plasmid after nebulisation. To study the response and its interactions across a range of plasmid sizes and possible device frequencies, a plasmid size at the lower limit (5.7 kb) and higher limit (20 kb) was chosen for the study. Similarly, a nebuliser device operating at a lower frequency (U03 nebuliser) of 65 kHz and a higher frequency (U22 nebuliser) of 175 kHz was employed. The frequencies of the two devices were constrained by device design. A nozzle size of 3μm was used for the U03 and U22 nebuliser devices. The variables and levels chosen for the experimental design are shown in Table 7.5.

Table 7.5: Variables and levels chosen for factorial design of experiments

Variables	**Levels**	
	-	+
Plasmid size (kb)	5.7	20
Frequency (kHz)	65	175

7.3.2 Experimental design

The experimental design chosen was a full factorial design ($2^2 = 4$) for a two variable experimental design with two levels. The experimental design consisting of 4 runs with the levels of the variables are shown in Table 7.6.

Table 7.6: A 2^2 factorial experimental design for plasmid size and frequency as variables

Run	**Plasmid size (kb) (Coded units)**	**Frequency (kHz) (Coded units)**
1	5.7 (-)	175 (+)
2	20 (+)	175 (+)
3	20 (+)	65 (-)
4	5.7 (-)	65 (-)

The response of % damage to the sc structure was determined from average values of triplicate measurements from the densitometric scans of separate agarose gels.

7.3.3 Analysis of factorial experimental design

The analysis of 2^2 factorial design was done using Minitab® 15.1 (Stat-Ease, Inc., Minneapolis, USA), and the results from the statistical analysis, model adequacy plots, contour plots and response surface plots are reported.

The results of the factorial fit for % damage to sc structure versus plasmid size and nozzle size are given in Tables 7.3 & 7.4. The estimated effects and coefficients for % damage are shown in Table 7.3. This table indicated the coefficient of determination R^2 and adjusted R^2 values for this model are good with predictable response.

Table 7.8 shows the results of analysis of variance (ANOVA) for % damage to the sc structure. Significant interactions for the main effects and two way interactions are predicted.

Table 7.7: Estimated effects and coefficients for % damage in coded units

Term	**Effect**	**Coefficient**	**SE Coefficient**	**T**	**P**
Constant		55.769	0.7037	79.25	0.000
Plasmid size (kb)	78.502	39.251	0.7037	55.78	0.000
Frequency (kHz)	-7.413	-3.706	0.7037	-5.27	0.006
Plasmid size (kb) * Frequency (kHz)	11.882	5.941	0.7037	8.44	0.001
S (Standard deviation) = 1.99046					
PRESS (Predicted Residual Sum of Squares) = 63.391					
R^2 (Coefficient of determination) = 99.88%					
R^2 (Predicted) = 99.5%					
R^2 (Adjusted) = 99.78%					

Table 7.8: Analysis of variance (ANOVA)

Source	**Degrees of freedom (df)**	**Sequential Sum of Squares**	**Adjusted Sum of Squares**	**Adjusted Mean Sum of Squares**	**F value**	**p-value (Prob >F)**
Main effects	2	12435.2	12435.2	6217.59	1569.33	0.000
2-Way interactions	1	282.4	282.4	282.39	71.28	0.001
Residual error	4	15.8	15.8	3.96		

The significant variables of the model are plasmid size, nozzle size, and interaction between plasmid and nozzle size. The response equation for % damage to sc structure in terms of estimated coefficients (determined using data in uncoded units) and variables is given in equation 7.2.

$$\text{Damage}_{sc} = 16.6093 + (3.6767 * X_{plasmid}) - (0.2615 * f) + (0.0151 * X_{plasmid} * f) \ldots\ldots$$

.....Equation 7.2

The next section will analyse the model adequacy plots, contour plots and response plots, and check the significance of the variables predicted in the model.

7.3.4 Model adequacy plots

The adequacy of the model and the significance of the variables are discussed in Figures 7.6 and 7.7. Figure 7.6 shows the normal plot of the standardized effects in the model. In confirmation of the results in the earlier section, the main variables and interactions were predicted to have a significant effect on the model.

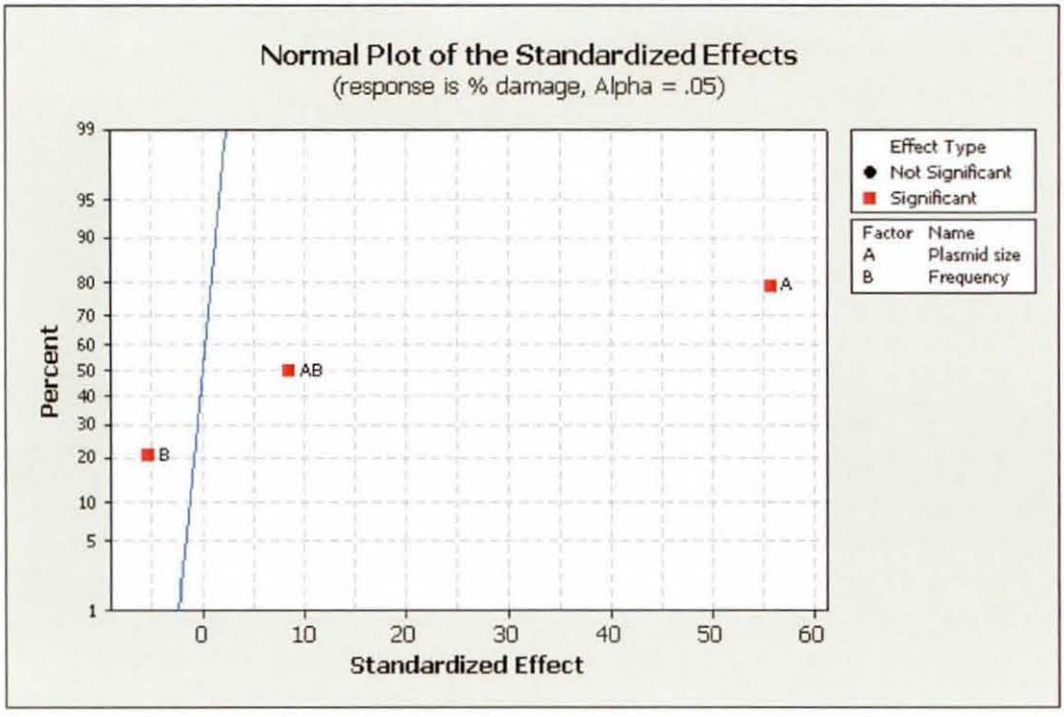

Figure 7.6: Normal plot of standardised effects for plasmid size and device frequency

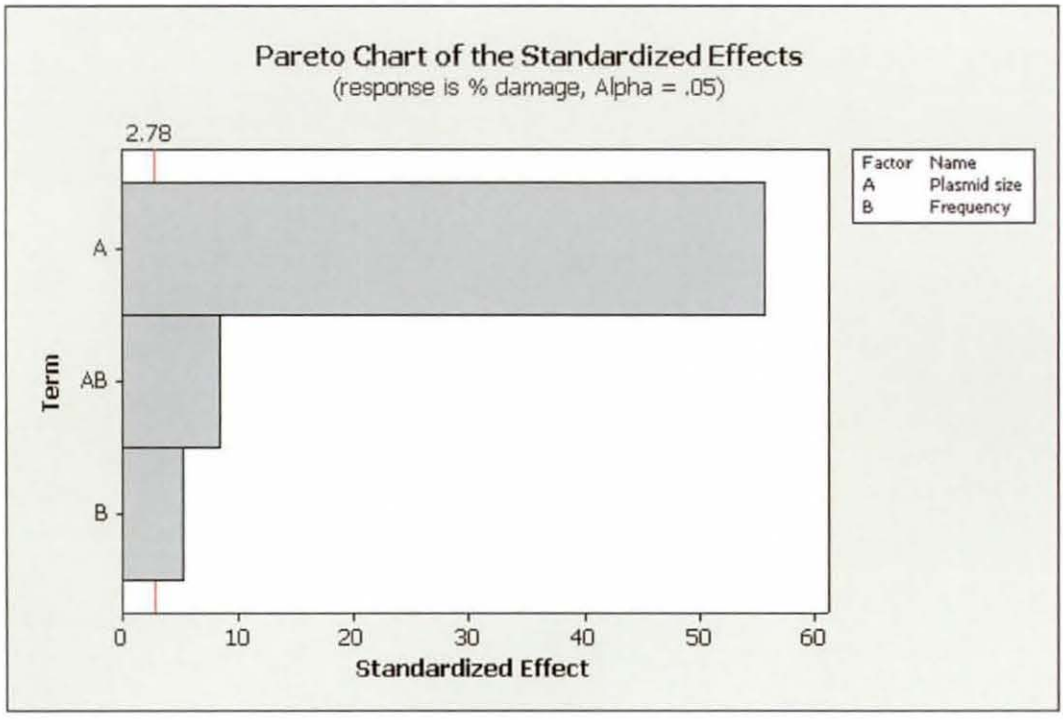

Figure 7.7: Pareto chart of standardised effects for plasmid size and device frequency.

As shown in the figure 7.6, plasmid size was predicted to have a positive effect resulting in increased damage to the sc structure. However, frequency was predicted to have a slight negative effect with decreased damage to sc structure. As observed in the figure, the interaction between the two variables had a significant effect on the response.

The Pareto chart of standardized effects shown in Figure 7.7 also showed similar results as in Figure 7.6. Plasmid size was predicted to have a greater influence on damage compared to frequency. However, as observed in Table 7.7, the combined effect of interaction between the variables was predicted to be more significant than frequency of the device.

7.3.5 Model predictions: Main effects and interaction plots

The main effects and interaction plots for damage to sc structure of plasmids are shown in Figures 7.8 and 7.9 respectively. The main effects plot (Figure 7.8) showed the 5.7 kb plasmid to be subjected to minimum damage compared to the 20 kb plasmid. This plot also showed that damage using the nebuliser device at 65 kHz was slightly more than that at 175 kHz. This was due to the increased aerosolisation time with the 65 kHz device perhaps exposing the fragile sc structure of the plasmid to hydrodynamic forces and cavitation. The non-parallel lines of plasmid size and nozzle frequency in the interaction plots (Figure 7.9) suggested interaction between the variables.

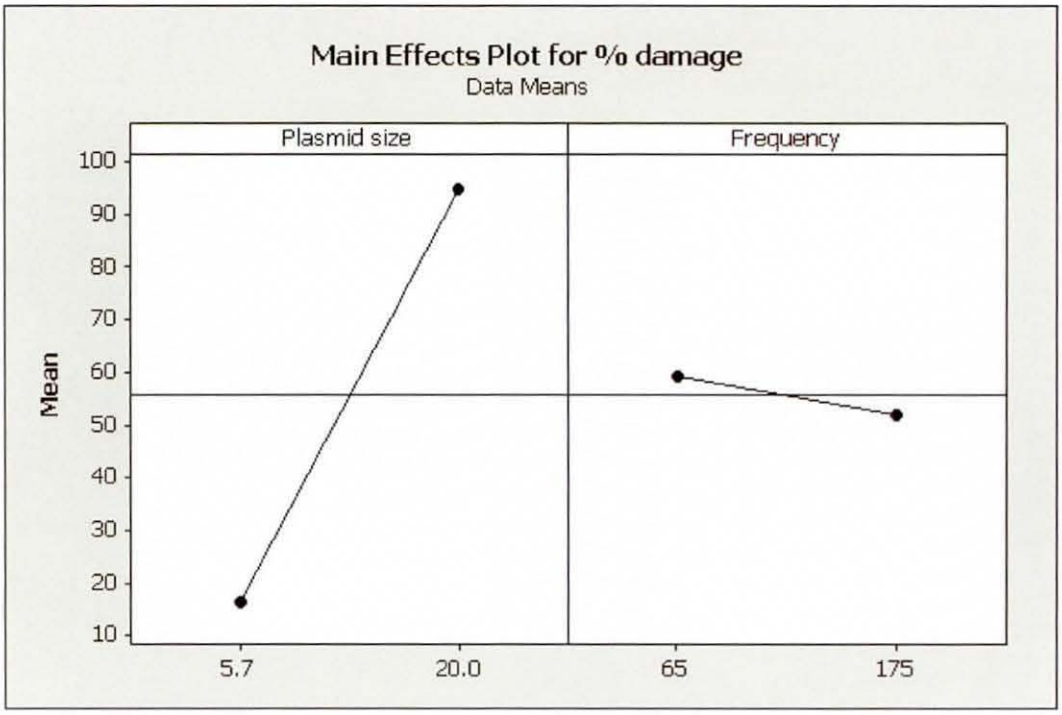

Figure 7.8: Main effects plot of plasmid size and device frequency for % damage to sc structure.

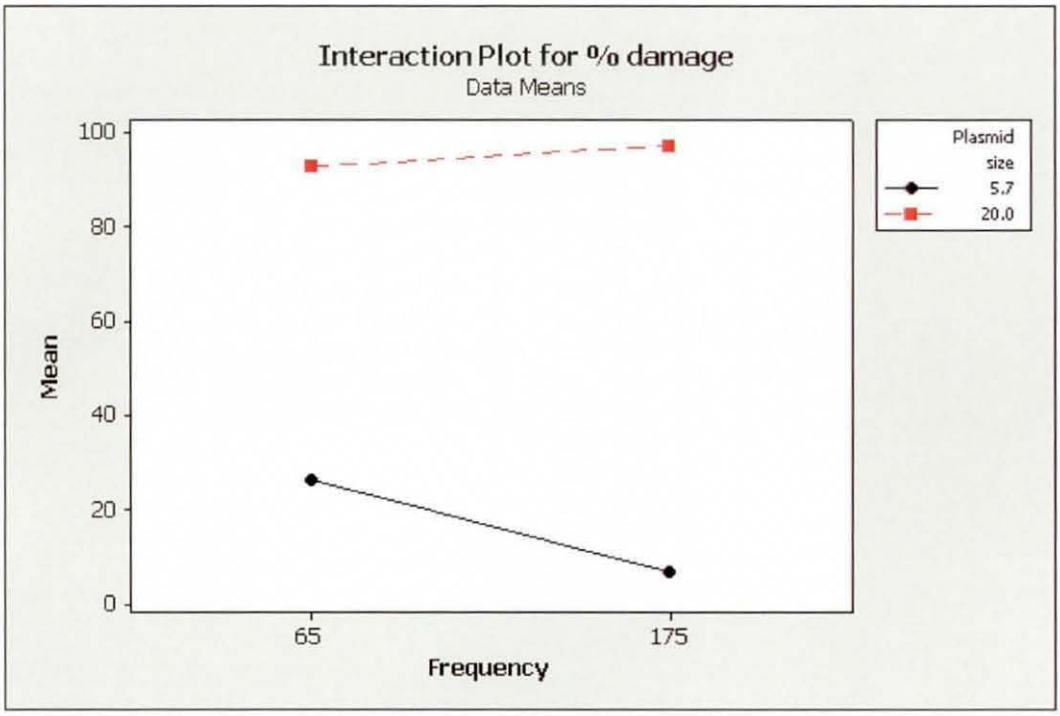

Figure 7.9: Interactions plot of plasmid size and device frequency for % damage to sc structure.

7.3.6 Model predictions: Contour and surface plots

The contour plot of % damage versus frequency and plasmid size in figure 7.10, provides information on sc structural damage for plasmid sizes from 5.7 kb to 20 kb and frequencies from 65 kHz to 175 kHz.

At 65 kHz, damage was predicted to increase with increasing size of plasmid. Damage was predicted to be independent of device frequency for plasmid DNA sizes >16 kb due to the greater influence of nozzle size on DNA damage. For a device frequency >100 kHz, damage to the sc structure of 5.7 kb plasmid was predicted to be minimum. Damage levels of 40-60% were predicted for an intermediate plasmid of size 13 kb. At 175 kHz, sc structural damage was predicted to be less than at 65 kHz for plasmid size <16 kb.

7.3.7 Predicted damage at intermediate frequencies

The model predictions from the contour and surface plots provided data on damage to the sc structure at intermediate frequencies. Figure 7.11 shows the predicted damage to the sc structure of 5.7 and 20 kb plasmids between 65 and 175 kHz respectively. The droplet size computed from equations 6.1 and 6.2 is observed to be linearly dependent on the frequency of the device. Aerosol particle size from the vibrator horn is a parameter which influences damage to the sc structure for a fixed nozzle size of 3 μm at different device frequencies. Hence, figure 7.11 is expected to provide a reasonable prediction of damage to the sc structure for 5.7 and 20 kb plasmids at intermediate frequencies for a fixed nozzle size.

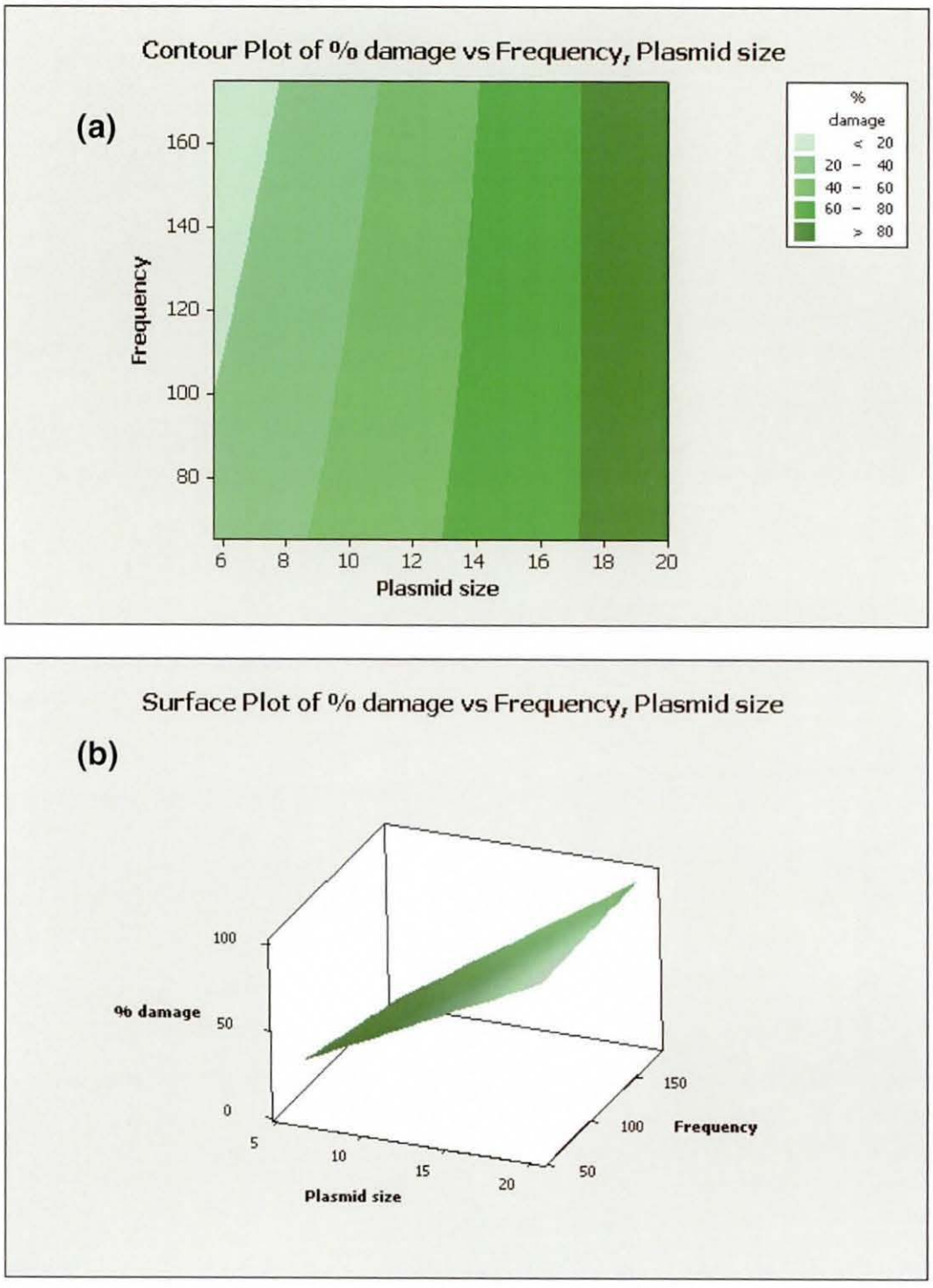

Figure 7.10: Model predictions from factorial design of plasmid size and device frequency: a) contour and b) surface plots of damage to sc structure of the plasmid.

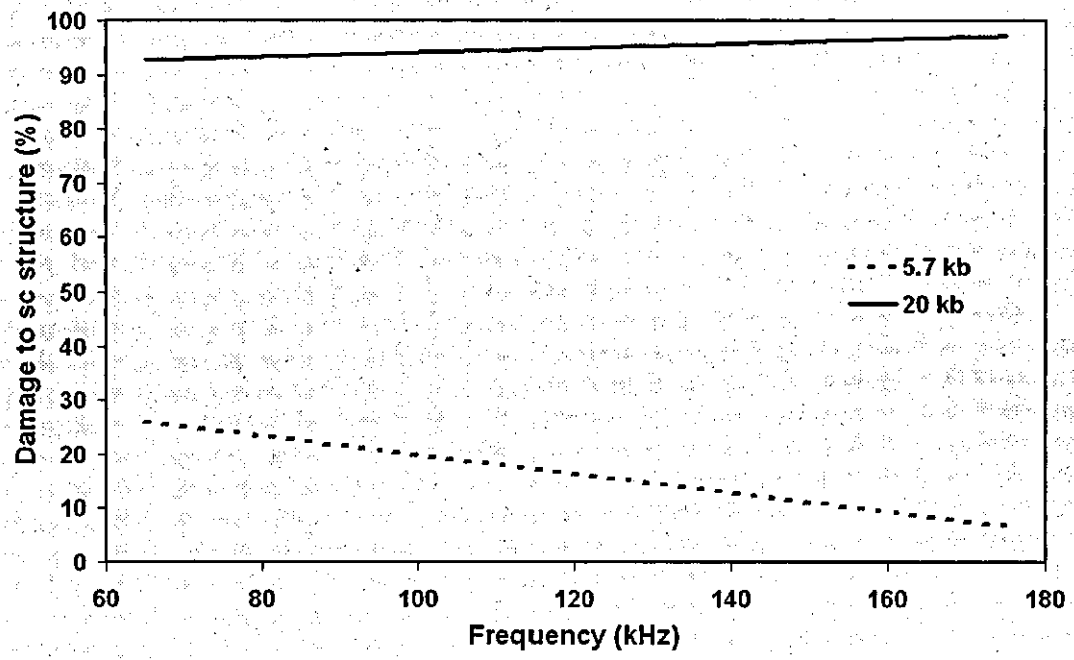

Figure 7.11: Prediction of damage to the sc structure of 5.7 kb and 20 kb plasmid at intermediate frequencies at a nozzle size of 3 μm.

7.3.8 Discussion

The factorial design of experiments using plasmid DNA size and device frequency as the variables provide information on the potential damage to the sc structure at intermediate plasmid sizes and frequencies. Statistical analysis of results has shown the size of plasmid DNA to have a more significant impact than device frequency. Predictions from the contour plot at low frequency (65 kHz) have shown damage to be dependent on plasmid DNA size.

Figure 7.11 shows the damage to the sc structure of the plasmid at device frequencies from 65 kHz to 175 kHz. Lower damage to sc structure of the 5.7 kb plasmid was predicted at high frequency (175 kHz) than at low frequency (65 kHz). Higher damage to sc structure of the 20 kb plasmid was predicted at low frequencies. However, Engineering studies in chapter 6 have shown maximum damage to the sc structure of the 20 kb plasmid due to exposure to hydrodynamic forces on passage through the mesh nozzles of the nebuliser device operated at high frequency. However, partial

damage was also observed to the sc structure of the plasmid due to cavitation on aerosolisation without mesh. As shown in Figure 7.8, damage to the sc structure of the 20 kb plasmid at low frequency was less than at high frequency, possibly due to lower hydrodynamic forces as a result of a lower nebulisation rate. However, higher damage to plasmids of smaller size (5.7 kb) at low frequency was perhaps due to effects of cavitation, as a result of increased residence time (low nebulisation rate) in the device.

7.3.9 Summary

The contour plot for damage to sc structure of plasmids of size from 5.7 kb to 20 kb at device frequencies from 65 kHz to 175 kHz provides useful information for device design and formulation for the delivery of plasmid DNA. This approach of factorial design of experiments promises to provide additional information by capturing the interaction between the variables which would not have been possible from a univariate analysis [Martendal et al., 2007]. Interaction between the variables, plasmid and nozzle sizes, and plasmid size and device frequency indicated a mutual influence on the percentage damage to the sc structure.

7.4 Conclusions

Nebulisation of plasmid DNA results in damage to the sc structure of large plasmids. Damage to the sc structure of plasmid DNA depends on device parameters such as nozzle size and frequency, in addition to formulation. This chapter has employed a 2^2 factorial design of experiments to investigate the main effects of the variables such as plasmid size, nozzle size and device frequency and the interactions between them. Damage to sc structure of plasmid DNA was more pronounced at 3 μm nozzle size than at 5 μm. Nebulisation at 65 kHz device frequency resulted in more damage to plasmids of size <13 kb than at 175 kHz. The main advantage of the results from such experiments is the information on the interaction between the variables for the limits chosen in the experimental design. This will assist device design and formulation for the delivery of plasmid DNA as a non-viral gene therapeutic.

CHAPTER 8. FORMULATION OF 20 KB PLASMID DNA FOR NEBULISATION

8.1 Introduction

Formulation of large size plasmid DNA is essential to protect the super-coiled (sc) structure against damage during the aerosolisation process. Intensive research is being pursued to develop suitable non-viral formulations for delivery of plasmid DNA [Anchordoquy et al., 2004]. Currently formulation substrates such as cationic liposomes [Lasic, 2000] and polymers [Munier et al., 2005] are being employed for condensing the plasmid from a very loose molecular structure to a compact, small biomolecule. Cationic liposomes have been used for the ultrasonic nebulisation of a small plasmid (size unknown) for airway administration [Pillai et al., 1998]. Although cationic liposomes are being evaluated in clinical trials, it is reported that pulmonary surfactants may inhibit cationic liposome-mediated gene delivery to respiratory epithelial cells [De Smedt et al., 2000]. Cationic polymers (CPs) used for gene delivery can be a homo-polymer with a linear backbone such as DEAE-dextran (Diethylaminoethyl-dextran), pLL (poly(L-lysine), pVP (poly(N-ethyl-4-vinylpyridinium bromide)), linear pEI (poly(ethyleneimine)), Chitosan, or a branched backbone such as branched pEI, or a co-polymer such as pEG-pLL (poly(ethylene glycol)-poly(L-lysine)) [Schmieder et al., 2007; Lee and Kim, 2005].

DEAE-dextran has been reported to enhance uptake of protein and nucleic acid by cells [Rigby, 1969]. Although, DEAE-dextran as a DNA condensing agent is reported to be simple, effective and still widely used for *in vitro* transfection, it has been observed to be cytotoxic and unsuitable for *in vivo* systems [Luo & Saltzman, 2000]. However, DEAE-dextran DNA transfection of adherent primary cultured human macrophages resulted in superior transfection compared to cationic liposome and calcium phosphate precipitation methods [Mack et al., 1998]. It is shown recently that adenovirus complexed with DEAE-dextran can enhance gene transfer to the sodium caprate treated airways upon intra-nasal administration in mice, and is envisaged in the clinical setting to enhance the gene therapy efficiency for cystic

fibrosis via airway delivery [Gregory et al., 2003]. Gene therapy is an attractive target for unmet clinical diseases like cystic fibrosis and is a perfect example as a target for pulmonary delivery of gene therapeutic containing cystic fibrosis transmembrane conductance regulator (CFTR) gene. Complexes of CFTR gene in an adenovirus with DEAE-dextran have been reported for gene therapy [Welsh and Fasbender, 1999]. *In vivo studies* in large animal models such as sheep have been used for optimising aerosol gene delivery of plasmid DNA/PEI complexes aimed at developing cystic fibrosis gene therapy protocols [McLachlan et al., 2007]. McLachlan et al report the use of Pari LC plus jet nebulisers with a delivery rate of 0.25 mL/min for their study. The partial resistance of pDNA/PEI complexes to DNase degradation can improve the efficiency of gene delivery, due to the administration of rhDNase (Pulmozyme) to clear the thick mucus in CF patients. It has been reported that gene expression levels of 5% to the target cells is sufficient to restore the malfunctioning of the CFTR protein in cystic fibrosis diseased patients.

Studies on the aerosol delivery of plasmid DNA using conventional jet nebulisation [Lentz et al., 2005] and ultrasonic nebulisation [Smart et al., 2002] showed damage to sc structure of plasmids. An alternative electro-hydrodynamic technique [Davies et al., 2005] for pulmonary aerosol delivery is promising [Zimlich et al., 2002]. The aerosol delivery of plasmid DNA in the intact supercoiled (sc) form is crucial to meet the stringent drug quality requirements [Levy et al., 2000a]. Since the size of a complete CFTR gene is approximately 10 kb [Lee et al., 2005], it is expected that a typical plasmid vector with a therapeutic gene insert would be of the order of 15 kb. Plasmids of size >13 kb are damaged in rotating shear devices at shear/strain rates $>5x10^5$ s^{-1} [Levy et al., 1999].

Earlier studies in chapter 4 have shown sc structure of a naked 5.7 kb plasmid to be safely delivered using a mesh nebuliser, while that of an unformulated 20 kb plasmid was completely degraded [Arulmuthu et al., 2007]. In addition to plasmid size, CFD (computational fluid dynamics) study and high speed imaging of aerosol generation predicted a 300 pN hydrodynamic force on large plasmids that would damage the DNA strands in sc structure. Hence, formulation of plasmid DNA is essential to ensure protection of the shear-sensitive super-coiled structure during aerosolisation.

The aerosol delivery of non-viral plasmid formulation with cationic liposomes complexed to plasmid DNA using a clinical nebuliser was the first to be demonstrated and resulted in transgene expression restricted to the lungs [Stribling et al., 1992]. However, in spite of the impressive initial results, a low DNA delivery efficiency (0.083%) was obtained using this approach.

In chapter 6, experimental and theoretical studies on damage to a naked sc plasmid upon nebulisation showed the size of sc structure of a 20 kb plasmid to be of the order of the nozzle size of the device studied. Earlier studies in chapter 7 showed this nozzle size of 3 μm was crucial for the generation of fine respirable aerosols using the mesh nebuliser. In this chapter, formulation of a 20 kb plasmid is reported to reduce the size of the plasmid to ensure safe delivery of the sc structure upon passage through the micron-sized nozzles of the mesh nebuliser.

8.2 Formulation of 20 kb plasmid

Nebulisation of naked 20 kb plasmid in TE buffer resulted in substantial damage to the sc structure of the plasmid. Condensation of the sc structure in ionic strength buffer (150-300mM NaCl) also resulted in damage to the plasmid (Chapter 4). Nebulisation of the unformulated 20 kb plasmid at different DNA concentrations was performed in order understand levels of damage at low DNA concentrations. The study discussed in the following section was intended to provide information on whether damage to the sc structure of the 20 kb plasmid upon nebulisation was concentration-dependent. Formulation of plasmid DNA using cationic substrates has been reported to reduce hydrodynamic diameter based on charged attraction between the negatively charged DNA phosphate backbone and cationic substrate [Lentz et al., 2005], therefore formulation of 20 kb plasmid with cationic liposomes and polymers has been attempted and the results are discussed below.

8.2.1 Nebulisation of unformulated 20 kb plasmid

Earlier studies reported in Chapter 4, showed nebulisation of 20 kb plasmid to substantially damage the sc structure. In order to gain information and improve understanding of the extent of damage to sc structure at plasmid DNA (pDNA) concentrations used for formulation, nebulisation of naked 20 kb plasmid at 150 mM NaCl in distilled water was carried out. Naked plasmid formulations at 15, 7.5 and 5 µg/mL DNA concentrations were subjected to nebulisation in the mesh nebuliser. The damage to the sc structure was assessed by agarose gel electrophoresis and DNA concentration at UV absorbance of 260 nm.

8.2.1.1 Analysis of DNA damage

As shown in the densitometric scans in figure 8.1, the band intensity corresponding to the sc peak was assessed after nebulisation to determine the percentage damage to the sc structure. Agarose gel electrophoresis of 20 kb plasmid after nebulisation indicated substantial damage to the sc structure at all pDNA concentrations (Figure 8.1). As is evident from Table 8.1, the purity of plasmid DNA in the before and after nebulisation sample was observed to be acceptable for gene therapy with a DNA ratio (A_{260}/A_{280}) of 1.8-1.95. An increase in DNA concentration in the after nebulisation sample was due to increased absorbance (A_{260}) of the DNA fragments resulting from the degradation of the supercoiled structure. Determination of the percentage damage to the sc structure of the 20 kb plasmid after nebulisation from the densitometric scans of the agarose gel (Figure 8.1) revealed that damage is independent of plasmid DNA concentration.

Table 8.1: Nebulisation of unformulated 20 kb plasmid (n=2)

Plasmid DNA sample (µg/mL)	Nebulisation stage	DNA ratio (A_{260}/A_{280})	DNA conc in µg/mL (UV-abs at 260 nm)	% damage to sc structure
15	Before	1.891	15.92	
	After	1.796	38.10	92.18
7.5	Before	1.899	8.261	
	After	1.825	14.42	93.19
5	Before	1.925	4.508	
	After	1.823	8.889	91.56

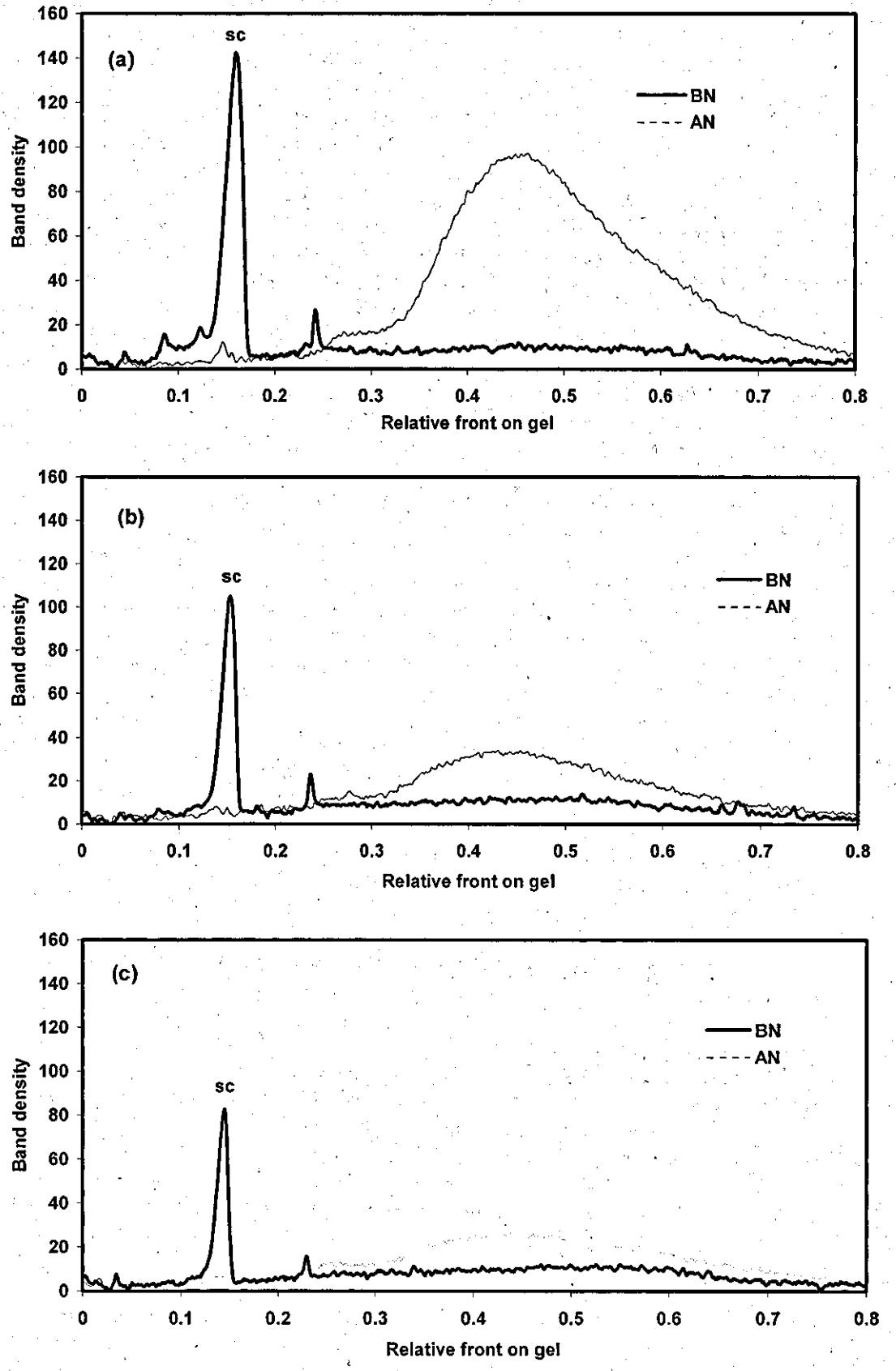

Figure 8.1: Densitometric scans of agarose gel from nebulisation of 20 kb pDNA at DNA concentrations of: a) 15, b) 7.5, c) 5 μg/mL.

8.2.2 Nebulisation of pDNA formulation with liposomes

Formulation of 20 kb plasmid was performed using cationic liposomes, DOTAP/DOPE and DOTAP-Cholesterol as described in Chapter 3. A plasmid DNA concentration of about 30μg/mL was used for formulation with cationic liposomes as per the prescribed protocol [Megafectin™ catalogue]. Nebulisation of unformulated 20 kb was carried out at 30 μg/mL concentration. Nebulisation of the formulated 20 kb plasmid with DOTAP/DOPE and DOTAP-Cholestersol resulted in no aerosol generation, perhaps due to increased viscosity of the formulation at the same DNA concentration. Agarose gel electrophoresis of complexed DNA from the nebuliser chamber showed no damage to the sc structure (Figure 8.2), similar to that observed with a naked 20 kb plasmid.

8.2.3 Nebulisation of pDNA formulations with DEAE-dextran

DEAE-dextran is a polycationic derivative of Dextran and the very first chemical reagent to be used for DNA delivery [Liu et al., 2004]. Aerodynamically light high molecular weight water-soluble particles of DEAE-dextran are reported for pulmonary drug delivery [Edwards et al., 2002]. In this study, DEAE-dextran has been used as a substrate to form an aggregate/ complex with a 20 kb plasmid to develop a non-viral formulation. Due to its wide applications in gene therapy [Kaplan et al., 1998], protein and nucleic acid uptake by the cells [Fox et al., 1977], adjuvant in vaccine production [Joo and Emod, 1988] and stabilisation of proteins [Gibson et al., 1992], DEAE-dextran was used as substrate for development of non-viral DNA formulations. Plasmid DNA forms a complex with polycationic DEAE-dextran (DD) due to electrostatic forces. In these experiments, it was attempted to preserve the sc structure of plasmid DNA during aerosolisation by forming a complex with DD. DD/DNA formulations with varying DD Nitrogen to DNA Phosphate (N/P) ratios as reported in Chapter 3 were subjected to nebulisation.

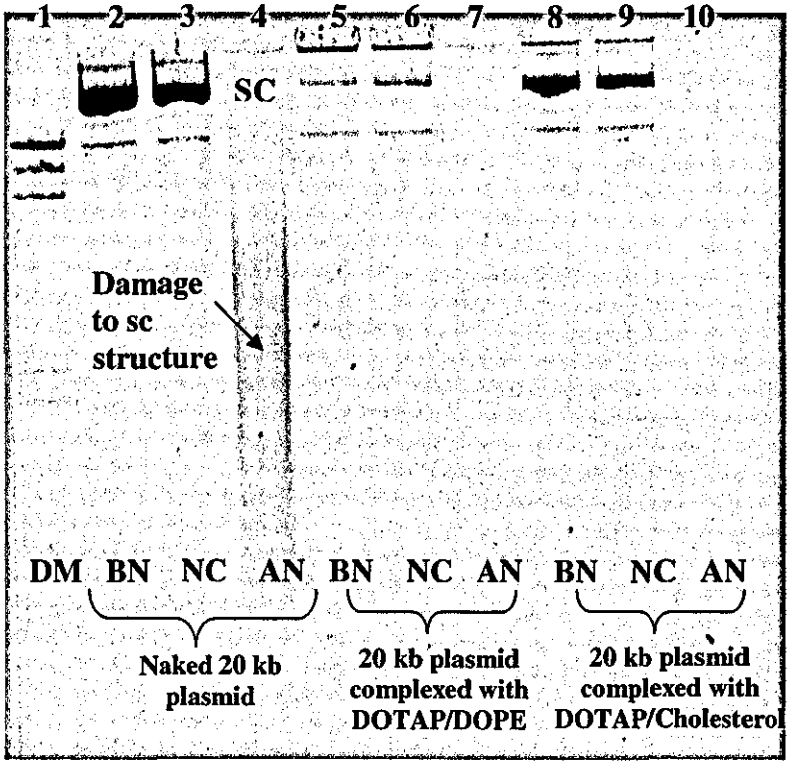

Figure 8.2: Agarose gel electrophoresis of nebulisation samples of (i) naked 20 kb plasmid, (ii) 20 kb plasmid complexed with DOTAP/DOPE and (iii) 20 kb plasmid complexed with DOTAP/Cholesterol; damage to the sc structure of naked plasmid observed, DM – DNA marker, BN – before nebulisation, NC – Nebuliser chamber and AN – after nebulisation. Note: AN samples of complexed plasmid were not loaded due to an absence of aerosol generation from the non-viral cationic lipid/DNA formulations.

8.2.3.1 Analysis of pDNA damage

The DD/DNA formulations with N/P ratios of 0.1, 0.2 and 0.4 resulted in complete aerosolisation and the percentage damage to the sc structure was analysed using an agarose gel electrophoresis. From the densitometric scans of the agarose gel shown in Figure 8.3, the sc structure of the plasmid and linear DNA fragments decreased at increasing N/P ratios. However, damage to the positively-charged DD/DNA complex was observed to be similar as shown in Table 8.2. The decrease in sc

structure at higher DD concentrations was perhaps due to the complexation of the pDNA sc structure with DD. The decrease in DNA concentration at higher N/P ratios was due to protection of the sc structure in the DD/sc complex. Nebulisation of formulated 20 kb plasmid with DD at N/P ratio of 0.45 was attempted, but resulted in inefficient aerosolisation. The damage to the sc structure in this case was observed to be around 20%.

Table 8.2: Analysis of DNA damage to pDNA formulations of DEAE-dextran (n=2)

DD/pDNA formulation	**Nebulisation stage**	**A_{260}/A_{280}**	**DNA (µg/mL)**	**% damage to**	
				sc	**sc/DD complex**
N/P = 0.1	Before	1.819	25.18		
	After	1.868	22.91	91.08	74.57
N/P= 0.2	Before	1.671	23.99		
	After	1.715	26.03	87.45	75.94
N/P= 0.4	Before	1.528	27.89		
	After	1.642	12.58	83.16	74.15

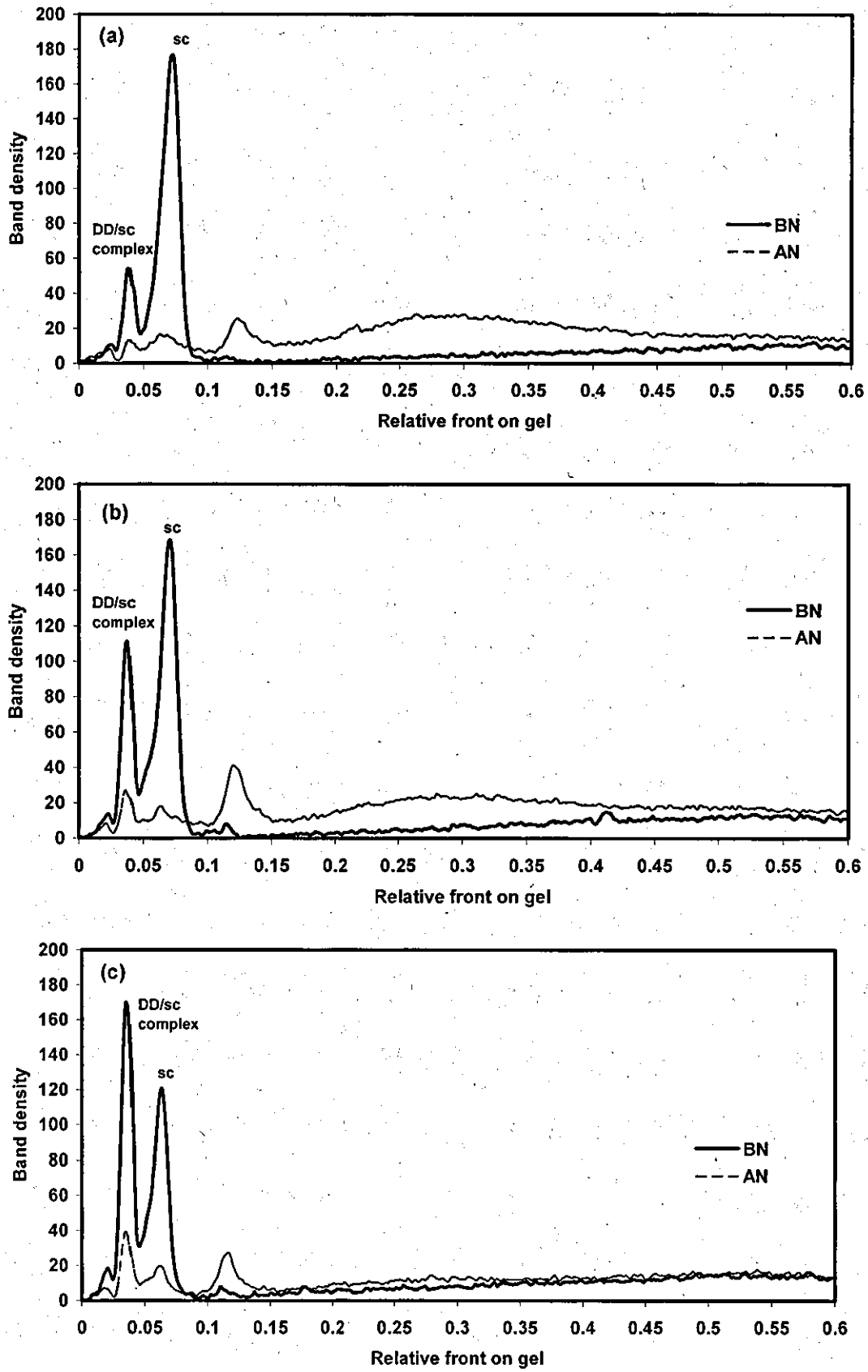

Figure 8.3: Densitometric scans of agarose gel from nebulisation of 20 kb pDNA complexed with DEAE-dextran at N/P ratios of: a) 0.1, b) 0.2 and c) 0.4.

8.2.3.2 Atomic force microscopy

Atomic force microscopy of the nano-particulate formulations were carried out to examine the extent of complexation of sc DNA with DD and the relative size of the nano-sized particles.

8.2.3.2.1 Visualisation of pDNA/DD formulations

AFM images of the nanoparticles show a visual representation of the effect of different DD concentrations on complexation of sc structure. They provided additional information on the structure of DD/pDNA formulations.

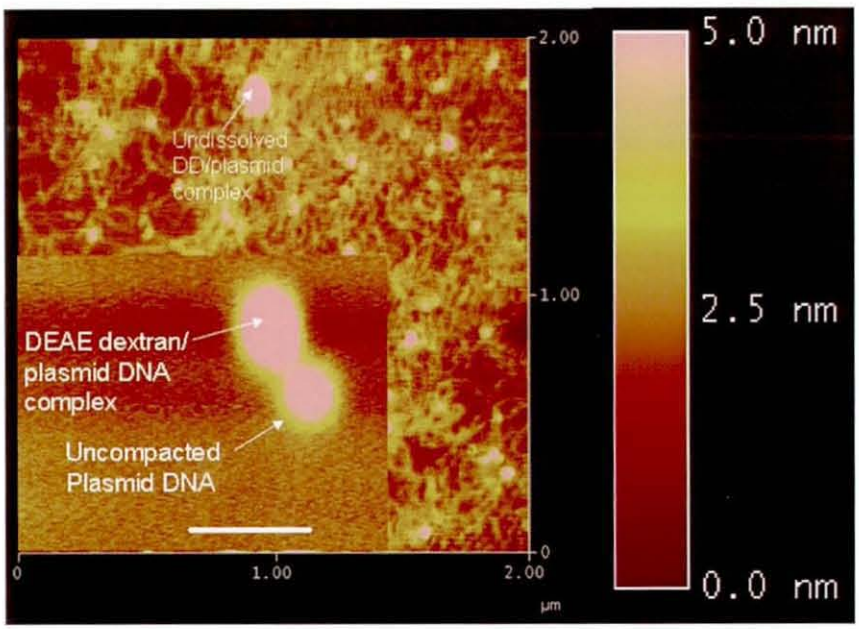

Figure 8.4: AFM image of sc structure and DD/sc pDNA complex (N/P ratio 0.1) before nebulisation. Inset shows DD/sc pDNA complex with protruding strands of pDNA after nebulisation (scale bar for inset – 250 nm, height – 5 nm).

Figure 8.4 shows an AFM image of a pDNA/DD formulation with a N/P ratio of 0.1. The AFM image shows the presence of a major portion of the sc structure in the formulation is uncomplexed with DD. A few nanoparticles of DD/sc pDNA complex are also observed. The inset shows a plasmid DNA nanoparticle at N/P ratio of 0.1 after nebulisation in the form of an ellipsoid/spheroid complex with a compact centre and a "fluffy" periphery with plasmid DNA protrusions due to incomplete condensation. This suggested that for a DD/pDNA formulation with N/P ratio of 0.1, the concentration of DD was limiting to ensure efficient condensation. The results agree with the densitometric scans of the agarose gel shown in Figure 8.3a, which suggested that a significant percentage of the sc structure remained uncomplexed. The loose sc structure of plasmid DNA before nebulisation in figure 8.4 suggests in-efficient condensation of sc structure at N/P ratio of 0.1 and the formation of less dense nanoparticles.

Plasmid DNA/DD formulations prepared with higher DD concentration at N/P ratio of 0.2 resulted in condensation with plasmid DNA to form loose nanoparticles as seen in Figures 8.5(a) & 8.5(b). The protrusions of plasmid DNA strands from the complex DD/sc complex suggest incomplete condensation. However, due to the higher DD concentration at N/P ratio of 0.2, the DD/sc complex was more compacted when compared with that at a N/P ratio of 0.1. Figures 8.5(c) & 8.5(d) show compaction of the DD/plasmid DNA complex after nebulisation into dense nanoparticles and aggregates. This agrees with parallel literature [Kleemann et al., 2004] which suggests that ultrasonic nebulisation results in compact condensation of linear pEI-plasmid DNA complexes to form dense particles or aggregates.

As observed in the densitometric scan of Figure 8.3b, a higher proportion of nanoparticles are formed due to the increase in DD concentration when compared to that at a N/P ratio of 0.1. However, the sc structure was still observed to be uncomplexed with the possibility of a few loosely complexed DD/sc DNA nano-particles as observed in Figure 8.6. In this figure, unwinding of DNA strands from the nanoparticle complex was observed as a result of inadequate condensation of DD with plasmid DNA at N/P ratio of 0.2 before nebulisation. Similar images of DNA strands protruding outside uncondensed plasmids were observed by Dunlap et al. [1997].

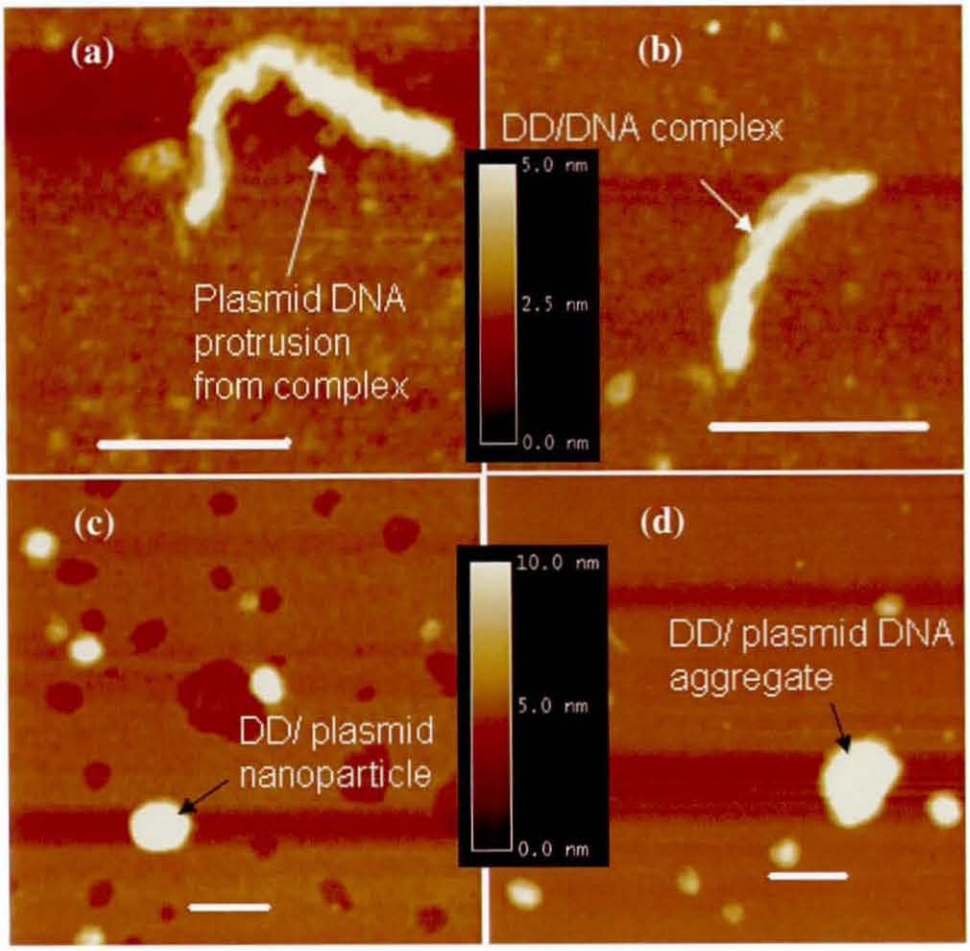

Figure 8.5: AFM images of DD/plasmid DNA complex (N/P ratio 0.2) before nebulisation (height – 5 nm), (c) & (d) after nebulisation (height – 10 nm); scale bar – 250 nm for all the images.

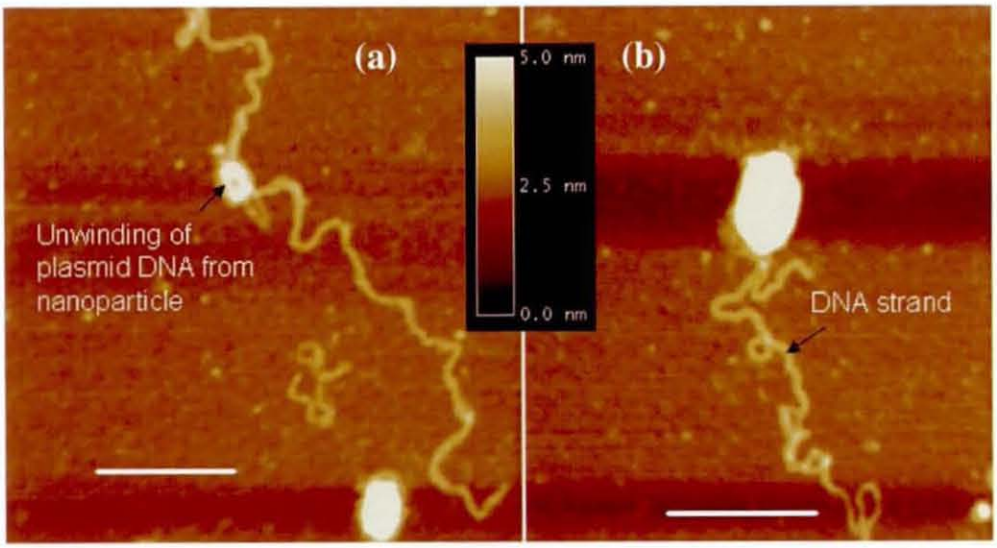

Figure 8.6: AFM images of unwinding of DNA strand from DD/sc pDNA complex at N/P ratio of 0.2 before nebulisation (height – 5 nm); scale bar – 250 nm.

At pDNA/DD formulations with N/P ratio of 0.4 the formation of compact nanoparticles before nebulisation was observed as shown in Figures 8.8 (a) & (b). Nebulisation of these formulated nanoparticles resulted in the formation of more compact nanoparticles as shown in Figure 8.9. Similar observations have been reported by Kleemann et al. [2004]. This may be due to the hydrodynamic conditions induced on the fluid by the ultrasonic vibrations of the horn, resulting in the formation of aggregates/ dense nanoparticles.

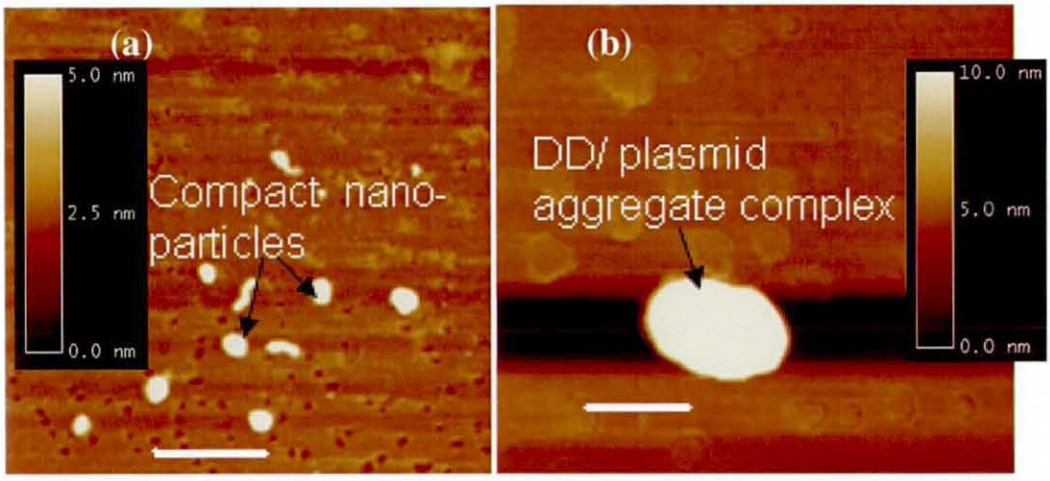

Figure 8.7: AFM images of DD/plasmid DNA complex at N/P ratio of 0.4 before nebulisation (a) nanoparticles (scale bar – 600 nm, height – 5 nm), (b) aggregates (scale bar – 250 nm, height – 10 nm).

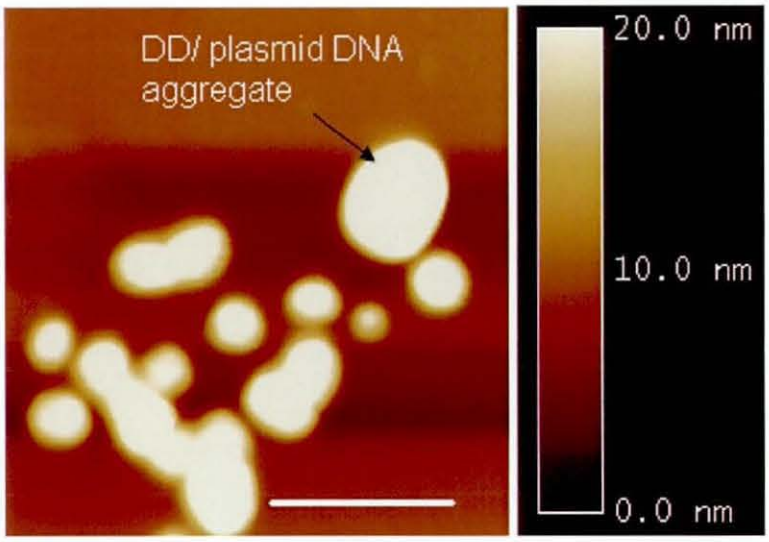

Figure 8.8: AFM images of DD/plasmid DNA complex at N/P ratio of 0.4 after nebulisation (scale bar – 250 nm, height – 20 nm).

8.2.3.2.2 Size of pDNA/DD formulations

The sizes of non-viral DD formulations of 20 kb plasmid were obtained by analysis of AFM images using the Dimension 300 software and are summarised in Table 8.3. With increasing DD concentration, the size of the single nanoparticle and aggregated complex increased for samples before nebulisation. The size of the single nanoparticles and aggregated particle complex at N/P ratio of 0.1 after nebulisation was higher than before nebulisation possibly due to inefficient condensation. However, the size of single nanoparticles in the recovered aerosols after nebulisation was smaller for formulations with N/P ratios of 0.2 and 0.4 when compared to the size before nebulisation. This may due to better compaction of the DD/plasmid DNA complexes upon nebulisation, as reported in a study of ultrasonic nebulisation of pDNA formulations [Kleemann et al., 2004].

Table 8.3: Size of DD/plasmid DNA nanoparticles determined by AFM

Plasmid/ DD formulation	Nebulisation stage	Single particle complex (nm)*	Aggregated particle complex (nm)*
N/P ratio = 0.1	Before	39.06 ± 3.90	104.27 ± 18.34
	After	115.27 ± 17.62	274.87 ± 114.71
N/P ratio = 0.2	Before	103.56 ± 13.72	161.27 ± 36.27
	After	82.03 ± 11.72	161.69 ± 28.88
N/P ratio = 0.4	Before	123.90 ± 30.15	199.95 ± 88.62
	After	94.50 ± 27.12	343.85 ± 109.47

* Particle size data are mean with SD from n=3 to 7 measurements for each sample.

8.2.4 Nebulisation of pDNA formulations with PEI

Polyethyleneimine (PEI) has been shown to be an effective agent for DNA delivery both *in vitro* and *in vivo* [Kichler 2004]. Complex formation between cationic PEI and anionic plasmid DNA occurs by counter-condensation of oppositely charged polymers. PEI-based pDNA formulations have proven stable during nebulisation and resulted in efficient transfection through the airways [Densmore, 2003]. However,

the size of the plasmid DNA used for PEI formulation and nebulisation to date have been less than 5 kb [Kleemann et al., 2004]. It is envisaged that the size of the plasmids used for future gene therapy trials may be larger in order to harbour therapeutic genes of size >5 kb and even up to 50 kb [Levy et al., 2000].

As discussed in the following section, a 20 kb plasmid has been formulated with branched PEI (molecular weight 25 kDa) at an N/P ratio of 10. Nebulisation of PEI/pDNA formulations in the mesh nebuliser resulted in complete nebulisation. In order to quantify the damage to plasmid DNA in PEI/pDNA formulation, a PicoGreen assay was carried out. AFM imaging enabled visualisation of the formulated nanoparticles and determination of the molecular size and structure. Agarose gel electrophoresis was not performed since it required decomplexation of the PEI from the pDNA and would result in the dissociation of the formulated nanoparticle.

8.2.4.1 Analysis of pDNA damage

The PicoGreen assay enables quantification of dsDNA by binding with the fluorescent PicoGreen dye with sensitivity up to picogram DNA concentrations. Figure 8.9 shows the relative fluorescence in a PicoGreen assay of a 20kb plasmid formulated in TE buffer and a PEI/plasmid complex formulated in PBS. There is a significant increase in fluorescence from the plasmid formulated in TE buffer after nebulisation due to the increased binding of PicoGreen dye to the dsDNA fragments generated from the degradation of the sc structure (as observed in Figure 8.1). The reduction in fluorescence of PEI complexed 20 kb plasmid before nebulisation compared to unformulated 20 kb is due to the condensation of the sc structure of the plasmid with PEI, resulting in binding of PicoGreen dye to fewer exposed dsDNA fragments. The PEI plasmid complex shows no increase in fluorescence after nebulisation, suggesting that the DNA sc structure was not degraded during the aerosolisation process. The reduction in the relative fluorescence of the PEI formulation after delivery is likely to be due to compaction of the formulated PEI particles during aerosolisation, resulting in less exposure of the DNA to the fluorescent dye.

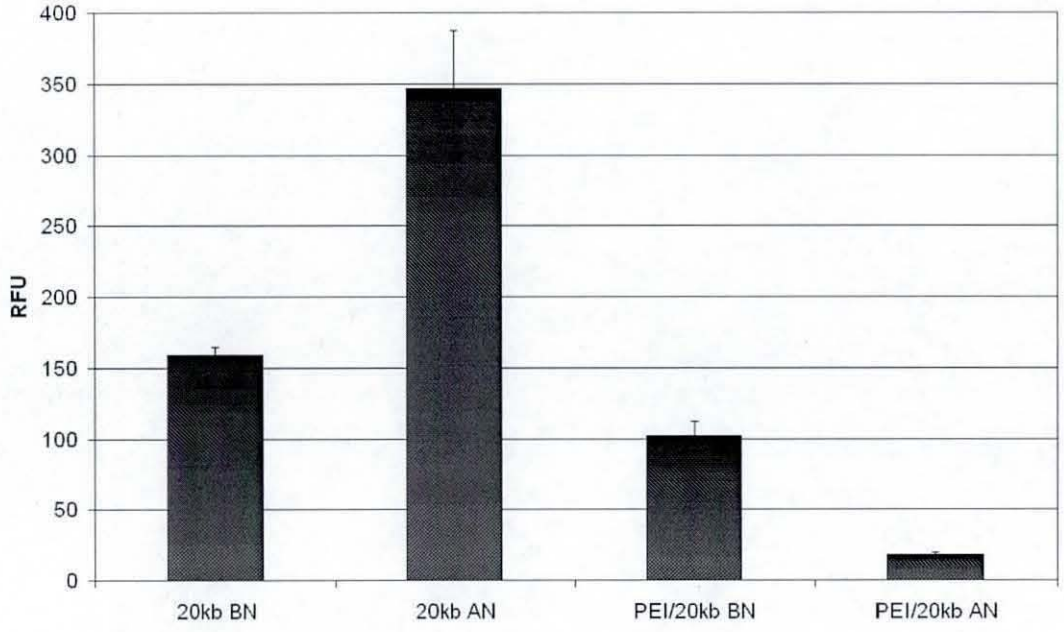

Figure 8.9: Formulation studies of 20kb plasmid DNA: PicoGreen assay results showing relative fluorescence unit (RFU) of plasmid formulated in TE buffer and PEI/20 kb plasmid DNA before (BN) and after nebulisation (AN) (n=3).

8.2.4.2 Atomic force microscopy

AFM imaging of the 20 kb plasmid formulated with PEI was performed to determine the size and structure of formulated plasmid before and after nebulisation. Figure 8.10 shows AFM image of the nanoparticles of PEI/plasmid complex formulated in PBS indicating a reduced size of ~400 nm before nebulisation. The size of PEI/plasmid formulated nanoparticles was higher than DD/plasmid formulated nanoparticles, perhaps due to a higher N/P ratio. The appearance of protruding plasmid DNA strands from the complex indicated a less compact PEI/plasmid nanoparticle. The release of DNA strands from the uncompacted PEI/plasmid complex may be due to sample preparation for AFM imaging. This confirmed the presence of the sc structure of the plasmid in the formulated nanoparticle. However, no unwinding of the DNA from the nanoparticles was observed after nebulisation suggesting formation of dense, compact nanoparticles during the aerosolisation process (Figure 8.10).

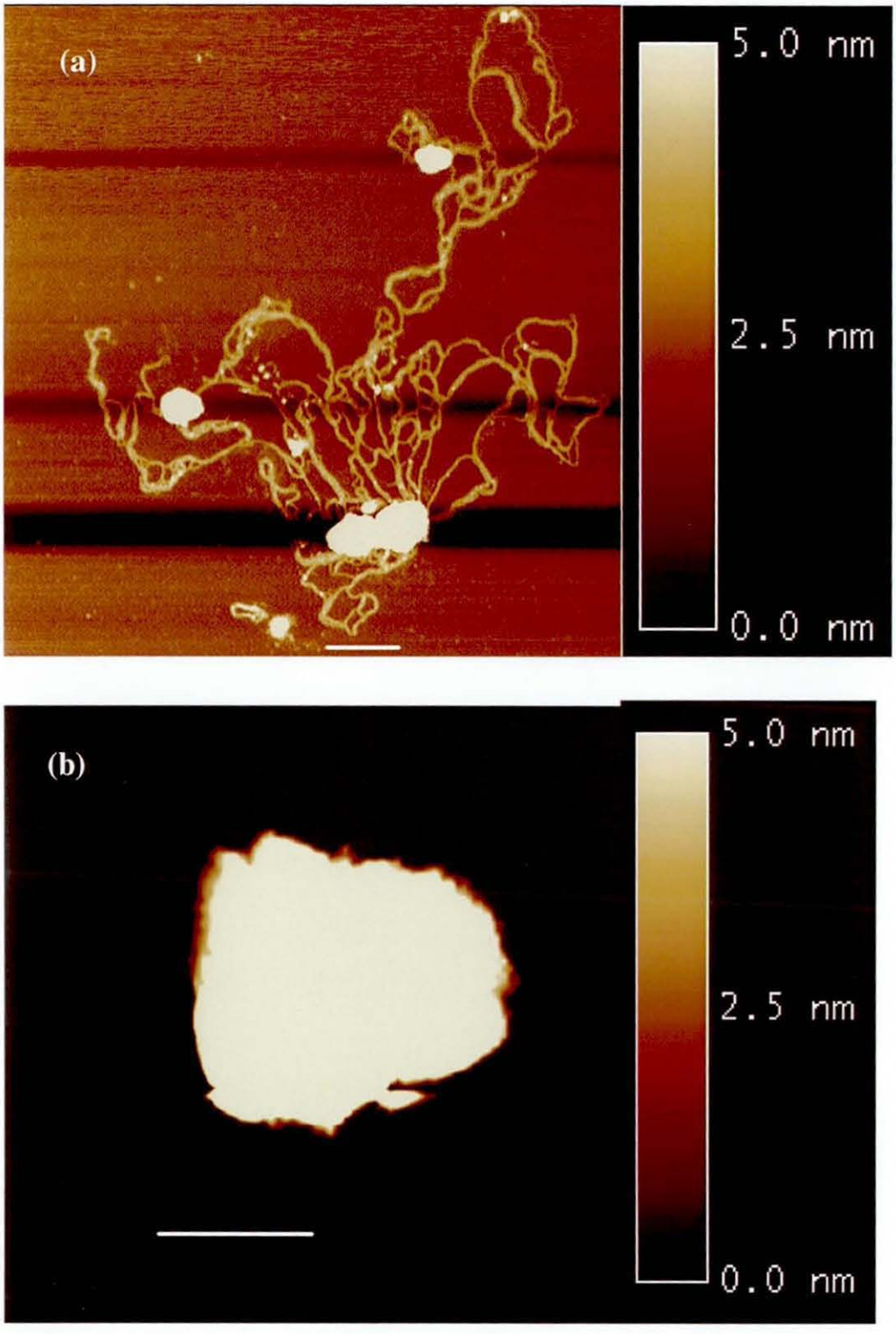

Figure 8.10: Formulation studies of 20kb plasmid DNA: Structural analysis by AFM imaging in air of PEI/20 kb plasmid formulated in PBS after washing the samples with de-ionised water; a) before nebulisation; scan size of 4.35 x 4.35 μm, scale bar – 500 nm; b) after nebulisation, scan size of 0.8 x 0.8 μm, scale bar – 200 nm; height 5 nm for both images.

8.3 Discussion

The safe delivery of ~15% of the sc structure of 20 kb plasmid using DEAE-dextran promises to deliver the therapeutic effect required in important diseases such as cystic fibrosis. DD being a linear polymer exhibits a loose condensation with plasmid DNA, similar to a scheme predicted for linear PEI [Kleemann et al., 2004]. AFM imaging of the formulated 20 kb plasmid showed the formation of compact nanoparticles after nebulisation, resulting in no DNA damage based on fluorescence. The formation of dense aggregates of 100 nm has been observed for a 4.3 kb plasmid complexed with PEI after ultrasonic nebulisation [Kleemann et al.., 2004]. The formation of nanoparticles of size 400 nm for the PEI-complexes 20 kb plasmid suggests a similar size ratio. With an increase in plasmid size, the hydrodynamic forces on the plasmid are larger resulting in damage to the sc structure. Hence the molecular dimensions of the sc structure of large plasmids must be reduced by adequate formulation to ensure undamaged passage of the particles through the mesh nozzle holes during aerosol delivery using a mesh nebuliser of this configuration.

8.4 Conclusions

Formulation is a prerequisite for safe delivery of sc structure of large-sized plasmids. The main objective of formulation is to reduce the size of the sc structure to that of a 5.7 kb plasmid (about 400 nm) to ensure protection against the hydrodynamic forces prevalent during aerosolisation. Formulation of 20 kb plasmid in ionic strength buffer did not result in efficient condensation of sc structure. Formulation with a cationic gene delivery agent and adjuvant such as DEAE-dextran resulted in protection of sc structure by about 15%. However, formulation of 20 kb plasmid with more cationic PEI resulted in total protection of the sc structure as evident from the PicoGreen fluorescence assay. Although research on formulation is widely reported, testing the efficacy of the bio-therapeutic following delivery via a device is an important step towards achieving the fruits of gene therapy. In the next chapter, transfection studies on Chinese Hamster Ovary cells using aerosolised plasmid DNA are presented that check the transfection efficiency and hence integrity of the aerosolised sc structure.

CHAPTER 9. TRANSFECTION OF CHINESE HAMSTER OVARY CELLS USING PLASMID DNA

9.1 Introduction

Earlier results have shown the supercoiled structure of a 5.7 kb plasmid to be intact after nebulisation using the U22 mesh nebuliser using analytical tools such as a UV spectrophotometer (for absorbance measurements), a microplate reader (for fluorescence measurements based on PicoGreen assay), agarose gel electrophoresis and an atomic force microscope. However, it is crucial to validate the performance of nebulised plasmid DNA for gene delivery into cells. The main objective of the work reported in this chapter was to check the integrity of the sc structure of the 5.7 kb plasmid bearing a Green Fluorescent Protein (GFP) marker gene after nebulisation, by carrying out *in vitro* transfection studies to quantify GFP gene expression into the cells.

An ideal cell line for studying the transfection of aerosolised plasmid DNA would have been a human epithelial cell line [Forbes and Ehrhardt, 2005]. However, due to the constraints in the handling of such a cell line, a common mammalian cell line, suspension-adapted Chinese Hamster Ovary (CHO-S) cells, was used for transfection studies as reported in this chapter. Since the suspension culture environment resulted in inefficient transient transfection of the naked plasmid [Tait, 2006], it was necessary to formulate the plasmid prior to transfection in order to achieve integration of the GFP gene in the cells. Hence the plasmid to be tested for transfection was formulated with a cationic formulation substrate, in order to protect the plasmid DNA and achieve DNA integration into the cells.

The structure of this chapter starts with a presentation of the reasons for the choice of the formulation substrate and concentration levels used for transfection. The twin strategy adopted for transient transfection of CHO-S cells with formulated 5.7 kb plasmid DNA includes:

(i) Formulation of the 5.7 kb plasmid with a cationic substrate → nebulisation → transfection → GFP gene expression and

(ii) Nebulisation of the 5.7 kb plasmid in a biological buffer → formulation with a cationic substrate → transfection → GFP gene expression.

The order of the formulation and nebulisation operations was primarily carried out to (i) quantify the expression of the GFP gene from the 5.7 kb plasmid into the CHO-S cells and (ii) examine the influence of formulation on transient gene expression. The GFP gene expression in the CHO-S cells was quantified using a fluorometer and flow cytometer. Cell density and viability measurements were carried out to study the influence of formulation and transfection on the CHO-S cells.

9.2 Choice of formulation substrate and concentration

Polyethylenimine (PEI) has been widely employed as a cationic substrate to complex plasmid DNA for aerosol gene delivery [Gautam et al., 2001, Densmore et al., 2000]. Branched PEI (25 kDa) has been reported to have higher reporter gene expression compared to linear PEI for gene delivery to the lungs [Rudolph et al., 2005]. The final DNA concentration of PEI/pDNA formulation used for *in vitro* serum-free transfection was 1 μg/mL [Tait, 2006], and *in vivo* transfection using aerosol delivery was 50 μg/mL [Densmore et al., 2000]. Hence, a pDNA concentration of 1 μg/mL was employed for *in vitro* transfection studies. A PEI/DNA ratio of 10:1 was the commonly used composition for preparation of pDNA formulations for aerosol gene delivery [Gautam et al., 2001].

9.3 Transfection of CHO-S cells

Transient transfection of suspension-adapted Chinese hamster ovary cells with uncomplexed plasmid DNA has been reported to result in insignificant transfection [Tait et al., 2004]. Hence, transfection studies were carried out using the 5.7 kb plasmid DNA formulated with PEI according to a protocol described by Tait [2006].

The formulation of 20 kb plasmid with PEI resulted in protection of the sc structure as reported in Chapter 8.

In this chapter, transfection of CHO-S cells was carried out using two formulations of sc 5.7 kb plasmid, namely: (i) PEI complexed with 5.7 kb plasmid and subsequently nebulised, and (ii) 5.7 kb plasmid nebulised and subsequently complexed with PEI. The 5.7 kb plasmid used for formulation adhered to the quality specifications for non-viral gene therapy in terms of purity and sc plasmid DNA homogeneity. The CHO-S cells were maintained up to passage 24 as per the protocol described in Chapter 3. The CHO-S cells used for transfection were taken from the mid-exponential phase of growth and resuspended in CHO-S SFM (Serum free medium) to achieve an initial viable cell density of about $2.1x10^5$ cells mL^{-1}. The pDNA concentration used for transfection in the ultra low binding 24 well plate was 1 μg/mL and each condition was carried out in triplicate. The cell density and GFP expression in the CHO-S cells transfected with samples of the complexed plasmid taken before and after nebulisation were quantified after an incubation time of 24 to 48 hours. The results are discussed below.

9.3.1 PEI complexed 5.7 kb plasmid

The 5.7 kb plasmid was complexed with 25 kDa branched PEI at a PEI Nitrogen to DNA Phosphate (N/P) ratio of 10 to 1 (corresponding to PEI:DNA weight ratio of 1.3:1) and incubated for 15 min prior to nebulisation. Nebulisation of formulated and unformulated 5.7 kb plasmid was carried out using the U22 mesh nebuliser. The aerosols of plasmid DNA from nebulisation were condensed and collected using an in-house fabricated aerosol collection apparatus described in Chapter 3. The transfection of CHO-S cells was carried out using the "before nebulisation" and "after nebulisation" samples of the formulated plasmid. The viable cell density of CHO-S cells and fluorescence measurements for GFP expression in untransfected and transfected cells are compared.

9.3.1.1 Cell density measurements

As shown in Figure 9.1, the viable cell density of untransfected CHO-S cells was observed to be higher than the formulated plasmid samples after an incubation time of 48 hours. However, viable cell density of cells transfected with un-nebulised formulated plasmid was observed to be lower than that after nebulisation. The compaction of PEI in the formulated 5.7 kb plasmid after nebulisation is likely to have occurred due to the oscillatory motion of the vibrator horn prior to aerosol formation during the nebulisation process. A higher viable cell density was observed for cells transfected with pDNA after nebulisation at the end of transfection.

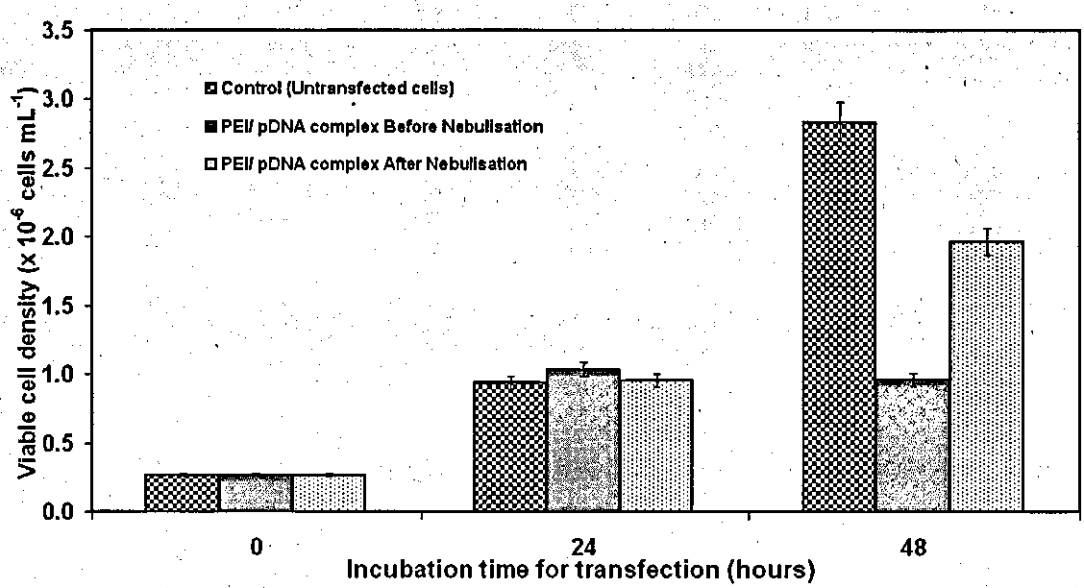

Figure 9.1: Viable cell density of Chinese hamster ovary cells transfected with before and after nebulisation samples of PEI formulated 5.7 kb plasmid. Control refers to untransfected CHO-S cells (n=2).

9.3.1.2 Fluorescence measurements

Figure 9.2 shows the cell specific RFU for transfected CHO cells before and after nebulisation of 5.7 kb plasmid formulated with PEI. From Figure 9.2, GFP quantification in terms of cell specific RFU showed a significant ($p = 0.001$) increase in transfection for the PEI formulated plasmid before nebulisation. However, there was a less significant increase ($p = 0.047$) in fluorescence in the cells transfected

with formulated plasmid after nebulisation than the untransfected cells. The fluorescence of the untransfected cells is due to auto-fluorescence exhibited by the cells. The variation in the cell-specific RFU of PEI/pDNA complex before nebulisation was perhaps due to the variation in the formation of less compacted nanoparticles. The cell-specific fluorescence in the cells transfected with formulated plasmid before nebulisation samples was higher than the formulated plasmid after nebulisation due to perhaps two reasons, namely: (i) release of PEI/pDNA complex from uncompacted PEI formulated plasmid and (ii) increased burden on the cells for transient gene expression. The PEI/pDNA complex after nebulisation resulted in the formation of compact nanoparticles (as reported in section 8.3). A higher viable cell density of the cells transfected with pDNA after nebulisation (Figure 9.1) was due to lower transient gene expression of the compact PEI/pDNA complex. The low cell-specific RFU after nebulisation was due to the inability of the pDNA to transfect the cells, resulting in less integration of the plasmid DNA and consequently lower GFP expression (Figure 9.2).

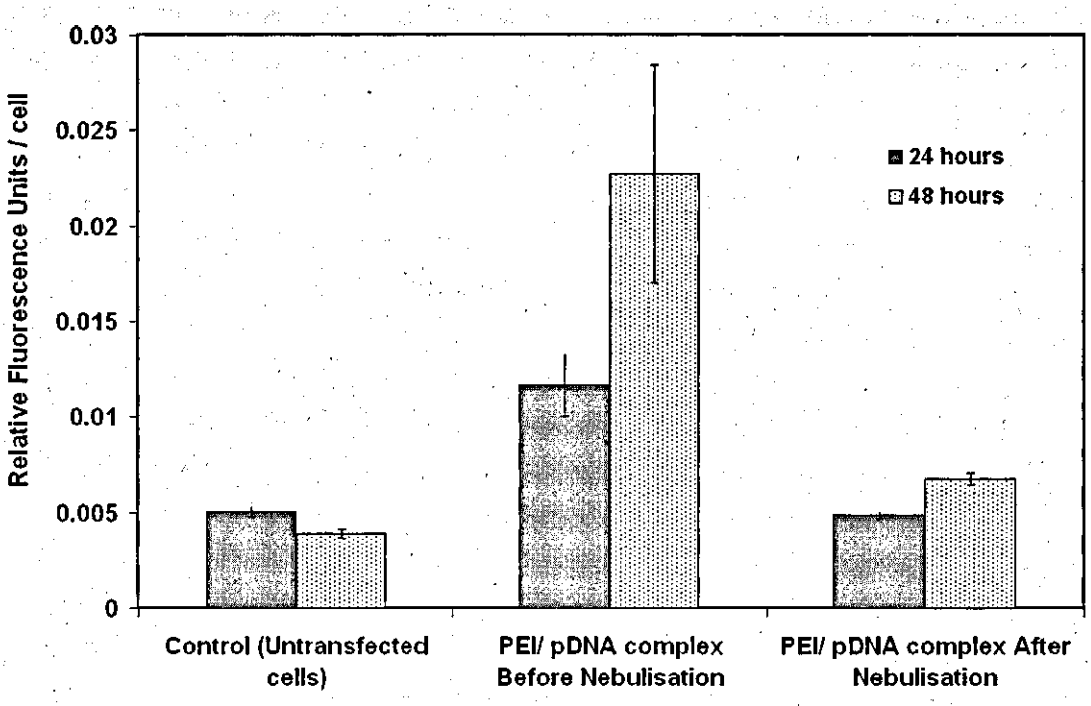

Figure 9.2: Cell specific relative fluorescence units for untransfected and transfected CHO-S cells based on fluorescence measurements using a microplate reader at excitation wavelength of 483nm and emission wavelength of 530nm for GFP quantification after 24 and 48 hours of incubation (n=3).

The transfection of CHO-S cells with formulated plasmid subjected to nebulisation clearly showed that there was an inverse relationship between viable cell density and fluorescence due to GFP expression by the transfected cells. The formulated PEI plasmid upon nebulisation was perhaps compacted during the nebulisation process resulting in no transfection of the pDNA into CHO cells. Since the RFU of the transfected samples were low, the transfection efficiency was determined using a flow cytometer.

9.3.2 Nebulised 5.7 kb plasmid complexed with PEI

Transfection studies with PEI formulated plasmid before nebulisation showed a significant increase in transfection compared to that formulated after nebulisation. The main objective of the transfection studies was to investigate the effect of plasmid DNA nebulisation on DNA delivery into the cells. Hence, it was essential to first nebulise the 5.7 kb plasmid DNA, and then formulate the un-nebulised and nebulised samples with PEI, prior to transfection. Using this approach, the compaction of PEI/pDNA complex during the nebulisation process can also be avoided. Although, this approach is not practically relevant to studying the aerosol delivery of plasmid DNA in pre-clinical trials, it was carried out mainly to check the integrity of the sc structure of plasmid after nebulisation by determination of the transfection efficiency in the transfected CHO cells.

9.3.2.1 Plasmid in TE buffer

In order to investigate the influence of formulation on GFP expression in CHO-S cells, the 5.7 kb plasmid in TE buffer (at 20 μg/mL DNA concentration) was nebulised and then formulated with PEI for transient transfection studies. An unnebulised plasmid sample was also formulated with PEI to study the effect of nebulisation on the transfection of the 5.7 kb plasmid.

9.3.2.1.1 Cell density measurements

The viability of untransfected and transfected CHO-S cells after an incubation time of 48 hours for all the plasmid DNA samples was observed to be ~95%. As shown in Figure 9.3, there was no significant difference ($p = 0.17$) between the cell densities determined in terms of viable and total cell count for the unnebulised and nebulised pDNA complexed with PEI.

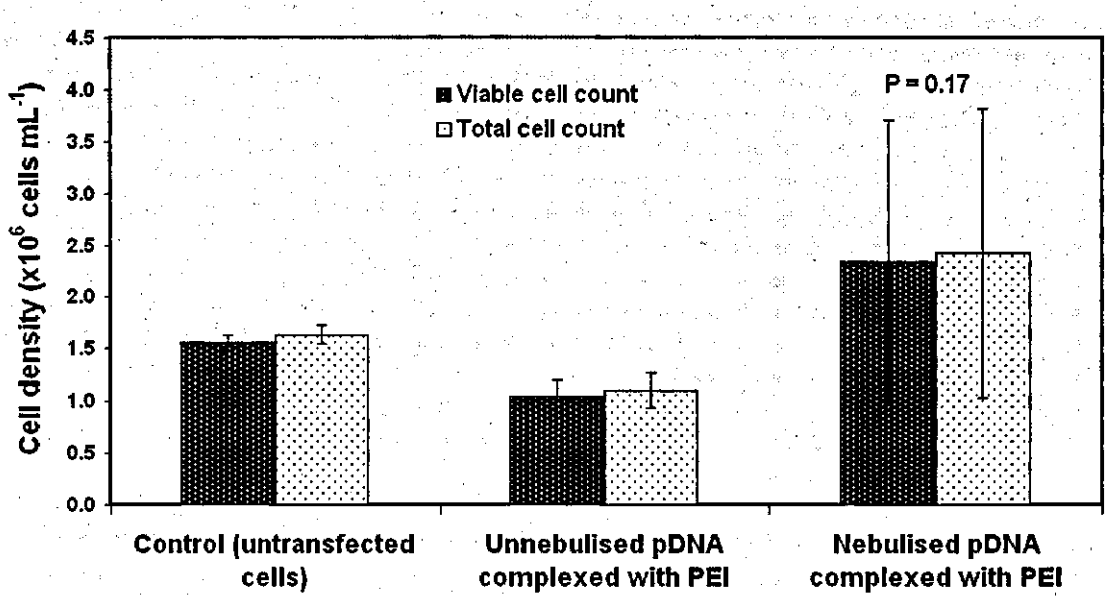

Figure 9.3: Cell density of CHO-S cells transfected with unebulised and nebulised samples of 5.7 kb plasmid complexed with PEI after an incubation time of 48 hours. Control refers to untransfected CHO-S cells (n=3).

In chapter 4, it has been shown that the 5.7 kb plasmid on nebulisation resulted in generation of linear dsDNA fragments from the degradation of the open-circular (oc) structure. A large variability for the cell density of the nebulised sample may be due to the cytotoxic effect from the complexation of linear dsDNA fragments with PEI. A cell viability of 95% for both the transfected samples suggested that there was no influence of formulation and nebulisation on them. However, there was a significant difference ($p = 0.007$) in the cell densities between the untransfected cells and cell transfected with unnebulised plasmid DNA formulations.

9.3.2.1.2 Flow cytometry analysis

A flow cytometric analysis was carried out to determine the transfection efficiency of the CHO-S cells and the protocol is described in detail in Chapter 3. The transfection efficiency is defined as the percentage of eGFP positive cells in a transfected cell population.

In Figure 9.4, GFP intensity in CHO-S cells for un-nebulised and nebulised 5.7 kb pDNA samples complexed with PEI is shown. The percentage values indicate the percent of cells expressing GFP as determined by the ADC software (as discussed in 3.2.9.6). The GFP intensity in the untransfected cells (Fig. 9.4a) was used to determine background fluorescence, and therefore the transfection efficiency of other samples. Although the transfection efficiency in the CHO-S cells transfected with un-nebulised (Fig. 9.4b) and nebulised (Fig. 9.4c) 5.7 kb plasmid at 20 μg/mL DNA concentration was the same, more expressing cells (GFP intensity up to 100) were observed for un-nebulised plasmid. The insignificant difference in cell densities and transfection efficiencies between un-nebulised and nebulised 5.7 kb plasmid suggested no effect on pDNA delivery in the transfected CHO-S cells due to the nebulisation process.

In order to examine the influence of plasmid DNA concentration on transfection of CHO-S cells, the 5.7 kb plasmid at 30 μg/mL DNA concentration was nebulised and formulated with PEI, prior to transfection. As observed in Fig. 9.4d, a corresponding increase in transfection efficiency proportional to the plasmid DNA concentration was obtained. This result showed that the low transfection efficiency achieved using a DNA concentration of 20 μg/mL can be increased by increasing the plasmid DNA concentration used for nebulisation.

Earlier results in Chapter 4 showed nebulisation of 5.7 kb plasmid DNA in TE buffer resulted in a slight damage (about 5%) to the sc structure. The sc structure of the 5.7 kb plasmid in an ionic buffer such as phosphate buffered saline (PBS), HEPES buffered saline (HBS) resulted in better protection to the sc structure upon nebulisation. The next section investigates the impact of formulation and nebulisation of 5.7 kb plasmid in ionic buffer on transfection.

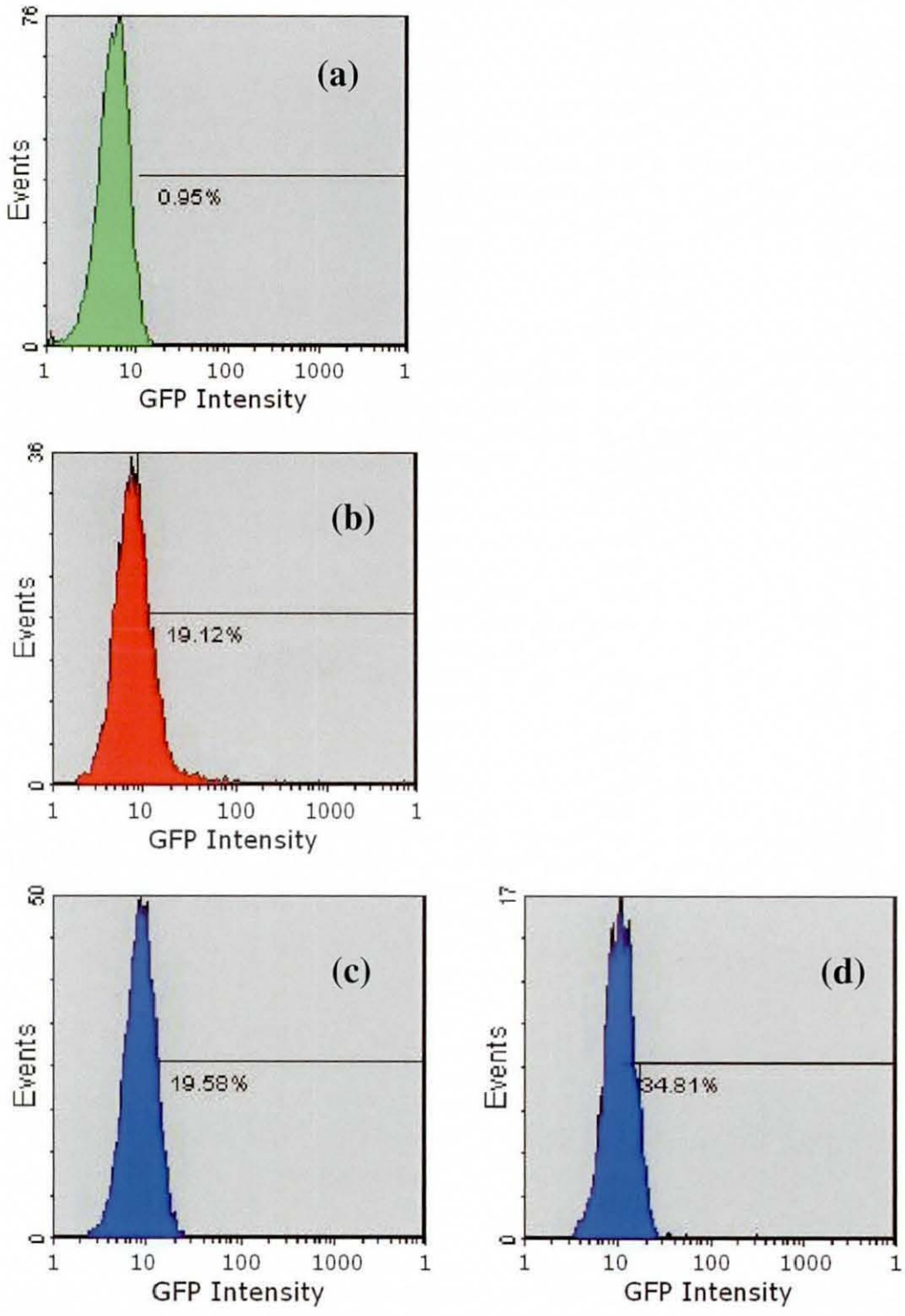

Figure 9.4: Effect of nebulisation and DNA concentration on transient transfection: GFP intensity measured using a Flow cytometer for a) untransfected CHO-S cells, b) unnebulised and c) nebulised pDNA at 20 μg/mL DNA concentration, d) nebulised pDNA at 30 μg/mL DNA concentration in TE complexed with PEI, after incubation time of 48 hours; % values indicate the transfection efficiency in terms of the percent of eGFP positive cells in a transfected cell population.

9.3.2.2 Plasmid in HBS buffer

This experiment was conducted to investigate the influence of an ionic buffer such as HEPES buffered saline (HBS) on transfection of 5.7 kb plasmid DNA. HBS has been used as a common biological buffer for the preparation of biological samples. Unnebulised and nebulised 5.7 kb plasmid in HBS (20 μg/mL DNA concentration) was complexed with PEI and transfected in CHO-S cells to study the effect of plasmid DNA condensed in ionic buffer on DNA delivery into the cells.

9.3.2.2.1 Flow cytometry analysis

Flow cytometry analysis was carried out on the nebulised and unnebulised transfected CHO-S cells to determine the transfection efficiency from the GFP expression in the cells. As shown in Figure 9.5a, the untransfected cells exhibited background fluorescence due to auto-fluorescence of the cells and not GFP expression. The transfection efficiency of the cells transfected with unnebulised plasmid DNA was higher with a significant difference ($p = 0.02$) compared to the cells transfected with nebulised plasmid DNA. The decrease in transfection efficiency of the nebulised sample (Table 9.1) was possibly due to compaction of condensed sc structure of the 5.7 kb plasmid in ionic buffer during nebulisation. However, the effect of this compaction may be lower than that observed with the PEI formulated 5.7 kb plasmid, discussed in section 9.2.1.2.

Table 9.1: Average cell density and transfection efficiency (n=3) for 5.7 kb plasmid.

Sample	**Average cell density ($x10^6$ cells per mL)**	**Transfection efficiency (%) mean ± SD**
Control (Untransfected)	2.80	
Unnebulised 5.7 kb in HBS	2.30	17.18 ± 0.57
Nebulised 5.7 kb in HBS	1.74	12.96 ± 2.11
pDNA delivery efficiency of nebulised over unnebulised pDNA = 75.43%		

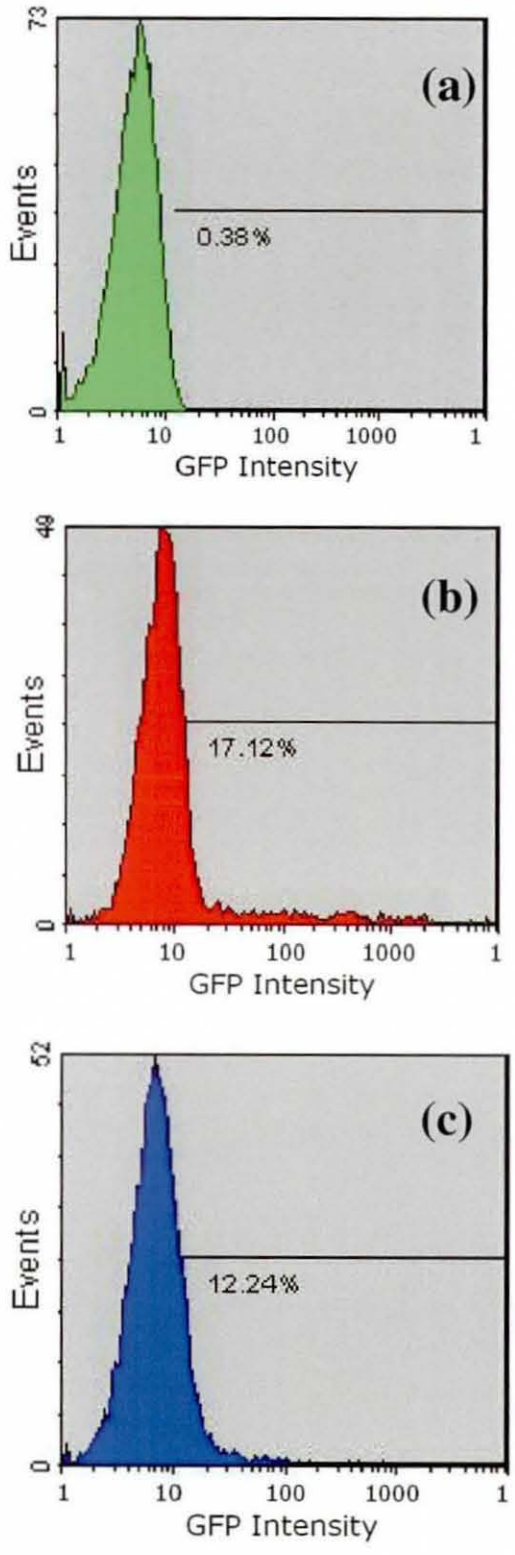

Figure 9.5: Effect of nebulisation and formulation on transient transfection: GFP intensity measured using a Flow cytometer for a) untransfected CHO-S cells, b) unnebulised and c) nebulised pDNA at 20 μg/mL concentration, in HBS complexed with PEI, after incubation time of 48 hours; % values indicate the percent of eGFP positive cells in a transfected cell population (n=3).

The plasmid DNA delivery efficiency (Table 9.1) using a U22 mesh nebuliser was determined from a ratio of the transfection efficiency of the cells transfected with nebulised over unnebulised plasmid DNA. A pDNA delivery efficiency of ~75% was observed using plasmid DNA formulated in ionic buffer. The results show that plasmid DNA after nebulisation can be transfected in suspension-adapted CHO cells and high pDNA delivery efficiencies can be obtained depending on the buffer used for plasmid DNA formulation.

9.3.2.2.2 Microscopy

The transfected and untransfected cells were visualised in a microscope using fluorescent light. As shown in Figure 9.6, strong fluorescence was observed in the transfected cells due to the incorporation of plasmid DNA containing the GFP marker gene. Since the pDNA concentration used for transfection was 1 μg/mL, the number of cells showing fluorescence was low. However, earlier studies in section 9.2.2.1.2 showed that the transfection efficiency and hence fluorescence of the transfected cells was dependent on the plasmid DNA concentration used for transfection.

9.4 Discussion

Direct *in vivo* gene transfer with naked DNA was first demonstrated when efficient transfection of myofibers was observed following injection of pDNA into skeletal muscle [Wolff et al., 1990]. Delivery of naked DNA to cells elicits minimal immune response when compared to DNA encapsulated in lipids or cationic polymers. The lack of immunogenicity of naked DNA makes it a good prospect for gene therapy. However, the susceptibility of naked DNA to degradation from nucleases and the need for DNA to have target specificity has resulted in the development of physical methods aimed at targeting DNA to tissues. The physical delivery methods for naked DNA reported in literature are (i) high pressure delivery, (ii) electroporation, (iii)

laser beam gene transduction, (iv) ultrasound, (vi) photochemical internalisation [Conwell and Huang, 2005] and (v) magnetofection [Dobson, 2006]. Systemic delivery of naked plasmid DNA for gene transfer into the liver holds promise for the treatment of metabolic diseases [Liu and Tyagi, 2005].

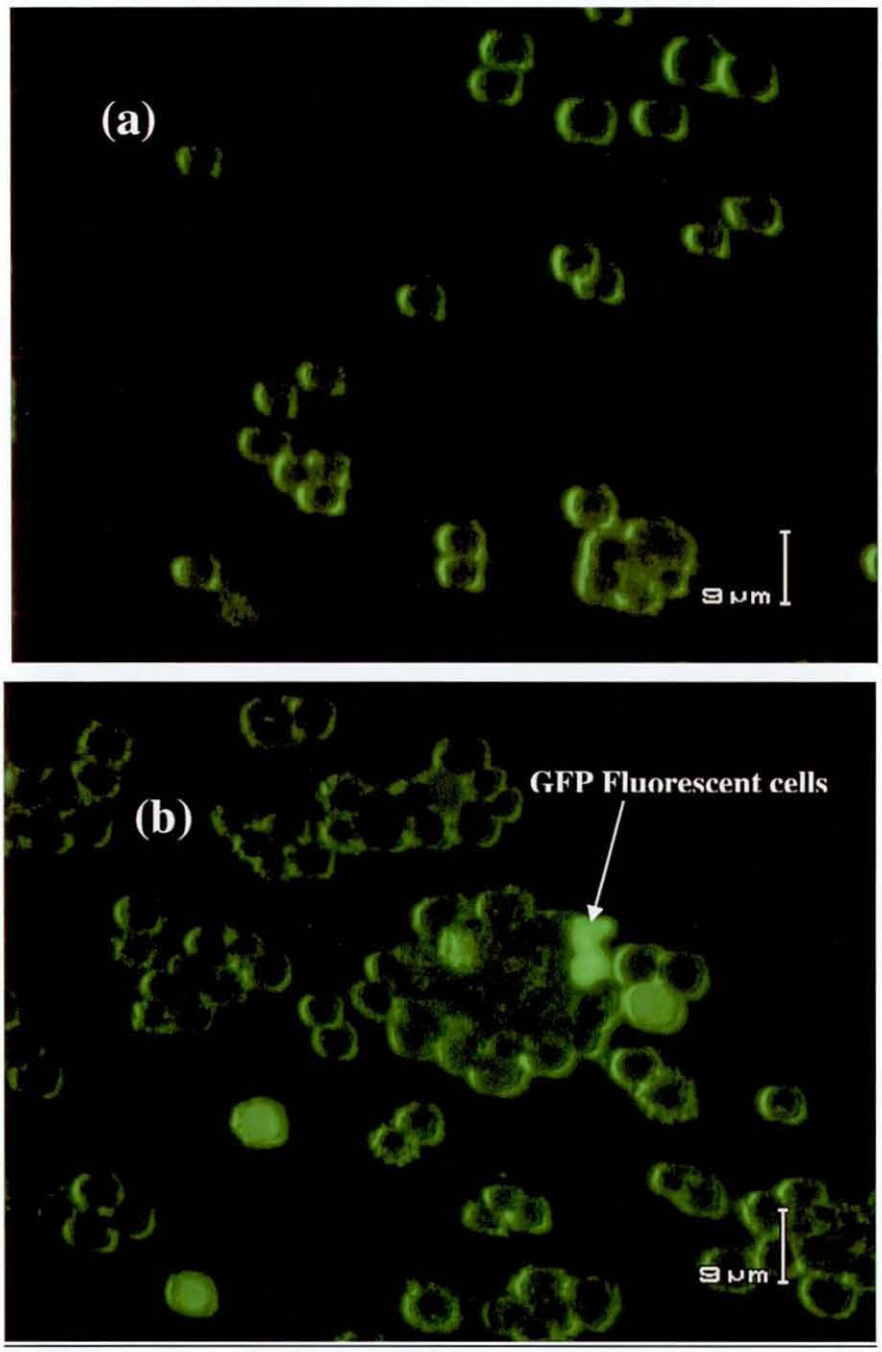

Figure 9.6: Microscopic image of a) untransfected and b) transfected CHO-S cells.

After the cloning of the cystic fibrosis gene, inhalation gene therapy was predicted to be an ideal non-invasive mode of gene delivery to the airway epithelial and other lung surfaces [Densmore, 2003]. However, the delivery of the CFTR (Cystic fibrosis transmembrane-conductance regulator) gene into the airways using existing respiratory devices such as jet nebulisers was limited due to the damage to DNA during the aerosolisation process and the difficulty in getting through the mucous. Nebulisation has a long history in the delivery of non gene-based drugs to the airways. In view of the damage to plasmid DNA during nebulisation, intensive research was pursued to protect plasmid DNA by formulation using cationic substrates such as PEI [Rudolph et al., 2005]. However, newer technologies employing nebulisation by single pass through a porous membrane offer promise as an ideal delivery system [Davies and Alton, 2005], without the need for formulation of naked plasmid DNA prior to delivery.

In the earlier chapters, safe aerosol delivery of sc structure of a naked 5.7 kb plasmid DNA has been experimentally and analytically determined. However, it is crucial to validate the performance of the aerosolised plasmid to confirm the integrity of the sc structure for its intended application in non-viral gene therapy. Transfection of adherent cells in culture has been reported to be straightforward because the complexes can reach the cell easily, cells are metabolically active and in a mitotic state [Demeneix and Behr, 2005]. In this chapter, transient transfection of plasmid DNA was carried out using suspension-adapted CHO cells. These cells have potential applications for the production of recombinant therapeutic proteins [Tait, 2006].

Transfection of PEI formulated 5.7 kb plasmid after nebulisation was observed to result in higher cell viability (Figure 9.1) and lower GFP fluorescence (Figure 9.2) than the before nebulisation sample. This was possibly due the cytotoxic effect of PEI from the less compact formulated plasmid DNA in the before nebulisation sample. Nebulisation in the mesh nebuliser resulted in the formation of condensed nanoparticles and it is possible that PEI/pDNA complexes after nebulisation may have been compacted. Earlier results reported in chapter 8 (section 8.3) supports this hypothesis. This probably resulted in limited dissociation of the PEI/pDNA complex leading to lower transfection.

Nebulisation of 5.7 kb plasmid in buffers with ionic strength has resulted in protection to the sc structure of the plasmid after nebulisation. In order to study the influence of plasmid DNA formulated in ionic buffer on transfection, nebulisation of plasmid DNA in buffer with and without ionic strength was carried out in addition to PEI formulation prior to transfection. As observed in figures 9.3 and 9.4, insignificant differences in cell densities and transfection efficiency in CHO-S cells transfected with un-nebulised and nebulised plasmid in TE buffer were obtained. However, a significant difference in transfection efficiency was observed for the plasmid formulated in ionic buffer. Nebulisation of plasmid formulated in ionic buffer resulted in a lower transfection efficiency than the un-nebulised plasmid. The formulation of plasmid with PEI in ionic buffer resulted perhaps in the formation of large cationic PEI/pDNA complexes formed by aggregation when Van der Waals attraction becomes stronger than Coulombic repulsion, since the latter is weakened by shielding with salt [Demeneix and Behr, 2005]. However, a plasmid DNA delivery efficiency of over 75% after nebulisation compared to before nebulisation, confirmed the earlier results on retention of the sc structure of the 5.7 kb plasmid upon aerosolisation.

The safe aerosol delivery of the sc structure of 5.7 kb plasmid DNA using a U22 mesh nebuliser has been validated for the non-viral aerosol gene delivery by the successful *in vitro* transfection studies in suspension-adapted Chinese hamster ovary cells. Hence, aerosol delivery of plasmid DNA using a mesh nebuliser promises to be useful respiratory drug delivery device for non-viral aerosol gene delivery.

9.5 Conclusions

Nebulisation of 5.7 kb plasmid subsequently complexed with PEI resulted in higher GFP expression compared to the plasmid formulated with PEI prior to nebulisation. The low fluorescence of the formulated 5.7 kb plasmid after nebulisation could be possibly due to efficient complexation of the PEI with the sc structure resulting in low GFP expression in the cells. However, the sc structure was not damaged after nebulisation and when complexed with PEI just before transfection resulted in

release of plasmid DNA from the PEI complex into CHO cells leading to higher GFP expression than that with the formulated plasmid. The results demonstrate that the nebulisation process does not affect the expression from pDNA during transfection by retention of the supercoiled structure, which confirms the results presented in previous chapters. However, the data presented on the transfection of CHO-S cells with PEI/pDNA complex after nebulisation does show that nebulisation can affect expression by altering the nature of the PEI-pDNA complex in some way. This could be due to compaction of the PEI/pDNA complex during the nebulisation process. Nebulised plasmid DNA formulated in buffers with and without ionic strength resulted in appreciable transfection of the CHO cells.

This research has led to (i) proof-of-principle of safe aerosol delivery of sc plasmid DNA using a mesh nebuliser and (ii) transfection of aerosolised plasmid DNA, which offers immense potential for the application of mesh nebulisation technology for the aerosol delivery of shear-sensitive therapeutics such as plasmid DNA, siRNA, etc into the airways for the treatment of respiratory diseases such as cystic fibrosis, influenza and lung cancer.

CHAPTER 10. CONCLUSIONS

10.1 Introduction

Aerosol delivery of plasmid DNA has potential for applications in the treatment of acute respiratory diseases such as cystic fibrosis, lung cancer, influenza and SARs. This thesis has indicated the growing importance of plasmid DNA as a future gene therapeutic vector as shown by activity in gene therapy clinical trials. With the recent approval of insulin delivery through the respiratory route, pulmonary delivery promises to be an attractive non-invasive route for the treatment of chronic respiratory and systemic diseases. With the recent success in large-scale production of sc plasmid DNA, delivery remains a key outstanding issue.

The main results in the thesis that enable such delivery are summarised below:

- Nebulisation of plasmid DNA of sizes from 5.7 to 20 kb using a state-of-the-art mesh nebuliser for safe aerosol delivery of the supercoiled (sc) structure
- The development of method for the analysis of damage to the plasmid DNA sc structure using gel electrophoresis, the PicoGreen assay and AFM
- Engineering analysis to estimate the maximum hydrodynamic force and limiting size for safe delivery of the sc structure using the mesh nebuliser
- DOE studies to enable prediction of the damage due to different nozzle sizes and frequencies
- Formulation of plasmid DNA for safe aerosol delivery of the sc structure using ionic buffers, DEAE-dextran and PEI
- *In vitro* transfection studies in CHO-S cells to determine the transfection efficiency and validate the safe aerosolisation of the sc structure.

10.2 Conclusions

Purification and delivery of plasmid DNA in its supercoiled (sc) form is crucial for its application in non-viral gene therapy clinical trials and subsequently in therapies. Damage to the sc structure has been reported in bioprocessing operations involved in the purification of plasmid DNA on a large-scale. In this investigaton, typical plasmids of size from 5.7 to 20 kb were purified in the supercoiled form and formulations of plasmid DNA aerosolised using a commercially available and clinically approved mesh nebuliser. In order to facilitate quick adoption of a potential plasmid DNA based genetic drug, the Omron U22 mesh nebuliser was selected for the studies rather than unproven and unapproved device that would require both drug and device approval. While nebulisation of the naked 5.7 kb plasmid formulated in ionic buffer resulted in safe aerosol delivery of the sc structure, damage to the open-circular (oc) structure of the 5.7 kb plasmid and sc structure of 8.7, 13 and 20 kb plasmids was detected using gel electrophoresis, atomic force microscopy and the PicoGreen assay. Safe delivery of the sc structure of the 5.7 kb plasmid using the U22 mesh nebuliser suggested that damage is dependent on the size of the molecular sc structure and mesh nozzle, and device frequency.

A Box-Behnken design of experiments using nozzle size, DNA and NaCl concentrations as variables was used to create a three-dimensional response surface methodology (RSM) model to predict the damage to the sc structure of the 20 kb plasmid in the U22 mesh nebuliser. The model enables better understanding of the damage to the sc structure upon nebulisation at intermediate levels of the variables. Lower damage to the sc structure of 20 kb plasmid was predicted at nozzle sizes >3 μm. However, the requirement to use a nozzle size ≤ 3 μm to provide inhalable aerosols for respiratory delivery suggests that a 20 kb plasmid needs to be further condensed by formulation in order to circumvent damage. From the model predictions and analysis, it is concluded that the physical size of 20 kb plasmid remains the main bottleneck for aerosol delivery of the sc structure.

Engineering analysis of the aerosolisation of liquid from the nebuliser provided an insight into the process with the help of high-speed imaging. High-speed imaging of aerosolisation from the vibrator horn with and without a mesh provided data on the velocity and pressure amplitudes due to the ultrasonic motion of the vibrator horn.

Partial damage to the sc structure without the mesh, suggested the influence of cavitation due to the oscillatory motion of the horn. Aerosolisation without mesh resulted in the generation of non-uniform large droplets due to the effect of vibrations of the horn on the fluid. For a mesh nebuliser, the out-of-phase vibrations of the horn and mesh result in a single-pass droplet generation through the mesh nozzle. Damage to sc of the 20 kb plasmid and safe delivery of 5.7 kb plasmid is explained by estimations of the maximum hydrodynamic force computed from the strain rates predicted using CFD modelling and sizing of the sc structure using AFM imaging. Such a determination of hydrodynamic force levels for damage to DNA in micro-scale flow environments has not yet been reported in the literature and allows the degradation of such shear-sensitive therapeutics in drug-delivery device combinations to be explored. In addition to hydrodynamic force levels, a semi-log plot of plasmid DNA degradation against molecular size enabled a linear extrapolation of the limiting size for safe passage of the sc structure on aerosolisation in the mesh nebuliser. It was estimated that the sc structure of an unformulated plasmid of size less than 6.7 kb and 3.8 kb could be safely delivered using the U22 and U03 mesh nebulisers respectively. The influence of hydrodynamic force on damage to the sc structure was observed to be a significant parameter affecting delivery. A reduction in the size of the sc structure ensures lower levels of hydrodynamic force and consequently safe aerosol delivery. This method of estimating plasmid DNA size for safe delivery in a mesh nebuliser will assist in the design of plasmid DNA based gene therapeutics.

Damage to the sc structure of plasmid DNA depends on device parameters such as nozzle size and frequency, in addition to formulation. A factorial design of experiments investigated the main effects of the variables including plasmid size, nozzle size and device frequency and the interactions between them. Damage to the sc structure of plasmid DNA was more pronounced at 3 μm nozzle size than at 5 μm. Nebulisation at 65 kHz device frequency resulted in more damage to plasmids of smaller size than nebulisation at 175 kHz. The DOE showed positive interaction between the DNA plasmid and the nozzle size and frequency. The main advantage of the results from such experiments is that the potential for damage to the sc structure can be inferred with respect to the interactions between the variables chosen for the experimentation. This approach also will help in determining the design parameters of a device for safe aerosol delivery of plasmid DNA as a non-viral gene therapeutic.

The work above has shown that formulation is a prerequisite for safe delivery of the sc structure of large plasmids. Here, the main objective of formulation is to reduce the size of the sc structure to that of a 5.7 kb plasmid (about 400 nm) to ensure protection against the hydrodynamic forces during aerosolisation. Formulation of 20 kb plasmid with cationic PEI resulted in protection of the sc structure as shown by the PicoGreen fluorescence assay and AFM imaging. Transient transfection studies using a PEI formulated 5.7 kb plasmid bearing a Green Fluorescent Protein (GFP) marker gene in suspension-adapted Chinese Hamster Ovary (CHO-S) cells showed DNA delivery efficiency of >75% using aerosolised plasmid DNA compared to before nebulisation. This confirmed the earlier results on retention of the sc structure of the 5.7 kb plasmid upon aerosolisation.

10.3 Key parameters for delivery of supercoiled plasmid

The significant parameters for safe delivery of supercoiled structure of a plasmid using a mesh nebuliser are determined using design of experiments can be characterised into (i) device and (ii) formulation parameters and are summarised in Table 10.1.

10.4 Scope for future work

This research has demonstrated the potential of delivering intact supercoiled plasmid DNA using a mesh nebuliser. Scope exists for future research in the following areas:

- Engineering studies on multiphase fluid flow modelling through the device with modification of the key device parameters of the mesh nebuliser, nozzle size and frequency, to generate very fine aerosols for high efficiency of drug delivery to the lungs.

- The next steps of testing of the mesh nebuliser in pre-clinical and clinical gene therapy trials for non-invasive delivery of gene therapeutics. Use of a mesh

nebuliser for targeted delivery of nanoparticles including plasmid DNA delivery for cystic fibrosis holds considerable promise for the future.

Table 10.1: Summary of the key parameters for delivery of supercoiled plasmid

Key parameter	**Operating conditions**	**Damage to sc structure (%)**	**Effect on delivery**	**Recommended future work**
Nozzle size	3 μm	5.7 kb: Nil	Safe delivery	*In vivo* study
		20 kb: 93-98%	Not suitable	pDNA formulation
	4 μm	20 kb: 18-36%	Not suitable	Nozzle size unsuitable
	5 μm	20 kb: 22-30%	Not suitable	Nozzle size unsuitable
Formulation		Formulated 20 kb: Nil	Safe delivery	*In vivo* study
	0 mM NaCl	20 kb: 96% (3 μm)	Not suitable	Change nozzle frequency
	300 mM NaCl	20 kb: 93% (3 μm)	Not suitable	Change nozzle frequency
Nozzle frequency	175 kHz	5.7 kb: Nil	Safe delivery	*In vivo* study
		Formulated 20 kb: Nil	Safe delivery	*In vivo* study
		20 kb: >95%	Not suitable	Change nozzle size
		Limiting plasmid size: < 6.7 kb	Safe delivery	
	65 kHz	Limiting plasmid size: < 3.8 kb	Safe delivery	

10.4.1 Studies on multiphase modelling and device parameters

Engineering studies on multiphase modelling of flow through the device would be expected to provide additional information for device design. The influence of cavitation and dynamics of droplet formation on damage to the sc structure of the plasmid can be studied by their incorporation in a multiphase model. A freely jointed chain model that assumes the shape of the sc structure can be incorporated in the multiphase model to understand the vulnerable regions of the sc structure more likely

to be damaged during the aerosolisation process. A multiphase model with the plasmid nanoparticle, the solvent used for formulation and air as the three phases could predict the strain rates during the fluid flow through the nozzle. An evaluation of the strain rates encountered during the fluid flow could perhaps provide information on the nozzle frequency and nozzle size to be adopted to ensure safe delivery of the fragile sc structure of the plasmid.

Engineering studies reported in this thesis have shown that nozzle size and device frequency are the two main device parameters which influence the aerosolisation process resulting in the generation of fine respirable aerosols. Since this research has focussed on the use of an existing mesh nebuliser to deliver plasmid DNA, the next steps for the progress of this work could be focussed towards device development. Although the development of newer devices requires regulatory approval of the device, there are opportunities for the development of newer mesh nebulisers. Further device development should be focussed on increasing the frequency of the device and the nozzle size. An increase in frequency results in the generation of finer respirable aerosols. Although an increase in frequency can lead to higher strain rates, a corresponding increase in nozzle size would reduce its effects potentially leading to safe delivery of the sc structure of plasmids. Optimisation of the nozzle frequency and nozzle size promises to deliver devices with better performance in the aerosol delivery of shear-sensitive sc structure of plasmid DNA. The result reported in this thesis has shown that more damage to the sc structure is observed using a low frequency device than a high frequency device with the same nozzle size. Improved knowledge of the operating conditions of the device will provide the necessary background for further formulation development for the efficient delivery of the fragile gene therapeutic.

10.4.2 Nebulisation for cystic fibrosis gene therapy

Gene therapy holds considerable promise for the treatment of genetic and highly infectious respiratory diseases. With gene therapy still in clinical trials, the recent report by UK Gene Therapy Advisory Committee (GTAC) [http://www.advisorybodies.doh.gov.uk/genetics/gtac/flagging.htm] on the lack of vector integration and recombination using plasmid DNA suggests delivery is still an issue

for the successful application of non-viral gene therapy. Cystic fibrosis is a common lethal hereditary disease causing chronic lung inflammation. An ideal vector for gene therapy should have an adequate gene handling capability and delivery efficiency, and low immunogenicity. Plasmid DNA has a large transgene handling capability and low immunogenicity. However, aerosol delivery of large sized plasmids to the lungs has been a bottleneck for gene delivery. In order to improve the efficacy of CFTR gene delivery using plasmid DNA for cystic fibrosis patients, it is essential that the integrity of the fragile gene therapeutic is not damaged during the aerosolisation process and delivered as inhalable aerosols to reach the epithelial cells. An approved mesh nebuliser for the aerosol delivery of plasmid DNA studied in this research has shown that this device can be used for *in-vitro* and *in-vivo* assessment of cystic fibrosis gene therapy clinical trials. Further, the key steps required to take cystic fibrosis forward are the development of specific formulations to carry the plasmid containing the CFTR gene (~10 kb) and experiments to confirm its safe delivery in an ultrasonic mesh nebuliser. PEI formulations are an excellent starting point for the safe delivery of CFTR gene in the clinical trials. Magnetofection-assisted plasmid DNA delivery promises to deliver plasmid DNA bound to magnetic nanoparticles using an aerosolisation device such as the mesh nebuliser to the targeted cells resulting in improved efficacy of the gene therapeutic.

To summarise, testing the efficacy of a plasmid DNA-based gene therapeutic at the pre-clinical/clinical stage is crucial towards achieving the promise of gene therapy. This research has led to (i) demonstrated proof-of-principle of safe aerosol delivery of sc plasmid DNA using a mesh nebuliser and (ii) transfection of aerosolised plasmid DNA in a mammalian cell line such as CHO-S cells. The application of this mesh nebulisation technology for the aerosol delivery of shear-sensitive therapeutics such as plasmid DNA and siRNA into and via the airways offers immense potential for the treatment of unmet medical needs such as influenza, SARs, lung cancer.

References

Agami R. 2002. RNAi and related mechanisms and their potential use for therapy. Curr. Opin. Chem. Biol. 6:829-834.

Agarwal A, Unfer R, Mallapragada SK. 2005. Novel cationic pentablock copolymers as non-viral vectors for gene therapy. J. Controlled Release. 103:245-258.

Agu RU, Ugwoke MI, Armand M, Kinget R, Verbeke N. 2001. The lung as a route for systemic delivery of therapeutic proteins and peptides. Respir. Res. 2:198-209.

Anchordoquy TJ, Armstrong TK, Molina MDC, Allison SD, Zhang Y, Patel MM, Lentz YK, Koe GS. 2004a. Formulation considerations for DNA-based therapeutics. In Cellular drug delivery: Principles and practice, First ed., Liu DR, Oie S. Eds. 1:237-263. Totowa, NJ: Humana Press Inc.

Anchordoquy TJ, Armstrong TK, Molina MDC, Allison SD, Zhang YE, Patel MM, Lentz YK, Koe GS. 2004b. Physical stabilization of plasmid DNA-based therapeutics during freezing and drying. In: Lyophilization of Biopharmaceuticals, Costantino HR, Pikal MJ. Eds., Springer.

Anderson RJ, Schneider J. 2007. Plasmid DNA and viral vector-based vaccines for the treatment of cancer. Vaccine (in press).

Andrieu-Soler C, Bejjani R, de Bizemont T, Normand N, Benezra D, Behar-Cohen F. 2006. Ocular gene therapy: a review of nonviral strategies. Mol. Vis. 12:1334-1347.

Arulmuthu ER, Williams DJ, Baldascini H, Versteeg HK, Hoare M. 2007. Studies on aerosol delivery of plasmid DNA in a mesh nebuliser. Biotechnol. Bioeng. (in press).

Baatz JE, Zou Y, Korfhagen TR. 2001. Inhibitory effects of tumor necrosis factor-[alpha] on cationic lipid-mediated gene delivery to airway cells in vitro.

Biochimica Et Biophysica Acta (BBA) - Molecular Basis of Disease. 1535:100-109.

Banga AK, Prausnitz MR. 1998. Assessing the potential of skin electroporation for the delivery of protein- and gene-based drugs. Trends Biotechnol. 16:408-412.

Baraldo K, Leforestier N, Bureau M, Mignet N, Scherman D. 2002. Sphingosine-based liposome as DNA vector for intramuscular gene delivery. Pharm.Res. 19:1144-1149.

Barrero A, Loscertales IG. 2007. Micro- and nanoparticles via capillary flows. Annu. Rev. Fluid Mech. 39:89-106.

Barry PW. 2002. The future of nebulisation. Respir Care, 47:1459-1469.

Bassett JD, Bright AW. 1976. Observations concerning the mechanism of atomisation in an ultrasonic fountain. Journal of Aerosol Science 7:47-51.

Batchelor GK. 1967. An introduction to fluid dynamics. Cambridge, UK: Cambridge University Press. p79-130

Bensimon D, Simon A, Croquette V, Bensimon A. 1995. Stretching DNA with a receding meniscus: Experiments and models. Phys. Rev. Lett. 74:4754-4757.

Birchall J. 2006. Pulmonary delivery of nucleic acid derived therapies. Journal of Pharmacy and Pharmacology 58:A96-A96.

Bloquel C, Bourges JL, Touchard E, Berdugo M, BenEzra D, Behar-Cohen F. 2006. Non-viral ocular gene therapy: Potential ocular therapeutic avenues. Adv. Drug Del. Rev. 58:1224-1242.

Borras T. 2003. Recent developments in ocular gene therapy. Exp. Eye Res. 76:643-652.

Box GEP, Behnken DW. 1960. Some new three-level designs for the study of quantitative variables. Technometrics. 30:1-40.

Brown M. 2002. Gene therapy trials for cystic fibrosis. Drug Discov. Today. 7:788-789.

Bustamante C, Bryant Z, Smith SB. 2003. Ten years of tension: single-molecule DNA mechanics. Nature 421:423-427.

Bustamante C, Smith SB, Liphardt J, Smith D. 2000. Single-molecule studies of DNA mechanics. Curr. Opinion Structural Biology 10:279-285.

Cao T, Wang XJ, Doop DR. 2000. Regulated cutaneous gene delivery: the skin as a bioreactor. Human Gene Therapy. 11:2297-2300.

Chowdhury EH, Akaike T. 2005. Rapid isolation of high quality, multimeric plasmid DNA using zwitterionic detergent. J Biotechnol. 119:343-347.

Cipolla DC, Gonda I. 1994. Method for collection of nebulized proteins. In Formulation and delivery of proteins and peptides. 355-360.

Coelho-Castelo AAM, Santos Jr RR, Bonato VLD, Jamur MC, Oliver C, Silva CL. 2003. B-Lymphocytes in Bone Marrow or Lymph Nodes Can Take Up Plasmid DNA After Intramuscular Delivery. Human Gene Therapy 14:1279-1285.

Conwell CC, Huang L. 2005. Recent advances in non-viral gene delivery. In: Non-viral vectors for gene therapy. Second ed. Part II. Huang L, Hung M-C, Wagner E. Eds. London, UK:Elsevier Academic Press. 217-230.

Cryan SA, Holohan A, Donohue R, Darcy R, O'Driscoll CM. 2004. Cell transfection with polycationic cyclodextrin vectors. Eur. J. Pharm. Sci. 21:625-633.

Dailey LA, Schmehl T, Gessler T, Wittmar M, Grimminger F, Seeger W, Kissel T. 2003. Nebulization of biodegradable nanoparticles: impact of nebulizer technology and nanoparticle characteristics on aerosol features. J. Controlled Release. 86:131-144.

Dalby R, Suman J. 2003. Inhalation therapy: technological milestones in asthma treatment. Adv. Drug Deliv. Rev. 55:779-791.

Davies JC. 2006. Gene and cell therapy for cystic fibrosis. Pediatric Respiratory Reviews. 7S:S163-165.

Davies LA, Hannavy K, Davies N, Pirrie A, Coffee RA, Hyde SC, Gill DR. 2005. Electrohydrodynamic comminution: A novel technique for the aerosolisation of plasmid DNA. Pharm Res. 22:1294-1304.

Davies LA, Hyde SC, Gill DR. 2005. Plasmid inhalation: delivery to the airways. In: DNA pharmaceuticals: formulation and delivery in gene therapy, DNA vaccination and immunotherapy. Schleef M. Ed. Wiley-VCH Verlag Gmbh & Co. Weinheim.

Davis JC, Alton EWFW. 2005. Airway gene therapy. In: Non-viral vectors for gene therapy. Second ed. Part II. Huang L, Hung M-C, Wagner E. Eds. London, UK:Elsevier Academic Press. 291-314.

Davis ME. 2002. Non-viral gene delivery systems. Curr. Opin. Biotechnol. 13:128-131.

Davis PB, Ziady AG. 2003. Non-viral methods of gene transfer to airway epithelium. Gene Therapy and Regulation 2:77-90.

Davis SS. 2006. The use of soluble polymers and polymer microparticles to provide improved vaccine responses after parenteral and mucosal delivery. Vaccine. 24:S7-S10.

De Smedt SC, Demeester J, Hennink WE. 2000. Cationic polymer based gene delivery systems. Pharm. Res. 17:113-126.

Demeneix B, Behr J-P. 2005. Polyethylenimine (PEI). In: Non-viral vectors for gene therapy. Second ed. Part II. Huang L, Hung M-C, Wagner E. Eds. London, UK:Elsevier Academic Press. 217-230.

Denet A, Vanbever R, Preat V. 2004. Skin electroporation for transdermal and topical delivery. Adv. Drug Deliv. Rev. 56:659-674.

Dennis JH, Pieron CA. 2004. Quality control and standards in nebulizer performance and use. In: Practical handbook of nebulizer therapy. Taylor & Francis Group: London. p19-40.

Dennis JH. 2004. New developments in nebulizer technology. In: Practical handbook of nebulizer therapy. Taylor & Francis Group: London. p41-60.

Densmore CL, Orson FM, Xu B, Kinsey BM, Waldrep JC, Hua P, Bhogal B, Vernon K. 2000. Aerosol delivery of robust polyethyleneimine-DNA complexes for gene therapy and genetic immunization. Molecular Therapy 1:180-188.

Densmore CL. 2003. The re-emergence of aerosol gene delivery: a viable approach to lung cancer therapy. Curr. Cancer Drug Targets 3:275-286.

Deshpande D, Blanchard J, Srinivasan S, Fairbanks D, Fujimoto J, Sawa T, Wiener-Kronish J, Schreier H, Gonda I. 2002. Aerosolization of lipoplexes using AERx pulmonary delivery system. AAPS Pharm Sci. 4:1-10.

Dhand R. 2002. Nebulizers that use a vibrating mesh or plate with multiple apertures to generate aerosol. Respir. Care 47:1406-1410.

Dhand R. 2003. New nebuliser technology – aerosol generation by using a vibrating mesh or plate with multiple apertures. Business Briefings: Long term healthcare strategies. 1-4.

Dobson J. 2006. Gene therapy progress and prospects: Magnetic nanoparticle-based gene delivery. Gene Therapy 13:283-287.

Dobson J. 2007. Toxicological aspects and applications of nanoparticles in paediatric respiratory disease. Paediatr. Respir. Rev. 8:62-66.

Doi M, Edwards SF. 1986. The theory of polymer dynamics. Oxford university press: New York.

Doukas AG, Kollias N. 2004. Transdermal drug delivery with a pressure wave. Adv. Drug Deliv. Rev. 56:559-579.

Dunlap DD, Maggi A, Soria MR, Monaco L. 1997. Nanoscopic structure of DNA condensed for gene delivery. Nucleic Acid Research. 25:3095-3101.

Edwards DA, Caponetti G, Hrkach JS, Lotan N, Hanes J, Ben-Jebria A, Langer RS. 2002. Aerodynamically light particles for pulmonary drug delivery. US Patent 2002141947.

El-Aneed A. 2004. An overview of current delivery systems in cancer gene therapy. J.Controlled Release 94:1-14.

Elhissi AMA, Taylor KMG. 2005. Delivery of liposomes generated from proliposomes using air-jet, ultrasonic and vibrating-mesh nebulisers. J. Drug Deliv. Sci. Tech. 15:261-265.

Elouahabi A, Ruysschaert J. 2005. Formation and Intracellular Trafficking of Lipoplexes and Polyplexes. Molecular Therapy. 11:336-347.

Erbacher P, Zou S, Bettinger T, Steffan A, Remy JE. 1998. Chitosan-Based Vector/DNA Complexes for Gene Delivery: Biophysical Characteristics and Transfection Ability. Pharm. Res. 15:1332-1339.

Ewert K, Ahmad A, Evans HM, Safinya CR. 2005. Cationic lipid-DNA complexes for non-viral gene therapy: relating supramolecular structures to cellular pathways. Exp. Opin. Biol. Ther. 5:33-53.

Fabre JW. 2005. Hydrodynamic gene delivery. In: DNA pharmaceuticals: formulation and delivery in gene therapy, DNA vaccination and immunotherapy. Schleef M. Ed. Wiley-VCH Verlag Gmbh & Co. Weinheim.

Ferrari S, Geddes DM, Alton EWFW. 2002. Barriers to and new approaches for gene therapy and gene delivery in cystic fibrosis. Adv. Drug Deliv. Rev. 54:1373-1393.

Ferreira GNM, Monteiro GA, Prazeres DMF, Cabral JMS. 2000. Downstream processing of plasmid DNA for gene therapy and DNA vaccine applications. Trends Biotechnol. 18:380-388.

Ferreira SLC, Bruns RE, Ferreira HS, Matos GD, David JM, Brandao GC, da Silva EGP, Portugal LA, dos Reis PS, Souza AS, dos Santos WNL. 2007. Box-

Behnken design: an alternative for the optimization of analytical methods. Analytica Chimica Acta. 597:179-186.

Fink TL, Klepcyk PJ, Otte MS, Gedeon CR, Hyatt SL, Kowalczyk TH, Moen RC, Cooper MJ. 2004. Effective transgene expression in the murine lung using compacted nanoparticles formulated with plasmid DNAs of 5, 10, and 20 kbp. Molecular Therapy. 9:S192.

Finlay WH. 2001. The mechanics of inhaled pharmaceutical aerosols: An introduction. Associated Press.

Flament MP, Leterme P, Gayot A. 1999. Influence of the technological parameters of ultrasonic nebulisation on the nebulisation quality of α1 protease inhibitor (α1P1). Int. J. Pharm. 189:197-204.

Forbes B, Ehrhardt C. 2005. Human respiratory epithelial cell culture for drug delivery applications. European Journal of Pharmaceutics and Biopharmaceutics . 60: 193-205.

Forde GM. 2005. Rapid-response vaccines-does DNA offer a solution? Nat. Biotechnol. 23:1059-1062.

Fox RM, Mynderse JF and Goulian, M. 1977. Biochem.16:4470–4480.

Gautam A, Densmore CL, Golunski E, Xu B, Waldrep JC. 2001. Transgene expression in mouse airway epithelium by aerosol gene therapy with PEI-DNA complexes. Molecular Therapy. 3:551-556.

Genc S, Koroglu TF, Genc K. 2004. RNA interference in neuroscience. Mol. Brain Res. 132:260-270.

Georgiou CD, Papapostolou I. 2006. Assay for quantification of intact/fragmented genomic DNA. Anal. Biochem. 358:247-256.

Gersting SW, Schillinger U, Lausier J, Nicklaus P, Rudolph C, Plank C, Reinhardt D, Rosenecker J. 2004. Gene delivery to respiratory epithelial cells by magnetofection. J. Gene Med. 6:913-922.

Gibson TD et al. 1992. Analyst 117:1293-1297.

Gill HS, Prausnitz MR. 2007. Coated microneedles for transdermal delivery. J. Controlled Release. 117:227-237.

Glasspool-Malone J, Somiari S, Drabick JJ, Malone RW. 2000. Efficient Nonviral - Cutaneous Transfection. Molecular Therapy. 2:140-146.

Gregory LG, Harbottle RP, Lawrence L, Knapton HJ, Themis M, Coutelle C. 2003. Enhancement of adenovirus-mediated gene transfer to the airways by DEAE Dextran and Sodium caprate in vivo. Mol. Therapy. 7:19-26.

Han S, Mahato RI, Sung YK, Kim SW. 2000. Development of biomaterials for gene therapy. Mol. Therapy. 2:302-317.

Hanes J, Dawson M, Har-el Y, Suh J, Fiegel J. 2003. Gene delivery in the lung. In Pharmaceutical Inhalation Aerosol Technology, 2nd ed., Hickey AJ Ed. 16:1-51, New York: Marcel Dekker.

Hansma HG, Laney DE. 1996. DNA binding to mica correlates with cationic radius: assay by atomic force microscopy. Biophys. J. 70:1933-1939.

Hellermann G, Mohapatra S. 2003. Genetic therapy: on the brink of a new future. Genetic Vaccines and Therapy 1:1.

Hess DR. 2000. Nebulizers: principles and performance. Respir. Care. 45:609-622.

Hirko A, Tang F, Hughes JA. 2003. Cationic Lipid Vectors for Plasmid DNA Delivery. Curr. Med. Chem. 10:1185-1193.

Hoare M, Levy S, Bracewell DG, Doig SD, Kong S, Titchener-Hooker N, Ward JM, Dunnill P. 2005. Bioprocess engineering issues that would be faced in producing a DNA vaccine at up to 100 m^3 fermentation scale for an influenza pandemic. Biotechnol.Prog. 21:1571-1592.

Hofland HEJ, Sorgi FL, Spack EG. 2004. Development of nonviral DNA delivery systems. In Cellular drug delivery: Principles and practice. Lu DR, Oie S. eds., 67-80. New Jersey: Humana Press Inc.

Howard KA, Li XW, Somavarapu S, Singh J, Green N, Atuah KN, Ozsoy Y, Seymour LW, Alpar HO. 2004. Formulation of a microparticle carrier for oral polyplex-based DNA vaccines. Biochimica Et Biophysica Acta (BBA) - General Subjects. 1674:149-157.

Huth S, Lausier J, Gersting SW, Rudolph C, Plank C, Welsch U, Rosenecker J. 2004. Insights into the mechanism of magnetofection using PEI-based magnetofectins for gene transfer. J. Gene Med. 6:923-936.

Illum L, Jabbal-Gill I, Hinchcliffe M, Fisher AN, Davis SS. 2001. Chitosan as a novel nasal delivery system for vaccines. Adv. Drug Deliv. Rev. 51:81-96.

Jeffs LB, Palmer LR, Ambegia EG, Giesbrecht C, Ewanick S, MacLachlan ERI. 2005. A Scalable, Extrusion-Free Method for Efficient Liposomal Encapsulation of Plasmid DNA. Pharm.Res. 22:362-372.

Joo I, Emod J. 1988. Adjuvant effect of DEAE-dextran on cholera vaccines. Vaccine. 6:233-237.

Kai E, Ochiya T. 2004. A method for oral DNA delivery with N-acetylated chitosan. Pharm. Res. 21:838-843.

Kalia YN, Naik A, Garrison J, Guy RH. 2004. Iontophoretic drug delivery. Adv. Drug Deliv. Rev. 56:619-658.

Kamiya H, Tsuchiya H, Yamazaki J, Harashima H. 2001. Intracellular trafficking and transgene expression of viral and non-viral gene vectors. Adv. Drug Deliv. Rev. 52:153-164.

Kaneda Y, Nakajima T, Nishikawa T, Yamamoto S, Ikegami H, Suzuki N, Nakamura H, Morishita R, Kotani H. 2002. Hemagglutinating virus of Japan (HVJ) envelope vector as a versatile gene delivery system. Molecular Therapy. 6:219-226.

Kaplan, J.M. et al. 1998. Hum Gene Ther 9:1469–1479.

Kawano T, Okuda T, Aoyagi H, Niidome T. 2004. Long circulation of intravenously administered plasmid DNA delivered with dendritic poly(l-lysine) in the blood flow. J.Control.Release. 99:329-337.

Khatri L, Taylor KMG, Craig DQM, Palin K. 2001. An assessment of jet and ultrasonic nebulisers for the delivery of lactate dehydrogenase solutions. Int. J. Pharm. 227:121-131.

Kichler A, Chillon M, Leborgne C, Danos O, Frisch B. 2002. Intranasal gene delivery with a polyethylenimine-PEG conjugate. J.Controlled Release. 81:379-388.

Kichler A. 2004. Gene transfer with modified polyethylenimines. J. Gene Med. 6:S3-S10.

Kinsey BM, Densmore CL, Orson FM. 2005. Non-Viral Gene Delivery to the Lungs. Current Gene Therapy 5:181-194.

Kircheis R, Wightman L, Wagner E. 2001. Design and gene delivery activity of modified polyethylenimines. Adv. Drug Deliv. Rev. 53:341-358.

Kishida M, Okada M, Izawa M, Shimoda M, Saito M, Takeshita Y, Koshibu T, Nakazono H, Suzuki I, Shinomiya N, Aoki T. 2003. Clinical examination of miniature mesh nebuliser MicroAIR®, Allergology and Immunology, Vol. 10, pp. 136-140

Kleemann E, Dailey LA, Abdelhady HG, Gessler T, Schmehl T, Roberts CJ, Davies MC, Seeger W, Kissel T. 2004. Modified polyethylenimines as non-viral gene delivery systems for aerosol gene therapy: investigations of the complex structure and stability during air-jet and ultrasonic nebulization. J Controlled Release 100:437-450.

Klink D, Schindelhauer D, Laner A, Tucker T, Bebok Z, Schwiebert EM, Boyd AC, Scholte BJ. 2004. Gene delivery systems--gene therapy vectors for cystic fibrosis. Journal of Cystic Fibrosis. 3:203-212.

Knight JD, Adami RC. 2003. Stabilization of DNA utilizing divalent cations and alcohol. Int.J.Pharm. 264:15-24.

Knoch M, Keller M. 2005. The customised electronic nebuliser: a new category of liquid aerosol drug delivery systems. Expert Opin. Drug Deliv. 2:377-390.

Kobayashi N, Kuramoto T, Chen S, Watanabe Y, Takakura Y. 2002. Therapeutic Effect of Intravenous Interferon Gene Delivery with Naked Plasmid DNA in Murine Metastasis Models. Molecular Therapy, 6:737-744.

Kobayashi N, Nishikawa M, Takakura Y. 2005. The hydrodynamics-based procedure for controlling the pharmacokinetics of gene medicines at whole body, organ and cellular levels. Adv. Drug Deliv.Rev. 57:713-731.

Kohli AK, Alpar HO. 2004. Potential use of nanoparticles for transcutaneous vaccine delivery: effect of particle size and charge. Int. J. Pharm. 275:13-17.

Kong S, Titchener-Hooker N, Levy MS. 2006. Plasmid DNA processing for gene therapy and vaccination: Studies on the membrane sterilisation filtration step. Journal of Membrane Science 280:824-831.

Konrad MW, Bolonick JI. 1996. Molecular dynamics simulation of DNA stretching is consistent with the tension observed for extension and strand separation and predicts a novel ladder structure. J Am Chem Soc. 118:10989-10994.

Koping-Hoggard M, Issa MM, Kohler T, Varum KM, Artursson P. 2005. A miniaturized nebulisation catheter for improved gene delivery to the mouse lung. J Gene Med 7:1215-1222.

Langer R. 2004. Transdermal drug delivery: past progress, current status, and future prospects. Adv. Drug Deliv. Rev. 56:557-558.

Larson RG, Magda JJ. 1989. Coil-stretch transition in mixed shear and extensional flows of dilute polymer solutions. Macromolecules. 22:3004-3010.

Larson RG. 1999. The structure and rheology of complex fluids. Oxford University Press, New York.

Lasic DD. 2000. Liposomes in gene delivery. CRC Press, Boca Raton, Florida.

Lavery R, Lebrun A, Allemand J, Bensimon D, Croquette V. 2002. Structure and mechanics of single biomolecules: experiment and simulation. J. Phys.: Condens. Matter 14:R383-R414.

Lavon I, Kost J. 2004. Ultrasound and transdermal drug delivery. Drug Discov. Today. 9:670-676.

Le Brun PPH, de Boer AH, Heijerman HGM, Frijlink HW. 2000. A review of the technical aspects of drug nebulization. Pharm. World Sci. 22:75–81.

Lebrun A, Lavery R. 1996. Modelling extreme stretching of DNA. Nucleic Acids Research 24:2260-2267.

Lechardeur D, Verkman AS, Lukacs GL. 2005. Intracellular routing of plasmid DNA during non-viral gene transfer. Adv. Drug Deliv. Rev. 57:755-767.

Lee M, Kim SW. 2005. Polyethylene glycol-conjugated copolymers for plasmid DNA delivery. Pharm. Res. 22:1-10.

Lee TWR, Mathews DA, Blair GE. 2005. Novel molecular approaches for cystic fibrosis gene therapy. Biochem. J. 387:1-15

Lengsfeld CS, Anchordoquy TJ. 2002. Shear-induced degradation of plasmid DNA. J Pharm Sci. 91:1581-1589.

Lentz YK, Anchordoquy TJ, Lengsfeld CS. 2006a. DNA acts as a nucleation site for transient cavitation in the ultrasonic nebuliser. J Pharm Sci. 95:607-619.

Lentz YK, Anchordoquy TJ, Lengsfeld CS. 2006b. Rational for selection of an aerosol delivery system for gene delivery. J Aerosol Medicine 19:372-384.

Lentz YK, Worden LR, Anchordoquy TJ, Lengsfeld CS. 2005. Effect of jet nebulization on DNA: identifying the dominant degradation mechanism and mitigation methods. J Aerosol Sci. 36:973-990.

Levy MS, Ciccolini LAS, Yim SSS, Tsai JT, Titchener-Hooker N, Ayazi Shamlou, Dunnill P. 1999a. The effect of material properties and fluid flow intensity on plasmid DNA recovery during cell lysis. Chem. Eng. Sci. 54:3171-3178.

Levy MS, Collins IJ, Tsai JT, Ayazi Shamlou P, Ward JM, Dunnill P. 2000a. Removal of contaminant nucleic acids by nitrocellulose filtration during pharmaceutical-grade plasmid DNA processing. J.Biotechnol. 76:197-205.

Levy MS, Collins IJ, Yim SS, Ward JM, Titchener-Hooker N, Ayazi Shamlou P, Dunnill P. 1999. Effect of shear on plasmid DNA in solution. Bioprocess Eng 20:7-13.

Levy MS, Lotfian R, O'Kennedy RD, Lo-Yim MY, Ayazi-Shamlou P. 2000b. Quantitation of supercoiled circular content in plasmid DNA solutions using a fluorescence-based method. Nucleic Acids Research. 28:e57.

Levy MS, O'Kennedy RD, Ayazi-Shamlou P, Dunnill P. 2000c. Biochemical engineering approaches to the challenges of producing pure plasmid DNA. Trends Biotechnol. 18:296-305.

Li AF, Escher A. 2003. Intradermal or Oral Delivery of GAD-Encoding Genetic Vaccines Suppresses Type 1 Diabetes. DNA Cell Biol. 22:227-232.

Liaw J, Chang SF, Hsiao FC. 2001. In vivo gene delivery into ocular tissues by eye drops of poly(ethylene oxide)-poly(propylene oxide)-poly(ethylene oxide) (PEO-PPO-PEO) polymeric micelles. Gene Therapy. 8:999-1004.

Liu F, Tyagi P. 2005. Naked DNA for liver gene transfer. In: Non-viral vectors for gene therapy. Second ed. Part II. Huang L, Hung M-C, Wagner E. Eds. London, UK:Elsevier Academic Press. 217-230.

Liu MA, Ulmer JB. 2005. Human clinical trials of plasmid DNA vaccines. Advances in Genetics. 55:25-40.

Luo D, Saltzman WM. 2000. Synthetic DNA Delivery Systems. Nat. Biotechnol. 18:33-37.

Luo D. 2004. A new solution for improving gene delivery. Trends Biotechnol. 22:101-103.

Lyubchenko Y, Shylakhtenko LS. 1997. Visualization of supercoiled DNA with atomic force microscopy *in situ.* Proc. Natl. Acad. Sci. USA 94:496-501.

MacColl G, Bunn C, Goldspink G, Bouloux P, Gorecki DC. 2001. Intramuscular plasmid DNA injection can accelerate autoimmune responses. Gene Therapy. 8:1354-1356.

Mack KD, Wei R, Elbagarri A, Abbey N, McGrath MS. 1998. A novel method for DEAE-dextran mediated transfection of adherent primary cultured human macrophages. J Immunological Methods 211:79-86.

Mahato RI, Smith LC, Rolland A. 1999. Pharmaceutical perspectives of nonviral gene therapy. Adv. Genetics. 41:95-156.

Mahato RI. 2005. Water insoluble and soluble lipids for gene delivery. Adv. Drug Deliv. Rev. 57:699-712.

Mandal TK. 2005. Inhaled insulin for diabetes mellitus. Am J Health-Syst Pharm. 62:1359-1364.

Martendal E, Budziak D, Carasek E. 2007. Application of fractional factorial experimental and Box-Behnken designs for optimization of single-drop microextraction of 2,4,6-trichloroanisole and 2,4,6-tribromoanisole from wine samples. J. Chromatogr. A. 1148:131-136.

Martin B, Sainlos M, Aissaoui A, Oudrhiri N, Hauchecorne M, Vigneron JP, Lehn JM, Lehn P. 2005. The design of cationic lipids for gene delivery. Curr. Pharm. Design. 11:375-394.

Mason RL, Gunst RF, Hess JL. 2003. Statistical design and analysis of experiments: With applications to engineering and science. John Wiley & Sons: New York.

McLachlan G, Baker A, Tennant P, Gordon C, Vrettou C, Renwick L, Blundell R, Cheng SH, Scheule RK, Davies L, Painter H, Coles RL, Lawton AE, Marriott C, Gill DR, Hyde SC, Griensenbach U, Alton EWFW, Boyd AC, Porteous DJ,

Collie DDS. 2007. Optimizing aerosol gene delivery and expression in the ovine lung. Molecular Therapy 15:348-354.

Meachem JM, Varady MJ, Degertekin FL, Fedorov AG. 2005. Droplet formation and ejection from a micromachined ultrasonic droplet generator: visualization and scaling. Phys. Fluids 17:100605-12.

Meacle FJ, Zhang H, Papantoniou I, Ward JM, Titchener-Hooker NJ, Hoare M. 2006. Degradation of supercoiled plasmid DNA within a capillary device. Biotechnol. Bioeng. 97:1148-1157.

Meyers RH, Montgomery DC. 2002. Response surface methodology: process and product optimization using designed experiments. John Wiley & Sons: New York.

Mikszta JA, Alarcon JB, Brittingham JM, Sutter DE, Pettis RJ, Harvey NG. 2002. Improved genetic immunization via micromechanical disruption of skin-barrier function and targeted epidermal delivery. Nature Medicine. 8:415-419.

Mishra S, Webster P, Davis ME. 2004. PEGylation significantly affects cellular uptake and intracellular trafficking of non-viral gene delivery particles. Eur. J. Cell Biol. 83:97-111.

Mitragotri S, Kost J. 2004. Low-frequency sonophoresis: A review. Adv. Drug Deliv. Rev. 56:589-601.

Montier T, Delepine P, Pichon C, Ferec C, Porteous DJ, Midoux P. 2004. Non-viral vectors in cystic fibrosis gene therapy: progress and challenges. Trends Biotechnol. 22:586-592.

Moraes TJ, Downey GP. 2004. Cystic fibrosis: potential options for gene-directed therapies. Drug Discovery Today: Therapeutic Strategies. 1:345-349.

Mountain A. 2000. Gene therapy: the first decade. Trends Biotechnol 18:119-128.

Munier S, Messai I, Delair T, Verrier B, Ataman-Onal Y. 2005. Cationic PLGA nanoparticles for DNA delivery: comparison of three surface polycations for

DNA binding, protection and transfection properties. Colloids and Surfaces B: Biointerfaces. 43:163-173.

Munkonge FM, Dean DA, Hillery E, Griesenbach U, Alton EWFW. 2003. Emerging significance of plasmid DNA nuclear import in gene therapy. Adv. Drug Deliv. Rev. 55:749-760.

Murakami M, Hirokawa H, Hayata I. 2000. Analysis of radiation damage of DNA by atomic force microscopy in comparison with agarose gel electrophoresis studies. J Biochem Biophys Methods 44:31-40.

Nagasaki T, Kawazu T, Tachibana T, Tamagaki S, Shinkai S. 2005. Enhanced nuclear import and transfection efficiency of plasmid DNA using streptavidin-fused importin-[beta]. J. Controlled Release. 103:199-207.

Newman S, Gee-Turner A. 2005. The Omron MicroAir vibrating mesh technology nebuliser, a 21st century approach to inhalation therapy. J. Appl. Therapeutic Res. 5:29-33.

Nishikawa M, Takakura Y, Hashida M. 2005. Theoretical considerations involving the pharmacokinetics of plasmid DNA. Adv. Drug Deliv. Rev. 57:675-688.

Niven RW, Ip AY, Mittelman S, Prestrelski SJ, Arakawa T. 1995. Some factors associated with the ultrasonic nebulization of proteins. Pharm. Res. 12:53-59.

Odell JA, Keller A, Rabin Y. 1988. Flow-induced scission of isolated macromolecules. J. Chem. Phys. 88: 4022–4028.

Oliver MJ, McKenzie L, Pritchard Y. 2001. Evaluation of pressurised metered dose inhalers for pulmonary delivery of proteins and peptides. J. Aerosol Med. 14:394.

Orive G, Hernandez RM, Gascon AR, Dominguez-Gil A, Pedraz JL. 2003. Drug delivery in biotechnology: present and future. Curr. Opin. Biotechnol. 14:659-664.

Page DT, Cudmore S. Innovations in oral gene delivery: challenges and potentials. Drug Discov. Today. 6:92-101.

Pardridge WM. 2004. Intravenous, non-viral RNAi gene therapy of brain cancer. Expert Opin. Biol. Ther. 4:1103-1113.

Perrie Y, Barralet JE, McNeil S, Vangala A. 2004. Surfactant vesicle-mediated delivery of DNA vaccines via the subcutaneous route. Int.J.Pharm. 284:31-41.

Pilewski JM. 2002. Gene therapy for airway diseases: continued progress toward identifying and overcoming barriers to efficiency. Am. J. Respir. Cell Mol. Biol. 27:117-121.

Pillai R, Petrak K, Blezinger P, Deshpande D, Florack V, Freimark B, Padmabandu G, Rolland A. 1998. Ultrasonic nebulization of cationic lipid-based gene delivery systems for airway administration. Pharmaceutical Research 15:1743-1747.

Pleyer U, Ritter T. 2003. Gene therapy in immune-mediated diseases of the eye. Prog. Retin. Eye Res. 22:277-293.

Podesta A, Imperadori L, Colnaghi W, Finzi L, Milani P, Dunlap D. 2004. Atomic force microscopy study of DNA deposited on poly L-ornithine-coated mica. J Microscopy. 215:236–240.

Pouton CW, Seymour LW. 2001. Key issues in non-viral gene delivery. Adv. Drug Deliv. Rev. 46:187-203.

Pouton CW. 1999. Biological barriers to gene transfer. In: Advanced gene delivery: from concepts to pharmaceutical products. Rolland A Ed. Harwood Academic Publ.:Singapore.

Prather KJ, Sagar S, Murphy J, Chartrain M. 2003. Industrial scale production of plasmid DNA for vaccine and gene therapy: plasmid design, production, and purification. Enzyme Microb. Technol. 33:865-883.

Prausnitz MR. 2004. Microneedles for transdermal drug delivery. Adv. Drug Deliv. Rev. 56:581-587.

Prazeres DMF, Ferreira GNM. 2004. Design of flowsheets for the recovery and purification of plasmids for gene therapy and DNA vaccination. Chem. Eng. Proc. 43:615-630.

Qiagen. 2004. Qiaprep Miniprep Handbook. West Sussex, UK: Qiagen Ltd.

Ragonese R, Macka M, Hughes J, Petocz P. 2002. The use of the Box-Behnken experimental design in the optimisation and robustness testing of a capillary electrophoresis method for the analysis of ethambutol hydrochloride in a pharmaceutical formulation. J. Pharm. Biomed. Anal. 27:995-1007.

Resse HR, Zimm BH. 1990. Fracture of polymer chains in extensional flow: experiments with DNA and a molecular-dynamics simulation. J. Chem. Phys. 92:2650-2662.

Richardson SCW, Kolbe HVJ, Duncan R. 1999. Potential of low molecular mass chitosan as a DNA delivery system: biocompatibility, body distribution and ability to complex and protect DNA. Int. J. Pharm. 178:231-243.

Rigby, P. 1969, Nature, vol. 221, pp. 968-970.

Robinson BWS, Erle DJ, Jones DA, Shapiro S, Metzger WJ, Albelda SM, Parks WC, Boylan A. 2005. Recent advances in molecular biological techniques and their relevance to pulmonary research. Thorax 55:329-339.

Rochat T, Morris MA. 2002. Gene Therapy for Cystic Fibrosis by Means of Aerosol. Journal of Aerosol Medicine. 15:229-235.

Rock C, Shamlou PA, Levy MS. 2003. An automated microplate-based method for monitoring DNA strand breaks in plasmids and bacterial artificial chromosomes. Nucleic Acids Res. 31:e65.

Rolland A. 2005. Gene medicines: The end of the beginning? Adv. Drug Deliv. Rev. 57:669-673.

Rots MG, Curiel DT, Gerritsen WR, Haisma HJ. 2003. Targeted cancer gene therapy: the flexibility of adenoviral gene therapy vectors. J.Controlled Release. 87:159-165.

Rubanyi GM. 2001. The future of human gene therapy. Mol. Aspects Med. 22:113-142.

Rudolph C, Ortiz A, Schillinger U, Jauernig J, Plank C, Rosenecker J. 2005. Methodological optimization of polyethylenimine (PEI)-based gene delivery to the lungs of mice via aerosol application. J. Gene Med. 7:59-66.

Ryskin G. 1987. Calculation of the effect of polymer additive in a converging flow. J Fluid Mech. 178:423-440.

Schleef M, Schmidt T. 2004. Animal-free production of ccc-supercoiled plasmids for research and clinical applications. J Gene Med. 6:S45-S53.

Schleef M. (ed). 2005. DNA pharmaceuticals: formulation and delivery in gene therapy, DNA vaccination and immunotherapy. Wiley-VCH Verlag Gmbh & Co. Weinheim

Schmidt-Wolf GD, Schmidt-Wolf IGH. 2003. Non-viral and hybrid vectors in human gene therapy: an update. Trends Mol. Med. 9:67-72.

Schmieder AH, Grabski LE, Moore NM, Dempsey LA, Sakiyama-Elbert SE. 2007. Development of novel poly(ethylene glycol)-based vehicles for gene delivery. Biotechnol. Bioeng. 96:967-976.

Shrewsbury PJ, Muller SJ, Liepmann D. 2001. Effect of flow on complex biological macromolecules in microfluidic devices. Biomedical Microdevices. 3:225-238.

Shroff KE, Marcucci-Borges LA, de Bruin SJ, Winter LA, Tiberio L, Pachuk C, Snyder LA, Satishchandran C, Ciccarelli RB, Higgins TJ. 1999. Induction of HSV-gD2 specific CD4+ cells in Peyer's patches and mucosal antibody responses in mice following DNA immunization by both parenteral and mucosal administration. Vaccine 18:222-230.

Singer VL, Jones LJ, Ye ST, Haugland RP. 1997. Characterization of PicoGreen reagent and development of a fluorescence-based solution assay for double-stranded DNA quantitation. Anal. Biochem. 249:228-238.

Smart J, Stangl R, Frtiz E. 2002. Touchspray Technology: A preliminary in vitro evaluation of plasmid DNA of different size and topology. Proc. Respiratory Drug Delivery VIII. I: 529-531.

Sminia T, Kraal G. 1999. Nasal-associated lymphoid tissue. In: Mucosal Immunology. Ogra PL, Mestecky J, Lamm ME, Strober W, Bienenstock J, McGhee JR. Eds. 2nd ed. 1:357-364. San Diego: Academic Press.

Smith IJ, Parry-Billings M. 2003. The Inhalers of the Future? A Review of Dry Powder Devices on the Market Today. Pulm. Pharmacol. Ther. 16:79-95.

Spack EG, Sorgi FL. 2001. Developing non-viral DNA delivery systems for cancer and infectious disease. Drug Discov. Today. 6:186-197.

Stechschulte SU, Joussen AM, von Recum HA, Poulaki V, Moromizato Y, Yuan J, D'Amato RJ, Kuo C, Adamis AP. 2001. Rapid ocular angiogenic control via naked DNA delivery to cornea. Invest. Ophthalmol. Vis. Sci. 42:1975-1979.

Stribling R, Brunette E, Liggitt D, Gaensler K, Debs R. 1992. Aerosol gene delivery *in vivo*. Proc. Natl. Acad. Sci. 89:11277-11281.

Sullivan VJ, Mikszta JA, Laurent P, Huang J, Ford B. 2006. Noninvasive delivery technologies: respiratory delivery of vaccines. Expert Opin. Drug Deliv. 3:87-95.

Tachibana R, Harashima H, Ide N, Ukitsu S, Ohta Y, Suzuki N, Kikuchi H, Shinohara Y, Kiwada H. 2002. Quantitative analysis of correlation between number of plasmids and gene expression activity after transfection with cationic liposomes. Pharm. Res. 19:377-381.

Tachibana R, Harashima H, Shinohara Y, Kiwada H. 2001. Quantitative studies on the nuclear transport of plasmid DNA and gene expression employing nonviral vectors. Adv. Drug Deliv. Rev. 52:219-226.

Tait AS, Brown CJ, Galbraith DJ, Hines MJ. Hoare M, Birch JR, James DC. 2004. Transient production of recombinant proteins by Chinese hamster ovary cells using polyethyleneimine/DNA complexes in combination with microtubule disrupting anti-mitotic agents. Biotechnol. Bioeng. 88:707-721.

Tait AS. 2006. PEI-mediated transient gene expression in cell culture for the rapid production of therapeutic proteins. PhD thesis. UCL, London.

Takamura S, Niikura M, Li T-, Takeda N, Kusagawa S, Takebe Y, Miyamura T, Yasutomi Y. 2004. DNA vaccine-encapsulated virus-like particles derived from an orally transmissible virus stimulate mucosal and systemic immune responses by oral administration. Gene Therapy. 11:628-635.

Tanaka S-, Yamakawa T, Kimura M, Aoki I, Kamei J, Okuda K, Mobbs C. 2004. Daily nasal inoculation with the insulin gene ameliorates diabetes in mice. Diabetes Res. Clin. Pract. 63:1-9.

Taylor G, Gumbleton M. 2004. Aerosols for macromolecule delivery: design challenges and solutions. Am. J. Drug Deliv. 2:143-155.

Taylor GI. 1964. Disintegration of water drops in an electric field. Proc. R. Soc. A 280:383-397.

Taylor KMG, McCallion ONM. 1997. Ultrasonic nebulizers for pulmonary drug delivery. Int. J. Pharm. 153:93-104.

Thomas M, Ge Q, Lu JJ, Chen J, Klibanov A. 2005. Cross-linked small polyethylenimines: while still nontoxic, deliver DNA efficiently to mammalian cells *in vitro* and *in vivo*. Pharm. Res. 22:373-380.

Thorstenson Y, Hunicke-Smith S, Oefner P, Davis R. 1998. An automated hydrodynamic process for controlled, unbiased DNA shearing. Genome Research 8:848-855.

Topp MN. 1973. Ultrasonic atomization – A photographic study of the mechanism of disintegration. Journal of Aerosol Science 4:17-25.

Tuschl T, Borkhardt A. 2002. Small Interfering RNAs: A Revolutionary Tool for the Analysis of Gene Function and Gene Therapy. Mol. Interv. 2:158-167.

Vadolas J, Williamson R, Ioannou PA. 2002. Gene Therapy for Inherited Lung Disorders: An Insight into Pulmonary Defence. Pulm. Pharmacol. Ther., 15:61-72.

Valenta C, Auner BG. 2004. The use of polymers for dermal and transdermal delivery. European Journal of Pharmaceutics and Biopharmaceutics. 58:279-289.

Valle F, Favre M, Rios PDL, Rosa A, Dietler G. 2005. Scaling exponents and probability distributions of DNA end-to-end distance. Phys. Rev. Lett. 95:158105-1-4.

Versteeg HK, Hargrave GK, Hind RJA. 2005. An optical study of aerosol generation in dry powder inhalers. Proc. Drug Delivery to the Lungs 16, 3-6.

Versteeg HK, Malalasekera W. 1995. An introduction to computational fluid dynamics: The finite volume method. London:Longman Scientific and Technical.

Voβ C, Schmidt T, Schleef M, Friehs K, Flaschel E. 2003. Production of supercoiled plasmid DNA for biopharmaceutical application. J Biotechnol. 105:205-213.

Wahlung PO, Gustavsson PE, Izumrudov VA, Larsson PO, Galaev IY. 2004. Precipitation of polycation as a capture step in purification of plasmid DNA from a clarified lysate. Biotechnol Bioeng. 87:675-684.

Wang S, Ma N, Gao SJ, Yu H, Leong KW. 2001. Transgene expression in the brain stem effected by intramuscular injection of polyethylenimine/DNA complexes. Molecular Therapy. 3:658-664.

Webb AK, Dodd ME, Bush A. 2004. Nebulised antibiotics in cystic fibrosis and non-CF bronchiectasis in children and adults. In: Practical handbook of nebulizer therapy. Taylor & Francis Group: London. p115-136.

Wells DJ. 2004. Gene therapy progress and prospects: Electroporation and other physical methods. Gene Therapy. 11:1363-1369.

Welsh MJ, Fasbender AJ. 1999. Complexes of adenovirus with cationic molecules. US Patent 5962429.

Williams LJ. 2007. Novel pulmonary delivery technology. Pharma Mag. Jan/Feb p4.

Wolff J. 2005. Nonviral vectorology: in a good place. Molecular Therapy. 11:333-333.

Wolff JA, Williams P, Acsadi G, Jiao S, Jani A, Chong W. 1991. Conditions affecting direct gene transfer into rodent muscle *in vivo*. Biotechniques. 11:474-485.

Wong PK, Lee Y, Ho C. 2003. Deformation of DNA molecules by hydrodynamic focusing. J. Fluid Mechanics. 497:55-65.

Xenariou S, Griesenbach U, Ferrari S, Dean P, Scheule R, Cheng S, Geddes D, Plank C, Alton E. 2004. Magnetofection to enhance airway gene transfer. Molecular Therapy. 9:S180.

Yamamoto H, Asai K. 2004. Ultrasonic atomizer, ultrasonic inhaler and method of controlling same. Patent US2004045547.

Yule AJ, Al-Suleimani Y. 2000. On droplet formation from capillary waves on a vibrating surface. Proc. Royal Soc. Lond. A. 456:1069-1085.

Zelphati O, Felgner J, Wang Y, Liang X, Wang X, Felgner PER. 2003. Medicinal chemistry of plasmid DNA with peptide nucleic acids: A new strategy for gene therapy. Lett. Peptide Sci. 10:309-323.

Zhang Y, Finlay WH, Matida EA. 2004. Particle deposition measurements and numerical simulation in a highly idealized mouth-throat. J Aerosol Sci 35:789-803.

Zhang Y, Schlachetzki F, Li JY, Boado RJ, Pardridge WM. 2003. Organ-specific gene expression in the rhesus monkey eye following intravenous non-viral gene transfer. Mol. Vis. 9:465-472.

Zidan AS, Sammour OA, Hammad MA, Megrab NA, Habib MJ, Khan MA. 2007. Quality by design: understanding the formulation variables of a cyclosporine A self-nanoemulsified drug delivery systems by Box-Behnken design and desirability function. Int. J. Pharm. 332:55-63.

Zimlich WC, Dvorsky JE, Busick DR, Peters RD. 2002. Pulmonary aerosol delivery device and method. US Patent 2002153006.

Zimm BH, Resse HR. 1990. The degradation of T7 DNA in converging flow. Nucleic Acids Research. 18:4469-4470.

Publications

Conference Attendance and Presentations

- Poster presentation at Medilink East Midlands Healthcare Innovation Day, Nottingham, UK, May 2005
- Poster presentation at Drug Delivery to the Lungs 16 (DDL 16), Edinburgh, UK, December 2005
- Podium presentation at Respiratory Drug Delivery X (RDD X), Florida, USA, April 2006
- Drug Delivery to the Lungs 17 (DDL 17), Edinburgh, UK, December 2006
- BioProcess UK, Edinburgh, UK, December 2006.

References

Arulmuthu ER, Williams DJ, Baldascini H, Versteeg HK, Hoare M. 2007. Studies on aerosol delivery of plasmid DNA in a mesh nebuliser. Biotechnol. Bioeng. 98:939-955.

Arulmuthu ER, Versteeg HK, Williams DJ, Tait A, Hoare M. 2007. Plasmid DNA nebulisation for gene delivery to the lungs. Proc. Drug Delivery to the Lungs 18.

Arulmuthu ER, Versteeg HK, Williams DJ, Baldascini H, Hoare M. 2005. Mechanics of plasmid damage in a mesh nebuliser. Proc. Drug Delivery to the Lungs 16. 89-92.

Arulmuthu ER, Versteeg HK, Baldascini H, Khoo YC, Hoare M, Williams DJ. 2006. Plasmid DNA damage in a mesh nebuliser – an initial high-speed imaging study. Proc. Respiratory Drug Delivery X. 3:671-674.

Arulmuthu ER, Versteeg HK, Williams DJ. Strategies for delivery of non-viral plasmid DNA based gene therapy (in revision for IEEE-EMBS magazine).

APPENDIX

Repeatability of gel electrophoresis experiments on the nebulisation of 5.7 kb plasmid

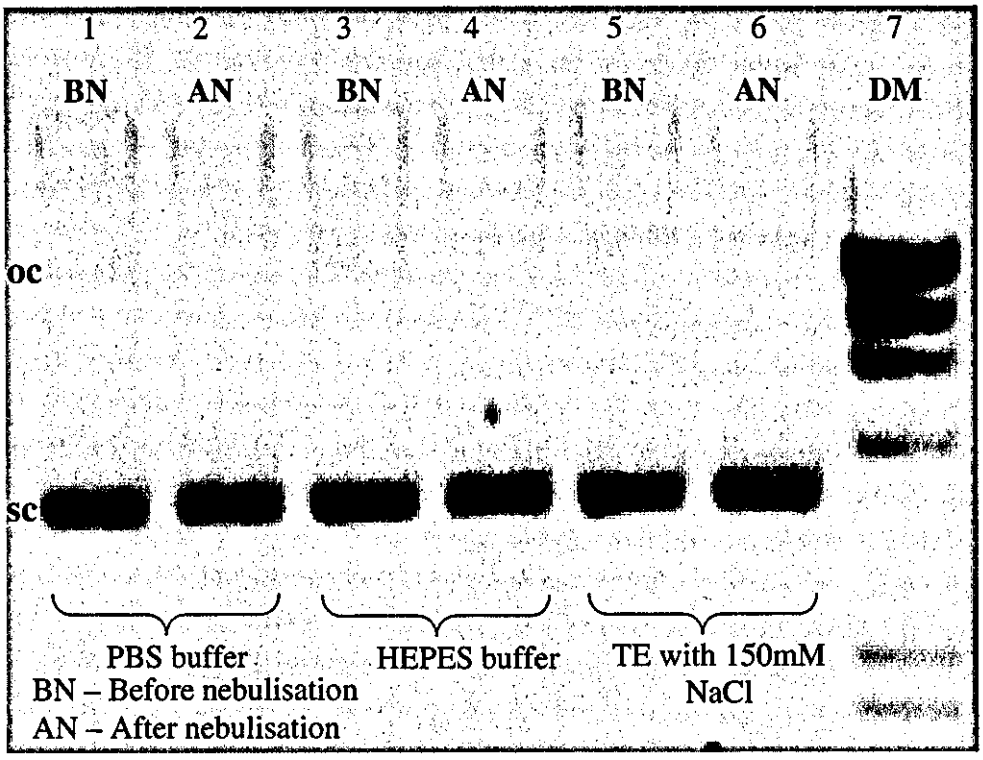

Figure A.1: Agarose gel electrophoresis of nebulisation of 5.7 kb plasmid in buffers showing the supercoiled (sc) and open-circular (oc) forms of the plasmid: lanes 1 and 2: BN and AN samples in PBS buffer; lanes 3 and 4: BN and AN samples in HEPES buffer; lanes 5 and 6: BN and AN samples in TE buffer with 150 mM NaCl; lanes 7 – DNA marker.

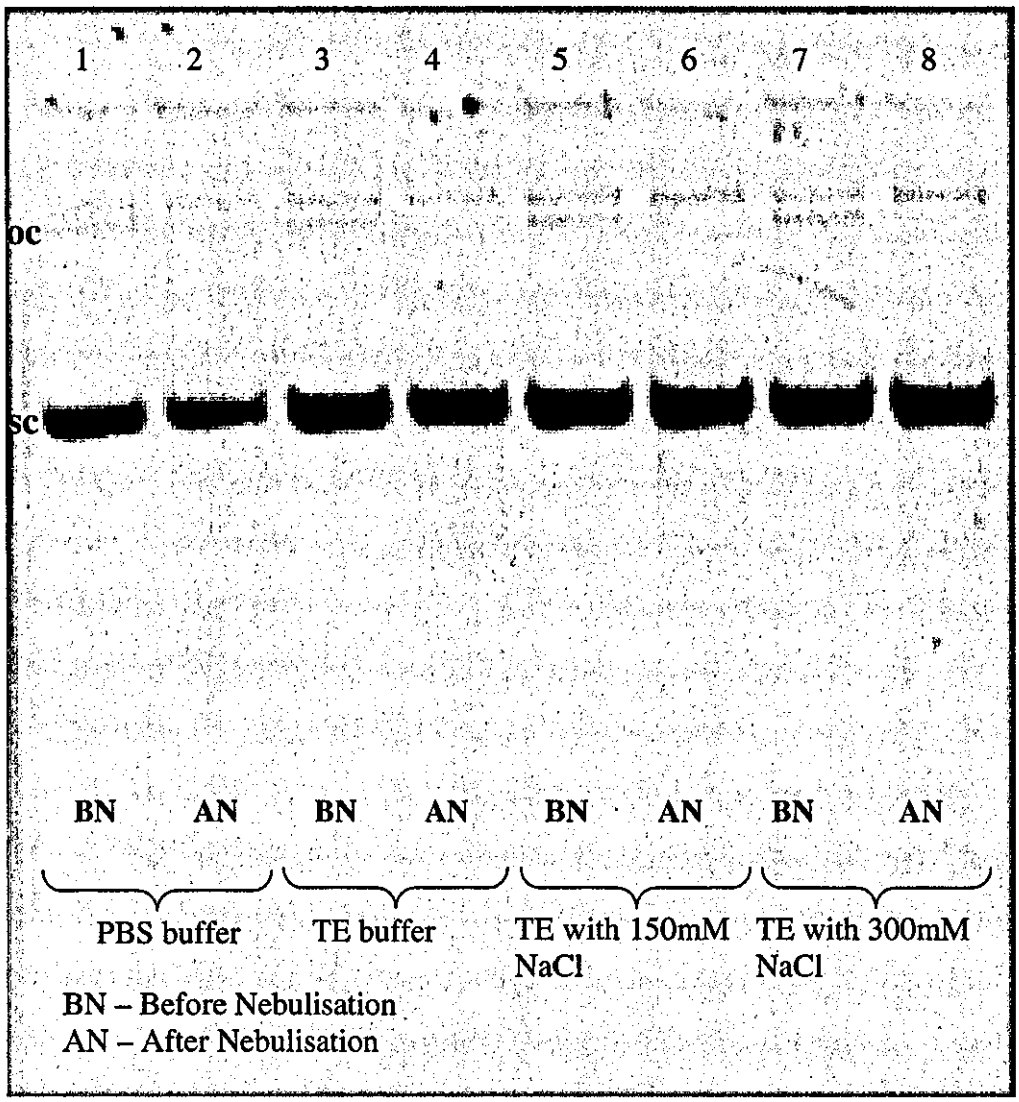

Figure A.2: Agarose gel electrophoresis of nebulisation of 5.7 kb plasmid in buffers showing the supercoiled (sc) and open-circular (oc) forms of the plasmid: a) PBS buffer; lanes 1 and 2: BN and AN samples in PBS buffer; lanes 3 and 4: BN and AN samples in TE buffer; lanes 5 and 6: BN and AN samples in TE buffer with 150 mM NaCl; lanes 7 and 8: BN and AN samples in TE buffer with 300 mM NaCl.

Repeatability of gel electrophoresis experiments on the nebulisation of 8.7 kb plasmid

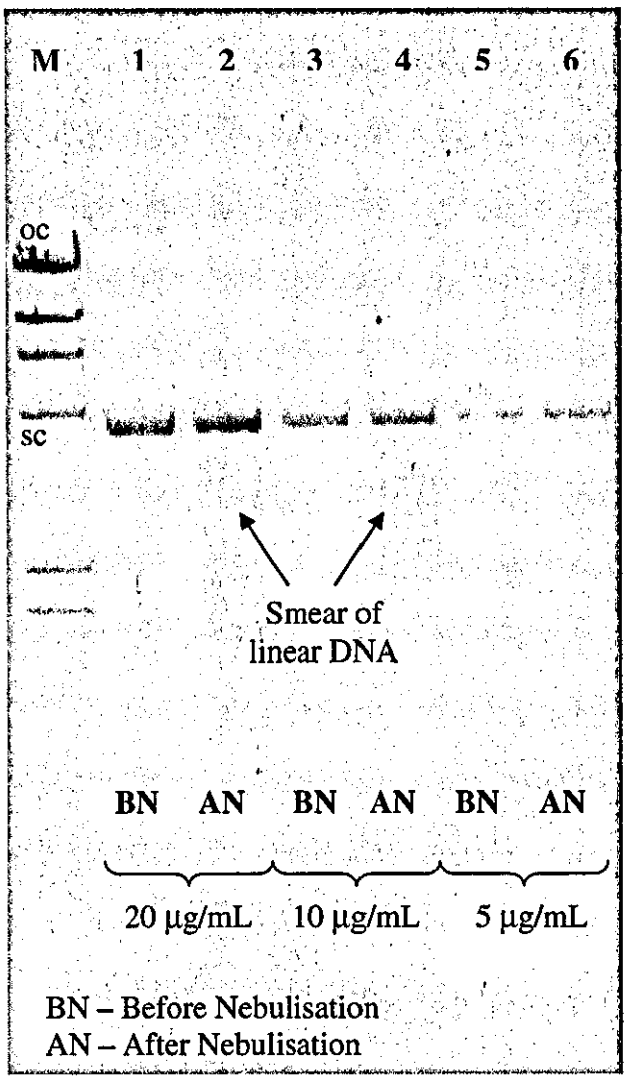

Figure A.3: Agarose gel electrophoresis of nebulisation of 5.7 kb plasmid in TE buffer showing the supercoiled (sc) and open-circular (oc) forms of the plasmid: lanes 1 – DNA Marker; lanes 2 and 3: BN and AN samples with 20 µg/mL DNA concentration; lanes 4 and 5: BN and AN samples with 10 µg/mL DNA concentration; lanes 6 and 7: BN and AN samples with 5 µg/mL µg/mL DNA concentration.

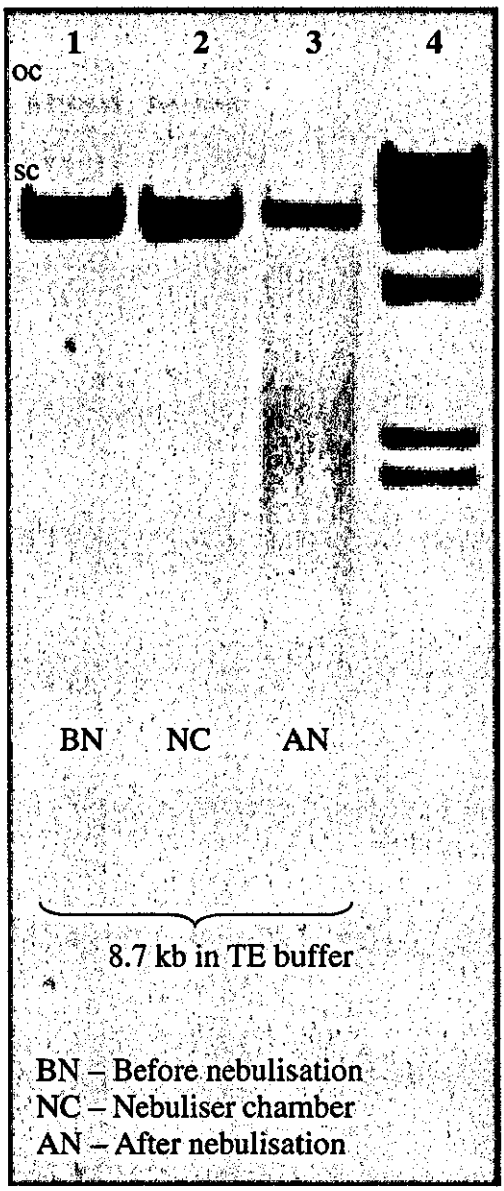

Figure A.4: Agarose gel electrophoresis of nebulisation of 8.7 kb plasmid in TE buffer showing the supercoiled (sc) and open-circular (oc) forms of the plasmid: lanes 1 – BN; 2 – NC; 3 – AN samples; 4 – Lamba HindIII DNA marker.

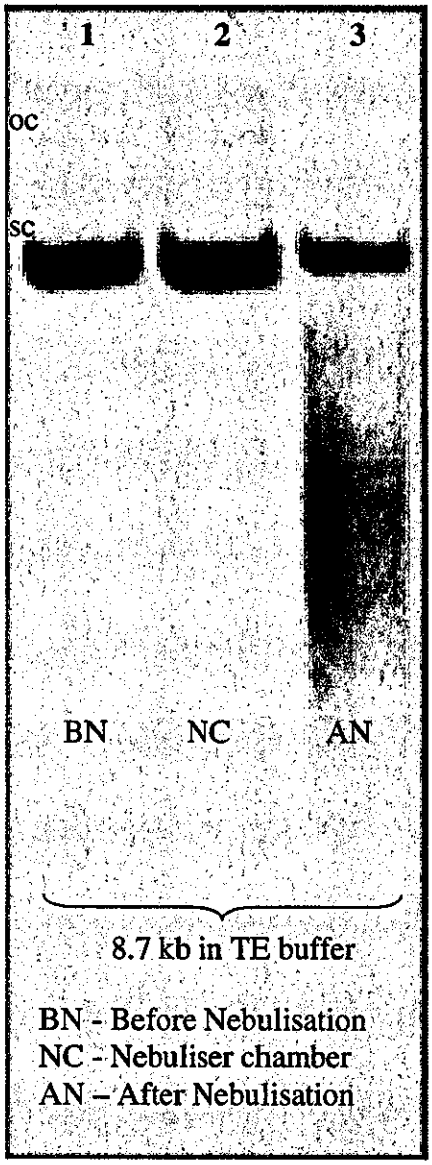

Figure A.5: Agarose gel electrophoresis of nebulisation of 8.7 kb plasmid in TE buffer showing the supercoiled (sc) and open-circular (oc) forms of the plasmid: lanes 1 – BN; 2 – NC; 3 – AN samples; 4 – Lamba HindIII DNA marker.

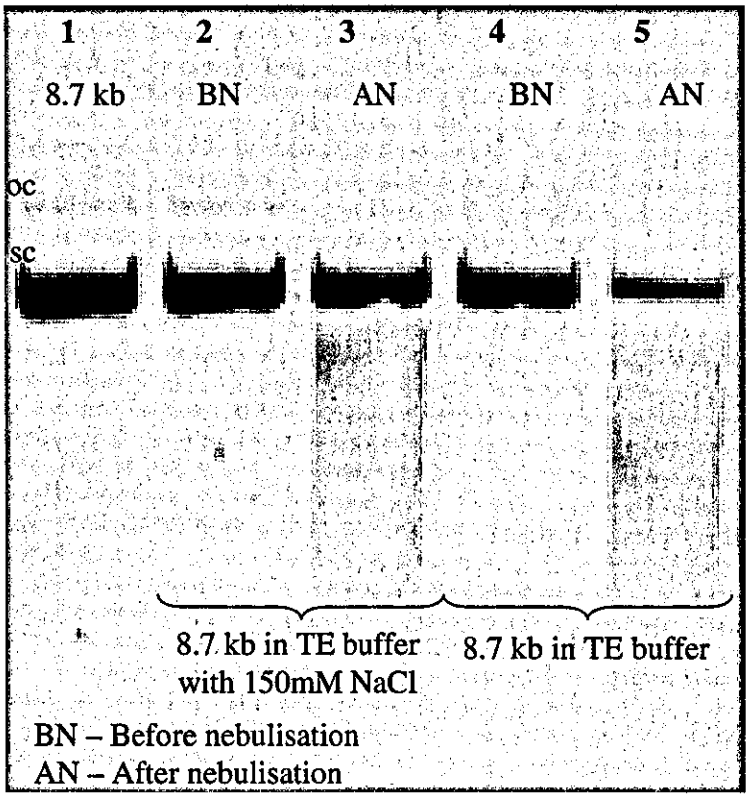

Figure A.6: Agarose gel electrophoresis of nebulisation of 8.7 kb plasmid in buffers showing the supercoiled (sc) and open-circular (oc) forms of the plasmid: TE Buffer – control; TE Buffer with 150mM NaCl, lanes 2 and 3 –BN and AN; TE Buffer, lanes 4 and 5 –BN and AN.